

**Assessment of the performance of three clear
coatings for use in heritage conservation by an
oxygen consumption technique**

Amber J. Lawson

Thesis submitted to Cardiff University
in candidature for the degree of PhD

September 2016

Declaration

This work has not been submitted in substance for any other degree or award at this or any other university or place of learning, nor is being submitted concurrently in candidature for any degree or other award.

Signed A. J. Lawson Date

STATEMENT 1

This thesis is being submitted in partial fulfillment of the requirements for the degree of PhD.

Signed A. J. Lawson Date

STATEMENT 2

This thesis is the result of my own independent work/investigation, except where otherwise stated.
Other sources are acknowledged by explicit references. The views expressed are my own.

Signed A. J. Lawson Date

STATEMENT 3

I hereby give consent for my thesis, if accepted, to be available for photocopying and for inter-library loan, and for the title and summary to be made available to outside organisations.

Signed A. J. Lawson Date

STATEMENT 4: PREVIOUSLY APPROVED BAR ON ACCESS

I hereby give consent for my thesis, if accepted, to be available for photocopying and for inter-library loans **after expiry of a bar on access previously approved by the Academic Standards & Quality Committee.**

Signed A. J. Lawson Date

Summary

Without the protection provided by anti-corrosive paints, vehicles, bridges and industrial heritage would not have survived for long. Where these coatings fail or are damaged, ferrous metal requires further protection. To provide insight into coating failure a survey of paint layers and corrosion products found on historic wrought iron and mild steel was carried out around Scotland. Corrosion has also been found to be a major contributor to structural damage of historic armoured vehicles.

When choosing coatings within conservation, decisions are based on qualitative data and practitioners' experience rather than evidence based standards for specific ferrous alloys in particular environmental conditions. Limited quantitative data exists hence this research seeks to produce quantified data via a standardised approach. To provide environmental context for the laboratory based tests, temperature and humidity data from the Tank Museum has been considered. Thus the anti-corrosive performances of clear coatings on historic armoured steel have been assessed in controlled temperature and relative humidity by using a sensitive corrosion monitoring technique.

For relevance to the conservation sector common materials, methodology and environmental conditions were considered and standardised. Aluminium oxide blasting of the steel removed contaminants and provided a keyed surface for Paraloid B72 and Cosmoloid H80, popular clear coatings within conservation and Siliglide 10, a modern silane based coating. All three coatings offered protection for the steel whether applied to cleaned surfaces or to pre-corroded surfaces. The best treatment method and thus the treatment recommended for protecting areas of paint-loss is to clean the surface and apply three layers of Paraloid B72.

The standardised approach used allows other researchers to contribute comparable data to the production of a database and future standards within conservation.

Acknowledgement

My foremost thanks go to Professor David Wakinson, for his supervision, advice and guidance over the past four years.

This project was funded by a Collaborative Doctoral Award from the Arts and Humanities Research Council (AHRC), with additional support and materials provided by Historic Scotland (now Historic Environment Scotland) and the Tank Museum, both partners in this project.

At Historic Scotland, my thanks goes to all the staff at the Conservation Centre for their support and welcome during my time in Edinburgh. The conservation science team - Alick Leslie for his guidance and support and Maureen Young for her assistance and training for X-ray fluorescence and X-ray diffraction. The painting conservation team, Damiana Magris and Ailsa Murray for their guidance with the paint layer cross sections and friendship as well as Heather Wood and Liz Wood for their continuing support and friendship.

At the Tank Museum, a special thanks goes Mike Hayton for his time and the donated materials as well as the hospitality he and his wife provided. Thanks also goes to the men in the workshop, particularly Ian 'Buzz' Aldridge who provided help with the equipment and Brian Frost who helped retrieve the data-loggers from inside the tanks and also provided a knee when I was stuck on a tank.

At Cardiff University many thanks goes to Melanie Rimmer, Eric Nordgren, Panagiota Manti and Phil Parkes for training on various pieces of equipment. I would also like to thank Paul Nicholson for his support as my second supervisor, Susan Virgo and Helen Szewczyk who both listened and provided support and guidance throughout the PhD process. Additionally, I would like to thank Nicola Emmerson for offering advice and guidance during my write up.

I would like to thank all those who have supported and encouraged me over the past four years - Eleanor Ford for putting up with me and providing lifts both to university and the airport; Duncan Slarke for listening and providing a practitioners perspective; Tamara Lawson-Rao for also listening and taking the time to reassure me and finally my parents for their unwavering support both emotionally and financially.

Dedication

This thesis is dedicated to my parents,

Albert James and Prunella Ann Lawson

For their unwavering support.

And

To the loving memory of

Suki

(† 2016)

Table of Contents

1	Introduction	1
1.1	The Importance of Conserving Historic Ferrous Metal	1
1.2	Research Context.....	1
1.3	Research Aims and Objectives	2
1.4	Advantages of Collaboration	3
1.5	Thesis Structure	3
2	Corrosion.....	4
2.1	The Corrosion Problem	4
2.2	Atmospheric Corrosion.....	5
2.3	Form of Corrosion	10
2.3.1	Uniform or General Corrosion	10
2.3.2	Non-uniform or Localised Corrosion.....	10
2.3.2.1	Differential Aeration Cells	12
2.3.2.2	Pitting Corrosion	13
2.3.2.3	Crevice Corrosion	16
2.3.2.4	Galvanic Corrosion	18
2.3.2.5	Filiform Corrosion.....	19
2.3.2.6	Stress Corrosion Cracking (SCC).....	21
2.4	Atmospheric Corrosion Products	22
2.5	Factors Governing Atmospheric Corrosion.....	27
2.5.1	Meteorological and Air Pollutant Factors.....	28
2.5.1.1	Solar Radiation and Wind	28
2.5.1.2	Temperature.....	31
2.5.1.3	Moisture	32
2.5.1.4	Deposition of pollutants: gases, particulates and aerosols	39
2.5.2	Environment Types.....	46
2.5.2.1	Rural Environments	48
2.5.2.2	Urban Environments	48
2.5.2.3	Industrial Environments	48

2.5.2.4	Marine Environments	48
2.5.3	Sheltered and Indoor Corrosion	49
3	Coating Systems: Properties and Performance	52
3.1	Introduction.....	52
3.2	Coatings	52
3.2.1	The Function of Coatings	52
3.2.2	Coating properties	54
3.2.2.1	The Rheology of Coatings: Flow and Levelling	54
3.2.2.1.1	Application Methods	55
3.2.2.1.2	Coating thickness	60
3.2.2.1.3	Wetting.....	63
3.2.2.2	Film formation	64
3.2.2.2.1	Curing/Drying.....	65
3.2.2.3	Coating Components and Chemical Characteristics.....	67
3.2.2.3.1	Binder System	67
3.2.2.3.2	Pigments.....	73
3.2.2.3.3	Solvents and Additives	74
3.3	Substrate Properties.....	78
3.3.1	Type of Substrate	78
3.3.2	Substrate Preparation.....	88
3.3.2.1	Cleaning Method.....	88
3.3.2.2	Surface Preparation	91
3.3.3	Coating Performance.....	92
3.3.3.1	Causes and Nature of Failure.....	93
3.3.3.2	Assessment of coating performance	95
4	Conservation Approaches & Experimental Design	103
4.1	Guidance and specification in conservation of heritage ferrous metal	103
4.2	Approaches to Extending the Lifespan of Heritage Ferrous Metals	104
4.2.1	Indoor approaches.....	104
4.2.2	Outdoor approaches	106

4.3	The Tank Museum, Bovington	114
4.3.1	The Environment	114
4.3.2	Vehicle Preparation	115
4.3.2.1	Surface Cleaning and Preparation	117
4.3.2.2	Coating.....	117
4.4	Clear Coatings.....	121
4.4.1	Requirements.....	121
4.4.2	Coating-Solvent Combinations and Application Techniques	121
4.4.2.1	Paraloid B72.....	122
4.4.2.2	Cosmoloid H80	124
4.4.2.3	Silanes, Polysiloxanes, Polysilazanes and Siliglide 10	126
5	Methodology.....	134
5.1	Aims and Objectives.....	134
5.1.1	Aims	134
5.1.2	Objectives	134
5.2	Field Testing and Data Collection	134
5.2.1	Sample Collection	134
5.2.2	Sample Analysis	137
5.2.2.1	Powder X-ray Diffraction (XRD).....	137
5.2.3	The Tank Museum – Environment data	138
5.2.3.1	Environmental Data Collection	138
5.3	Laboratory testing.....	140
5.3.1	Standardisation – Reliability and Validity of Research.....	140
5.3.1.1	Sample Preparation	140
5.3.1.1.1	Material selection and sampling cutting	140
5.3.1.1.2	Metallography	141
5.3.1.1.3	Surface preparation	142
5.3.1.1.4	Examination of Surfaces.....	142
5.3.1.2	Coatings: Concentrations, Solvents, Application and Oxygen Impact.....	142
5.3.1.2.1	Coating Application, Concentrations and Solvent Tests	142

5.3.1.2.2	Number of Coating Layers and Mass Applied.....	143
5.3.1.2.3	Solvent Choice and Impact on the Oxygen Measurements.....	144
5.3.1.3	Accelerated Corrosion: Chloride Deposition and Testing	147
5.3.2	Preparation and Testing of Coating Performance.....	149
5.3.2.1	Sample Material Corrosion Rates Uncoated	149
5.3.2.2	Coating Application Methodology	152
5.3.2.3	Oxygen Partial Pressure Measurements of Coated Steel Samples ..	153
5.3.3	Compatability of the Clear Coatings with Cromadex Paint	155
5.3.3.1	Effect of Cromadex Paint on the Oxygen Sensor Spots	155
5.3.3.2	Compatibility of Cromadex Paint and the Clear Coatings	155
6	Results and Analysis.....	157
6.1	Field Test Results.....	157
6.1.1	Corrosion Products From Around Scotland - X-Ray Diffraction.....	157
6.1.2	Internal Environment Data - The Tank Museum	163
6.1.2.1	Data collected by the Tank Museum (TM).....	163
6.1.2.2	Data collect inside tanks	166
6.2	Laboratory Results	171
6.2.1	Samples Material and Preparation	171
6.2.1.1	Metallography	171
6.2.1.2	Prepared Samples	172
6.2.1.3	Accelerated Corrosion and Chloride Deposition	174
6.2.1.3.1	Chloride Deposited	177
6.2.2	Oxygen Consumption of Armoured Steel Samples.....	179
6.2.2.1	Untreated Samples	179
6.2.2.2	Cleaned and uncoated samples	180
6.2.2.3	Partially pre-corroded uncoated samples	182
6.2.2.4	Comparison of uncoated samples	182
6.2.3	Clear Coatings: Application and Effect on Oxygen Measurements	185
6.2.3.1	Physical Appearance of Coatings Applied to Glass Slides	185
6.2.3.2	Mass of Coating Applied.....	188

6.2.3.2.1	Mass Applied on Glass Slides	188
6.2.3.2.2	Mass Applied on Ferrous Metal Samples.....	193
6.2.3.3	Impact of Coatings and Solvent Choice on Oxygen Sensors	197
6.2.4	Oxygen Consumption of Cleaned Coated Samples.....	200
6.2.5	Oxygen Consumption of Partially Pre-Corroded Coated Samples	204
6.2.6	Accelerated Corrosion at a Scribe through the Coatings.....	209
6.2.7	Images of samples.....	214
6.2.8	Images of cleaned, coated samples.....	219
6.2.9	Images of partially pre-corroded coated samples	224
6.2.10	Images of accelerated corroded scribed coated samples.....	228
6.2.11	Compatability of Coatings with Cromadex Paints	232
7	Discussion.....	239
7.1	Background field testing.....	239
7.1.1	Corrosion products	239
7.1.2	Environments at the Tank Museum.....	241
7.2	Laboratory Data.....	244
7.2.1	Sample Material.....	244
7.2.2	Sample size and surface preparation.....	244
7.2.3	Comparing the Oxygen Consumption of the Steel Samples.....	247
7.2.4	Clear Coatings	251
7.2.4.1	Availability and cost	251
7.2.4.2	Concentration, solvents, aesthetics and practicalities.....	251
7.2.5	Mass of coating, number of layers and distribution between layers	252
7.2.6	Effects on oxygen measurements	255
7.2.6.1	Solvent choice.....	255
7.2.6.2	Oxygen consumption of coated cleaned steel.....	255
7.2.6.3	Oxygen consumption of coated partially pre-corroded steel	257
7.2.6.4	Oxygen consumption of scribe coated cleaned steel.....	260
7.2.7	Aesthetics of coatings on samples	261
7.2.7.1	Cleaned and Coated Samples.....	262

7.2.7.2	Partially Pre-corroded and Coated Samples	264
7.2.7.3	Scribed coated samples	266
7.2.8	Compatibility of clear coatings with paints.....	268
8	Conclusion	270
9	Bibliography	273
10	Appendix	293
10.1	Summarised TM environment data.....	293

List of Figures

Figure 1 Rusting according to Stratmann	8
Figure 2 Summary of corrosion layer reactions discussed	9
Figure 3 Fe-H ₂ O-O ₂ system potential-pH diagram	10
Figure 4 Differential aeration cells	12
Figure 5 Current flow during the formation of pit from break in mill scale	14
Figure 6 Schematic of processes occurring in an actively growing pit in iron	15
Figure 7 Variations in cross sectional shape of pits.....	16
Figure 8 Typical schematic morphology - attack greatest at the mouth of the crevice.....	17
Figure 9 Basic wet corrosion cell schematic	18
Figure 10 Filiform corrosion of steel - chemical processes in a filament cell.....	20
Figure 11 Simultaneous conditions required for stress corrosion cracking	22
Figure 12 Rust layer modelling	24
Figure 13 Multi-scale model of corrosion - schematic	27
Figure 14 Atmospheric corrosion holistic model schematic	28
Figure 15 Effect of local wind speed on surf generated aerosol.....	29
Figure 16 Effect of distance from the coast and wind speeds on salt concentration (a) For surf-produced aerosols. (b) For ocean-produced salt.....	30
Figure 17 Map highlighting the proximity of Bovington Tank Museum to the coast	31
Figure 18 (a) Average daily minimum temperature; (b) Average daily mean temperature; (c) Average daily maximum temperature (°C) for summer 1971-2000	32
Figure 19 Representation of water adsorption on α -Fe ₂ O ₃	33
Figure 20 Airborne sea-salt particles class 5 distribution inland as a function of RH.....	34
Figure 21 Effects of surface RH on ocean generated aerosol - aerosol transport model	35
Figure 22 Momentary release rates of chromium, nickel, iron and manganese.....	36
Figure 23 (a) Annual average RH for 1961-1990. (b) Annual average RH for 1971-2000... ..	37
Figure 24 Average annual days of rain \geq 1 mm (a) for 1961-1990 (b) for 1971-2000.....	38
Figure 25 Change in annual days of rain $>$ 1mm between 1961-1990 and 1971-2000	39
Figure 26 Spatial and temporal scales of variability for atmospheric constituents	40
Figure 27 Deliquescence behaviour of mixed NaCl and KCl.....	42
Figure 28 Representation of a sulfate nest.....	44
Figure 29 Outline of overall transformation process	44
Figure 30 Schematic representation of a chloride agglomerate	45
Figure 31 The Vehicle Conservation Centre at the Tank Museum with over-head heating ..	51
Figure 32 Anticorrosive coating protective mechanisms	53
Figure 33 Factors affecting the longevity of an anticorrosive coating system	54
Figure 34 Different levelling (a-c) results after applying a coating to a rough surface.....	55
Figure 35 Paint application - various approaches.....	56
Figure 36 Illustration of a cross section of brush marks	58

Figure 37 Inadequate coating thickness at corners and edges	62
Figure 38 (a) Thick film at a corner (b) Surface tension causes a decrease in film thickness. (c) Thin film at the corner (d) Surface tension causes an increase in film thickness.....	62
Figure 39 (a) New film formed near an edge (b) Flow of material (c) Further flow of materials to the surrounding areas	63
Figure 40 Schematic illustration of good and poor wetting	64
Figure 41 Classification according to curing mechanism for binders.....	66
Figure 42 Deposition of siloxanes	67
Figure 43 Highly functional polysiloxane.....	71
Figure 44 Polydimethylsiloxane (PDMS) repeat unit	71
Figure 45 Polysilazane repeat unit.....	72
Figure 46 Idealised illustration of the effect of barrier pigments.	74
Figure 47 Anticorrosive coating systems classified according to solvent content	75
Figure 48 Effect of elements on corrosion based losses	82
Figure 49 Parameters involved in the blast cleaning process	90
Figure 50 Angle dependent erosion rate for typical ductile and brittle material	90
Figure 51 Quantitative service life data is available from three primary sources	92
Figure 52 External factors putting the coating-substrate bond under stress	93
Figure 53 Architectural coatings common failure modes	94
Figure 54 Idealised sketch of delamination and blistering	94
Figure 55 Common faults - root and basic associated with coating system failures	95
Figure 56 Fault tree - Underlying failure mechanisms	95
Figure 57 Oxygen-sensor spot inside container and light is transferred via fibre optic	99
Figure 58 Working principle behind optical O ₂ electrodes	99
Figure 59 Representation of attack mechanisms at scribe in the coating	100
Figure 60 (a) A hot-waxed lock; (b) A cold-waxed lock after Hurricane Katrina	105
Figure 61 South Gate of the Palace of Holyroodhouse	106
Figure 62 Dumfries Old Town Hall and stairway detail.....	110
Figure 63 Photograph of Dumfries Midsteeple ironwork.....	111
Figure 64 A “bagged up” tank in storage at the Imperial War Museum (IWM).	113
Figure 65 Front and back of two metal plates.....	113
Figure 66 Vehicle Conservation Centre (VCC) - View from balcony	114
Figure 67 Map of the Tank Museum site and locations of their data loggers	116
Figure 68 Machinery and safety equipment used by the Tank Museum for grit blasting. ...	118
Figure 69 Paints and painting equipment used at the Tank Museum.	119
Figure 70 Vehicle on display at the Tank Museum with historic paint detail left intact.....	120
Figure 71 Uses of Paraloid B72 and method preferred	123
Figure 72 Preferred solvents associated with the use of Paraloid B72	124
Figure 73 Uses of CH80 and preferred method.....	125
Figure 74 Preferred solvents associated with the use of CH80.....	125

Figure 75 Condensation of silanol groups to form a siloxane chain	126
Figure 76 Schematic of bonding mechanism - silane molecules and metal surface	127
Figure 77 Silanol terminated polydimethylsiloxane.....	128
Figure 78 Chemical structure of isoamyl acetate.....	128
Figure 79 Poly(1,1-dimethylsilazane) telomer repeat unit	129
Figure 80 Silane hydrolytic deposition	130
Figure 81 Wettability and contact angle.....	131
Figure 82 Effectiveness of silanes on inorganics.....	132
Figure 83 Sampling locations not including Orkney sites	136
Figure 84 Collection of corrosion products	137
Figure 85 The Sherman Firefly inside the New Display Hall	139
Figure 86 Sherman V Crab in the Discovery Centre	139
Figure 87 Both sides of the Saracen APV door	140
Figure 88 Corner section cut off the Saracen APV door.....	141
Figure 89 Sample with sides blanked-off.....	148
Figure 90 Spray bottle/sample set up.	148
Figure 91 Jar setup – with sensor spot, silica gel, data logger and sample.	150
Figure 92 Sealed reaction jar	150
Figure 93 Distance vs occurrence of akaganéite.....	158
Figure 94 Range in temperature experienced around the Tank Museum	163
Figure 95 Range in RH experienced around the Tank Museum	164
Figure 96 Temperature ranges for the sheds at the TM	165
Figure 97 Range of RH measured within the sheds at the Tank Museum	166
Figure 98 Average daily temperature and RH data - inside the Sherman Firefly	167
Figure 99 Summary of the temperature data collected inside the Sherman Firefly.....	167
Figure 100 Summary of the RH data collected inside the Sherman Firefly.....	168
Figure 101 Average daily temperature and RH data inside the Sherman V Crab.....	168
Figure 102 Summary of the temperature data collected inside the Sherman V Crab	169
Figure 103 Summary of the RH data collected inside the Sherman V Crab	169
Figure 104 Comparison of the average temperature data collected within the vehicles.	170
Figure 105 Comparison of the average RH data collected within the vehicles.	170
Figure 106 Sample dimensions.....	173
Figure 107 SEM SEI images summarising the changes to the surface profile.....	174
Figure 108 Sample corroded by salt solution applied by pipette	174
Figure 109 Trial 1-5 11 days after being sprayed with salt solution.	175
Figure 110 Trial 1-5 after being allowed to corrode for 11 days in the laboratory.	175
Figure 111 Chloride deposited by 10 drops of de-icing salt solution	177
Figure 112 Mass of chloride per spray of de-icing salt solution on a sample	178
Figure 113 Reduction in O ₂ partial pressure caused by untreated samples	179
Figure 114 Reduction in O ₂ partial pressure caused by untreated samples c.....	180

Figure 115 Reduction in O_2 partial pressure caused by samples air abraded clean.....	181
Figure 116 Reduction in O_2 partial pressure caused by samples air abraded clean.....	181
Figure 117 Reduction in O_2 partial pressure samples sprayed with salt solution.....	183
Figure 118 Comparison of the reduction in O_2 partial pressure for uncoated samples	184
Figure 119 Boxplot comparison of the uncoated samples.....	184
Figure 120 10% w/v Paraloid B72 in xylene on a glass slide	186
Figure 121 Zoomed area of figure 120	186
Figure 122 15% w/v Paraloid B72 in xylene	186
Figure 123 10% w/v Paraloid in acetone	186
Figure 124 Zoomed areas of figure 123.....	186
Figure 125 Coated with 10% w/v Paraloid in acetone	186
Figure 126 Zoomed areas of 10% w/v Paraloid B72 in acetone.....	187
Figure 127 10% Paraloid B72 in xylene applied to an air abraded slide	187
Figure 128 10% w/v Cosmoloid H80 in white spirit applied to an air abraded slide.	187
Figure 129 Comparison of mass distribution of Paraloid B72 coating over three layers for acetone and xylene as the solvents.....	191
Figure 130 Comparison of mass distribution of three layers of Cosmoloid H80.....	193
Figure 131 Comparison of the masses of the first layer of coatings.....	195
Figure 132 Comparison of the masses of the second layers of the clear coatings.	196
Figure 133 Comparison of the masses of the third layers of the clear coatings.....	196
Figure 134 Comparison of the total masses of the coatings.....	196
Figure 135 Comparison of the total masses of the coatings and surface preparations.	197
Figure 136 Reduction in PO_2 for Paraloid B72 in acetone not degassed glass slides	198
Figure 137 Reduction in PO_2 for Paraloid B72 in acetone on glass slides after de-gassing	198
Figure 138 Reduction in PO_2 for Cosmoloid H80 in white spirit not degassed glass slides	199
Figure 139 Reduction in PO_2 for Siliglidle 10 not degassed on glass slides	199
Figure 140 Reduction in O_2 partial pressure for Paraloid B72 coated clean samples.....	200
Figure 141 Reduction in O_2 partial pressure for Cosmoloid H80 coated cleaned samples.	201
Figure 142 Reduction in O_2 partial pressure for Siliglidle 10 coated cleaned samples	201
Figure 143 Comparison of the reduction in O_2 partial pressure for clean coated samples .	202
Figure 144 Boxplot of the reduction in O_2 partial pressure for clean coated samples.....	203
Figure 145 Boxplot comparing reduction in O_2 partial pressure for cleaned samples.....	203
Figure 146 Reduction in O_2 partial pressure - Paraloid B72 coated partially corroded	204
Figure 147 Reduction in O_2 partial pressure - Cosmoloid H80 coated partially corroded ...	205
Figure 148 Reduction in O_2 partial pressure - Siliglidle 10 coated partially corroded	206
Figure 149 Boxplot for the reduction in O_2 partial pressure by partially pre-corroded samples divided up into the types of coatings used.	206
Figure 150 Comparison of the average reduction in O_2 partial pressure of partially corroded samples coated and uncoated over 50 days.	207

Figure 151 Comparison of the average reduction in O ₂ partial pressure of the partially corroded samples coated and uncoated over 340 days	208
Figure 152 Comparison of the reduction in O ₂ partial pressure per day for the different types of coating on different surfaces	208
Figure 153 Reduction in O ₂ partial pressure for clean coated samples with salt solution applied to a scribe in the Paraloid B72 coating first for 70 days	209
Figure 154 Reduction in O ₂ partial pressure for clean coated samples with salt solution applied to a scribe in the Paraloid B72 coating - a further 148 days	210
Figure 155 Combined data for the reduction in O ₂ partial pressure for clean coated samples with salt solution applied to a scribe in the Paraloid B72 coating - 218 days	210
Figure 156 Reduction in O ₂ partial pressure for clean coated samples with salt solution applied to a scribe in the Cosmoloid H80 coating first 70 days.	211
Figure 157 Reduction in O ₂ partial pressure for clean coated samples with salt solution applied to a scribe in the Cosmoloid H80 coating - a further 148 days	211
Figure 158 Combined data for the reduction in O ₂ partial pressure for clean coated samples with salt solution applied to a scribe in the Cosmoloid H80 coating - 218 days	212
Figure 159 Reduction in O ₂ partial pressure for clean coated samples with salt solution applied to a scribe in the Siliglide 10 coating first 70 days	212
Figure 160 Reduction in O ₂ partial pressure for clean coated samples with salt solution applied to a scribe in the Siliglide 10 coating - a further 148 days.....	213
Figure 161 Combined data for the reduction in O ₂ partial pressure for clean coated samples with salt solution applied to a scribe in the Siliglide 10 coating - 218 days	213
Figure 162 Untreated (UT) sample 1 side A prior to exposure at 80% RH	215
Figure 163 UT1B prior exposure at 80% RH	215
Figure 164 UT1A after 163 days exposed to 80% RH.....	215
Figure 165 UT1B after 163 days exposed to 80% RH.....	215
Figure 166 Zoomed area of UT1A after 163 days exposed to 80% RH	215
Figure 167 Zoomed area of UT1B after 163 days exposed to 80% RH	215
Figure 168 Sample CS3A prior to air abrading clean	216
Figure 169 Sample CS3B prior to air abrading clean	216
Figure 170 CS3A after air abrading before exposure at 80% RH.....	216
Figure 171 CS3B after air abrading before exposure at 80% RH.....	216
Figure 172 CS3A after exposure at 80% RH for 65 days	216
Figure 173 CS3B after exposure at 80% RH for 65 days	216
Figure 174 Zoomed area of CS3B - effect of surface profile on the corrosion pattern	217
Figure 175 Zoomed areas of CS3B - a mix of filiform and general corrosion.....	217
Figure 176 Sample PC1A before air abrading clean	217
Figure 177 PC1B prior to air abrading clean.....	217
Figure 178 PC1A after cleaning by air abrasion	217
Figure 179 PC1B after cleaning by air abrasion	217

Figure 180 PC1A prior to exposure at 80% RH	218
Figure 181 PC1B after partially corroding with salt spray prior to exposure at 80% RH	218
Figure 182 PC1A after exposure at 80% RH for 48 days	218
Figure 183 PC1B change in corrosion after exposure at 80% RH for 48 days	218
Figure 184 Zoomed area of corrosion on PC1A filiform and general corrosion	218
Figure 185 Zoomed area of PC1B salt-spray corroded side	218
Figure 186 PB72CS5A cleaned by air abrasion	220
Figure 187 PB72CS5B cleaned by air abrasion	220
Figure 188 PB72CS5A after coating with 10% w/v Paraloid B72 in acetone	220
Figure 189 PB72CS5B after coating with Paraloid B72 in acetone	220
Figure 190 PB72CS5A after O ₂ monitoring for 341 days.....	220
Figure 191 PB72CS5B after O ₂ monitoring for 341 days.....	220
Figure 192 Zoomed area of PB72CS5A showing the corrosion formed and the coating	221
Figure 193 Zoomed area of PB72CS5B - corrosion patches and bubbles in the coating. ...	221
Figure 194 CH80CS5A cleaned by air abrasion	221
Figure 195 CH80CS5B cleaned by air abrasion	221
Figure 196 CH80CS5A after coating with Cosmoloid H80 in white spirit	221
Figure 197 CH80CS5B after coating with Cosmoloid H80 in white spirit	221
Figure 198 CH80CS5A after monitoring O ₂ levels for 341 days.....	222
Figure 199 CH80CS5A after monitoring O ₂ levels for 341 days.....	222
Figure 200 Zoomed area of general corrosion on sample CH80CS5A	222
Figure 201 Zoomed area of general corrosion on sample CH80CS5B	222
Figure 202 S10CS5A cleaned by air abrasion	222
Figure 203 S10CS5B cleaned by air abrasion	222
Figure 204 S10CS5A after being coated with Siliglide 10	223
Figure 205 S10CS5B after being coated with Siliglide 10	223
Figure 206 S10CS5A after monitoring O ₂ levels for 341 days.....	223
Figure 207 S10CS5B after monitoring O ₂ levels for 341 days.....	223
Figure 208 Zoomed area of S10CS5A displaying corrosion.....	223
Figure 209 Zoomed area of corrosion on sample S10CS5B	223
Figure 210 PB72PC1B – top side after cleaning by air abrasion.....	225
Figure 211 PB72PC1B – top side sprayed with salt solution, after corroding for 8 days	225
Figure 212 PB72PC1B – top side cleaned, corroded and coated	225
Figure 213 PB72PC1B after exposure at 80% RH for 342 days	225
Figure 214 Zoomed area of PB72PC1B - filiform corrosion and bubbles in the coating.	225
Figure 215 CH80PC sample 2 side B – top side after cleaning by air abrasion.....	226
Figure 216 CH80PC2B – top side sprayed with salt solution and corroded for 8 days	226
Figure 217 CH80PC2B – top side cleaned, accelerated corroded and then coated	226
Figure 218 CH80PC2B after monitoring O ₂ levels for 342 days.....	226
Figure 219 Zoomed area of CH80PC2B with loose corrosion and detaching coating	226

Figure 220 S10PC6B – top side after cleaning by air abrasion	227
Figure 221 S10PC6B – top side sprayed with salt solution, after corroding for 8 days	227
Figure 222 S10PC6B – coating applied over corrosion caused by sprayed salt solution ...	227
Figure 223 S10PC6B after exposure at 80% RH for 342 days.....	227
Figure 224 Zoomed area of S10PC6B revealing powdery corrosion	227
Figure 225 PB72SC1B with salt solution painted down the scribe to accelerate corrosion	229
Figure 226 PB72SC1B after 70 days, clearly showing filiform corrosion	229
Figure 227 PB72SC1B after a further 148 days – 218 days in total.....	229
Figure 228 Zoomed area around the scribe on PB72SC1B	229
Figure 229 CH80SC5A with salt solution painted down the scribe to accelerate corrosion	230
Figure 230 CH80SC5A after monitoring O ₂ levels for 70 days.....	230
Figure 231 CH80SC5A after monitoring O ₂ levels for a further 148 days (218 days)	230
Figure 232 Zoomed area around the scribe on CH80SC5A.....	230
Figure 233 S10SC4A with salt solution painted down the scribe to accelerate corrosion...	231
Figure 234 S10SC4A after 70 days, with corrosion mainly focused in the scribe	231
Figure 235 S10SC4A after a further 148 days – 218 days in total	231
Figure 236 Zoomed area around the scribe on S10SC4A.....	231
Figure 237 Panzer grey - Cromadex paint.....	233
Figure 238 Red oxide - Cromadex paint.....	234
Figure 239 Semi-gloss black - Cromadex paint.....	235
Figure 240 Matt green - Cromadex paint.....	236
Figure 241 Semi-gloss green - Cromadex paint	237
Figure 242 Green gloss - Cromadex paint.....	238
Figure 243 Reverse side of sample PC5 following exposure at 80% RH.....	246
Figure 244 Zoomed central area of sample PC5 after exposure at 80% RH	246

List of Tables

Table 1 Forms of localised corrosion	11
Table 2 Effect of NaCl concentration on pitting corrosion rate summarised.....	15
Table 3 Galvanic Series of Metals and Alloys.....	19
Table 4 Chemical compounds found in rust layers	23
Table 5 Key corrosion products formed in different locations within the rust layer.....	25
Table 6 Typical ground roughness values	30
Table 7 Deliquescence and efflorescence points for common aerosol components.....	41
Table 8 Temperature and humidity levels at which marine and deicing salts begin to absorb water and form a corrosive chloride solution.	42
Table 9 Atmospheric corrosivity categories and examples of typical environments.....	46
Table 10 Summary of gaseous concentration, aerosol type and rain water composition	47
Table 11 ISO classification of time of wetness	49
Table 12 Classification of corrosivity of indoor atmospheres.....	50
Table 13 Mass loss of uncoated and vinyl resin-coated cold-rolled steel samples in atmosphere containing SO ₂ and NaCl	53
Table 14 Miscellaneous wet coating methods	57
Table 15 Suitability of different bristle types for use with different paints	57
Table 16 Advantages and disadvantages of pads compared to brushes	59
Table 17 Minimum coating thickness of corrosion protection coating systems for steel	61
Table 18 Summary of chemically and physically drying paints.....	65
Table 19 Coating thickness for coating systems depending on the type of atmospheric	68
Table 20 Anticorrosive properties required of polymers for specific polymer classes	69
Table 21 Properties provided by the inorganic and organic portions	70
Table 22 Range of applications of siloxane materials	72
Table 23 Most commonly used liquid carriers of pigment and binders used in paints	75
Table 24 Solvent properties	76
Table 25 Uses of architectural ferrous metal	79
Table 26 Concentration limits of elements for classification as base or alloy metal	80
Table 27 Quality groups used to divide steel further in the standard EN 10 020	81
Table 28 Alloy elements and their effect on corrosion properties.....	84
Table 29 Corrosion rates of ferrous metals in different environments	86
Table 30 Cleaning Methods for Historic Ferrous Metalwork.....	89
Table 31 Some of the most common types of failure or defect and probable causes.....	96
Table 32 Summary of salt solutions used in the automotive industry.....	101
Table 33 Extract from the summary by Bos of some standardized accelerated tests.....	102
Table 34 Coatings used by conservators in indoor environments in the UK.....	105
Table 35 Coatings used outdoors by conservation practitioners	107
Table 36 Microscopy images of polished paint layer cross sections	107

Table 37 Cromadex paints used by the Tank Museum, Bovington	117
Table 38 Ingredients proportions in Siliglide 10 as stated on the MSDS.....	129
Table 39 Designation according to contact angle	131
Table 40 Sites and numbers of samples collected	135
Table 41 MadgeTech RHTemp101A data-logger manufacturer specifications.....	138
Table 42 Location and environment of vehicles and location of the data loggers	138
Table 43 Summary of the grades of abrasive and liquid used for grinding and polishing ...	141
Table 44 Coating and solvent tests run to test the impact on the O ₂ sensor spot.....	146
Table 45 Coating concentrations and solvents used	147
Table 46 Sample names, numbers, surface condition, coating and days of monitoring	151
Table 47 Content of different sample jars	152
Table 48 Content of jars containing samples.....	154
Table 49 Cromadex paint colour, finish and numbers involved in monitoring	155
Table 50 Drying and over-coating times for Cromadex paints.....	156
Table 51 Summary of the corrosion products detected around Scotland.....	157
Table 52 Corrosion products on historic wrought iron and mild steel around Scotland	159
Table 53 Data summary collected in the Discovery Centre on the Mark 10.....	164
Table 54 Summarised data collected in the New Display Hall on the Firefly	164
Table 55 Summary of data by the TM in the New Display Hall inside the Firefly	165
Table 56 Images of etched steel sample from a Saracen APV	171
Table 57 SEM analysis of Saracen APV Steel	172
Table 58 Masses and sample labels of 15 samples before treatment	172
Table 59 Samples PC1-5 after being sprayed with salt solution and allowed to corrode....	175
Table 60 Chloride deposited by pipette drop application.....	177
Table 61 Chloride deposition by spray application converted to µg	178
Table 62 Linear trendline analysis of figure 114	180
Table 63 Linear trendline analyses of figure 116.....	182
Table 64 Linear trendline analyses of figure 117.....	183
Table 65 Mass of each layer of 10% Paraloid B72 in xylene coated on a glass slide.....	188
Table 66 Percentage difference of each layer of Paraloid B72 in xylene and total mass ...	188
Table 67 Percentage of total coating mass in each layer of Paraloid B72 in xylene.....	189
Table 68 Mass of each layer of Paraloid B72 in acetone coated onto slides	189
Table 69 Percentage difference of each layer of Paraloid B72 in acetone.....	189
Table 70 Percentage of the total coating mass in each layer of Paraloid B72 in acetone. .	190
Table 71 Difference between using acetone and xylene as the solvent for the coating Paraloid B72: average mass for each layer	190
Table 72 Mass of each layer of Cosmoloid H80 in white spirit and slide used for coatings	191
Table 73 Percentage difference of each layer of Cosmoloid H80 in white spirit and the total mass in comparison to the highest mass.....	192

Table 74 Percentage of the total coating mass contained in each layer of Cosmoloid H80 in white spirit.	192
Table 75 Summarised distribution of Paraloid B72 over 3 layers on metal samples.....	193
Table 76 Summarised distribution of Cosmoloid H80 over 3 layers on metal samples.....	194
Table 77 Summarised distribution of Siliglilide 10 over 3 layers on metal samples	194
Table 78 Comparison of the clean coated samples with control data substracted.....	203
Table 79 Comparison of partially pre-corroded coated samples	207
Table 80 Comparison of data ranges and rate of reduction values	250
Table 81 Summary of environment in the British Steel Hall on the Tortoise Tank.	293
Table 82 Data summary collected in the Discovery Centre on the Mark 10.....	293
Table 83 Summarised data collected in the New Display Hall on the Firefly	293
Table 84 Summary of data by the TM in the New Display Hall inside the Firefly	294
Table 85 Summary of data collected by the TM in Nev's Shed	294
Table 86 Summary of the data collected by the TM in the New Shed.....	294
Table 87 Summary of data collected by the TM in Shed 1	294
Table 88 Summary of data collected by the TM in the Shed 1 Extension	294
Table 89 Summarised data collected in the Tamiya Hall, at the Sentry Post.....	295
Table 90 Summary of data collected by the TM in the WW1 Hall, display case	295
Table 91 Summary of data collected by the TM in the WW1 Hall, CW	295

Abbreviations and Symbols

AJMM	Air jet micro-machining	JIS	Japanese Standards Association
ASTM	American Society for Testing and Materials	ISO	International Standards Organisation
AHRC	Arts and Humanities Research Council	LED	Light emitting diode
APV	Armoured Personnel Vehicle	MIO	Micaceous iron oxide
ACAP	Automotive Corrosion and Protection	MIC	Microbiologically induced corrosion
BS	British Standard	MDRH	Mutual deliquescence RH
BSI	British Standards Institute	NHIG	National Heritage Ironwork Group
cSt	Centistokes	NSS	Neutral salt spray
CFD	Computational fluid dynamics	PDMS	Polydimethylsiloxane
CDA	Collaborative doctoral award	POF	Polymer optical fibre
CPS	Counts per second	RH	Relative humidity
CCT	Cyclic corrosion testing	RHA	Rolled homogeneous armour
DS/EN	Danish Standard/European Standard	RTV	Room temperature vulcanizing
DRH	Deliquescence RH	SEM	Scanning electron microscope
DIN	Deutsches Institut für Normung e. V.	SEI	secondary electron imaging
DSS	Duplex stainless steels	SAE	Society of Automotive Engineers
EIS	electrochemical impedance spectroscopy	SOHIC	Stress-oriented hydrogen-induced cracking
EBSD	Electron backscattered diffraction	SS	Stainless steel
EN	European Norm	SCC	Stress cracking corrosion
GM	General Motors	SSC	sulfide stress cracking
T_g	Glass transition temperature	SA	Surface area
GNP	Gross national product	TOW	Time-of-wetness
HIC	Hydrogen-induced cracking	TM	Tank Museum
IWM	Imperial War Museum, Duxford	UV	Ultra-violet
IMS	Industrial methylated spirit	UK	United Kingdom

US	United States	w/w	Weight to weight ratio
VCC	Vehicle Conservation Centre	WWI	World War 1
VDA	Verband der Automobilindustrie - German Association of the Automotive Industry	XRD	X-ray diffraction
VICT	Volvo indoor corrosion test		
v/v	Volume to volume ratio		
w/v	Weight to volume ratio		

Uncommon Symbols and Units

<i>D</i>	Eddy diffusivity
$\mu\text{eq l}^{-1}$	Microequivalent per litre
γ	Impaction-to-sedimentation ratio
\approx	Approximately equal to

Control and surface preparation

NS	No sample - Control
UT	Untreated
CS	Clean surface
PC	Partially Pre-corroded
SC	Scribe creep test

Coatings and solvents

PB72	Paraloid B72
CH80	Cosmoloid H80
S10	Siliglide 10
WS	White spirit

Corrosion Product Abbreviations

A	Akaganéite
G	Goethite
L	Lepidocrocite
M	Magnetite/Maghemite

Environment

I	Industrial
M	Marine
R	Rural
U	Urban

Tank Museum (TM) locations

BSH	British Steel Hall	TH	Tamiya Hall
DC	Discovery Centre	VCC	Vehicle Conservation Centre
NDH	New Display Hall	WW1 Hall	World War 1 Hall

Chemical Elements, Ions, Compounds and Corrosion Products

β -FeOOH	Akaganéite	Fe ₃ O ₄	Magnetite
Al	Aluminium	Mg	Magnesium
NH ₂	Amine	MgCl ₂	Magnesium chloride
NH ₃	Ammonia	Mn	Manganese
NH ₄ ⁺	Ammonium	MnS	Manganese sulfide
Br ⁻	Bromide ions	Mo	Molybdenum
Ca ²⁺	Calcium	Ni	Nickel
CaCl ₂	Calcium chloride	Nb	Niobium
CO ₂	Carbon dioxide	N	Nitrogen
Cl ⁻	Chloride ions	NO ₃ ⁻	Nitrate
Cl ₂	Chlorine	NO ₂	Nitrogen dioxide
Cr	Chromium	NO _x	Nitrogen oxides
Cu	Copper	O ₂ or O	Oxygen
δ -FeOOH	Feroxyhyte	O ₃	Ozone
FeCl ₃	Ferric chloride	P	Phosphorus
FeCl ₂	Ferrous chloride	K ⁺	Potassium
Fe(OH) ₂	Ferrous hydroxide	KCl	Potassium chloride
FeSO ₄	Ferrous sulfate	Si	Silicon
α -FeOOH	Goethite	SiC	Silicon carbide
α -Fe ₂ O ₃	Hematite	NaCl	Sodium chloride
HCl	Hydrochloric acid	S	Sulfur
H or H ₂	Hydrogen	SO ₄ ²⁻	Sulfate
H ₂ S	Hydrogen sulfide	H ₂ SO ₄	Sulfuric acid
•OH	Hydroxide radical	SO ₂	Sulfur dioxide
OH ⁻	Hydroxide ions	SO _x	Sulfur oxides
OH-	Hydroxyl	SO ₃	Sulfur trioxide
Fe	Iron	Sn	Tin
Pb	Lead	Ti	Titanium
γ -FeOOH	Lepidocrocite	H ₂ O	Water
Fe ₂ O ₃	Maghemite	Zn	Zinc

1 Introduction

1.1 The Importance of Conserving Historic Ferrous Metal

The survival of historic ferrous metal artefacts, machinery and vehicles is important for the enjoyment and education of future generations. To make appropriate recommendations about the long term management of ferrous metal objects it is crucial to understand what objects are made from and how significant they are (Williams, 2009b). Therefore, both humanities/arts and science influence conservation science and in order to produce a holistic programme of research and analysis, scientific techniques are only part of a well-executed inquiry.

1.2 Research Context

Analyses of vehicles at the Tank Museum (TM) revealed that corrosion was a major contributor to structural damage together with wear, fatigue/stress corrosion cracking (SCC), cracks and failures (Saeed, 2013). Thus, this collaborative doctoral award (CDA) was set up to research corrosion of ferrous metal and selected clear coating treatments within conservation.

Due to a lack of evidence-based heritage standards, choosing a treatment method for historic ferrous metal within conservation is difficult as it relies on unscaled comparisons and speculation. It is therefore the responsibility of conservation scientists to modify existing industrial standards or develop new ones that address heritage contexts. For this reason, in addition to providing insight into specific treatment methodology commonly used within conservation practice, this research also provides quantified comparable data for the treatment of historic armoured steel by using standardised methodology.

Potential Impact of this Study

This research benefits not only those responsible for the maintenance of historic armoured vehicles (e.g. The Tank Museum, Bovington) and outdoor wrought iron (Historic Scotland), but also benefits other museums, independent conservators and those with smaller private collections. The quantified data provided can contribute to informed decision-making for the treatment of ferrous metal. Producing achievable and reproducible quantified outcomes benefits the whole Heritage Sector as they are provided with supporting data for the creation of a management tool to

preserve a variety of ferrous metals. The quantified outcomes of this research provides some underpinning data required for the development of standards. It is by direct quantitative comparison of corrosion rate results that comparisons can be made between both uncoated samples and coated samples, in the same environment. This allows guidance to be offered for the best treatment method for the specified environmental conditions as the anti-corrosive performance of the coatings can be ranked according to quantitative corrosion rate data.

By providing a reproducible test methodology this project strives to encourage other researchers to contribute towards the creation of a database, by testing new coatings and different ferrous alloys. The results of this project can be used to support the development of evidence based conservation and management strategies.

1.3 Research Aims and Objectives

This research is designed to provide standardised methodology and quantitative, statistically evaluated data. It aims to determine the effectiveness of selected clear coatings for controlling the corrosion of modern historic steel in conservation contexts with specific reference to the needs of the TM. The occurrence of chloride contaminated surfaces at heritage sites around Scotland will also be assessed.

This will be accomplished by:

- Surveying the occurrence of chloride bearing corrosion products at historic sites in Scotland and contextualise this for heritage.
- Assessing the environmental context for use of coatings within the TM.
- Preparing samples of historic armoured steel donated by the TM for testing the efficacy of three clear coatings: Paraloid B72 (acrylic), Cosmoloid H80 (micro-crystalline wax) and Siliglide 10 (silane).
- Assessing the ability of these coatings to prevent corrosion in high relative humidity (RH) by monitoring the oxygen consumption of samples at 80% relative humidity.
- Determining if standardised pre-corrosion of samples with de-icing salt solution prior to applying coatings impacts on the protective performance of the coating.

1.4 Advantages of Collaboration

This thesis resulted from an Arts and Humanities Research Council (AHRC) funded CDA with additional support from the TM in Bovington, Dorset and Historic Scotland, Edinburgh, now part of the newly formed Historic Environment Scotland.

For this study, as the author is neither a conservator by training nor had direct experience of working in a museum or heritage environment, collaborative working was particularly useful. Within this project the participation of Historic Scotland and the TM was important for providing background context and access to historic materials. Time spent at the TM provided insight into the conservation methods they use and the placement carried out at Historic Scotland's Conservation Centre, Edinburgh permitted a sampling survey of corrosion products and historic paint layers to take place, providing further background context for the project.

1.5 Thesis Structure

This thesis is structured to address its research objectives and the interdisciplinary context. The corrosion problem is addressed initially, followed by an overview of atmospheric corrosion and relevant research within this area (Chapter 2). An outline of coating systems a common method used for preserving ferrous metal, is offered in chapter 3 addressing all aspects of the coating, the metal composition and the interface between the coating and metal, plus methods used to assess performance. Practices and coatings used within the conservation sector are considered in Chapter 4. This is followed by the methodology used for testing and data collection (Chapter 5). The results and analyses of the data are presented in chapter 6, with a discussion of the results and their implications presented in chapter 7. Chapter 8 summarises the key finding of this research project and includes some recommendations for coating methodology and areas for additional research.

2 Corrosion

2.1 The Corrosion Problem

Safety, economics and conservation are the three primary reasons for concern about and study of corrosion (Schweitzer, 2010). Safety issues resulting from corrosion can be extreme if machines and structures are not maintained; discovery of cracks on an aircraft, can ground an entire fleet (Evans, 1972).

Corrosion is an expensive problem and attempts to estimate its cost were made as early as 1922 (Bhaskaran et al., 2005). In 1969, Hoar (1976) was asked to chair a committee to investigate and assess the cost per annum in the UK of corrosion and what methods were available for reducing it. The report gave the total cost per annum as £1,365 million and the possible savings as £310 million. While the figures were conservative and did not include domestic dwellings or agriculture (Hoar, 1976), they represented approximately 3.5% of the gross national product (GNP) (Koch et al., 2001; Bhaskaran et al., 2005). Several years ago the National Institute of Standards in the United States (formerly the National Bureau of Standards) estimated the annual cost of corrosion to be in the range of \$9 billion to \$90 billion (Schweitzer, 2010).

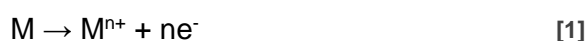
The UK's heritage is a big draw for foreign visitors, and is ranked 4th out of 50 nations for the quality of the heritage by potential visitors (Brightman, 2012). Many of the UK's heritage sites and objects contain metallic elements, thus the conservation of these metallic elements is of great importance, but funding can sometimes be an issue. In the heritage sector the majority of organisations responsible for cultural material rely on external funding and since central governments often control a large proportion of this funding, it can often be restricted or withdrawn for political, economic or philosophical reasons (Ashley-Smith, 2013). With restricted funds and corrosion being such a big problem questions need to be asked, e.g. 'how much from the past can be preserved?'. The majority of museums take charge of more and more material, but they must be selective. Preventing damage to and providing access to objects in museums costs money, but as long as the objects survive, providing access can generate income (Ashley-Smith, 2013). Decisions always need to be made, balancing expenditure between conservation and exploitation due to the need for revenue is a key decision that has to be made.

To meet their goals, retaining evidence of an object's cultural context and integrity while preserving it, metals conservators need to implement carefully thought out plans (Selwyn, 2004; Watkinson, 2010). Treatment plans are different for all metal heritage and the treatment decisions depend on numerous factors. There are differences between the core values of a conservator and corrosion scientist. For the conservator many values, often intangible, are associated with function, whereas to the corrosion scientist "function" is purely utilitarian (Cole et al., 2004c). However, a knowledge and understanding of corrosion science is vital for a good conservator.

2.2 Atmospheric Corrosion

In the presence of moisture and oxygen (O₂), iron (Fe) and steel are thermodynamically unstable and corrode during burial, immersion in water and exposure to moist air (Walker, 1982c). Atmospheric O₂ and moisture can support electrochemical corrosion of metals, which involves a number of processes occurring on and within the metal:

1. **A metallic circuit** – Electrons flowing between the anodic areas and cathodic areas in solid phase.
2. **Anodic area** – Oxidation of the metal occurs at the anodes.



3. **Cathodic area** – Where reduction occurs – electrons are consumed.

In neutral and acidic solutions exposed to ambient air, the reduction of dissolved O₂ is often observed [2] and [3] (Jones, 2013).



The reduction of hydrogen ions (H⁺) in acid solution does not occur at an appreciable rate above pH 4 (Turgoose, 1982) [4], and can occur in the absence of O₂. In certain circumstances, water (H₂O) can be reduced assuming it dissociates to H⁺ and hydroxide (OH⁻) ions [5]. With OH⁻ subtracted from both sides of the reaction [5] it is considered equivalent to [4].



4. **An electrolyte** – a thin aqueous layer on the metal surface in contact with both the anode and cathode (Walker, 1982c), which conducts electric current due to free ions (Groysman, 2010). It contains various species deposited from the atmosphere or originating from the corroding metal (Kucera and Mattsson, 1987). Pure H₂O is not an electrolyte owing to poor dissociation of H₂O molecules. During the initial stages of corrosion, the charge balance during oxidation of the metal is maintained by the reduction of dissolved O₂ or H₂O (Graedel and Frankenthal, 1990).

Since the anodic reaction is rapid in most media, the cathodic reaction controls the rate of corrosion as [2] and [3] are contingent upon the amount of dissolved O₂ in the H₂O (Walker, 1982c). However, where thickness of a liquid film exceeds several tenths of a micron (µm) or the corrosion product film develops, hindering electron or O₂ transport, O₂ transport can become rate-limiting (Morcillo et al., 2011). With this research focused on the corrosion of historic ferrous metal predominantly used for large historic armoured vehicles and structures, the cathodic processes will begin in aerated solutions and the Fe will oxidise to Fe²⁺ at the anode [6].



Atmospheric corrosion of iron can be split into two distinguishable stages: initiation and propagation (Kucera and Mattsson, 1987). A third stage, cessation, has been proposed (Schindelholz and Kelly, 2012). These three stages are controlled by the different wetting and drying phenomena that metal surfaces are exposed to in atmospheric environments.

Initiation

Initiation of corrosion is a slow process if both the atmosphere and metal surface are free from contaminants, even in atmospheres saturated with H₂O vapour (Kucera and Mattsson, 1987). In water free from contaminants, inclusions e.g. manganese sulfide (MnS) dissolve when the surface becomes wet initiating corrosion. The presence of deposited solid particles are more important for the initiation of corrosion (Kucera and Mattsson, 1987; Morcillo et al., 2011), as corrosion can be affected by absorbent and non-absorbent particles. Absorbent particles e.g. charcoal and soot are essentially inert but they have surfaces that adsorb sulfur dioxide (SO₂) by either co-adsorption of water vapour or condensation of H₂O within the structure, catalysing the formation of a corrosive acid electrolyte (Syed, 2006).

Non-absorbent particles can facilitate differential aeration processes at the point of contact.

During initiation, anodic spots become surrounded by cathodic areas (Kucera and Mattsson, 1987). In clean dry atmospheres, steel surfaces become covered by a thick oxide film (20-50 Å) with an inner layer of magnetite (Fe_3O_4) and an outer layer of polycrystalline ferric oxide, maghemite (Fe_2O_3), which almost stops further oxidation taking place (Kucera and Mattsson, 1987; Morcillo et al., 2011).

Lepidocrocite ($\gamma\text{-FeOOH}$) can form in atmospheres containing small amounts of water vapour (Kucera and Mattsson, 1987). During the electrochemical reduction of corrosion, Fe^{2+} , an intermediate is initially formed and creates a reduced surface layer on top of the FeOOH crystals (Stratmann et al., 1983).

Propagation

Propagation of the corrosion process requires the presence of an electrolyte film on the metal surface (Kucera and Mattsson, 1987; Morcillo et al., 2011). The propagation of corrosion can be stimulated by SO_2 , adsorbing and oxidising to sulfate (SO_4^{2-}) in the rust layers or by chlorides (Cl^-) in polluted atmospheres where corrosion of carbon steel proceeds in localised cells (Kucera and Mattsson, 1987).

Wetting and Drying Phenomena - Cyclic Corrosion

Atmospheric corrosion occurs when the temperature at the metal surface is sufficiently low for water to condense. The cycles of wet oxidation are followed by dry oxidation (Santarini, 2007). Atmospheric corrosion of iron or low-alloy steel is thus considered a wet-dry cyclic process, involving three stages (figure 1):

1. Wetting - electrolyte gradually covers the metal surface or corrosion layer
2. Wet - once wet the electrolyte layer remains constant at the surface
3. Drying - the electrolyte layer gradually disappears from the surface (Dillmann et al., 2004; Morcillo et al., 2011; Monnier et al., 2014)

Different physio-chemical mechanisms characterise each of these stages (Maréchal et al., 2007). Figure 1 provides a key for understanding the general trends in atmospheric corrosion and shows a marked peak in the corrosion rate occurs during the drying phase (Santarini, 2007), while the corrosion potential shifts to more anodic values (Cole, 2010). During the drying stage, due to the thinning of the electrolyte film on the inner surface of the rust layer the rate of diffusion limited O_2

reduction reaction is extremely fast (Morcillo et al., 2011), explaining the increased corrosion current during this phase (Cole, 2010).

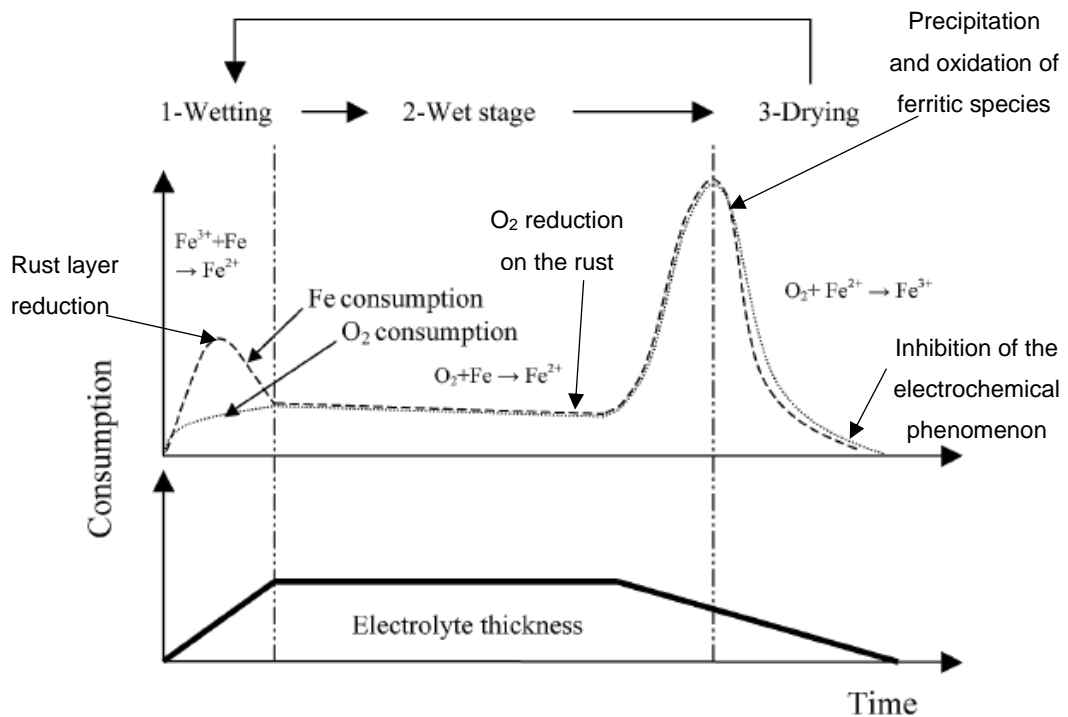
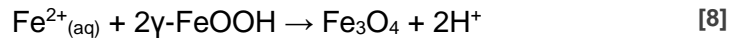
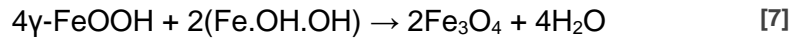


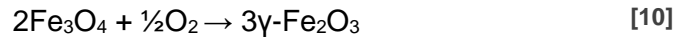
Figure 1 Rusting according to Stratmann, taken from Morcillo et al. (2011). Additional information from (Santarini, 2007). The upper sketch models the iron and oxygen consumptions rates at the different stages of wet-dry cycling and the lower schematic illustrates the variation of electrolyte thickness.

In the cyclic oxidation-reduction process γ -FeOOH acts as an O_2 carrier. Once a corrosion layer forms it is responsible for the continued corrosion during the wetting stage. The reduction of γ -FeOOH within the rust layer balances anodic dissolution of Fe (Hœrlé et al., 2004). Throughout the stages of aqueous oxidation, porous corrosion layers are wetted by an aqueous electrolyte (Santarini, 2007).

The reducing and oxidising conditions change within rust layers from one surface to the other as one side is in contact with iron and the other side with air. Evan's model states oxidising conditions prevail in dried-out layers, but if the pores are filled with water reducing conditions prevail in most of the layers (Stratmann et al., 1983). Whilst drying-out the "neutral level" between both conditions moves toward the iron, but during wetting of the sample it moves towards the atmosphere. The drying time of pores is significantly influenced by capillary action within corrosion layers, owing to minimisation of the liquid-air interface (Schindelholz and Kelly, 2012). In strong reducing conditions near the iron surface where sections of rust are reduced the reactions in [7] and [8] can follow:



If the pores in the corrosion layer dry out, access of O_2 becomes favoured at the site of the reduction of FeOOH , the conditions change to re-oxidation of the Fe^{2+} intermediate and Fe_3O_4 , resulting in [9] and [10].



The subsequent cycle of anodic dissolution of iron [6] then produces the electrons necessary for $\gamma\text{-Fe}_2\text{O}_3$ to be reduced to Fe_3O_4 . The reactions within the corrosion layer discussed by Stratmann et al. (1983) are summarised in figure 2.

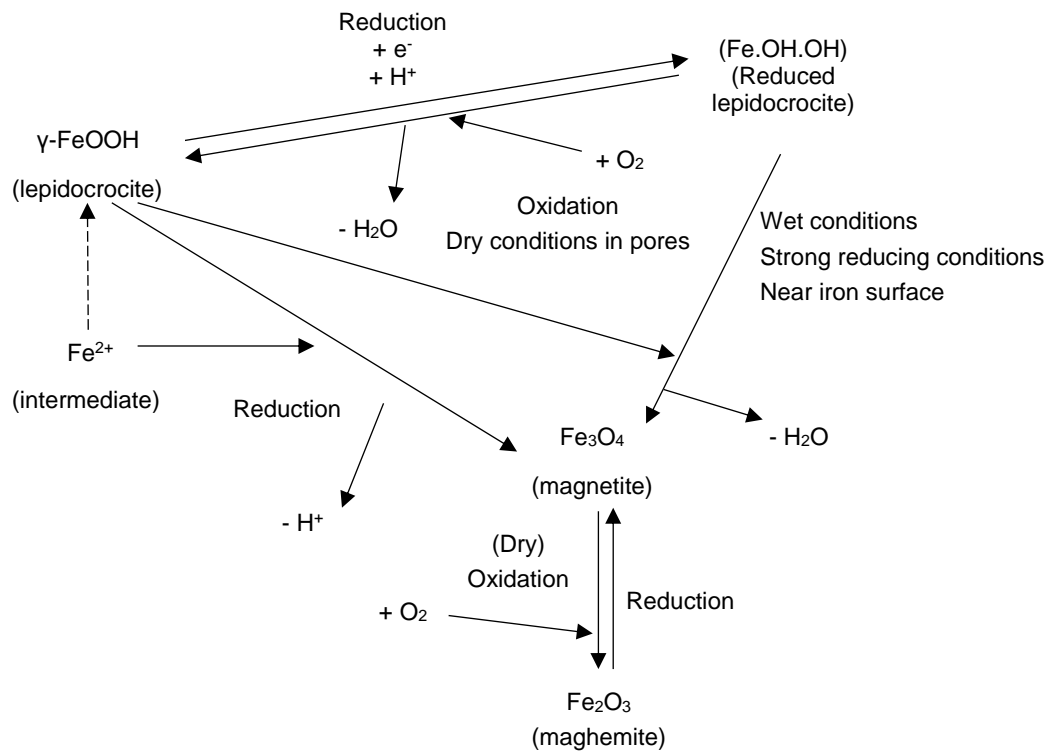


Figure 2 Summary of corrosion layer reactions discussed

Potential/pH Diagrams

Corrosion layers form according to prevailing conditions and pollutant gases and ions available in the corrosion environment. Stability fields of corrosion products

thermodynamically found in O_2 - H_2O systems normally represent the most common products occurring on Fe corroding in a damp unpolluted atmosphere (figure 3).

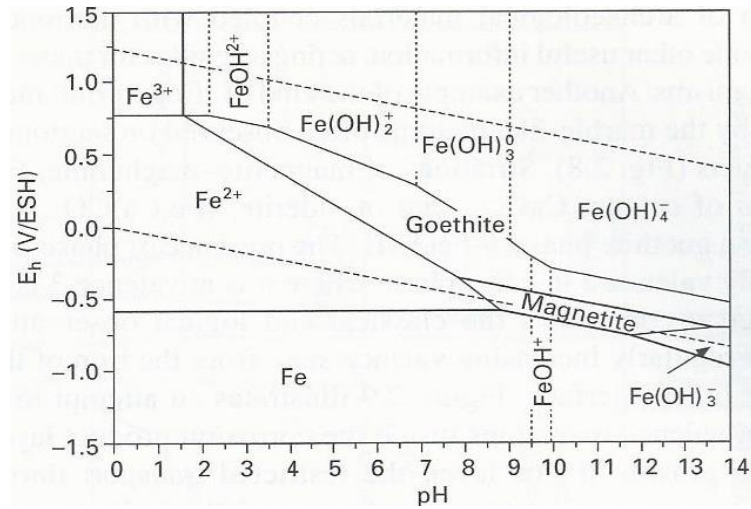


Figure 3 Fe- H_2O - O_2 system potential-pH diagram, $[Fe]_{total} = 10^{-5} \text{ mol.L}^{-1}$ (Santarini, 2007)

2.3 Form of Corrosion

While there are typical characteristics of corrosion relating to particular environments, corrosion attacks in different environments may still have common features (Chatterjee et al., 2001). Irrespective of the environment, some types or forms of attack are evident and corrosion is classified on the basis of these forms. Corrosion phenomena are of two types: uniform (general) and non-uniform (localised).

2.3.1 Uniform or General Corrosion

Corrosion attack that is evenly spread over a metal surface is uniform or general corrosion (Groisman, 2010), and seldom leads to failure of vehicles or structures. Its rate is generally measured in terms of the change of thickness (mm/year), mass loss of metal ($\text{g cm}^{-2} \text{ day}^{-1}$) or volume of hydrogen (H_2) formed, which can be converted to mass loss of the metal and used to calculate the corrosion penetration (Groisman, 2010). Atmospheric corrosion is normally uniform and takes place in wet and damp conditions (Chatterjee et al., 2001).

2.3.2 Non-uniform or Localised Corrosion

Localised corrosion is more prevalent than general corrosion, as it is caused by heterogeneities in the metal and local environment and in some instances mechanical factors are involved (Chatterjee et al., 2001; Groisman, 2010). It often results in the premature failure of metallic components (Chatterjee et al., 2001).

There are many forms of localised corrosion (table 1), but they all result in two main outcomes as pits and cracks, although blisters can also result inside the metals with hydrogen damage (Groysman, 2010). Some forms of corrosion listed are more frequently suffered by large military vehicles, industrial heritage or large metallic structures e.g. sculptures or gates and railings, than others and these are looked at in more detail below.

Table 1 Forms of localised corrosion – data largely taken from Groysman (2010), additional references included within the text.

Form of non-uniform corrosion	Type of deterioration	Influencing factors/causes and notes
Pitting Corrosion	Pits	Presence of Cl ⁻ anions in the environment and also a result of the existence of differential aeration cells, galvanic corrosion, microbiologically induced corrosion (MIC), erosion and cavitation.
Crevice Corrosion	Pits	Similar to pitting corrosion, there is an increased likelihood with increasing potential or Cl ⁻ and there is a critical crevice temperature comparable in certain respects to the critical pitting temperature ¹ (Laycock et al., 1997).
Galvanic Corrosion or dissimilar metal corrosion	Pits	Two different metals, alloys or conductor e.g. graphite in contact in general electrolyte, or in the atmosphere RH needs to be > 60% and the presence of salts in the air is required.
Microbiologically Induced Corrosion (MIC)	Pits	Only special kinds of bacteria, which are active contribute to metallic corrosion.
Dealloying or selective leaching	Pits	If a metal alloy is immersed in the electrolyte environment under specific conditions, e.g. naturally in acid or more quickly in an electrochemical system, the more reactive element in the metal alloy is selectively dissolved (Pickering, 1995; Stratmann and Rohwerder, 2001).
Intergranular Corrosion	Cracks	The selective dissolution of grain boundaries caused by electrochemical heterogeneity between precipitates at the grain boundaries and the grains themselves (occurs most often with stainless steels).
Exfoliation	Cracks	A specific form of intergranular corrosion – frequently seen on the surface of wrought aluminium alloys with an elongated grain strain in industrial or marine environments (Zhao and Frankel, 2007).
Filiform Corrosion or under-film corrosion	Pits (Filaments)	A specific type of crevice corrosion (Selwyn, 2004). High humidity (65 to 95% RH at room temperature), sufficient water permeability of the film, the presence of defects in the protective film, salt crystals or dirt/dust particles on the metal surface. The presence of O ₂ and an aggressive atmosphere are essential (Schweitzer, 2010).

¹ Critical pitting temperature – the lowest temperature at which stable pitting is possible.

Stress Corrosion Cracking (SCC) or environment induced cracking	Cracks	Caused by a combination of chemical attack and mechanical loading. Metals/alloys subjected to constant (static) tensile stresses and exposed to certain environmental conditions (type, temperature and concentration of aggressive species) within a certain electrode potential range may develop cracks.
Hydrogen Damage	Cracks, Blisters	Comparable to SCC but is only caused by hydrogen atoms and molecules and tensile stresses. There are four types: hydrogen blistering, hydrogen-induced cracking (HIC), stress-oriented hydrogen-induced cracking (SOHIC) and sulfide stress cracking (SSC).
Corrosion Fatigue	Cracks	Similar to SCC but fluctuating stresses exist instead of constant. It varies with mechanical (loading), metallurgical and environmental factors.
Erosion-Corrosion	Pits	The abrasive action of moving fluids and gases, accelerated by the presence of solid particles or liquid drops in gases. A conjoint action involving erosion (mechanical) and corrosion (chemical/electrochemical), due to the presence of aggressive species in the moving media (fluid or gas).
Cavitation	Pits	The formation and collapses of gaseous bubbles on the metallic surface.
Impingement Attack	Pits	Local hits against a metallic surface, of high velocity streams of fluids, gases, solid particles or together (it is a form of erosion-corrosion).
Fretting Corrosion	Pits	Between two materials under load, where they are in contact and subject to minute relative motion by vibration, (fretting where the environment participates in the destruction of the metal).

2.3.2.1 Differential Aeration Cells

Localised attack can be caused by a drop of electrolyte solution on a steel surface (figure 4). Slow diffusion of O_2 into the drop produces lower O_2 under the centre of the drop, producing an anode with the metal surface under the side edge of the drop as the cathode (Shreir, 1976). Anodic Fe^{2+} ions and cathodic OH^- ions form $Fe(OH)_2$ that is rapidly oxidised by dissolved O_2 to rust, $Fe_2O_3 \cdot H_2O$.

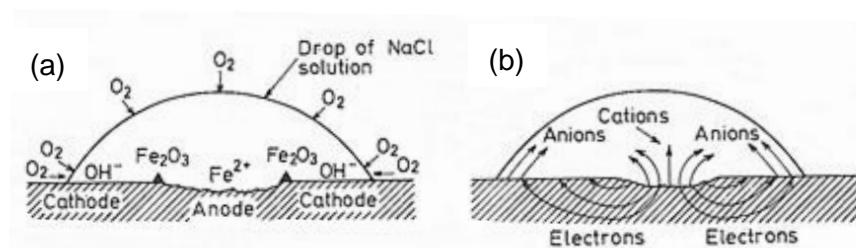


Figure 4 Differential aeration cells formed by the geometry of a drop of sodium chloride (NaCl) solution on a steel surface (Shreir, 1976)

In many corrosion processes where local O₂ depletion occurs, differential aeration is an important factor e.g. pitting corrosion and crevice corrosion, which are almost always affected by a differential aeration mechanism (Cole, 2010). Differential aeration cells can be considered macro-models for the initiation of pitting and crevice corrosion (Jones, 2013).

2.3.2.2 Pitting Corrosion

Pitting corrosion is localised metal loss that can develop as a deep, tiny hole in otherwise unaffected surfaces. Pitting is most likely to occur in the presence of Cl⁻ ions, combined with O₂ or oxidising salts (Uhlig, 1963). The driving forces for pitting corrosion include:

1. Surface irregularities in the metal
2. Chemical composition (including MnS inclusions)
3. Breaks in the continuity of a protective layer e.g. mill scale, coating or deposits
4. The presence of Cl⁻ or bromide ions (Br⁻)
5. Temperature
6. RH.

Mechanistically it has a range of steps (Punckt et al., 2004; Peguet et al., 2007; Tsutsumi et al., 2007; Pardo et al., 2008b; Hastuty et al., 2010). Pardo et al. (2008b) describe the pitting attack of stainless steel (SS) as a three stage process:

- i. Initiation* – In both carbon steel and SS pits are initiated at sulfide inclusions (Wranglen, 1974), on SS MnS is the most common site for pit nucleation. Where there is a passivation oxide layer, the local breakdown of this layer in the presence of aggressive anions is predominantly considered the initiation step (Pardo et al., 2008b). Breaks in the layer lead to differences of potential resulting in an electric current through the water or across the moist steel from the metallic anode to the nearby cathode (e.g. mill scale on steel) (figure 5) (Schweitzer, 2010).

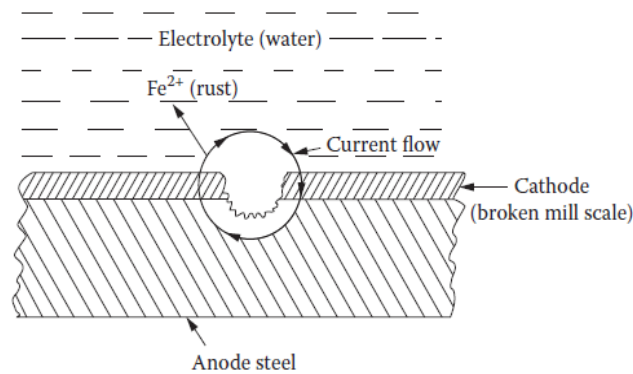
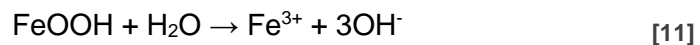


Figure 5 Current flow during the formation of pit from break in mill scale (Schweitzer, 2003; Schweitzer, 2010)

The corrosion reaction itself increases the corrosion rate (Pardo et al., 2008b) as differential aeration cells form (figure 4). As with differential aeration cells de-aeration, acidification and formation of localised anodes are caused by corrosion at the centre of a water drop. Cathodic reduction of the dissolved O_2 causes the perimeter area to become alkaline as there is greater access to the outer surface of the drop (figure 4) (Jones, 2013). The hydrated passive film represented by the $FeOOH$, dissolves slowly [11].

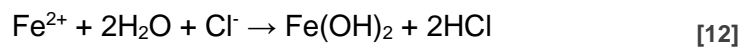


- ii. *Metastable propagation* – When the pits are still very small during the early stages of pit propagation they can be repassivated spontaneously. Until spontaneous repassivation is no longer possible pit growth is considered metastable (Pardo et al., 2008b)
- iii. *Stable propagation* – Propagation involves the formation of a concentration cell in which the pit solution has a lower O_2 content, but a higher salt and acid content than the bulk of the surrounding solution (Wranglen, 1974). Pits grow at an ever-increasing rate once initiated, as the conditions within them are self-propagating or autocatalytic with no external stimulus (Jones, 2013). Cáceres et al. (2009) determined the effect of NaCl concentration on the rate of carbon steel corrosion (table 2).

A model of an actively growing pit on SS is shown in figure 6. Negative anions e.g. Cl^- are attracted to the initiation site by the positively charged Fe^{2+} ions produced at the anode. Reduction in the local pH at the initiation site is caused by hydrolysis [12].

Table 2 Effect of NaCl concentration on pitting corrosion rate summarised from Cáceres et al. (2009)

NaCl concentration	Initial corrosion rate behaviour	Factors influencing the corrosion rate behaviour
High (0.5 – 1 M)	Continuously dropped with time	Continuous surface oxide layer forms - inhibitory influence - reduces the limiting current density for O ₂ reduction. This prevails over the increase of iron dissolution area linked to the steady increase in the number and size of pits.
Low (0.02 – 0.1 M)	Increased with time, peaked at 3 hours, before slowing	Pits become covered by iron oxide caps that inhibit O ₂ diffusion the corrosion rate slows, but the pits continue growing as separate entities



This acidic solution destroys the local passivity and creates an anode within the pit. The Cl⁻ in the pit, with an increasing concentration of Cl⁻ as hydrochloric acid (HCl) accelerates anodic dissolution (Jones, 2013).

Fe²⁺ diffusing out of the pit is oxidised to Fe³⁺ and precipitates as the corrosion products collect at the pit mouth forming an insoluble cap of Fe(OH)₃ (Jones, 2013). The pit retains high Cl⁻ concentration by migration of Cl⁻ into the pit but easy escape of Fe²⁺ is impeded. Without a cathodic reduction reaction to consume the electrons liberated by the pit anode reaction, pit growth will cease.

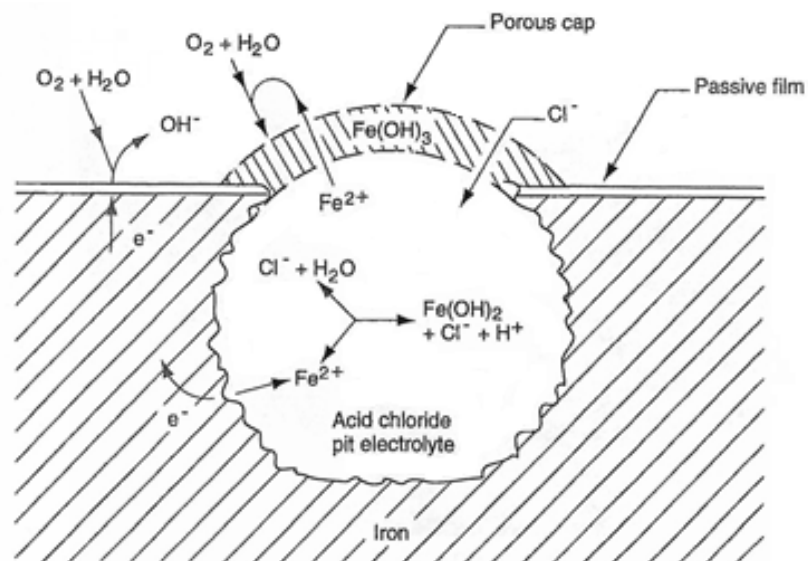


Figure 6 Schematic of processes occurring in an actively growing pit in iron (Jones, 2013)

Outcomes

When the anodic area is large in comparison to the cathodic area damage from pitting corrosion is spread out and usually negligible (Schweitzer, 2010). Based on results for Type 430 SS pit diameter and the probability of pitting corrosion decrease as the thickness and diameter of a droplet decrease as the effective cathode area is reduced and under droplets of Cl⁻ solution shallow pits form, indicating a preference for horizontal pit propagation (Hastuty et al., 2010).

When the anodic area is small the metal loss is concentrated and may be serious. Pit morphology depends on local chemistry and the metallurgy of the alloy (figure 7) (Jones, 2013). With damaged coating layers on many of the armoured vehicles at the Tank Museum, it is probable pitting corrosion will occur but the thickness of the steel means damage will be aesthetic rather than catastrophic.

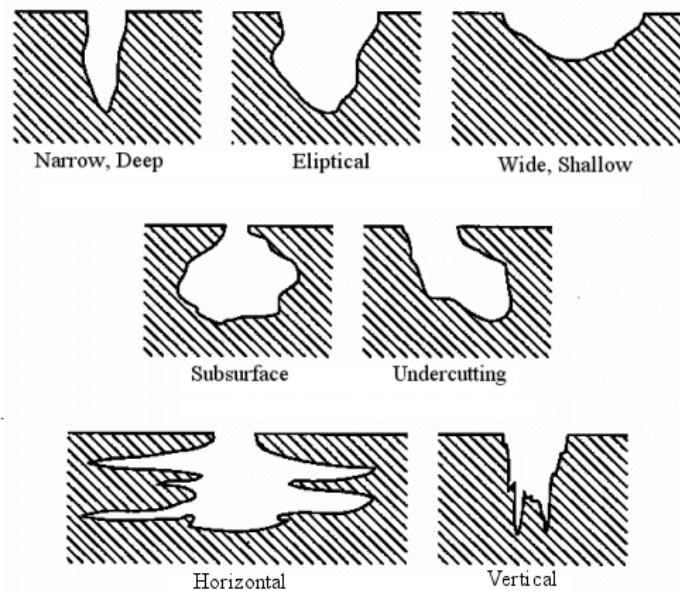


Figure 7 Variations in cross sectional shape of pits (Originally from Standard Practice G 46-76, Annual Book of ASTM Standards, Vol. 3.02, ASTM, Philadelphia, p197, 1988) (Jones, 2013).

2.3.2.3 Crevice Corrosion

While outer surfaces in the atmosphere are washed clean and then dry out, structural crevices often retain water and other solutions. Crevice corrosion can result from metal-to-metal or metal-to-non-metal contact with narrow gaps or openings that are not in excess of 3.18 mm, e.g. under bolts and around rivet heads. Here small amounts of liquid collect and become stagnant, creating local differences in O₂ concentrations (Schweitzer, 2010). Armoured vehicles and large metallic structures are susceptible to crevice corrosion due to the large number of joints and

bolts employed. Structural integrity of equipment can be challenged by crevice corrosion as it can be difficult to detect and can cause considerable damage under conditions in which high levels of uniform corrosion would not normally be expected (Kennell and Evitts, 2009) and can limit the service life of engineered structures (Walton et al., 1996).

Although crevice corrosion can take place in any corrosive environment and on any metal, dependence on an oxide film for corrosion resistance makes metals particularly prone to crevice corrosion (Schweitzer, 2010). The driving forces for crevice corrosion are:

1. Small gaps
2. Retained stagnant fluid

The gap defining a crevice is too small to permit the flow of liquid but large enough for the entrapment of a liquid (figure 8) (Schweitzer, 2010; Jones, 2013). The formation of differential aeration and Cl^- concentration cells are enhanced as the crevice shields part of the surface (Jones, 2013), with rapid progress and greater intensity in Cl^- environments (Schweitzer, 2010).

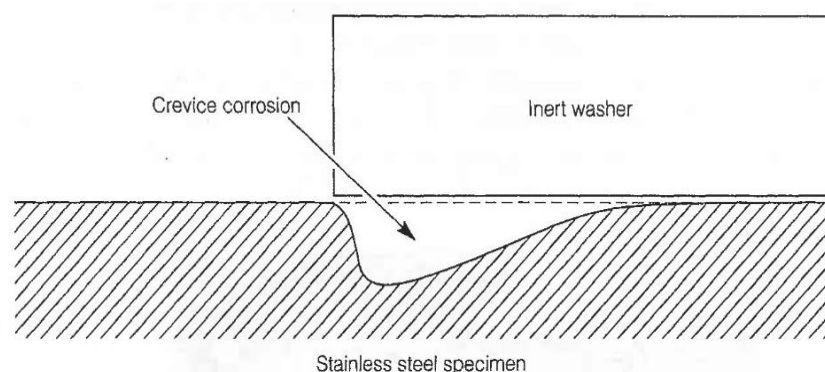


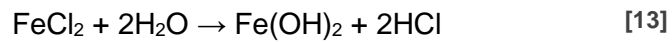
Figure 8 Typical schematic morphology with attack greatest at the mouth of the crevice (Jones, 2013)

Rashidi et al. (2007) use the Fontana and Greene (1967) model to describe a mechanism for crevice corrosion consisting of four stages:

1. Corrosion occurs as normal inside and outside the crevice [1] and [2] (Schweitzer, 2010) and the OH^- ions electrostatically counterbalance the Fe^{2+} ions (Rashidi et al., 2007).
2. Once most of the O_2 dissolved in the small volume of stagnated solution inside the crevice is consumed, dissolution continues because the electrons

travel through the metal to the outside of the crevice mouth where O_2 feeds the cathode reaction (figure 6).

3. Metal chloride is formed as Cl^- and OH^- ions diffuse into the crevice attracted by the accumulated Fe^{2+} and to maintain a minimum potential (Rashidi et al., 2007). The pH is lowered when HCl and iron (II) hydroxide are produced during the hydrolysis of the iron (II) chloride [13].



4. The rate of metal dissolution inside the crevice accelerates as HCl destroys the passive film and the crevice remains cathodically protected by the cathodic reduction outside it (Schweitzer, 2010).

2.3.2.4 Galvanic Corrosion

A result of two different metals coupled to form a basic wet corrosion cell also known as dissimilar metal corrosion and termed bimetallic corrosion or multi-metallic corrosion (Trethewey and Chamberlain, 1995). The potential difference between two metals linked in the solid phase and within a common solution creates galvanic corrosion (figure 9). The more energetic metal corrodes while the more noble metal acts as the cathode and is protected.

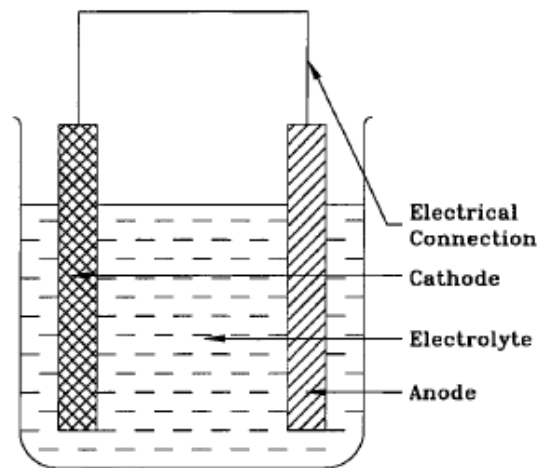


Figure 9 Basic wet corrosion cell schematic (Tavakkolizadeh and Saadatmanesh, 2001)

Due to their high corrosion resistance in various environments, galvanised steels are used extensively in vehicles and construction (Tada et al., 2004). When electrolyte is in contact with both metals, e.g. within a scratch in the zinc coating, the zinc corrodes and the iron becomes the cathode and is protected (table 3) (Tada et al., 2004).

Table 3 Galvanic Series of Metals and Alloys (Schweitzer, 2003)

<i>Corroded end (anodic)</i>	
Magnesium	Muntz metal
Magnesium alloys	Naval bronze
Zinc	Nickel (active)
Galvanized steel	Inconel (active)
Aluminum 6053	Hastelloy C (active)
Aluminum 3003	Yellow brass
Aluminum 2024	Admiralty brass
Aluminum	Aluminum bronze
Alclad	Red brass
Cadmium	Copper
Mild steel	Silicon bronze
Wrought iron	70/30 Cupro-nickel
Cast iron	Nickel (passive)
Ni-resist	Inconel (passive)
13% chromium stainless steel (active)	Monel
50/50 lead tin solder	18-8 Stainless steel type 304 (passive)
Ferretic stainless steel 400 series	18-8-3 stainless steel type 316 (passive)
18-8 stainless steel type 304 (active)	Silver
18-8-3 Stainless steel type 316 (active)	Graphite
Lead	Gold
Tin	Platinum
	<i>Protected end (cathodic)</i>

2.3.2.5 Filiform Corrosion

Filiform corrosion is a manifestation of differential aeration and crevice corrosion, and is sometimes termed under-film corrosion as it has been observed under thin organic coatings on steel (Slabaugh and Grotheer, 1954; Jones, 2013). It is characterised by the meandering, threadlike filaments of corrosion usually beneath semipermeable coatings or films (Schweitzer, 2010), which initially grow roughly perpendicular to the edge of the defects (Delplancke et al., 2001). Filiform corrosion requires humid conditions between 65 and 95% RH at room temperature to occur on steel (Delplancke et al., 2001; Schweitzer, 2010), but 80 to 85% RH is accepted as optimal for filiform corrosion to develop (Bautista, 1996). Contaminants such as chlorides, sulfates or carbonic acid are also a necessity for filiform to occur (Delplancke et al., 2001).

The mechanism for filiform corrosion involves:

- i. Initiation – Generally assisted by Cl⁻ ions at weak parts of the iron oxide film, a scratch or other defect in a coating. Once the metallic iron is exposed to the aqueous solution a differential aeration cell forms below the droplet and corrosion attack is initiated (Weissenrieder and Leygraf, 2004). Composition

and permeability of coating have little or no effect on initiation and growth characteristics of filiform corrosion (Jones, 2013).

- ii. Propagation – The active potential difference for filiform corrosion growth forms due to the aeration cell with its separated anodic and cathodic areas (figure 10). Hydrolysis and acidification to a pH of 1 - 4 accompanies O_2 consumption at the head by active corrosion. When Fe^{2+} from the head contacts aerated conditions in the tail of the filament precipitation of rusty-red iron (II) hydroxide ($Fe(OH)_3$) occurs. Porosity or micro-cracks in the coating over the filament tail allows essential H_2O and O_2 to migrate to the corroding filament head. As the filament advances the $Fe(OH)_3$ decomposes to $Fe_2O_3 \cdot 3H_2O$. Figure 10 show a schematic of these processes (Jones, 2013).

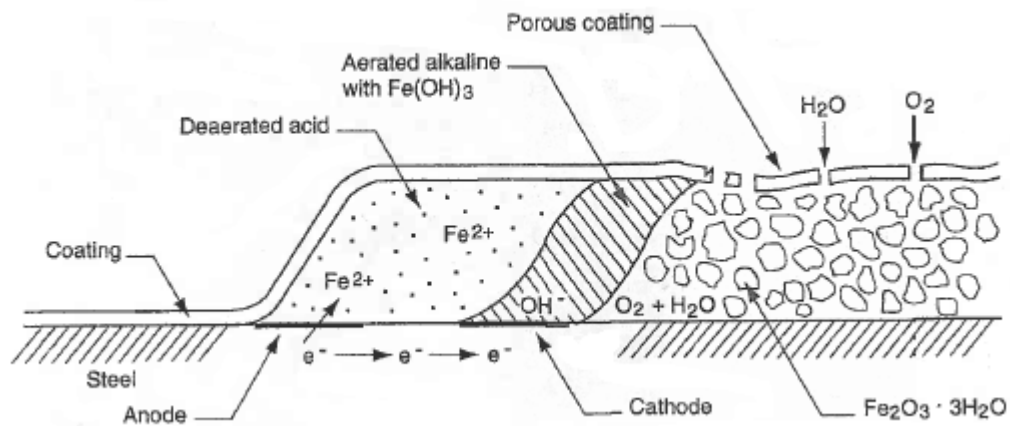


Figure 10 Filiform corrosion of steel - chemical processes in a filament cell (Jones, 2013)

Until the Cl^- ion concentration at the head is too low to rapidly create new anodic sites, filaments will continue to grow. On steel under transparent varnishes the active head of a filament usually appears blue, blue-green or grey and the tail is usually red-brown, indicating that the head is deaerated and contains Fe^{2+} ions, while the tail is aerated and contains Fe_2O_3 or $Fe_2O_3 \cdot 3H_2O$ as corrosion products (Schweitzer, 2010; Jones, 2013).

Penetration into the metal substrate is usually only superficial for filiform corrosion (Jones, 2013), typically 5-15 μm , essentially it is a cosmetic problem, but it is highly detrimental to the appearance of coated parts as it causes loss of paint adhesion (Delplancke et al., 2001; Schweitzer, 2010). Loss of paint adhesion can leave sites open to initiation of pitting or other forms of corrosion. Although the direct damage caused filiform corrosion is superficial, indirectly it could lead to more severe damage if pitting occurs.

Protection can be provided by films with very low permeability as well as other important factors such as preparation of the metal surface for coating, surface cleanliness, coating thickness, adherence, flexibility and the absence of voids. All these factors determine whether filiform corrosion will occur (Schweitzer, 2010).

Filaments can be deactivated by sealing the tail against water and O₂ transport, but reducing the RH below 60%, thus dehydrating the filament cell, is the only certain way to prevent filiform corrosion on steel (Jones, 2013).

2.3.2.6 Stress Corrosion Cracking (SCC)

SCC is one of the biggest causes of corrosion failure, with cracks frequently nucleating from corrosion pits, but depending on the environment and material, the cracks can be intergranular or trans-granular in nature (Marrow et al., 2006). The conjoint action of corrosion and stress is required, alternate applications of stress and corrosive environment will not produce SCC. It is at points of static tensile stress that SCC occurs, as fine cracks penetrate through the surface at the points of stress, the metal or alloy, which is usually free of corrosion over most of its surface. For stress corrosion the conditions needed and driving forces for structures such as bridges and armoured vehicles are (figure 11):

1. Tensile stress – due to an applied load
2. Sensitive metal (microstructure)
3. Suitable environment
4. Appropriate temperature and pH

Almost all alloys utilised for engineering purposes are subject to SCC, but the environments in which alloys are susceptible to SCC vary. The sensitivity of SS to SCC is determined by the alloy content (Schweitzer, 2010).

Due to the nature of the cracking unexpected failure can occur. It is hard to detect until extensive corrosion has developed. This form of corrosion is experienced by armoured vehicles at the TM and is of great concern.

SCC can be caused by specific steel alloy-environment combinations and although some vehicles within the TM are experiencing SCC, very few of the alloy-environment combination options can be applied to the historic vehicles displayed within the Museum.

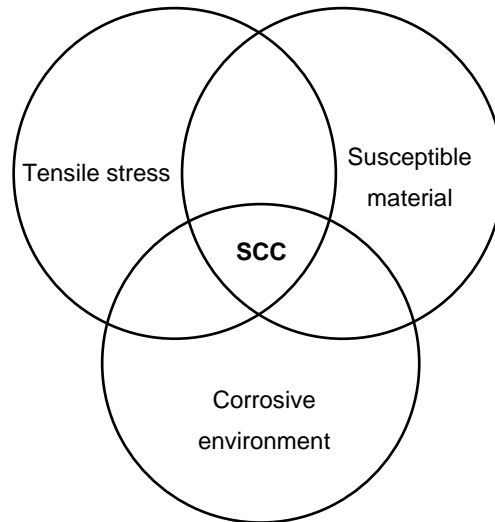


Figure 11 Simultaneous conditions required for stress corrosion cracking (Jones, 2013)

2.4 Atmospheric Corrosion Products

Rust layer compositions differ in different atmospheric conditions as they depend on pH and O₂ concentrations in the surface electrolyte (Kucera and Mattsson, 1987). Naturally occurring rust layers on iron and steels are complex with about a dozen different oxides and hydroxides of iron occurring within them (table 4) (Graedel and Frankenthal, 1990). On mild and low-alloy steels exposed to atmospheric corrosion, the main phases constituting the rust layers formed are either amorphous or crystallised iron oxyhydroxides (lepidocrocite γ -FeOOH, goethite α -FeOOH, akaganéite β -FeOOH and feroxyhyte δ -FeOOH) and iron oxides (magnetite Fe₃O₄) (Dillmann et al., 2004; Hoerlé et al., 2004).

Corrosion products can reveal whether there is active, aggressive corrosion taking place or whether a new equilibrium has been established and it has stabilised. The presence of akaganéite indicates active, aggressive corrosion is taking place, but for akaganéite to be formed Santana Rodríguez et al. (2002) deduced the chloride concentration must remain above 14-16 mg/m²/day. Rust layers which form due to atmospheric corrosion are often voluminous, porous, spalled, cracked and visually appear as loose black or orange–brown masses (Cornell and Schwertmann, 2006; Morcillo et al., 2011). This type of cracked rust layer is not protective as it allows corrosive species e.g. Cl⁻ ions easy access to the metallic substrate. Corrosion frequently consists of two layers and is always a mixture of phases. Loose outer layers consist of lepidocrocite and/or goethite and due to the reduced O₂ supply, magnetite is found at the iron/rust interface (Cornell and Schwertmann, 2006).

Ferrous hydroxide, $\text{Fe}(\text{OH})_2$ is only formed in neutral-basic solutions, so will not precipitate where the surface electrolyte is weakly acidic e.g. in SO_2 polluted atmospheres (Kucera and Mattsson, 1987).

Table 4 Chemical compounds found in rust layers (Morcillo et al., 2011)

Name	Composition
Oxides	
Hematite	$\alpha\text{-Fe}_2\text{O}_3$
Maghemite	$\gamma\text{-Fe}_2\text{O}_3$
Magnetite	Fe_3O_4
Ferrihydrite	$\text{Fe}_5\text{HO}_8 \cdot 4\text{H}_2\text{O}$
Hydroxides	
Ferrous hydroxide	$\text{Fe}(\text{OH})_2$
Ferric Hydroxide	$\text{Fe}(\text{OH})_3$
Goethite	$\alpha\text{-FeOOH}$
Akaganéite	$\beta\text{-FeOOH}$
Lepidocrocite	$\gamma\text{-FeOOH}$
Feroxyhite	$\delta\text{-FeOOH}$
Others	
Ferrous chloride	FeCl_2
Ferric chloride	FeCl_3
Ferrous sulfate	FeSO_4
Ferric sulfate	$\text{Fe}_2(\text{SO}_4)_3$

The long term growth of corrosion products is very dependent on the actual exposure conditions, influenced by the continuously repeated cycles of dissolution, coordination and precipitation; chemical composition, microstructure, crystallinity, thickness and other properties are all changed causing the corrosion product layer to age (Morcillo et al., 2011). Exposure time hardly affects the nature of rust constituents, as the species detected at a given site are independent of exposure and are nearly always the same at a given site due to the prevailing atmospheric conditions (de la Fuente et al., 2011; Morcillo et al., 2011). Thus where there is historic ferrous metalwork outdoors e.g. gates and railings etc., the corrosion products detected should be the same throughout the site. However, the proportion of the constituents and the appearance or disappearance of minor or intermediate compounds may alter with time (de la Fuente et al., 2011; Morcillo et al., 2011).

An ample supply of Fe^{2+} is associated with the frequent occurrence of green rusts, green-blue iron hydroxide compounds that are intermediate phases in the formation of iron oxides (goethite, lepidocrocite and magnetite). They occur under reducing

and weakly acidic to weakly alkaline conditions (Schwertmann and Fechter, 1994; Cornell and Schwertmann, 2006).

During atmospheric corrosion, the rust layer commonly formed on low-alloy steel presents a complex morphology, for which figure 12 presents a simplified model. Only the main characteristics have been labelled and are as follows:

- L - the rust layer thickness;
- d - the electrolyte thickness
- α/γ - the composition ratio of goethite (α -FeOOH) to lepidocrocite (γ -FeOOH), when a rust layer is considered to be formed of only these compounds;
- pores;
- Fe metal (Hœrlé et al., 2004; Maréchal et al., 2007).

The ability of the rust layer to be reduced and similarly its protective ability are characterised by the fraction of lepidocrocite in the rust layer and thus the amount of γ -FeOOH on the surface in the pores (described by α/γ) (Hœrlé et al., 2004).

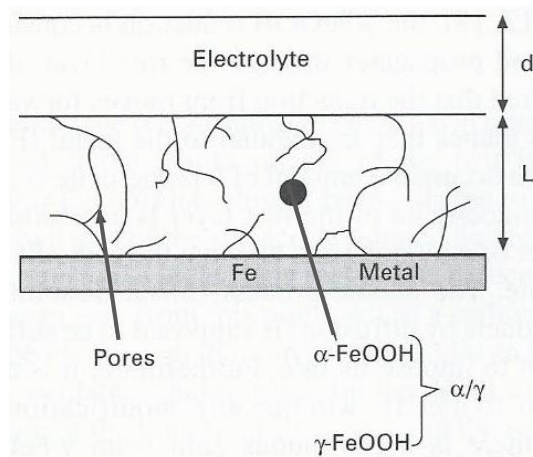


Figure 12 Rust layer modelling (Maréchal et al., 2007)

An insight into where key corrosion products are found within a rust layer and how they were formed, is offered by table 5. The inner dense region of the rust layers on ferrous metal generally includes amorphous FeOOH (Graedel and Frankenthal, 1990).

Table 5 Key corrosion products formed by different mechanisms in different locations within the rust layer

Corrosion Product	Formula	Position in the corrosion layer	Occurrence, properties and comment	References
Lepidocrocite	$\gamma\text{-FeOOH}$	Found in the outer loose crystalline assemblage. On weathering steel it is found in the more adherent inner layer.	Orange in colour. Formed in atmospheres containing small amounts of water vapour. Semi-conducting and electrochemically active. Paramagnetic (magnetic but only in the presence of an externally applied magnetic field) at room temperature – magnetic interactions are relatively weak.	(Kucera and Mattsson, 1987; Graedel and Frankenthal, 1990; Hoerlé et al., 2004; Cornell and Schwertmann, 2006)
Goethite	$\alpha\text{-FeOOH}$	Found in the outer loose crystalline assemblage. On weathering steel it is found in the more adherent inner layer.	Yellow-brown in colour. $\gamma\text{-FeOOH}$ is transformed into $\alpha\text{-FeOOH}$ in weakly acidic solutions – Cl ⁻ ions in lower concentrations facilitate this transformation. An insulating non-active species. The most stable ferric oxide hydroxide with 10 ⁵ times lower solubility than $\gamma\text{-FeOOH}$. Antiferromagnetically ordered at room temperature (interactions of neighbouring atoms make the spin of electrons align anti-parallel to one another, with zero net moment at temperatures below the ordering or Néel temperature).	(Kucera and Mattsson, 1987; Graedel and Frankenthal, 1990; Hoerlé et al., 2004; Cornell and Schwertmann, 2006; Ma et al., 2009)
Magnetite	Fe_3O_4	Some crystalline Fe_3O_4 is usually detected in the inner dense part of the rust adhering to steel surface, subjected to prolonged exposure, where depletion of oxygen may occur.	Black in colour. May form by the oxidation of $\text{Fe}(\text{OH})_2$ or intermediate ferrous-ferric species such as green rust – may occur during a drying phase. In the presence of a limited oxygen supply it may also be formed by reduction of FeOOH or $\gamma\text{-Fe}_2\text{O}_3$. Magnetite is considered as protective due to its thermodynamic stability and compactness although it is a good electronic conductor. Ferrimagnetic at room temperature. A pH > 7 is probably indicated by the presence of magnetite.	(Stratmann et al., 1983; Kucera and Mattsson, 1987; Hoerlé et al., 2004; Cornell and Schwertmann, 2006)

Maghemite	$\gamma\text{-Fe}_2\text{O}_3$	Occurs in the outer loose crystalline assemblage.	Brown coloured synthetic pigment. May form from the oxidation of Fe_3O_4 The oxidized form of magnetite with a similar crystal structure, but most of the iron is in the trivalent state. A semiconductor of electricity and ferrimagnetic at room temperature.	(Stratmann et al., 1983; Graedel and Frankenthal, 1990; Cornell and Schwertmann, 2006; Lyon, 2010)
Akaganéite	$\beta\text{-FeOOH}$	Generally distributed in the surface region of the rust layer, but also appears in the inner layer where water deposits containing chloride ions penetrate through cracks	Rare in nature, but can be formed in chloride-rich environments. Characteristic orange colour. Paramagnetic at room temperature – magnetic interactions are variable and depend on synthesis conditions.	(Cornell and Schwertmann, 2006; Scott and Eggert, 2009; Lyon, 2010; Morcillo et al., 2011)
Feroxyhyte	$\delta\text{-FeOOH}$	On weathering steel it is found in the outer layer.	Has not been reported in rust on carbon steel under atmospheric conditions. Mineral feroxyhyte has small particle size, poor crystallinity and is superparamagnetic at room temperature. Synthetic feroxyhyte is ferromagnetic at room temperature.	(Kucera and Mattsson, 1987; Graedel and Frankenthal, 1990; Cornell and Schwertmann, 2006)
Hematite	$\alpha\text{-Fe}_2\text{O}_3$	Not usually found in atmospheric corrosion products. However, it may be found within the passive layer	Bright red in colour. Usually require aqueous systems with elevated temperatures (> 250 °C) to be formed, although, it can be formed at room temperature. A semiconductor of electricity. Weakly ferromagnetic at room temperature.	(Cornell and Schwertmann, 2006; Lyon, 2010).

2.5 Factors Governing Atmospheric Corrosion

Modelling of scenario has become more common place over recent decades and for a corrosion model to be useful in making service life predictions, knowledge of the local environment and usage needs to be incorporated (Cole and Corrigan, 2011). A holistic multi-scale model for the prediction of service life subject to atmospheric corrosion was presented by Cole et al. (2011). By modelling the salt and water deposition, the basic holistic model combines processes that control atmospheric corrosion on a range of scales from electrochemical to macro (figure 13) (Cole and Corrigan, 2011; Cole et al., 2011).

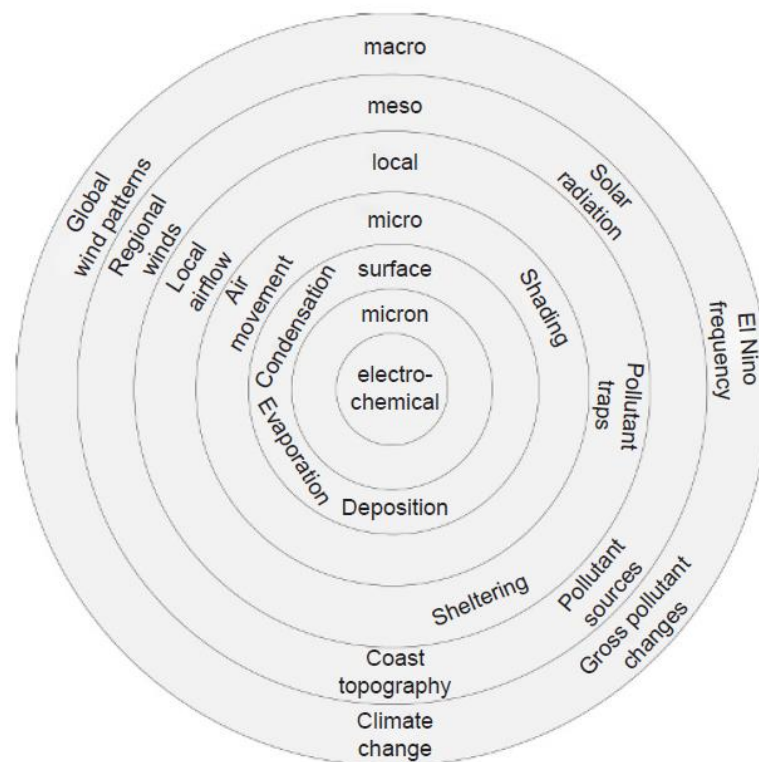


Figure 13 Multi-scale model of corrosion - schematic

The model outlined by Cole (Cole et al., 2003a; Cole et al., 2003b; Cole et al., 2003c; Cole et al., 2004a; Cole et al., 2004b; Cole and Paterson, 2004), is summarised in figure 14 (Cole et al., 2013). This holistic model focuses on corrosion by marine aerosols as it has primarily been designed for Australian conditions (Cole et al., 2011). For other locations, alterations must be made to the models to accommodate changes in the parameters within it (Ganther et al., 2011).

The chemical composition of the atmosphere, temperature and time-of-wetness (TOW) of the metallic surface are just a few of several factors which govern real-

time atmospheric corrosion of ferrous metal (Arroyave and Morcillo, 1995). These change significantly from outdoor, sheltered and indoor environments, in which historic structures and armoured vehicles are situated.

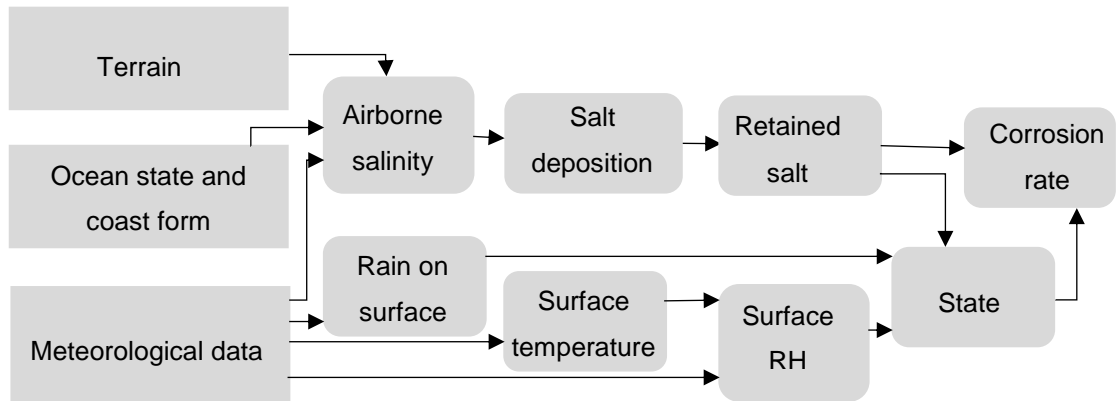


Figure 14 Atmospheric corrosion holistic model schematic

2.5.1 Meteorological and Air Pollutant Factors

Atmospheric corrosion is a complex process, which is directly affected by both meteorological and pollutant factors. For corrosion processes the most important climatic factors are RH, sunshine hours, temperature of the air and metal surface, wind velocity and, duration and frequency of the rain, dew and fog (Mendoza and Corvo, 1999). The TOW hinges mostly on meteorological parameters. The aggressiveness of atmospheric corrosion of metals is enhanced when pollutants are present in the water layer.

2.5.1.1 Solar Radiation and Wind

In addition to temperature, solar radiation and wind also affect the time that a surface remains wet (Brown and Masters, 1982). Solar radiation can trigger the deterioration of protective organic coatings, thus causing exposure of the underlying metal to atmospheric corrosion (Brown and Masters, 1982).

Wind can cause damage to metals directly and indirectly. In addition to catastrophic damage that can be caused by storms, wind can cause vibrations and deformations, which ultimately lead to metal fatigue (Godfraind et al., 2012), causing problems for some historic ferrous metal structures. Indirectly, wind contributes to the corrosion and the overall deterioration of metal, as the direction and velocity of wind affects both the dispersion of air pollutants and accumulation of particulates on metal surfaces (Brown and Masters, 1982). Generally, armoured vehicles at the Tank Museum are situated indoors, but a few are still located outdoors and others are

taken outdoors for use in displays. For those vehicles situated outdoors, those used in action displays and even those located in the vehicles conservation centre that has large roller doors on the side for ease of vehicle movement both inside the building and out of it, the wind will have an effect on the corrosion.

Wind convects and, although lifted by diffusion, aerosols may be dragged down by gravity (Cole, 2010). Gustafsson and Franzén (1996) found that sea-salt concentrations measured over land can vary due to wind speed and distance from the coastline. A rise in wind speed increases both the sea-salt aerosol generated by the surf (figure 15) and the concentration of salt found 1 km inland (figure 16 (a)) (Cole et al., 2003b).

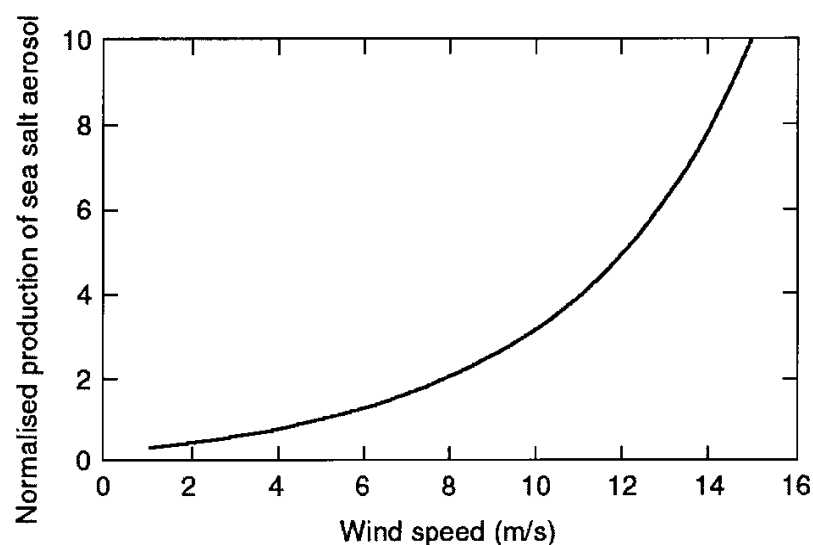


Figure 15 Effect of local wind speed on surf generated aerosol (Cole et al., 2003b)

In the open ocean, salt aerosols can be generated by either the wind tearing spume drops from the crests of ocean whitecaps or by bursting bubbles generated by ocean whitecaps (Cole et al., 2003b). Ocean generated salt aerosols can potentially travel much further inland than surf generated salt aerosols (figure 16 (a) and (b)). Turbulent diffusion lifts the salt up and the small salt aerosols are able to follow airstreams around obstacles, although medium to large salt aerosols are deposited on trees and man-made structures (Cole et al., 2003b). Although concentrations of ocean generated salt aerosol (figure 16 (b)) are initially much lower than surf generated salt aerosol (figure 16 (a)), they travel significantly further inland, up to 50 km compared to 1 km from the coast. Thus, wind speed plays an important role in both the generation of sea-salt aerosols and the distance it travels inland, since for higher wind speeds higher concentrations are detected further inland.

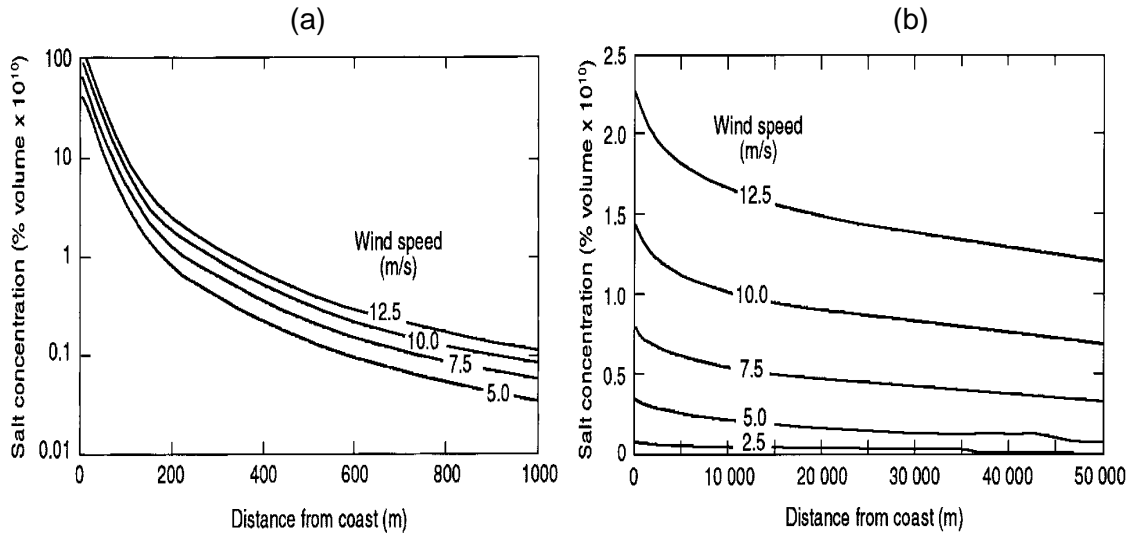


Figure 16 (a) Effect of distance from the coast of surf-produced aerosols and wind speeds on salt concentration (excluding ocean-produced aerosols) – 2 m height, 0.5 m ground roughness (table 6). (b) Effect of distance from coast for ocean-produced salt and wind speed on the salt concentration – 2 m height, 0.5 m ground roughness, 70% RH, 1200 mm year⁻¹ rainfall (Cole et al., 2003b; Cole, 2010)

Table 6 Typical ground roughness values (Cole et al., 2003b)

Roughness, m	Terrain
2	City buildings (10-30 m)
1	Forests
0.8	High density metropolitan
0.4	Centre of small town
0.2	Level wooded country; suburban buildings
0.06	Isolated trees, long grass
0.02	Uncut grass, airfields
0.008	Cut grass

The Tank Museum is ~ 8 km from the coastline (figure 17), thus, it is unlikely any sea-salt generated by the surf (waves breaking) will accumulate on vehicles left outside (figure 16 (a)). For both severe storms that can carry salt spray up to 15 km inland (Syed, 2006) and sea-salt generated by the English Channel (figure 16 (b)) at higher wind speeds, whether they reach the Tank Museum is dependent on the wind direction. Potentially any vehicle left outdoors could accumulate sea-salt, but due to the low concentration level this would take time.

Wind not only acts to distribute aerosols to the detriment of metals surfaces but, depending on the characteristics of both the wind and rain and the state of the surface, the surfaces themselves may be cleaned by either the wind or the rain (Cole, 2010). Unfortunately, removal of salts by wind is only significant when the

wind carries abrasive material or in climates where rain is very limited (Cole, 2010), which is not the case in the UK.

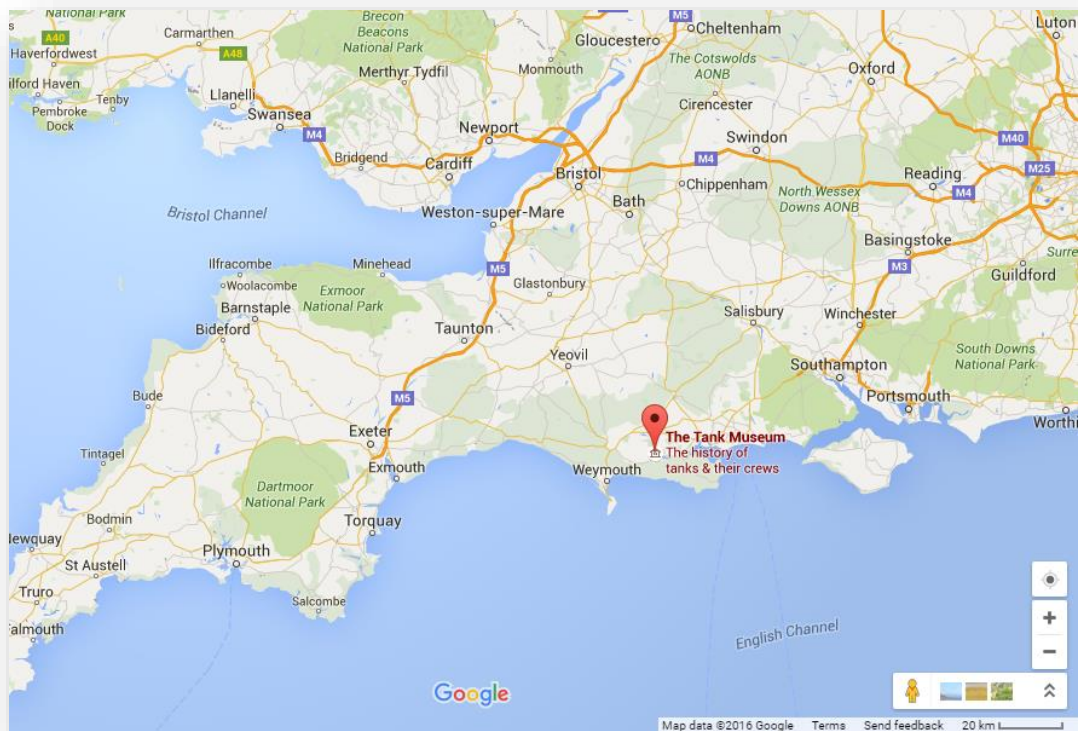


Figure 17 Map highlighting the proximity of Bovington Tank Museum to the coast – taken from Google maps July 2016, small scale bar included in the bottom right corner

2.5.1.2 Temperature

The kinetics of corrosion reactions are directly affected by changes in temperature, TOW, RH and dew point however, are affected indirectly (Brown and Masters, 1982). Higher temperatures increase the rate of electrochemical reactions and diffusion processes, speeding up corrosive attack. Increasing the temperature usually leads to a reduction in RH and more rapid evaporation of surface electrolyte, decreasing TOW, thus diminishing the overall corrosion rate (Syed, 2006). The RH close to a surface however, may be different from that of the ambient air if the temperature of the surface varies from that of the ambient air (Cole, 2010), as this is expected where radiant heating of a metal surface occurs. Temperature affects not only the corrosion reaction but the metals themselves. As metals have high thermal conductivities, and consequently very low thermal inertias, they are predisposed to developing films of condensation (Godfraind et al., 2012). Changes in temperature also cause variations in dimensions due to expansion and contraction stressing joints and interfaces, potentially leading to deterioration and damage of both the metal itself and the protective coating.

The average daily minimum, mean and maximum temperatures experienced in the summer within the UK from 1971-2000 are illustrated in figure 18. Care should be taken when comparing the three images as the colours on each image do not correspond with the same temperature ranges. Comparing the average daily minimum (figure 18 (a)) and maximum (figure 18 (c)) temperature ranges and images highlights the range in temperature that may be experienced within the summer period within the UK leading to expansion and contraction of ferrous metal and possible deterioration of coatings.

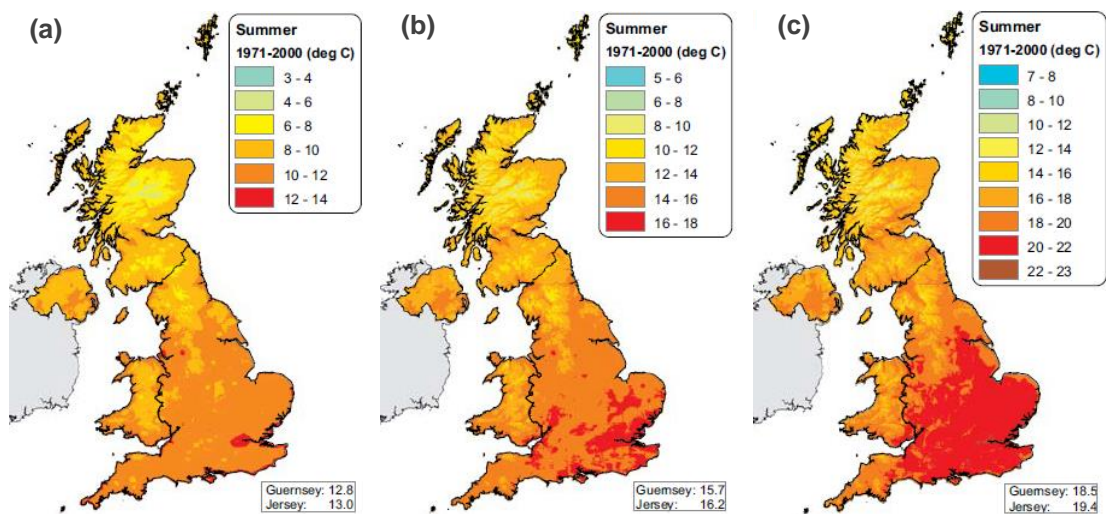


Figure 18 (a) Average daily minimum temperature (°C) for summer 1971-2000; (b) Average daily mean temperature (°C) for summer 1971-2000; (c) Average daily maximum temperature (°C) for summer 1971-2000 (Jenkins et al., 2008).

2.5.1.3 Moisture

Relative humidity (RH) is defined as the amount of water vapour present in the air expressed as a percentage of the amount needed for saturation at the same temperature and is the method used within this project to quantify the level of atmospheric moisture.

In non-polluted atmospheres saturated with water vapour, initiation of corrosion on a clean metal is a slow process (Kucera and Mattsson, 1987; Morcillo et al., 2011). Schindelholz and Kelly (2012) confirmed that a metal surface must be made wet by a sufficiently conductive liquid for atmospheric corrosion to occur in order to solvate the ions produced during the corrosion reactions (Lyon, 2010). Moisture forms on surfaces due to local RH via deposition of rain, fog and wet aerosols or hygroscopic salts on the surface (Cole, 2010).

The amount of water adsorbed is noticeably affected by the composition and morphological properties of the surface of ferrous metal (Graedel and Frankenthal, 1990). In atmospheric conditions as moisture is adsorbed, monolayers build up and a thin film of 'invisible' electrolytes is formed on metallic surfaces (Tullmin and Roberge, 2000; Cole, 2010). The number of monolayers are believed to be too few to sustain electrochemical corrosion processes below 60% RH, as at 40% RH the number of monolayers are estimated to vary from 1 to 2 layers, but increases to 2-5 monolayers at 60% RH and 6-10 monolayers at 100% RH (Cole, 2010). The corrosion processes during the RH cycles (wet-dry cycles) that typically occur during atmospheric corrosion are controlled by a layer of water 10–100 nm thick at the surface of the metallic substrate (Monnier et al., 2014). The equivalent of two layers of water, covers the surface at room temperature and approximately 60% RH (figure 19) (McCafferty and Zettlemyer, 1971; Graedel and Frankenthal, 1990).

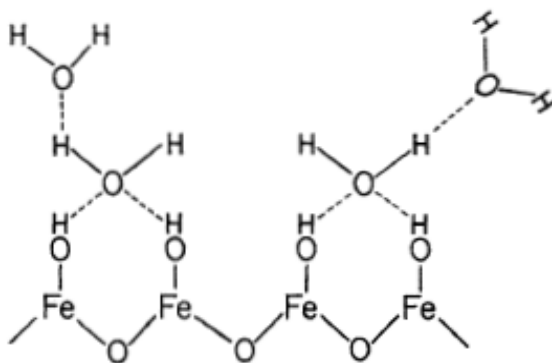


Figure 19 Representation of water adsorption on $\alpha\text{-Fe}_2\text{O}_3$ (McCafferty and Zettlemyer, 1971)

Transport of the electrolyte into or through corrosion layers is mostly linked to capillary action, the movement of liquid through crevices and pores in an object, which is driven by a balance between surface tension forces and gravity (Schindelholz and Kelly, 2012).

Although the first critical RH for iron and steel where corrosion commences at a very slow rate is 60%, there is a sharp increase in corrosion rate at 75 to 80% RH (Syed, 2006). However, Lyon (2010) reported that at $\leq 75\%$ RH corrosion of uncontaminated steel was negligible and consistent with a dry oxidation mechanism, but consistent with a critical RH of $\approx 80\%$ for the onset of aqueous atmospheric corrosion, he found at $\geq 85\%$ RH the corrosion rate rapidly increased.

Industry standards such as ISO-9223 define the basic TOW as the amount of time per year that the material of interest experiences a RH > 80% with the temperature > 0 °C (Otaduy and Karagiozis, 2010). Due to this definition for TOW and the sharp increase in corrosion rate at 80% RH, $\geq 80\%$ is an ideal RH to employ where static RH is being used for corrosion research, allowing comparisons to be made with other research. Wetness is influenced by the degree of coverage against rain, pollution in the atmosphere, the type of metal and presence of corrosion products, thus the 'actual' TOW may not be the same as determined by this definition (Kucera and Mattsson, 1987).

RH levels can have an indirect effect on the corrosion of ferrous metal as well as the direct effects discussed above. Gustafsson and Franzén (2000) report calculations by Rossknecht et al. (1973), regarding RH and the amount of airborne sea-salt recorded at 50 km from the Newport, Oregon coastline in the US; at < 40% RH the sea-salt concentration is 20 times that found at 99% RH (figure 20). Thus, a reduction in RH causes an increase in the dry deposition and concentration of sea-salt at 50 km from the coastline, increasing the number of contaminants e.g. Cl⁻ ions that may be deposited on metal surfaces and accelerate corrosion rates.

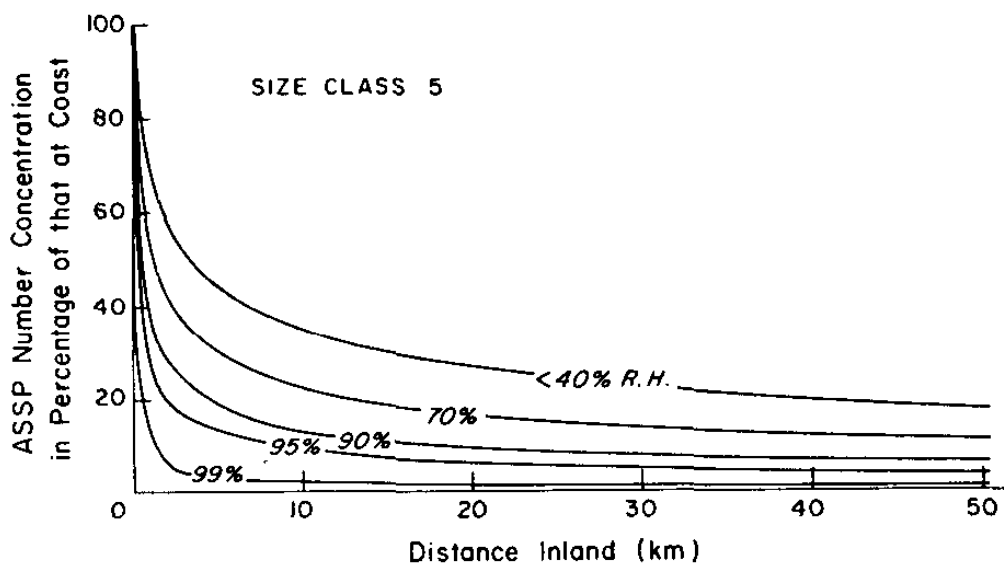


Figure 20 Airborne sea-salt particles class 5 distribution inland ($2.01 \mu\text{m} < d < 2.39 \mu\text{m}$) as a function of RH: $D = 10^4 \text{ cm}^2 \text{ sec}^{-1}$, $\gamma = 75.7$ (Rossknecht et al., 1973)

This trend is also visible in figure 21, where an RH of 70 or 90% causes a rapid decrease in salt concentration, but at 20 and 50% RH the decline is much slower, allowing salt concentrations to be noticeably higher inland when RH is low.

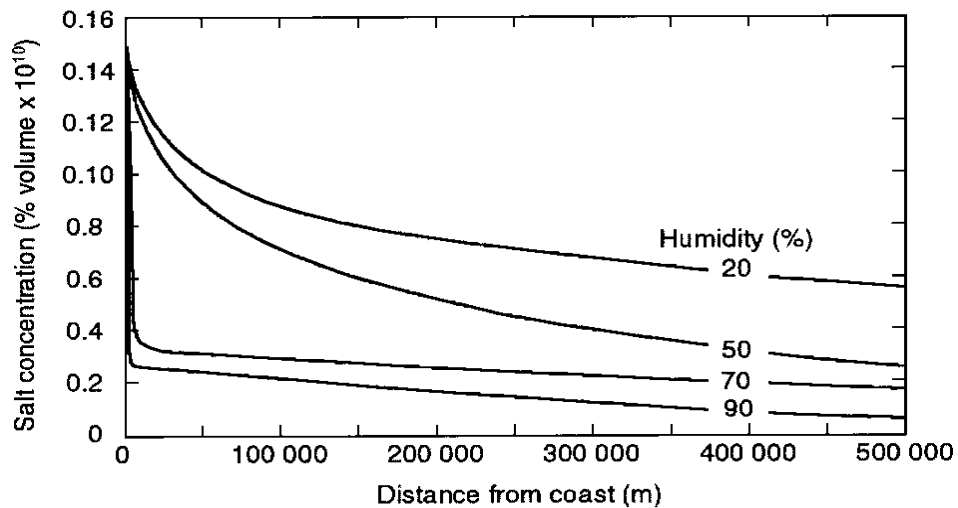


Figure 21 Effects of surface RH on ocean generated aerosol - 7.5 ms^{-1} wind speed, 800 mm year^{-1} rainfall – resulting from a computational fluid dynamics (CFD) based model of transport of aerosol (Cole et al., 2003b)

It is clear from figure 23 (a) and (b) that with the UK experiencing annual averages of $\text{RH} > 70\%$, the UK will not encounter the same levels of inland salt concentration as Australia does. The high RH also reduces the impact of salt aerosol transport by the wind.

It should be noted that in the UK the annual average RH for the period 1971-2000 (figure 23 (b)) has decreased slightly from the annual average RH for the period 1961-1990 (figure 23 (a)) and in some areas has decreased by as much as 1.6% RH (Jenkins et al., 2008). A decreasing trend in RH due to climate change could be good news for corrosion reduction in the UK.

Critical to the understanding of corrosion is a knowledge of the frequency of rain and the length of rain events. Herting et al. (2008) found that for stainless steel a time-dependent release of small amounts (low release rates) of the main metal alloy constituents from the stainless steel grades investigated, resulted from exposure to artificial rain. During the initial rain portion impinging the surface (first flush), higher rates were observed for all released metals. Through subsequent rain volumes lower and more constant release rates followed (steady-state) as illustrated in figure 22 (Herting et al., 2008). Reduced rainfall can mean a lack of rain-induced surface cleaning causing salts to build-up on exposed metal surfaces (Cole et al., 2013). Figure 24 (a) and (b) illustrate the average annual days of rain $\geq 1 \text{ mm}$ in the UK and although visually there is not a noticeable difference between the two, figure 25 highlights the change in annual days of rain between the two time periods. There is a clear East-West divide, however, with the number of days of rain experienced in

the UK, salts are unlikely to build-up on exposed metal surfaces of outdoor heritage structures, sculptures or railings, such as those looked after by Historic Scotland. Armoured vehicles and industrial heritage kept in sheds and under shelters will not experience rain-induced surface cleaning but they are also unlikely to experience the same extent of release of the main metal alloy constituents due to rain events.

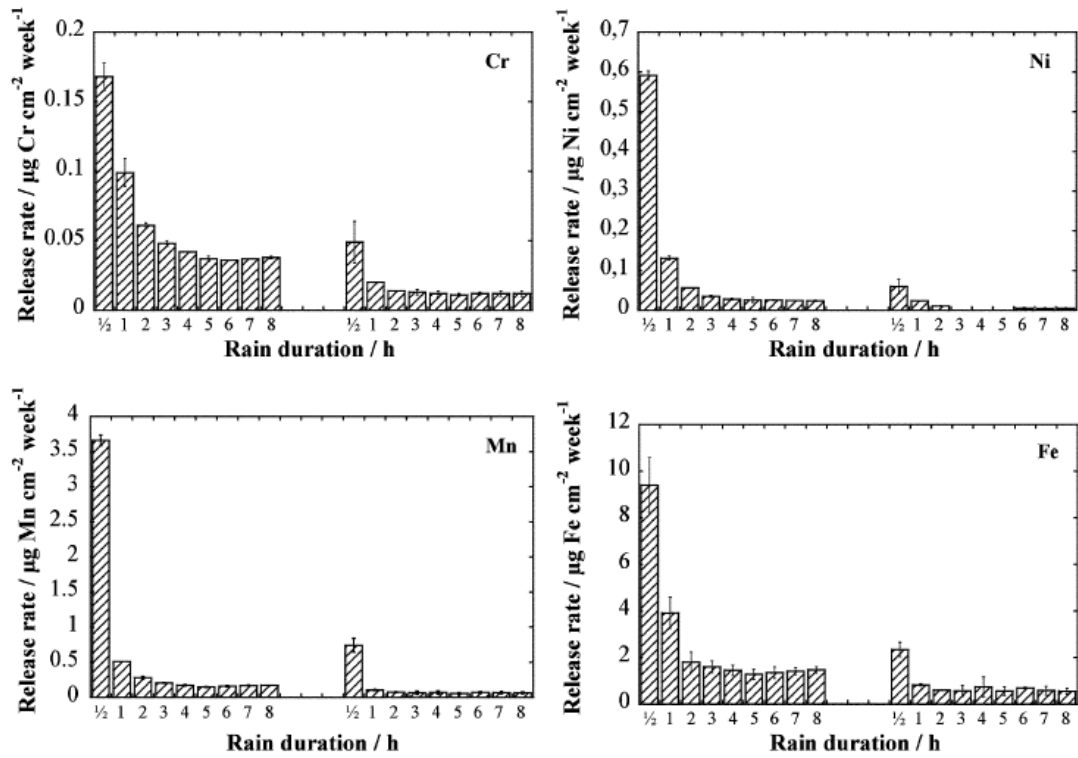


Figure 22 Momentary release rates of chromium (Cr), nickel (Ni), Fe and manganese (Mn) from as-received SS grade 4Ni exposed to two consecutive 8 hour rain events (pH 4.3, 4 mm h⁻¹)

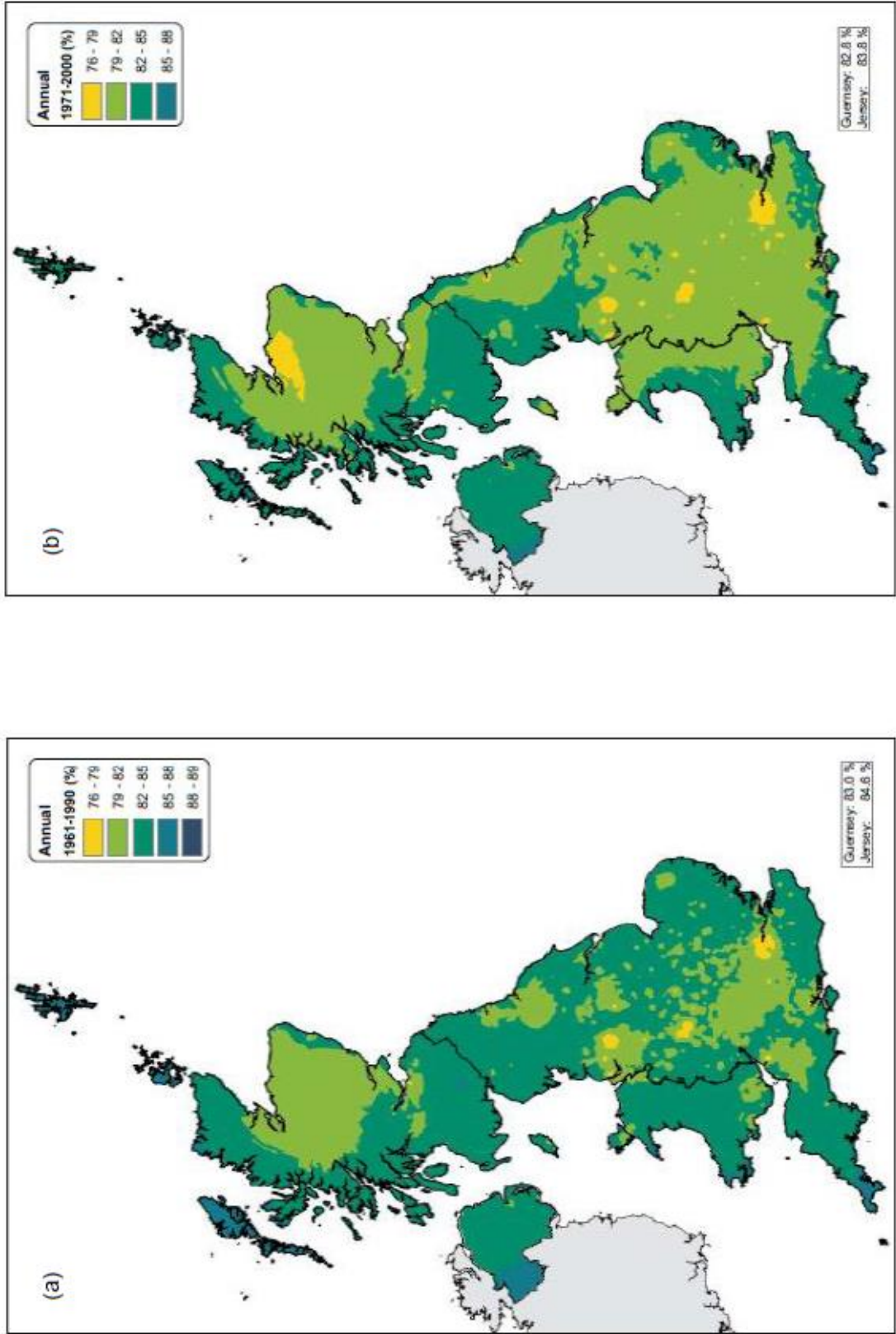


Figure 23 (a) Annual average RH (%) for 1961-1990. (b) Annual average RH (%) for 1971-2000 (Jenkins et al., 2008)

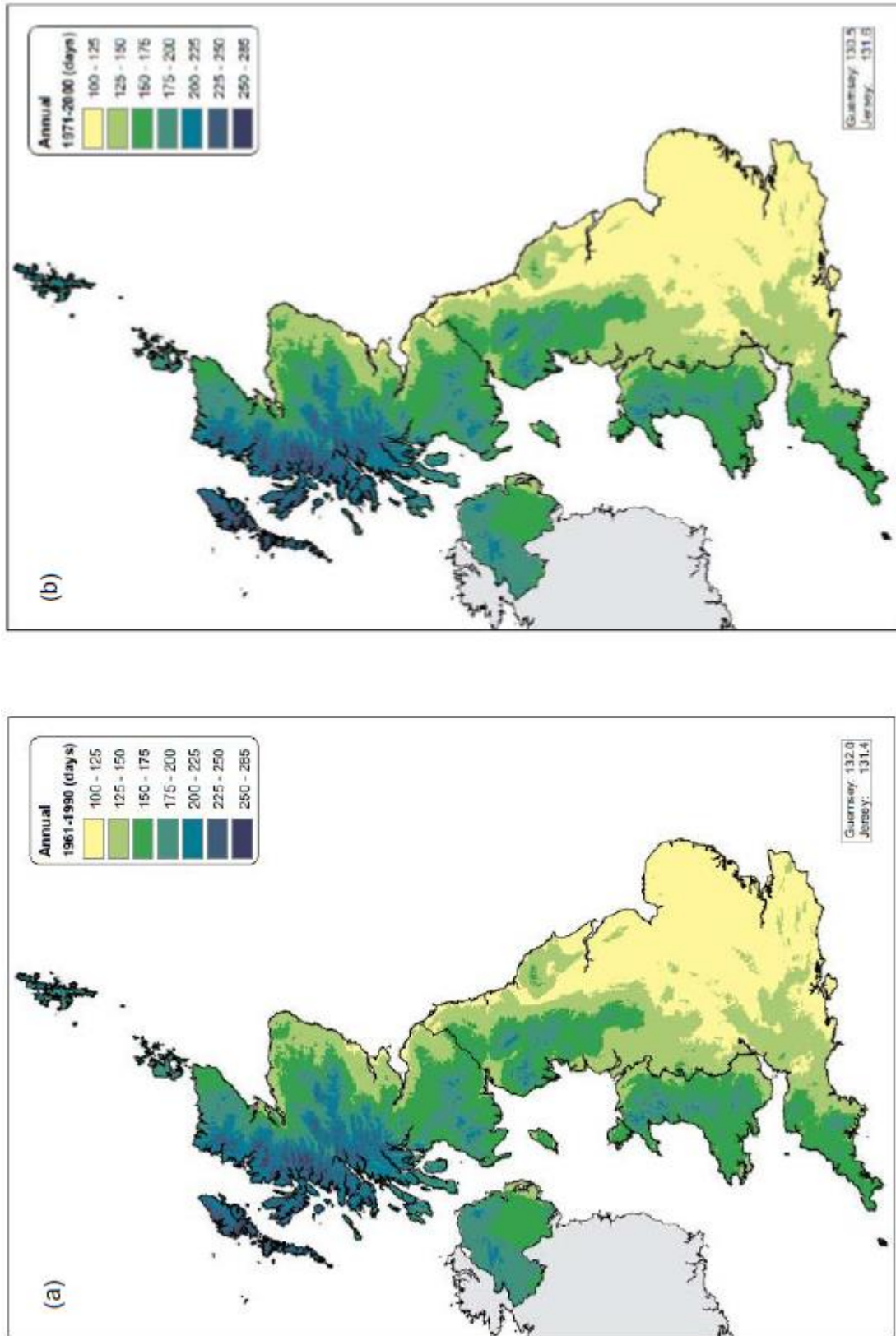


Figure 24 (a) Average annual days of rain ≥ 1 mm for 1961-1990. (b) Average annual days of rain ≥ 1 mm for 1971-2000 (Jenkins et al., 2008)

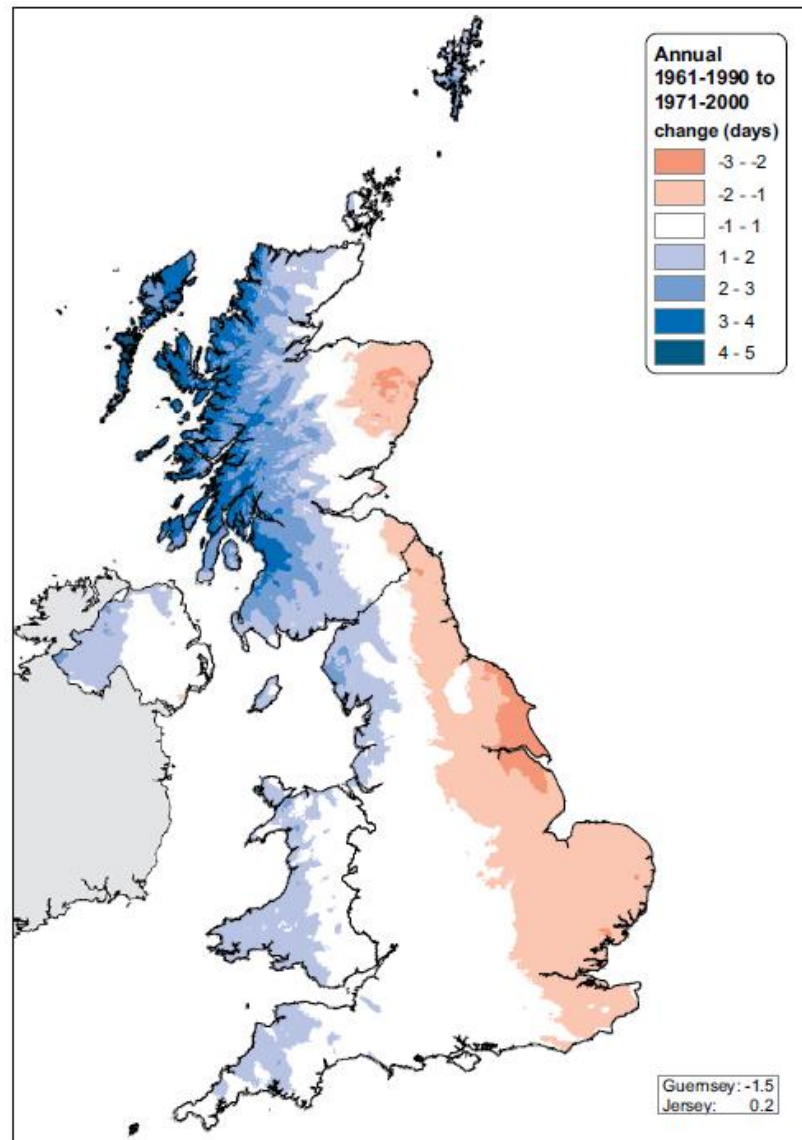


Figure 25 Change in annual days of rain > 1mm between 1961-1990 and 1971-2000 (Jenkins et al., 2008)

2.5.1.4 Deposition of pollutants: gases, particulates and aerosols

A variety of natural and anthropogenic pollutant gases, aerosols and particulates are constantly entering the atmosphere or being removed by raindrops or impact with the ground or ground-based objects (Cole, 2010). The distance travelled away from the source is dependent on the residence time, which is linked to its reactivity. Highly reactive species e.g. hydroxide radicals ($\cdot\text{OH}$) travel extremely short distances, oxidants e.g. nitrogen oxides (NO_x) and $\text{SO}_{2(g)}$ that oxidise and reduce both influence atmospheric pH, but travel limited distances and aerosols travel moderate distances from their source (figure 26). All of these substances have significant implications for atmospheric corrosion (Cole, 2010). As aerosols are moderately long lived species, they can travel considerable distances from their

source. Many common aerosol components contain corrosive Cl^- and SO_4^{2-} ions (table 7). Aerosols and salt mists formed from road-salt, can develop as tyres of moving vehicles spray tiny particles of salt water or dry salt into the air (Houska, 2009). Moving vehicles cause turbulence, which creates a vertical column of wet or dry salt particles that are transported away from the road by the wind. Accumulations usually stop within 1 km (0.6 miles) of a main roads, but they have been found 1.9 km (1.2 miles) downwind of a major road. Smaller wet droplets and dry particles travel much further away from roads than large saltwater droplets, which generally land within 'splash zone', 15 m (49 ft) from the road (Houska, 2009). The critical humidity level for corrosion can be lowered to 45% at 0 °C if calcium chloride (CaCl_2) is included in the de-icing salt. The transport of de-icing salt aerosols, although largely seasonal, may cause bigger issue for the UK in terms of corrosion, than sea-salt. De-icing salt is likely to be used on the roads and in the car parks of museum sites e.g. the TM and historic buildings with ornate gates and railings. Thus, de-icing salt could cause significant damage to ferrous metal. Fortunately, the TM is remote, away from main roads.

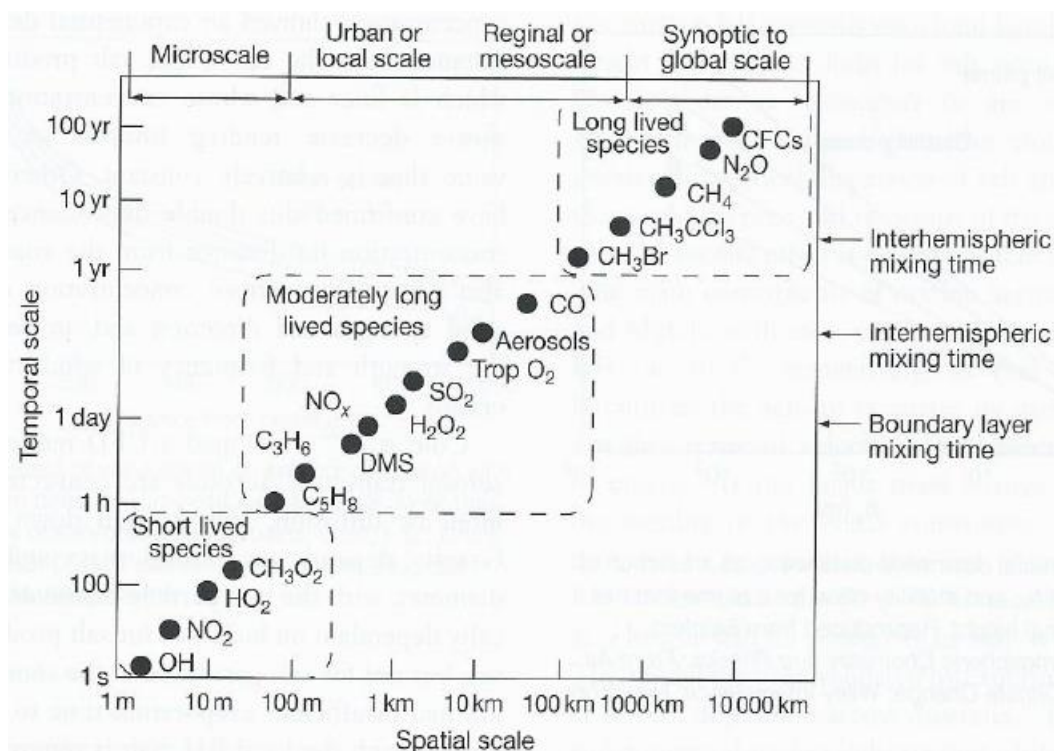


Figure 26 Spatial and temporal scales of variability for atmospheric constituents. Taken from (Schweitzer, 2003); Cole (2010); reproduced from Seinfeld, J. and S. Pandis 1997 Atmospheric Chemistry and Physics: From Air Pollution to Climate Change; Wiley Interscience: New York

Table 7 Experimentally determined deliquescence and efflorescence points for common aerosol components at or around ground 25 °C (Schindelholz and Kelly, 2012).

Compound	Chemical formula	Deliquescence RH (%)	Efflorescence RH (%)*	References
Halides	HCl	Liquid	Liquid	
	CaCl ₂	20	N/A	(Cohen, Flagan, & Seinfeld, 1987)
	MgCl ₂	33	N/A	(Tang, 1979)
	NaBr	45–58	N/A	(Cohen et al., 1987)
	NaCl	75	42–45	(Orr, Hurd, & Corbett, 1958; Tang, 1979)
	NH ₄ Cl	80	70	(Cohen et al., 1987; He, Cheng, Zhu, Wang, & Zhang, 2009)
	KBr	80–82	N/A	(Cohen et al., 1987)
	KCl	84–85	48	(Freney, Martin, & Buseck, 2009; Tang, 1979)
Nitrates	HNO ₃	Liquid	Liquid	
	Ca(NO ₃) ₂	18	N/A	(Tang & Fung, 1997)
	NH ₄ NO ₃	60–61	<30	(Lightstone, Onasch, Imre, & Oatis, 2000; Tang, 1979)
	NaNO ₃	75	35	(Tang & Fung, 1997)
	KNO ₃	93	N/A	(Freney et al., 2009)
Sulfates	H ₂ SO ₄	liquid	liquid	
	NH ₄ HSO ₄	39	N/A	(Cziczo, Nowak, Hu, & Abbatt, 1997; Tang, 1979)
	2NH ₄ NO ₃ ·(NH ₄) ₂ SO ₄	56	N/A	(Tang, 1979)
	(NH ₄) ₂ H(SO ₄) ₂	69	N/A	(Tang, 1979)
	(NH ₄) ₂ SO ₄	80	30–40	(Cziczo, et al., 1997; Orr et al., 1958; Tang, 1979)
	Na ₂ SO ₄	80	N/A	(Koloutsou-Vakakis & Rood, 1994)
	MgSO ₄	85	N/A	(Ha & Chan, 1999)
	K ₂ SO ₄	96	60	(Freney et al., 2009)

* Efflorescence – crystallisation point of a salt during drying cycle.

N/A denotes behaviour that was not measured or observed in the cited references.

‘Wet’ and ‘dry’ deposition are two methods for pollutants to combine with surface moisture layers (Arroyave and Morcillo, 1995). Wet deposition involves precipitation (rain, snow, fog) (Arroyave and Morcillo, 1995), whereas dry deposition involves adsorption of gas onto material surfaces or impaction of particles. Armoured vehicles situated outdoors will experience both wet and dry deposition, as will those located within lightweight buildings if condensation occurs, but if condensation does not occur those under shelter or indoors will only be subject to dry deposition.

Aerosols play a significant role in corrosion. Gradual changes in the composition of the rust result from variations in the size and composition of the aerosol (Lau et al., 2008). The corrosion resulting from fine aerosol particles has a composition related to SO₄²⁻, but those from coarse particles are mostly linked to Cl⁻. Lau et al. (2008) reported sea-salt (Na⁺Cl⁻) aerosols contributed the most to corrosion of mild steel, SO₄²⁻, ammonium (NH₄⁺), potassium (K⁺), magnesium (Mg²⁺) and nitrate (NO₃⁻) had a much smaller impact, while calcium (Ca²⁺) significantly inhibited corrosion.

Corrosion processes at humidity levels below that required for adsorption-induced wetting at a clean surface are initiated and sustained by deliquescence of deposited hygroscopic species. Deliquescence RH (DRH) values occur over a wide RH range (table 7) (Schindelholz and Kelly, 2012) and for CaCl₂ (table 8) they decrease with increasing temperature and vice versa.

Table 8 Temperature and humidity levels at which marine and deicing salts begin to absorb water and form a corrosive chloride solution (Houska, 2009).

Temperature		Critical Humidity Level (%)		
°F	°C	NaCl	CaCl ₂	MgCl ₂ *
77	25	76	30	50
50	10	76	41	50
32	0	-	45	50

*MgCl₂ – Magnesium chloride

Surface contaminants are more accurately represented as mixed salts, whose mutual deliquescence RH (MDRH), is lower than that of their pure salt components (figure 27). This has implications for corrosion as CaCl₂ is used with NaCl in de-icing salts (Houska, 2009) and although the DRH for NaCl is 75% RH, for CaCl₂ it is 20% RH (table 7).

Fossil fuels release SO₂ into the atmosphere. SO₂, is also a moderately long-lived species within the atmosphere (figure 26), with moderately long transport distances. In the atmosphere about 30% of the SO₂ is converted to the acid sulfate aerosol [14], which is removed through wet or dry deposition (The World Bank Group, 1999) forming sulfuric acid (H₂SO₄) (Walker, 1982c; Tullmin and Roberge, 2000; Syed, 2006).

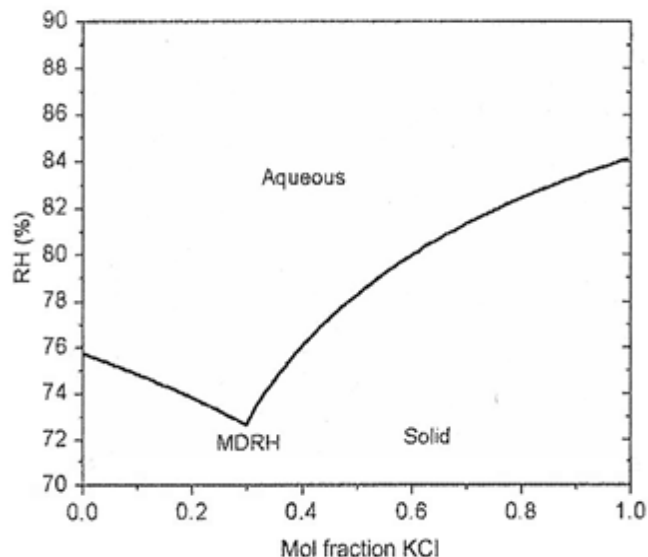
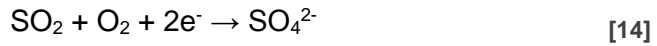
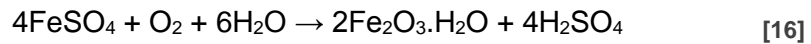
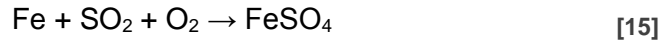


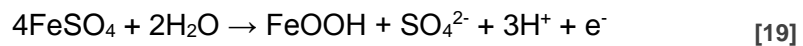
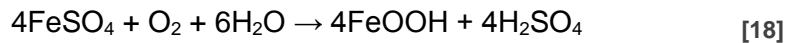
Figure 27 Deliquescence behaviour of mixed NaCl and KCl constructed using Analyzer Studio strong electrolyte modeling software (OLI Systems) (Schindelholz and Kelly, 2012)



Walker (1982c) speculated that the following equations [15] to [17] may occur when SO₂ gas is dissolved in rain. The soluble ferrous sulfate (FeSO₄) salt is formed when the dissolved SO₂ reacts with Fe.



Sulfuric acid is regenerated by the hydrolysis of FeSO₄ forming oxides [16] (Walker, 1982c), [18] (Badea et al., 2010), [19] (Syed, 2006)).



Liberating the corrosion-stimulating SO₄²⁻ ions, leads to an autocatalytic type of attack on Fe (Syed, 2006). A relatively low pH at the anodic site is maintained as a result of the pH-regulating effect of FeSO₄ and thus iron hydroxides are prevented from precipitating directly on the metal surface. As the sulfate accelerates the anodic dissolution of Fe, favourable conditions for corrosion in the active state are created. Crystalline iron (II) sulfate at the steel/rust interface was identified as tetrahydrate FeSO₄·4H₂O (Morcillo et al., 2011). Within the sulfate nests (figure 28) exist a reservoir of soluble ferrous sulfate, which contribute to their high stability. A semi-permeable membrane of hydroxide, formed by oxidative hydrolysis of iron ions, develops enclosing the sulfate nest.

Although the surfaces appear dry, in recesses corrosion can continue under moist conditions, as H₂SO₄ is difficult to remove (Walker, 1982c). Sulfur (S) has also been found to accumulate during winter at the metal-oxide interface, when steel is exposed in SO₂ polluted atmospheres (Morcillo et al., 2011). The S then becomes concentrated in nests with the arrival of summer, and is diffused throughout the thickness of the rust layer.

Although Cl⁻ in the atmosphere typically originate from the sea, they can also originate from general industrial pollution (Walker, 1982c). Cl⁻ increases the conductivity of solutions and as many Cl⁻ compounds are hygroscopic they

encourage electrochemical corrosion (Walker, 1982c). Where large amounts of Cl^- ions are deposited (within 100 m from the sea), the presence of Cl^- is conducive to the formation of $\beta\text{-FeOOH}$ which accelerates the corrosion process as it deteriorates the atmospheric resistance of low carbon steel (Ma et al., 2009). Chloride ions need to accumulate and reach a critical concentration level before their effects are seen. At 95 m from the coastline where Cl^- deposition is high, it was 9 months before $\beta\text{-FeOOH}$ formed in the inner layer as a result of Cl^- ions (Ma et al., 2009). Where small amounts of Cl^- ions are deposited and the concentration level is below the critical concentration, the Cl^- ion facilitates the transformation of $\gamma\text{-FeOOH}$ to $\alpha\text{-FeOOH}$ (Ma et al., 2009). The overall transformation process is outlined in figure 29. Corrosion at lower Cl^- concentration levels is still accelerated and the conditions for self-propagating pits and crevices still arise, and both of these forms of corrosion could cause problems on armoured vehicle and structures.

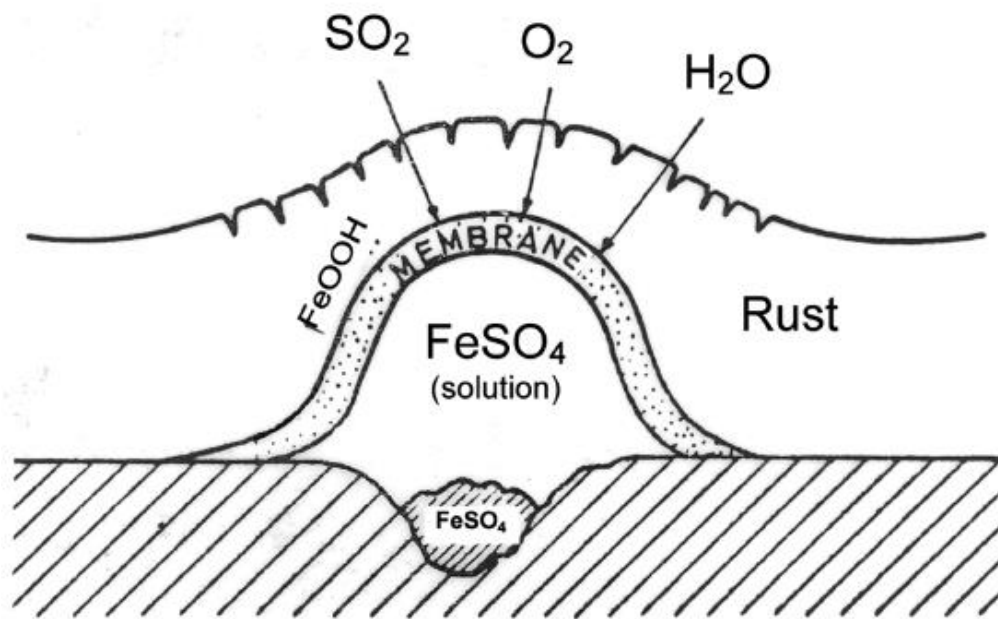


Figure 28 Representation of a sulfate nest (Morcillo et al., 2011)

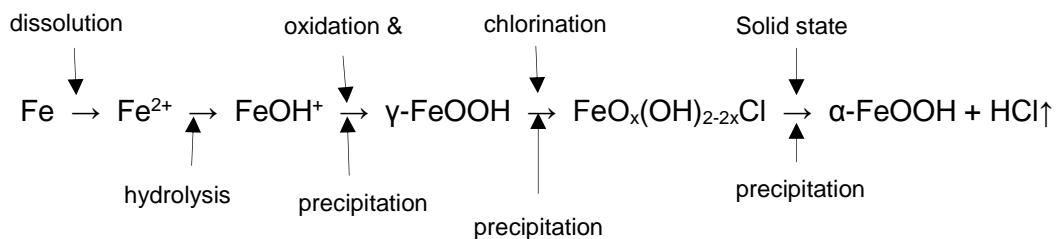


Figure 29 Outline of overall transformation process

The acceleration rate caused by Cl^- ions on the atmospheric corrosion of steel depends on the rain regime characteristics, i.e. the higher the volume of rain and the longer the period of time, the lower acceleration on corrosion rate for a given Cl^- deposition rate (Corvo et al., 2005).

Not only do Cl^- ions affect the rate of corrosion, but they affect the type of attack and products found in the corrosion layers. Protective and insoluble OH^- ions on metal surfaces can be replaced by soluble metal products causing local attack such as pitting. The Cl^- ion is small and relatively mobile, which allows it to diffuse to the metal surface (Walker, 1982c). The characteristics of rust layers are remarkably influenced by the level of Cl^- deposition (Ma et al., 2009). Corrosion of carbon steel with Cl^- proceeds in local cells which resemble SO_4^{2-} nests (Morcillo et al., 2011). The local cells arise around the Cl^- particles deposited on the surface, where the FeOOH passivating film is destroyed locally by the concentrated Cl^- solution. The development of differential aeration cells can lead to pitting. Unlike with SO_2 polluted atmospheres, nests are not formed as no amorphous oxide/hydroxide membrane is formed (figure 30). The ability of ferrous and ferric chlorides (FeCl_2 and FeCl_3) to form complexes is a factor which influences the corrosive activity, with oxidant hydrolysis giving rise to the complex $n\text{FeOOH}\cdot\text{FeCl}_3$, or a solution of FeCl_3 in FeOH in gel form (Morcillo et al., 2011).

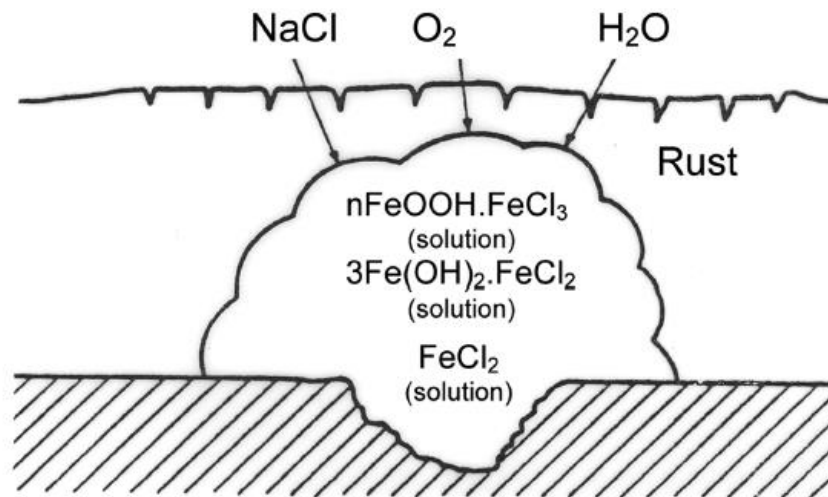


Figure 30 Schematic representation of a chloride agglomerate (Morcillo et al., 2011)

Iron chlorides are commonly found amongst the iron corrosion products, they tend to migrate to the steel/rust interface and accumulate (Morcillo et al., 2011).

2.5.2 Environment Types

The meteorological and air pollution factors discussed above have varying effects on different locations and environments due to terrain, proximity to the coast, mountainous regions or anthropogenic pollution sources. Understanding atmospheric corrosivity categories and examples of typical environments can make generalised service life predictions of steel possible or predict thickness loss of the armoured steel at the TM. The ‘corrosivity’ and ‘environment categories’ presented in table 9 are based upon those given in the Standards BS EN ISO 12944-2 and BS EN ISO 9223 (Tata Steel et al., 2015) (Standards are discussed in more detail in the next chapters).

Table 9 Atmospheric corrosivity categories and examples of typical environments (BS EN ISO 12944-2: 1998, Paints and varnishes – Corrosion protection of steel structures by protective paint systems – Part 2: Classification of environments, BSI)

Corrosivity category and risk	Low-carbon steel Thickness loss (μm) ^a	Examples of typical environments in a temperate climate (informative only)	
		Exterior	Interior
C1 very low	≤ 1.3	-	Heated buildings with clean atmospheres, e.g. offices, shops, schools, hotels
C2 low	> 1.3 to 25	Atmospheres with low level of pollution Mostly rural areas	Unheated buildings where condensation may occur, e.g. depots, sports halls
C3 medium	> 25 to 50	Urban and industrial atmospheres, moderate SO ₂ pollution Coastal area with low salinity	Production rooms with high humidity and some air pollution e.g. food-processing plants, laundries, breweries, dairies
C4 high	> 50 to 80	Industrial areas and coastal areas with moderate salinity	Chemical plants, swimming pools, coastal, ship and boatyards
C5-I very high (industrial)	> 80 to 200	Industrial areas with high humidity and aggressive atmosphere	Buildings or areas with almost permanent condensation and high pollution
C5-M very high (marine)	> 80 to 200	Coastal and offshore areas with high salinity	Buildings or areas with almost permanent condensation and high pollution

Note: ^a The thickness loss values are after the first year of exposure. Losses may reduce over subsequent years.

The loss values used for the corrosivity categories are identical to those given in BS EN ISO 9223: 2012, Corrosion of metals and alloys – Corrosivity of atmospheres – Classification, BSI

In coastal areas in hot, humid zones, the mass or thickness losses can exceed the limits of category C5-M. Special precautions must therefore be taken when selecting materials.

BS British Standard; EN European Norm; ISO International Standards Organisation.

Four types of environments are frequently used for corrosion testing – rural, marine, industrial and urban. In generalised terms, rural environments are the least corrosive, followed by urban, industrial and then marine environments. Although, Cole (2010) lists data for some key parameters for particular locations (table 10) these should only be taken as indicative especially as they are based on data collected in Australia, Japan, China, Brazil, Turkey, Mexico and South Africa and not the United Kingdom, also explaining the inclusion of remote locations as a fifth type of environment.

Table 10 Summary of gaseous concentration, aerosol type and rain water composition ($\mu\text{eq l}^{-1}$) for varying types of location in Australia (Cole, 2010)

Location type	Marine	Industrial	Urban	Rural	Remote
Gaseous (mixing ratio)					
SO ₂ (ppt)	260	1500	160-1500	160	20
H ₂ S (ppt)	65	365	365	35-60	3.6-7.5
NO _x (ppb)	0.2-1000	10-1000	10-1000	0.2-10	0.02-0.08
O ₃ (ppb)	20-40	100-400	100-400	20-40	20-40
Aerosols					
pH	0-9.5	-1-2.4	1.9-3		
Major species	NaCl, MgCl	H ₂ SO ₄ , (NH ₄) ₂ H(SO ₄) ₂ , (NH ₄) ₂ SO ₄ , NH ₄ HSO ₄	NH ₄ NO ₃ , NH ₄ Cl, (NH ₄) ₂ SO ₄		Dust, pollen, plant waxes
Secondary species	Na ₂ SO ₄ , H ₂ SO ₄ , NH ₄ HSO ₄ , (NH ₄) ₂ SO ₄ and NH ₄ NO ₃ .NaHSO ₄		NaNO ₃		
Rain water					
pH	4-5.6	4.2-7.3	4.4-6.1	3.6-5.8	5.6-6
Cl ⁻	100-1300	9-142	10-27	3-25	1-1300
NO ₃ ⁻	3-10	40-140	13-140	3-25	3-10
SO ₄ ²⁻	3-10	70-240	12-60	4-60	3-10
Na ⁺	100-1200	5-60	20-60	3-30	100-1200
NH ₄ ⁺	2-10	30-200	10-30	2-20	2-10
Ca ²⁺		20-300	2-35	2-20	80

2.5.2.1 Rural Environments

The principal corrosives in rural environments are moisture and relatively small amounts of carbon dioxide (CO₂) and sulfur oxides (SO_x) from various combustion products, as rural environments are usually free of aggressive agents, with deposition rates of SO₂ and NaCl lower than 15 mg m⁻² day⁻¹ (Syed, 2006). The decomposition of farm fertilizers may also result in ammonia (NH₃) being present.

2.5.2.2 Urban Environments

In an urban environment, a highly corrosive wet acid can develop on exposed surfaces with the addition of fog or dew as the atmosphere is characterized by pollution mainly composed of SO_x and NO_x from domestic emissions and motor vehicles (Syed, 2006). Although urban pollution is characterized by NO_x and SO_x emissions, there is little industrial activity and the atmosphere is similar to that found at rural locations with deposition rates of NaCl lower than 15 mg m⁻² day⁻¹, but the deposition rate of SO₂ is higher than this value (Syed, 2006).

2.5.2.3 Industrial Environments

In an industrial atmosphere, the most potent causes of corrosion are SO_x and NO_x formed by combustion reactions of fuel in motor vehicles and fossil fuels in power stations. Concentrations of phosphates, hydrogen sulfate, Cl⁻, NH₃ and its salts are also associated with these atmospheres (Syed, 2006).

2.5.2.4 Marine Environments

Marine atmospheres are usually highly corrosive, however, this is dependent on the RH, prevailing winds, wave action at the surf line and topography of the shore (Syed, 2006). The Cl⁻ ion from NaCl is the main culprit in marine atmospheres and due to marine fog and wind-blown spray droplets NaCl is deposited on steel surfaces at a rate higher than 15 mg m⁻² day⁻¹ (Syed, 2006). Severe corrosion is induced by this contamination at RH > 55%. The proximity to the ocean and salt characterize the marine environment and although the corrosiveness decreases rapidly with increasing distance from the ocean (figure 16 (a) and (b)), the salt spray can be carried as much as 15 km inland in a severe storm (Syed, 2006).

2.5.3 Sheltered and Indoor Corrosion

Other criteria appear to be valid under sheltered and indoor environments as the expression previously used for TOW does not correlate well in these conditions (Kucera and Mattsson, 1987) and the standard ISO 9223, does not differentiate conditions sufficiently (table 11) (Roberge et al., 2002). Another system of classification has been developed; standards ISO 11844 parts 1, 2 and 3 – *Corrosion of metals and alloys – Classification of indoor atmospheres* (table 12). Important pollutants are specified as SO₂, NO₂, ozone (O₃), H₂S, chlorine (Cl₂), Cl⁻, NH₃, organic acids and aldehydes, and particles (dust deposits and soot). Compared to the outdoor environment, the effects of corrosion in the indoor environment are more complicated and difficult to predict (Tidblad, 2013).

IC1 to IC3 (table 12) correspond to the more widely known corrosivity category C1 (table 9), and IC4 to IC5 corresponds to C2. The new display hall within the Tank Museum is likely to fall within the C1 corrosivity category as it was installed with radiant heating. The Vehicle Conservation Centre at the Tank Museum part of which is shown in figure 31 also reveals an over-head heating system, thus placing it in the C1 category. However, this building is also fitted with very large shutter for moving tanks in and out, which will also allow the movement of atmospheric pollutants into the building, potentially altering the corrosivity category it should fall within. There are also buildings, sheds and workshops without heating at the Tank Museum and these will fall under C2, which is also equivalent to an outdoor rural environment in term of corrosivity.

Table 11 ISO classification of time of wetness (Roberge et al., 2002)

Wetness category	Time of wetness (%)	Time of wetness (hours per year)	Examples of environments
T1	<0.1	<10	Indoor with climatic control
T2	0.1-3	10-250	Indoor without climatic control
T3	3-30	250-2500	Outdoor in dry, cold climates
T4	30-60	2500-5500	Outdoor in other climates
T5	>60	>5500	Damp climates

Table 12 Classification of corrosivity of indoor atmospheres based on corrosion rate measurements by mass loss determination of standard specimens. The values have been calculated from the values in the standard into $\mu\text{m year}^{-1}$ using the density 7.8 for carbon steel (Tidblad, 2013)

Corrosivity	Indoor Category	Carbon Steel
IC1	Very Low	≤ 0.01
IC2	Low	0.01-0.13
IC3	Medium	0.13-1.3
IC4	High	1.3-9
IC5	Very High	9-25

Under ventilated sheds, in both coastal and rural stations the average Cl^- deposition rate decreases sharply (Mendoza and Corvo, 1999). However, in sheltered conditions the influence of Cl^- could be higher than outdoors, as no rain wash occurs (Corvo et al., 2008). This accumulation of Cl^- and other pollutants combined with high RH may produce a corrosion rate higher than for outdoors, but maximum corrosion rates for steel normally occur outdoors, possibly due to the formation of a thick and adherent layer of corrosion products (Corvo et al., 2008). In closed space conditions it is practically impossible for the Cl^- ions to get into the indoor space of the sheds, whereas for gaseous sulfur compounds (SO_2 , sulfur trioxide (SO_3), etc.), there is not a marked decrease (Mendoza and Corvo, 1999). Small metallic boxes such as those used in the TROPICORR project can model indoor environments of steel fabricated buildings similar to some used at the Tank Museum, particularly when considering deposition of possible contaminants. The Vehicle Conservation Centre (VCC) employs over-head heating to avoid condensation forming on the surface of the Tanks (figure 31). The international collaborative project TROPICORR, found deposition of contaminants inside metallic boxes and corrosion rates reduced considerably in these conditions, but steel had the highest corrosion rate (Corvo et al., 2008).



Figure 31 A small area of the Vehicle Conservation Centre at the Tank Museum with over-head heating employed

Air temperature, RH, concentration of the pollutants SO_2 , NO_x , O_3 , NH_3 , HCl , sulfates, dispersed chlorides, organic acids, other volatile compounds and dust particles all influence corrosion indoors (Prosek et al., 2013); but heritage institutions mostly control and monitor, temperature and RH (as is the case for the Tank Museum), largely due to the cost and technical challenges of monitoring (Prosek et al., 2013). Indoors, RH plays a significant role in corrosion, with condensation forming the aqueous layer that acts as the electrolyte, and at 65% RH or above, this layer approaches the behaviour of bulk water (Høerlé et al., 2004; Selwyn, 2004). Indoor dust particles often contain salts and other contaminants and these hygroscopic pollutants can cause the local RH to be raised enough to initiate corrosion (Selwyn, 2004).

3 Coating Systems: Properties and Performance

3.1 Introduction

If ships, vehicles, aeroplanes, bridges and industrial plants were not given the protection afforded by anti-corrosive paints they would not function for long (Guy, 2004). This chapter discusses coating systems (coating, substrate and interface), focusing on ferrous metal, coating choice, coating properties and assessment of performance. The appearance, corrosion resistance, usage, need for coatings, and surface preparation for coating of ferrous metals used for large structures, machines and vehicles will also be considered. Finally, industrial coatings, processes and standards relative to heritage conservation are addressed.

3.2 Coatings

3.2.1 The Function of Coatings

In addition to being in the business of decoration, the coatings industry has always been concerned with conservation (Marrion, 2004). The lifespan, safety, operating efficiency, appearance and economy of structures and heritage metal can all be influenced by a protective coating (Bortak, 2002). Coatings purposes include:

- The prevention of corrosion – either actively or passively.
 - Actively – the inclusion of anticorrosive pigments
 - Passively – providing an adhesive and impermeable barrier
- Providing slip or slip resistance
- Abrasion and impact resistance
- Contamination resistance
- Providing hygienic properties
 - Bacterial, fungal or antifouling resistance (Marrion, 2004).

Irrespective of the end property, all coatings provide economic benefit by saving energy, reducing downtime, increasing lifetime, saving capital and allowing material substitution (Marrion, 2004).

Coatings significantly reduce corrosion rates (table 13) and quantifying the performance of coatings in terms of their anti-corrosion performance is central to this research. For anticorrosive coatings there are three basic mechanisms of

protection, barrier protection, passivation of the substrate surface (inhibitive effect) and sacrificial protection (galvanic effect) (figure 32) (Sorensen et al., 2009).

Table 13 Mass loss of uncoated and vinyl resin-coated cold-rolled steel samples after exposure for 21 days to an atmosphere containing SO₂ and NaCl (Baumann and Bender, 2008)

Atmospheric contamination*, (%)		Mass loss, (g/m ²) of steel,	
SO ₂	NaCl	not coated	coated
0.008		52.0	17.0
0.016		280.0	41.4
	0.0017	214.6	0
	5.0	385.2	0
0.008	0.0017	160.3	0
0.008	5.0	183.2	43.5
0.016	0.0017	791.0	235.2
0.016	5.0	195.7	80.5

* The exposure to SO₂ or NaCl in the last four experiments was carried out separately in daily alternation

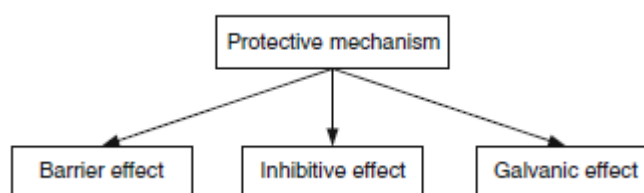


Figure 32 Anticorrosive coating protective mechanisms (Sorensen et al., 2009)

For organic coatings without active pigments, barrier properties regarding O₂ and H₂O are not the critical aspects describing the corrosion protection properties (Deflorian and Fedrizzi, 1999). Their low ionic conductivity can protect the substrate from atmospheric corrosion by isolating the anodic and cathodic areas (Arroyave and Morcillo, 1995; Deflorian and Fedrizzi, 1999).

Coating systems with low permeability for liquids, gases and ions provide *barrier* protection by impeding surface access to aggressive species. A chemical conversion layer or including inhibitive pigments in a coating can provide passivation of the substrate surface (an inhibitive effect) and the galvanic effect works by means of sacrificial protection provided electrical contact with the substrate is maintained. Metallic, organic, and inorganic coatings, have all been used in this way (Sorensen et al., 2009).

Internal and external variables affect performance and durability of a coating system, making it very difficult to assess (figure 33) (Sorensen et al., 2009).

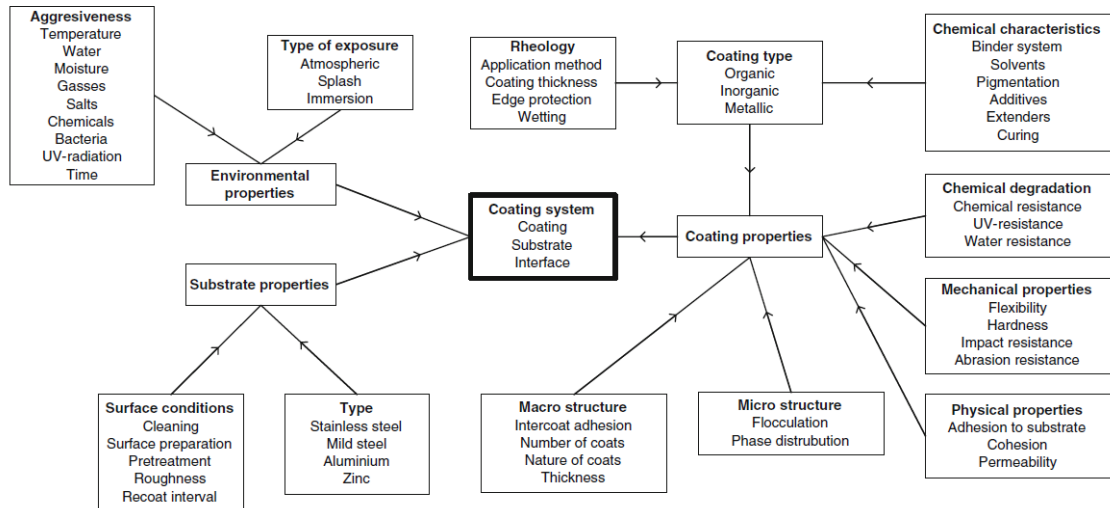


Figure 33 Factors affecting the longevity of an anticorrosive coating system (Sorensen et al., 2009)

3.2.2 Coating properties

3.2.2.1 *The Rheology of Coatings: Flow and Levelling*

Settling of pigment during storage, how much paint is picked up on the brush, film thickness applied, levelling of the applied film and control of sagging of the film are all governed by the flow properties of a paint (Wicks et al., 2006e). Coatings need to ‘hold up’, possibly on a vertical surface without dripping or running and ‘flow out’ (level) so that there are no visible surface imperfections or undulations, and a smooth film of the required thickness is achieved. Gravity is not a major influence as paint applied to a ceiling does not level any less effectively than paint applied to a floor (Wicks et al., 2006d). Rheology is considered during coating formulation (Marrion, 2004).

Achieving the best coating properties often requires compromise. Over a rough substrate, good levelling (figure 34 (a)) may be undesirable as thin areas provide limited protection, however, equal film thickness (figure 34 (b)) may also be undesirable due to the appearance. Controlling volatility offers a compromise with reasonable film smoothness without places where film thickness is very thin (figure 34 (c)) (Wicks et al., 2006d).

Levelling increases with high surface tension, but high surface tension can also lead to defects such as crawling, retraction and cratering (section 3.2.2.1.3). Thicker films promote levelling, but increase both the probability of sagging on vertical surfaces and cost (Wicks et al., 2006d). Levelling is fastest when the wavelength (λ in figure 36, determined by application condition) is small, the surface tension is

high, the viscosity is low and the film is thick. The principal means of control left is viscosity, which usually changes whilst the coating levels as solvent evaporation increases the viscosity (Wicks et al., 2006d) or for reaction systems like epoxy as they cross-link. The viscosity of a coating is its resistance to flow and must be adjusted to the method of application to be used (Wicks and Jones, 2013). Additionally, appearance is crucial in heritage contexts.

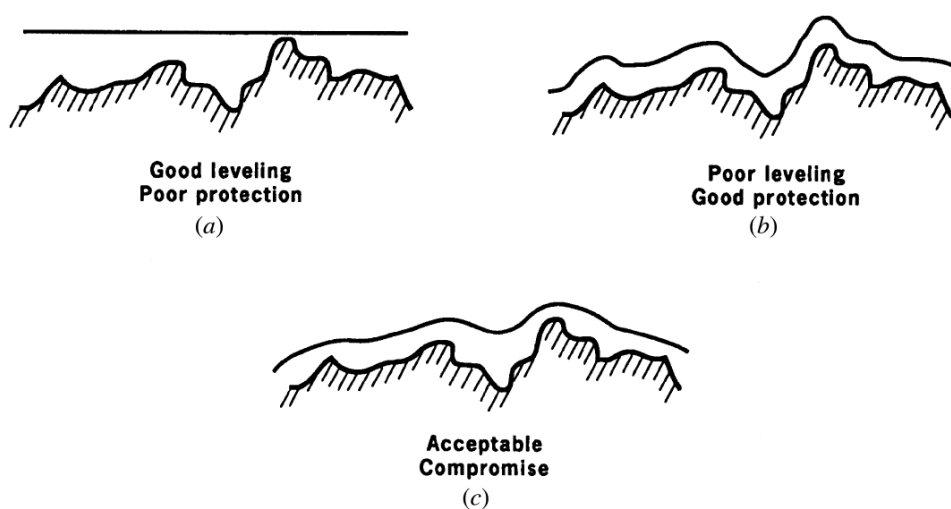


Figure 34 Different levelling (a-c) results after applying a coating to a rough surface (Finnie, 1995; Wicks et al., 2006d)

3.2.2.1.1 Application Methods

Coatings may be applied by a variety of methods, brushing, dipping, electro-deposition, curtain-coating, flow-coating, and spraying (compressed air, airless, electrostatic and aerosol spraying) (figure 35) (Turner, 1988) and these have various advantages and disadvantages (table 14) (Stoye and Freitag, 2007b). Coating application methods used for the maintenance and restoration of large metal objects will be considered in further detail, thus dip coating and flow, flood and curtain coating will not be discussed.

Although different consistencies of paint are required by different application methods, the application principle remains the same: greater viscosity requires larger quantities of dissolved polymer in the coating. Irregularities in the wet film surface are left by most methods of application such as brush marks, roller stipple and spray mottle, which can be lessened or removed by wet film flow, while avoiding 'run' if applied to a vertical surface (Turner, 1988).

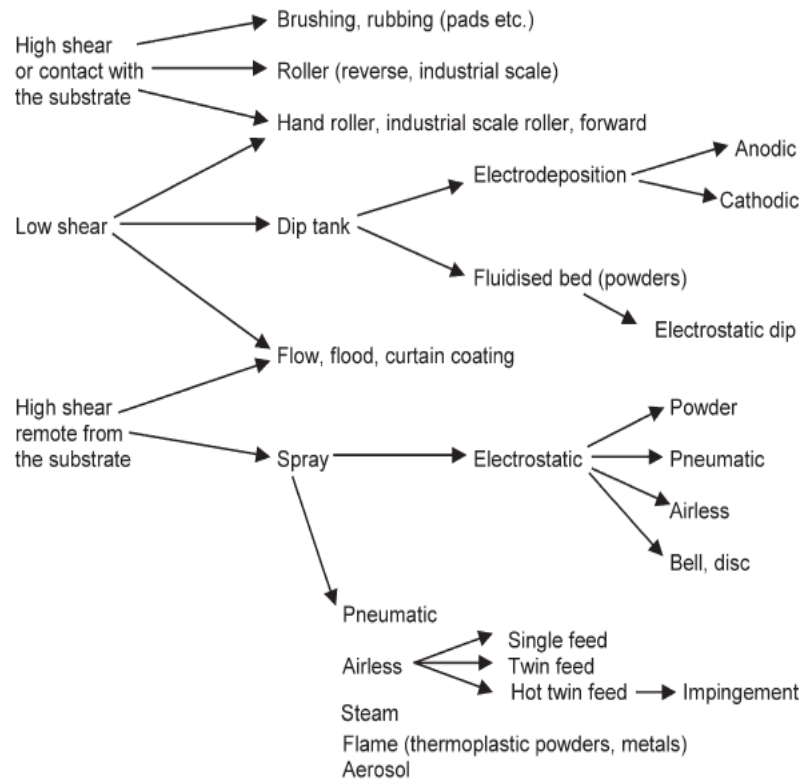


Figure 35 Paint application - various approaches (Marrion, 2004)

Brush and Pad Application

To avoid time-consuming and labour-intensive brush application industry uses more rapid and efficient methods. For maintenance of small areas, for coating awkward or restricted areas where spray application can be difficult or prohibited for health and safety, and for stripe coating of sharp edges, brushing remains suitable (Whitehouse, 2010). Hence, brush application is one of the methods used for maintenance of vehicles at the Tank Museum.

The brushes available vary in several ways: width, handle length and bristle type (e.g. nylon, polyester, and hog hair) (Wicks et al., 2006b). The suitability of a paint brush for a particular type of coating task is determined by its size, shape and bristle type (table 15). Armoured vehicles have many areas that are relatively inaccessible. Thus wetting and good adhesion are promoted by brushing paint into these spaces and forcing the coating into contact with the surface (Whitehouse, 2010).

Table 14 Miscellaneous wet coating methods, adapted from Stoye and Freitag (2007b) to include only methods suitable for large metal objects.

Application Method	Advantages	Disadvantages	Examples of areas of use
Brushing	<ul style="list-style-type: none"> • Simple equipment • High paint yield • No specially trained work-force required • Universally applicable • Good wetting of the substrate. 	<ul style="list-style-type: none"> • Highly labour-intensive (high wage costs) • Non-uniform film thickness • Danger of brush marks 	<ul style="list-style-type: none"> • Steel superstructures • Lattice constructions • Handicrafts • Do-it-yourself
Roller application	<ul style="list-style-type: none"> • Fast and easy to master • High paint yield • Uniform film thickness 	<ul style="list-style-type: none"> • Only suitable for smooth surfaces • Worse wetting of the substrate • Labour-intensive 	<ul style="list-style-type: none"> • Steel superstructures • Handicrafts • Do-it-yourself
Wiping	<ul style="list-style-type: none"> • Fast application • Uniform film thickness • High paint yield 	<ul style="list-style-type: none"> • Unsuitable for work pieces with complex shapes 	<ul style="list-style-type: none"> • Exterior coating of pipes • Application of bitumen to pipelines • Wood coating
Rolling, printing, strip (coil) coating	<ul style="list-style-type: none"> • High degree of automation • High paint yield • High economy • Very uniform coating 	<ul style="list-style-type: none"> • Only suitable for flat surfaces (strips) • High investment in plant and equipment • Limited potential uses 	<ul style="list-style-type: none"> • Strip and panel coating (sheet metal, wood, films, paper, paperboard)
Flow coating	<ul style="list-style-type: none"> • Good material yield • Easily automated 	<ul style="list-style-type: none"> • Non-uniform film thickness • Danger of paint slurry formation 	<ul style="list-style-type: none"> • Large, bulky articles (radiators, frames for commercial vehicles, etc.)

Table 15 Suitability of different bristle types for use with different paints (information extracted from (Finnie, 1995; Wicks et al., 2006b))

Bristle type	Suitability/response to paints	
	Water-borne	Solvent-borne
Hog bristle	✗	✓
Nylon bristles	✓	✗ (Swollen by some solvents)
Polyester bristles	✓	✓

Brushes hold paint in the spaces between their bristles and the paint is forced out from between the bristles due to pressure when it is applied. The paint layer is split via the forward motion of the brush, so part of the paint is applied to the surface and part remains on the brush. When using brushes, paint viscosity characteristics are critical, with a low shear rate (~ 15 to 30 s^{-1}) controlling the pick of paint on the brush and a high shear rate (~ 5000 to 20000 s^{-1}) between the brush and the substrate giving a low viscosity for ease of brushing (Wicks et al., 2006b). Paints aid their own application process as they are frequently highly shear thinning or thixotropic with their viscosity decreasing when a stress is applied e.g. stirring, but return to a semisolid state on standing. For the duration of the application the structure within the paint is destroyed by the high shear rates generated by the application methods, increasing the ease with which they flow in such processes (Reynolds, 1994, 2004). Since brushing generates a high shear rate ($10^4 - 10^6 \text{ s}^{-1}$), shear viscosity can be used to compare brushing characteristics of a series of paints and relate it to their rheology.

Increasing viscosity leads to increased film thickness and higher “brush drag”, this is slowed by using solvents with relatively slow evaporation rates (Wicks et al., 2006b). Paint applied by brush results in furrows (brush marks) in the surface of the wet film. These do not result from the individual bristles but form as the paint is applied and the wet film is split between the brush and the substrate (Wicks et al., 2006b). Levelling of brush marks is widely studied. A sine wave profile is used for the model of an idealised cross section of a wet film exhibiting brush strokes (figure 36) (Wicks et al., 2006d). As the thickness of the coating increases and the pressure on the brush increases, the wavelength (λ) also increases. Although levelling of brush marks should be promoted, it should only be to the extent where the seriousness of the surface irregularities is acceptable (Overdiep, 1986).

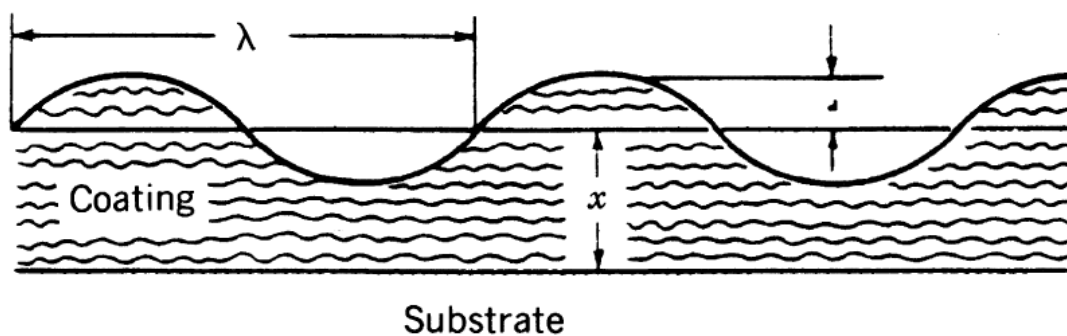


Figure 36 Illustration of a cross section of brush marks (Wicks et al., 2006d)

Pad applicators are also used in the do-it-yourself market instead of, or in addition to, brushes. Pad application is not used at the TM due to their disadvantages (table 16).

Table 16 Advantages and disadvantages of pads compared to brushes (information taken from Wicks et al. (2006b))

Advantages	Disadvantages
Holds more paint than a brush of similar width	Requires the use of a tray
Can apply paint twice as fast	Use of a tray results in some loss of paint
Generally leaves a smoother layer than brush application	Use of a tray also results in some solvent evaporation
Extension handles can be used, reducing the need for moving ladders	Cleaning pads is more difficult than paint brushes
Pads and refills are less expensive than paint brushes	

Hand-Roller Application

Although hand-roller application is used at the Tank Museum, it is not appropriate for this research where the focus is on small areas of coating maintenance.

Hand-roller application is the fastest method of hand application (Wicks et al., 2006b) being up to four times faster than brushing (Whitehouse, 2010). Hand-roller application is commonly used for applying architectural paint to walls and ceilings (Wicks et al., 2006b), but to coat corners and edges satisfactorily brushes may still be needed (Whitehouse, 2010). Hand-roller and brush application have similar viscosity requirements and both involve film splitting during application. However, for hand-roller application, the film stretches as the roller moves, leaving a ribbed surface as the film breaks at different times due to imbalances of pressures (Wicks et al., 2006b). Appearance wise whether this is acceptable depends on the desired surface finish and the levelling properties of the coating once it has been applied. An advantage of hand-roller application (table 14) is the resulting uniform coating thickness, which allows for more predictive corrosion protection and an even build-up of coating layers.

Spraying (Atomisation)

Although spraying is unlikely to be a method used in situ for maintenance, due to practicalities and health and safety considerations, it can be used in workshops for restoration of large vehicles. It is fast and is particularly useful for coating irregularly shaped articles, although it is also used on flat surfaces.

Spraying equipment works by atomising the liquid coating into droplets (Wicks et al., 2006b). Atomisation in conventional spraying is the result of external forces, the exchange of momentum between two free jets (air and paint) (Stoye and Freitag, 2007b). As the paint reaching the surface does not have the same composition as the paint leaving the spray-gun, the formulation of coatings is further complicated. Compared with the volume, the surface area of each droplet from which evaporation occurs is large (Turner, 1988) and a great deal of liquid can be lost this way, which adds to the cost. Since only a fraction of the spray particles are deposited on the object being sprayed, the principal disadvantage is the inefficiency of the application (Wicks et al., 2006b).

3.2.2.1.2 Coating thickness

Coating thickness and uniformity can be affected by application method, coating formulation and substrate surface profile. For the success of any coating system, an adequate film thickness is essential. Premature failure will generally result from under-application, solvent entrapment and subsequent loss of adhesion or splitting of primer coats can result from gross over-application. Table 17 shows how coating thickness needs to vary for different service life requirements of different binders in a coastal environment.

The substrate shape and surface can also have a significant effect on coating thickness. Pits in the substrate surface and blasting to clean and create an adhesive surface both have an impact on the thickness of the coating and uniformity (figure 34). The thickness of coatings at edges and corners can also lead to concern about their protection.

Table 17 Minimum coating thickness of corrosion protection coating systems for steel in a coastal atmosphere (Baumann and Bender, 2008)

Binder	Service Life, (in years)			
	2 to 5	5 to 10	10 to 20	> 20
	Minimum coating thickness, μm			
Oil	75-125	125-200		
Alkyd resin¹	75-100	100-125	125-150	>150
Phenol resin¹	75-100	100-175	175-275	
Vinyl resin²	50-75	75-100		
Chlorinated rubber²	50-75	75-100	100-275	
Epoxy resin²	100-125	125-150	125-200	

1 Mean value of six different degrees of cleanliness

2 Blasted surface

Edge and Corner Protection

For ease and uniformity of paint application, structures in critical chemical atmospheres often use cylindrical sections. It is difficult to coat edges and corners uniformly (figure 37), and this leaves thinly coated protrusions susceptible to corrosion (Jones, 2013). It is a problem with the many angular aspects of armoured vehicles.

Surface tension minimises the surface area of the film when it is applied around a corner, causing a decrease or increase in the film thickness (figure 38 (b) and (d)) (Chan and Venkatraman, 2006). An increase in the thickness of the film at edges, is related to variations in the surface tension with the solvent concentration. A decrease in film thickness at the edge for a newly formed film is due to surface tension of the film. As there is a larger surface area per unit volume near the edge, the solvent evaporates much faster at the edge of the film creating a higher surface tension causing material transport towards the edge from region 2 to 1 (figure 39). Due to the exposure of the underlying material in region 2, which has a higher solvent concentration, the newly formed surface will have a lower tension. The surface tension gradient across the regions (figure 39 (c)), causes more materials to be transported from region 2 to the surrounding areas (regions 1 and 3) (Chan and Venkatraman, 2006).

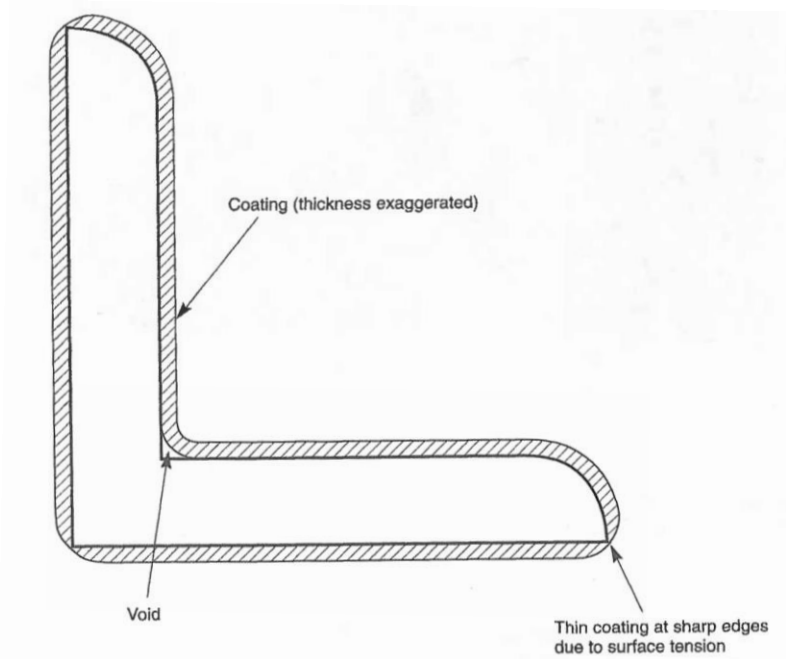


Figure 37 Inadequate coating thickness at corners and edges (Jones, 2013)

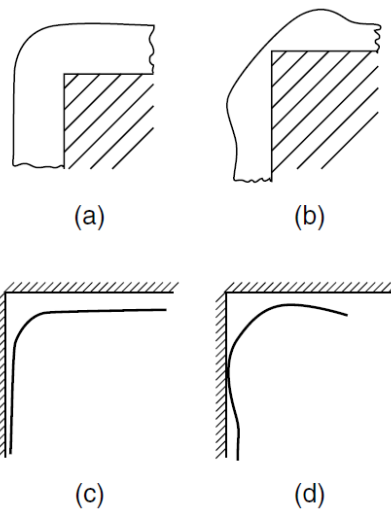


Figure 38 (a) Thick film at a corner – newly applied. (b) Surface tension causes a decrease in the film thickness. (c) Thin film at the corner – newly applied. (d) Surface tension causes an increase in film thickness at the corner (Chan and Venkatraman, 2006).

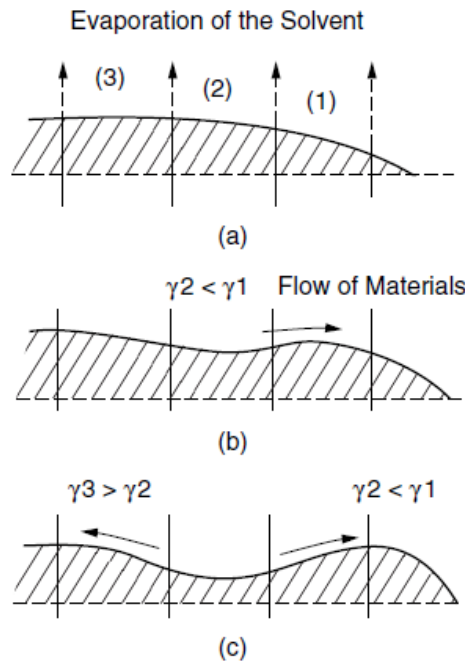


Figure 39 (a) New film formed near an edge. (b) Flow of material from regions 2 to 1. (c) Further flow of materials from region 2 to the surrounding areas (Chan and Venkatraman, 2006)

3.2.2.1.3 Wetting

In the adhesion of a coating to a substrate, wetting is a major and perhaps limiting factor (Chan and Venkatraman, 2006; Wicks et al., 2006a). There cannot be interactions and hence there will be no contribution to adhesion if a coating does not spread spontaneously over a substrate surface so that there is intermolecular contact between the substrate surface and the coating (Wicks et al., 2006a). The ability of a coating to wet and adhere to a substrate, is determined by its surface tension. Thus, solvents with lower surface tensions can be used to improve the ability of paint to wet a substrate (Chan and Venkatraman, 2006) making choice of solvent and its quantity of crucial importance (figure 40).

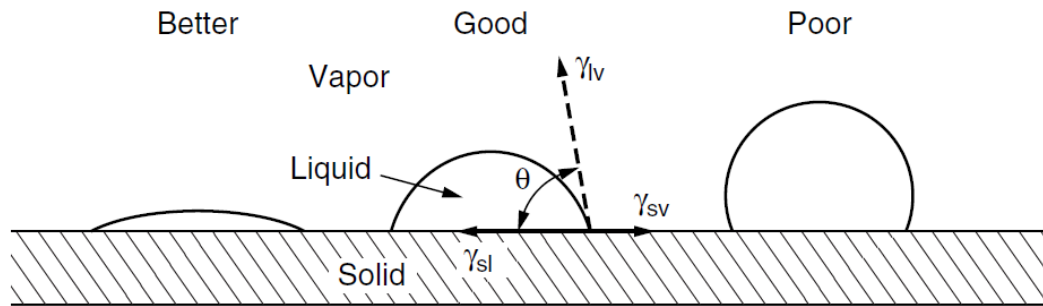


Figure 40 Schematic illustration of good and poor wetting (Chan and Venkatraman, 2006)

3.2.2.2 Film formation

Film formation is a crucial process in coatings technology (Wicks and Jones, 2013) and when it occurs by solvent evaporation from a solution two stages are involved:

1. *First stage of solvent evaporation.* Evaporation increases viscosity and coatings reach the 'dry to touch' stage quickly, but they retain several percent of the solvent (Wicks and Jones, 2013). Evaporation is largely dependent on three factors:
 - i. The vapour pressure at the temperature encountered during the evaporation
 - ii. The ratio of surface area to volume of the film
 - iii. The rate of air flow over the surface
2. *The diffusion control stage.* Evaporation increases glass transition temperature (T_g) and decreases the free volume. Solvent loss becomes dependent on how fast the solvent molecules can diffuse to the surface, which depends on the following:
 - i. Solvent structure
 - ii. Solvent-polymer interactions
 - iii. Temperature
 - iv. T_g of the film
 - v. Film thickness

Diffusion is faster for smaller, linear solvent molecules than large, branched-chain ones.

To formulate coatings from low molecular weight resins containing oligomers and monomers considerably less solvent is required as they can polymerise further after application and solvent evaporation. Cross-linking reactions occur, reducing the solvent usage and yielding a more solvent resistant insoluble film.

Latex paints undergo film formation by coalescence of polymer particles from a dispersion system, via evaporation, deformation and coalescence, which is how powder coatings form films. To reduce the film formation temperature it has been common to include a coalescing solvent in the formula (Wicks and Jones, 2013).

3.2.2.2.1 Curing/Drying

The film-forming element of a coating or adhesive is the binder (or resin) (BASF, 2011), which for practical coatings must adhere to the substrate and have a minimum level of strength, it is not sufficient just to form a film (Wicks and Jones, 2013). Binders can be classified as physically or chemically drying. The transition to a solid coating from a liquid can occur in three ways: solvent evaporation, chemical reaction or a combination of both. Basic information about chemically and physically drying coatings has been summarised in table 18.

Table 18 Summary of chemically and physically drying paints. Information extracted from Stoye and Freitag (2007c)

	Physically drying paints	Chemically drying paints
Polymer type	Thermoplastic polymers	Thermosetting coatings
Special requirements	-	Usually elevated temperatures or radiation - causes cross-linking of the binder forming a polymer network
Molecular masses	> 20,000	~800 – 10,000
Solids content	Low - due to low solubility	High
Solvent content	High (> 60%)	Low (30 to 60%)

The type of chemical reaction or agent used to liquefy the coating can be used to further divide chemically curing and physically drying coating into subgroups as illustrated in figure 41 (Sorensen et al., 2009). The information provided in figure 41 is not definitive as for example, moisture cure siloxane binders exist and siloxanes can be combined with other binders to improve their performance, e.g. epoxy siloxanes and acrylic siloxanes.

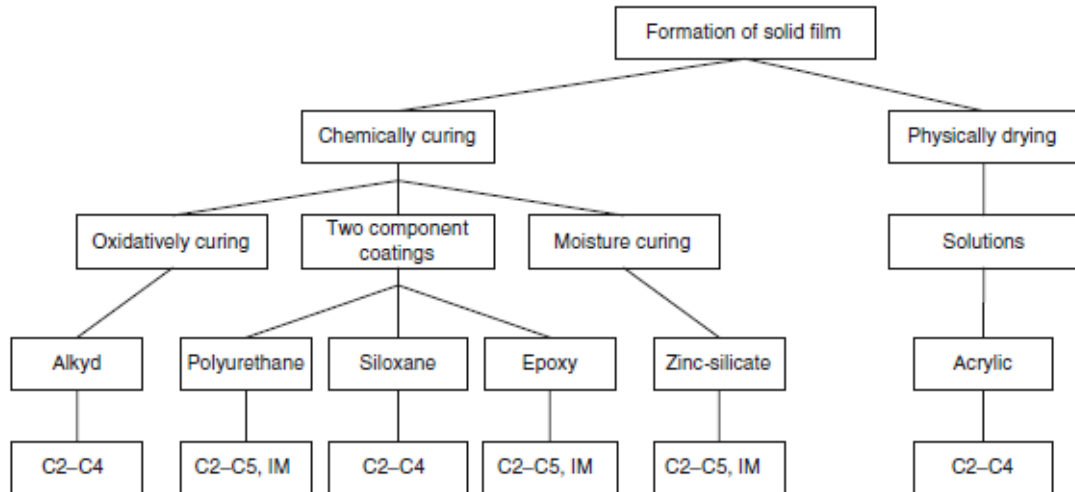


Figure 41 Classification according to curing mechanism for binders, with suggested areas of application from low to heavy impact (C2-C5), and immersion in seawater (IM) (Sorensen et al., 2009)

The curing time and conditions selected affect the performance of a coating. For example, adhesion to a subsequent layer can be adversely affected in an under-cured paint system and paints layers can become brittle or yellow if the maximum curing temperature is exceeded (Stoye and Freitag, 2007b). In protective coatings, the binders or polymers used that dry or cure at ambient temperatures do so by either solvent evaporation, air oxidation, or chemical reaction of components mixed together before application (Guy, 2004). Both types of curing methods can proceed in parallel or overlap where there is a suitable combination of binder (Stoye and Freitag, 2007b).

Figure 42 illustrates an example of chemical curing, in this case a polysiloxane molecule (a polymer molecule with a silicon-oxygen (Si-O) backbone) is attracted closer to the surface of the metal substrate and the attached hydroxyl (OH-) groups by H-bonding forces of attraction. The reaction progresses with H₂O molecules being evolved and Si-O-Metal bonds being formed, but in many cases heat is required.

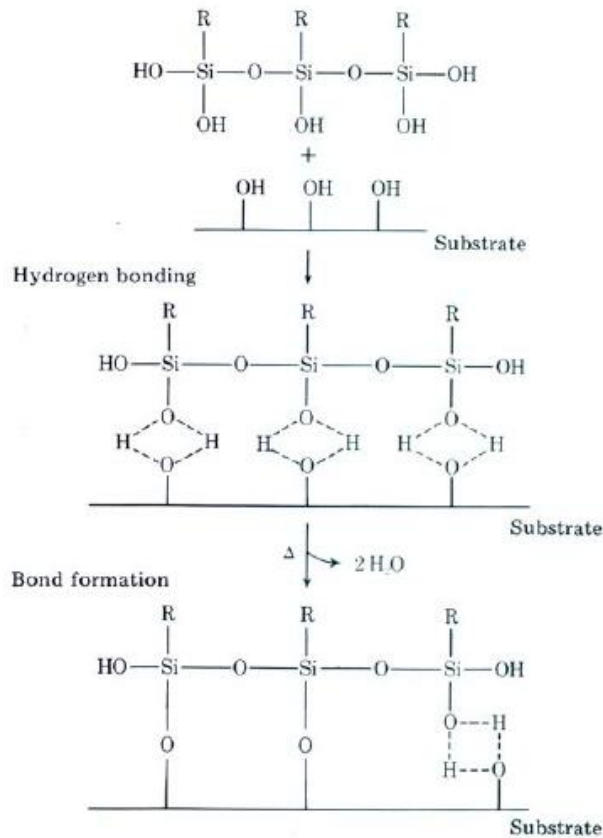


Figure 42 Deposition of siloxanes Arkles (1977)

3.2.2.3 Coating Components and Chemical Characteristics

A liquid corrosion-protective coating is comprised of primary materials from three classes: binders, pigments and solvents and additives. In a general coating, prior to application the polymer volume fraction ranges from 20 to 50%, the pigment volume concentrations range from 0 to 35%, the solvent composition by volume ranges from 10 to 50% (0% in powder coatings), and additives are usually 15% or less (Bierwagen and Huovinen, 2010). The polymeric matrices of coatings are the binders; pigments assist the coating in supplying colour and other functions including protection of the substrate and are solid, insoluble particles. The use of solvents is abandoned when using powder coatings but clear, liquid coatings are the focus of this research, and thus solvents are considered in more detail below.

3.2.2.3.1 Binder System

Binders determine durability, flexibility and gloss, as well as providing adhesion to the substrate and binding the pigments and extenders together (BASF, 2011). The binder is normally used for classifying paints e.g. alkyd, acrylic, polyester, nitrocellulose, epoxy, and oil-based paints (Stoye and Freitag, 2007c). Binder type

also influences the recommendations made for minimum coating thickness and the suitability of the coating for particular atmospheric environments (table 19).

Table 19 Coating thickness for coating systems depending on the type of atmospheric exposure in an external climate (Baumann and Bender, 2008)

Binder	Atmosphere			
	Rural	Urban	Industrial	Marine
	Coating thickness, μm			
Alkyd resin	120-160	160-240	240	240*
Alkyd resin blend	120-160	160-240	240	240*
Epoxy resin ester	120-160	160-240	240	240*
Bitumen/oil blends		220	220-250	220-250
Vinyl chloride copolymers		240	240	240
Chlorinated rubber		240	240	240
Vinyl chloride copolymer blends	160	160-240	240	240
Chlorinated rubber blends	160	160-240	240	240
Acrylic resin copolymer blends	160	160-240	240	240
Acrylic resin copolymer	240	240	240	240
Epoxy resin ¹ , polyurethane		160	240-320	240
Epoxy resin- or polyurethanehydrocarbon resin blend				360-420
Ethyl silicate-zinc dust	80-140	80-140		140
Silicone resin	130	130	130*	130*

* For a comparatively low exposure

1 Polyacrylate/polyisocyanate system for the last coat for outdoor exposure

To formulate a corrosion-protective coating, the properties of the polymer used needs to meet specific requirements:

1. Wet/dry adhesion – keeping the coating in contact with the substrate.
2. Low permeability to ions, H_2O and O_2 – physical barrier effect.
3. Low conductivity – inhibit flow of current in local corrosion cells and stop ion and electron motion in the film – electrical barrier effects.
4. Stability in its environment, stability to OH-driven basic hydrolysis and ultra-violet (UV) radiation, thermal stability, etc.
5. Strong adsorption of coating polymer to substrate interface – reinforces the wet adhesion of the polymer mentioned in property 1 and provides good wetting of substrate by coating system (Bierwagen and Huovinen, 2010).

Polymer composition and additives can alter all these properties (table 20)

Table 20 Anticorrosive properties required of polymers for specific polymer classes (Bierwagen and Huovinen, 2010)

Polymer	Properties					
	Wet adhesion	Chemical barrier	Electrical resistance	Exterior durability	Substrate wetting	Relative cost
Epoxies	✓	✓	✓	✓	✓	Medium
Polyurethanes/polyureas	✓	✓	✓	✓	✗	Medium to high
Acrylics	✗	✗	✗	✗	✗	Medium
Alkyds	✗	✗	✗	✗	✗	Low
Silicones	✗	✗O ₂ /✓H ₂ O	✗	✓	✗	Medium
Inorganic/sol-gels, etc.	✗/✓	✗	✗	✓	✓	Medium to high
Vinyls	✗	✓	✓	✗	✗	Low

Epoxies

The epoxy class of polymers is possibly the most commonly used in corrosion protective organic coatings (Bierwagen and Huovinen, 2010). For steel, epoxy-amine coatings are particularly effective as corrosion-protective primers as in the presence of H₂O, the amine groups resulting from the cross-linking reaction promote adhesion and the cross-linked resins are resistant to hydrolysis (Wicks and Jones, 2013). In addition to meeting all the specific anticorrosive properties required of polymers, the crosslinking can be controlled relatively easily. Their disadvantages include:

- i. A relatively strong tendency to pick up water – they are plasticised by water resulting from high humidity effects and immersion.
- ii. Poor UV resistance – as many precursors for epoxies have chromophoric phenyl groups in their structure, therefore they are often used as primers.

Isocyanate-based polymers: polyurethanes and polyureas

For corrosion protection isocyanate-based polymers are the second most commonly used class of polymer, but are less tolerant compared to epoxy coatings, having less wetting and adhesion properties (Bierwagen and Huovinen, 2010). Their three main advantages are:

1. High mechanical resistance
2. Outstanding chemical resistance
3. Excellent lightfastness and weather resistance (in the case of aliphatic polyisocyanates) (Stoye and Freitag, 2007d).

Due to their excellent UV resistance and barrier properties, aliphatic polyurethane (PUR) coatings are often used as topcoats in corrosion-protective systems.

Acrylics and Alkyds

UV stability and application range make acrylic resin paints one of the largest groups in use (Stoye and Freitag, 2007d). Thermoplastic acrylics have been applied as “flow and reflow” automotive topcoats and are typically mostly poly(methyl methacrylate) with a molecular weight in the order of 10^5 (Marrion, 2004).

Polyacrylate copolymers are made up of acrylate and methacrylate esters. Crosslinking chemistries with many other polymer types are allowed due to the vast number of side-groups of acrylic monomers available (Bierwagen and Huovinen, 2010).

Low cost and wide application range mean alkyds are amongst the longest employed polymer classes but their use in purely corrosion-protective systems is in decline, as this class of polymers is sensitive to basic hydrolysis.

Inorganic and hybrid coatings including silicones

During the past 50 years or so most polymer materials used in coatings have been organic (Cameron, 2004), due to low cost, ease of chemical manipulation and resulting properties.

A mixture of organic groupings and inorganic elements are the basis for most corrosion-protective systems, with very few purely inorganic polymers. Inorganic atoms and organic portions provide different properties (table 21).

Table 21 Properties provided by the inorganic and organic portions

Inorganic atoms provide	Organic portion provides
Heat resistance	Solubility
Fire resistance	Functionality (e.g. for crosslinking)
Radiation resistance	Hydrophobicity and other surface properties
Biological inertness	Many other characteristics
Electrical conductivity	

Vinyl polymers

The most common polymers with inorganic side chains are probably represented by vinyl systems (Cameron, 2004), which are normally physically drying but a few are chemically cross-linked with other reactants via incorporated reactive groups (Stoye

and Freitag, 2007d). The ubiquitous use of these systems has been curtailed by the need to use large amounts of strong solvent and the volatile organic compound (VOC) regulations. In UV exposure, as a class they have poor outdoor durability but they have excellent barrier properties, especially water resistance (Bierwagen and Huovinen, 2010). Often multiple layers are applied to produce thick films which contributes to their success.

Poly(organosiloxanes) (or silicones) and other silicon based polymers
 Polysiloxanes containing silicon (Si) and oxygen (O) are very well established as pigments and fillers in coatings as they are found in glass and other mineral silicates (Cameron, 2004). Polysiloxane chains are very brittle without modification as there are very few atoms between the network junction points (figure 43). This can be improved by replacing some of the siloxane groups with organic groups.

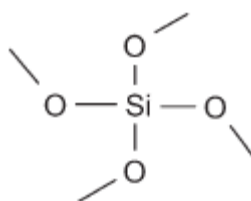


Figure 43 Highly functional polysiloxane (Cameron, 2004)

The best known example, polydimethylsiloxane (PDMS) (figure 44) is used for car polishes and stop-cock grease.

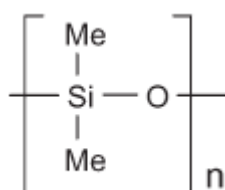


Figure 44 Polydimethylsiloxane (PDMS) repeat unit (Cameron, 2004)

Siloxane systems have many desirable properties and modification can improve their properties (table 22). High crosslink density with as big a difference as possible between the solubility parameter of the inorganic polymer and the organic or other liquids it may be in contact with produces a very high chemical resistance except to alkali, as the Si-O-Si bond is not resistant to hydrolysis (Cameron, 2004). Water repellent coatings are almost entirely based on siloxane chemistry presenting

a hydrophobic organic surface to any incoming moisture and binding to the substrate.

Table 22 Range of applications of siloxane materials (Cameron, 2004)

Property	Possible application
Low surface energy	Easy clean surface
Thermal stability	Heat resistant coatings
UV stability	Durable coatings
Interfacial activity	Adhesion promotion
	Corrosion protection
Low VOC	Compliant coatings

Despite their hydrophobicity, eventually moisture reaches the metal-silane interface (Ooij et al., 2005). If the substrate's metal hydroxide is soluble to some degree, the hydrolysis reaction that formed the Si-O-Me bonds is especially reversible. Walker (1982a) found that the initial adhesion of two-pack polyurethane and epoxide paints was dramatically increased by pre-treatment with organo-functional silanes on steel and aluminium, even after exposure to cyclic humidity under condensation conditions and accelerated weathering (Walker, 1982a). With a backbone comprised entirely of Si atoms polysilanes have as yet found little application in coatings (Cameron, 2004).

There is much interest in *polysilazanes*, which are the nitrogen (N) analogues of poly(organosiloxanes) with an Si-N repeat unit (figure 45) as curing reactions or organic modification is provided by the reactive secondary amino groups (Cameron, 2004). Their potential as heat resistant and corrosion protective coatings has been the source of interest over recent years.

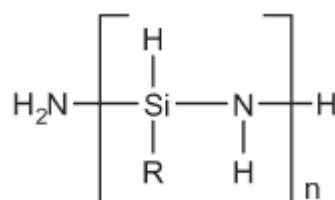


Figure 45 Polysilazane repeat unit (Cameron, 2004)

3.2.2.3.2 Pigments

For ferrous metals pigments can interrupt or slow down aspects of the corrosion process and reduce the rate of corrosion by either inhibiting the corrosion reactions or being sacrificial anodes (Guy, 2004).

Anti-corrosive pigments need to be near to the metal surface, so are included in the primer (Guy, 2004). Passivating oxide layers can be extremely effective inhibitors of corrosion but the porous loosely adhering oxide layer that forms on iron and steel provides very poor protection. The partially soluble inhibitive pigments work by releasing oxidative and other species into the film close to the metal surface and react with it to form a tightly adhering impermeable film that prevents dissolution of the metal at the anode (Guy, 2004). For ferrous metals, these inhibitive pigment oxides include chromates, phosphates, molybdates, borates and complexes formed from these families of compounds (Guy, 2004; Bierwagen and Huovinen, 2010).

If possible, a primer should also act as a barrier coat (Guy, 2004). Pigments can have considerable influence on moisture transport in paint films as they decrease the volume fraction of the binder material, where moisture transport primarily takes place (van der Wel and Adan, 1999). Due to their hydrophobic and lamellar properties, extender pigments are often used in the primer, which also acts as a barrier coat. Coatings formulated with lamellar pigments impede the transport of aggressive species by providing a tortuous path of diffusion as they often align parallel to the substrate surface during film formation (Sorensen et al., 2009; Bierwagen and Huovinen, 2010). Extender pigments or fillers are less costly than coloured pigment or other special pigments, but they play a very important role in the formulation of paint (Guy, 2004). In coatings insufficiently pigmented with spherical pigments, the aggressive species can migrate almost straight through the coating (figure 46) (Sorensen et al., 2009). Including anti-corrosive pigments in the build coats or finishes is pointless and a waste of expensive pigment as it is not next to the substrate surface. In a build coat film extenders are used, the type and volume of extender dictating its barrier properties. The additional barrier properties provided by the build coat give maximum impermeability (Guy, 2004). Micaceous iron oxide (MIO), essentially a type of hematite (Fe_2O_3) is the most widely used lamellar pigment for anticorrosive barrier coatings (Sorensen et al., 2009).

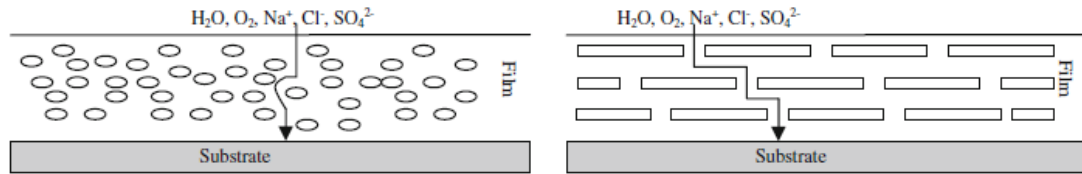


Figure 46 Idealised illustration of the effect of barrier pigments. The aggressive species can migrate almost straight through the coating, in coatings pigmented with spherical pigments. The aggressive species are provided a tortuous path of diffusion, when the coating contains lamellar pigments (Sorensen et al., 2009)

The formation of a barrier layer over anodic areas, passivating the surface is promoted by passivating pigments, which should have minimum solubility to avoid leaching out of the coating film (Wicks et al., 2006c). However, after exposure to humid conditions the use of passivating pigments may lead to blistering. Since the mid-nineteenth century red lead (Pb) pigment Pb_3O_4 (2 to 15% PbO), has been used as a passivating pigment in oil primers, and was used on rusty, oily steel for air dry application (Wicks et al., 2006c). Widespread prohibition of its use has resulted because of its toxicity.

As long as highly hydrophilic pigments are avoided, high pigmentation reduces O_2 and H_2O permeability of the final combined film (Wicks and Jones, 2013). Pigments are in fact the least expensive component of most primers (Wicks and Jones, 2013).

Metallic pigments (essentially small particles of zinc or alloys of zinc of 4-7 μm in size) are included in primers to prevent electro-chemical dissolution by acting sacrificially as the anode in the corrosion mechanism. Media such as inorganic and organic silicates, epoxy, chloro-rubber and other inert polymers are used to formulate zinc-rich primers (Guy, 2004).

3.2.2.3.3 Solvents and Additives

Solvents

Added to dissolve or disperse other constituents of the formulation, solvents reduce the viscosity of liquid coatings and are traditionally a major part of an organic coatings (Sorensen et al., 2009). Anticorrosive coatings can be classified by their solvent content (figure 47 and table 23). Cost, environmental and legal arguments place severe restrictions on the type of solvents that can be used and restrict their quantities (Bierwagen and Huovinen, 2010).

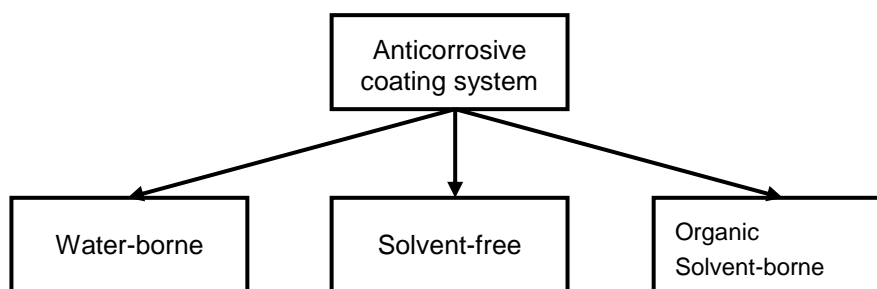


Figure 47 Anticorrosive coating systems classified according to solvent content (Sorensen et al., 2009)

Table 23 Most commonly used liquid carriers of pigment and binders used in paints extracted from Turner (1988)

Liquid	Comments
Water	The main ingredient of the continuous phase of most emulsion paints. Can be used alone or blended with alcohols or ether-alcohols to dissolve water-soluble resins or dyestuffs. Advantages: availability, cheapness, lack of odour, non-toxic and non-flammable. Disadvantages: limited miscibility with other liquids and the film-formers designed to be dissolved or dispersed in it usually remain permanently sensitive to it.
Aliphatic hydrocarbon mixtures: chiefly paraffins	Usually supplied as mixtures due to the difficulty of separating the individual compounds. Many of the mixtures also contain a percentage of aromatic hydrocarbons e.g. white spirit (155-195 °C) approximately 15% aromatic.
Terpenes	Commonly used versions are turpines, dipentene and pine oil. <ul style="list-style-type: none"> • Turpentine varies with grade – principally α-pinene. Replaced by white spirit as the main solvent for house paints. • Dipentene is mainly limonene • Pine oils are mixtures mainly of terpene alcohols Can be used as anti-skinning agents
Aromatic hydrocarbons Alcohols Esters Ketones	Supplied to the paint industry as fairly pure named compounds, but proprietary names are used for some aromatic mixtures which are sold cheaply.
Ethers and ether-alcohols	Ethers are not commonly used. Ether-alcohols are very common (contain both the ether (-C-O-C-) and alcohol (-C-O-H-) groups).
Nitroparaffins	Uncommon solvent due to cost and evidence of toxicity
Chloroparaffins	Uncommon solvent as rather toxic

For solvents, the most important properties are:

1. Solvency
2. Viscosity or consistency
3. Boiling point and evaporation rate
4. Flash point
5. Chemical nature
6. Toxicity and smell
7. Cost

These properties are considered in more detail in table 24 with numerical data for properties 1-4 (Turner, 1988) but only solvents linked with this research have been presented.

Table 24 Solvent properties – data extracted from Turner (1988)

Solvent	Formula	Solvency		Viscosity at 20 °C (centipoises)	Boiling point (°C)	Flash point (closed cup) (°C)
		H-bonding group	Solubility parameter			
Water	H ₂ O	III	23.4	1.002	100	None
Aliphatic Hydrocarbons						
White spirit (WS)		I	6.9		155-195	33 ^m
Odourless WS		I				180-207
Aromatic Hydrocarbons						
Toluene	C ₆ H ₅ .CH ₃	I	8.9	0.55*	111	4
Xylene	C ₆ H ₄ .(CH ₃) ₂	I	8.8	0.586	138-144	27
Alcohols						
Ethanol	C ₂ H ₅ OH	III	12.7	1.200	78	14
Esters						
Butyl acetate	CH ₃ .CO.O.C ₄ H ₉	II	8.5	0.671*	127	23
Ketones						
Acetone	CH ₃ .CO.CH ₃	II	10.0	0.316*	56	-17

* at 25 °C; ^m = minimum

The solvent remaining in the coating long enough for the coating to complete film formation, and then evaporating without compromising the development of the coating properties, is a primary consideration for coatings protecting against corrosion (Bierwagen and Huovinen, 2010). The time required to convert a coating to a dry film and the appearance and physical properties of the final film are affected by evaporation rate (Wicks et al., 2006f), which changes flow rate, due to increased consistency caused by a rise in 'solids' (Turner, 1988). Barrier properties are reduced by residual solvent, which acts as a plasticizer lowering the effective T_g . Where polymer crosslinking occurs, full development of coating properties will not occur if the solvent leaves the film before reactions are complete.

The evaporation rate of water acting as a solvent is affected by RH, in addition to the four variables below which also affect evaporation rates of other solvents (Wicks et al., 2006f):

1. temperature
2. vapour pressure
3. surface/volume ratio
4. flow rate over the surface.

The temperature at and near the metal surface decreases as solvents evaporate. Thermal diffusion from within the sample and its surroundings warms the sample, whilst latent heat of evaporation cools the surface. Rapid thermal diffusion maintains the surface temperature so it will not fall much during evaporation, but if it is slow a sharp drop in surface temperature results (Wicks et al., 2006f).

While a combination of several solvents are used in organic solvent-borne coatings to balance the evaporation rate and dissolution of the viscous polymeric binder (Sorensen et al., 2009), this research utilises a single solvent.

Additives

Paints typically contain between 0.01 and 1% additives along with resins, solvents and pigments. Some properties required by a paint are difficult to achieve, thus paint additives can be used to impart these specific properties to the paint (e.g. better slip, flame retardance, UV stability) or they can be used to prevent defects in the coating (e.g. foam bubbles, flocculation, sedimentation) (Stoye and Freitag, 2007a). Additives can be classified by the following groups:

1. Corrosion inhibitors
2. Defoamers
3. Driers and catalysts
4. Light stabilisers
5. Preservatives
6. Rheological control agents
7. Surface additives
8. Wetting and dispersing additives

3.3 Substrate Properties

The performance and durability of an anti-corrosive coating is affected by a number of variables (figure 33) (Sorensen et al., 2009). A coating system also includes the substrate and coating/substrate interface and therefore the substrate type and its surface condition that is influenced by cleaning, surface preparation, pre-treatment, roughness and recoat interval.

3.3.1 Type of Substrate

The selection of metals for making building components, large structure, vehicles and machinery depends on the properties needed in each case (table 25) (Godfraind et al., 2012). Ferrous alloys where Fe content is higher than any other element and the carbon content is < 2% is steel.

Chemical composition divides steel into unalloyed and alloyed grades in line with EN 10 020. To be classed as an alloy steel, the limiting values quoted in table 26 must be reached or exceeded by the content of an individual element in at least one case. For unalloyed steels, the level of an individual element should not reach or exceed the limiting concentrations (Schauwinhold et al., 2003). The addition of other elements can often improve the protective nature of some corrosion layers that form on metals and alloys. The corrosion rate of mild steel can be reduced to roughly the same rate as wrought iron if 0.2% copper (Cu) can be added to it (Evans, 1972).

Table 25 Uses of architectural ferrous metal (adapted from Metals from the English Heritage Practical Building Conservation Series (Godfraind et al., 2012))

Ferrous Metal	Characteristics	Appearance		Corrosion resistance	Architectural applications, period of common use and other comments
		Cut section	Oxidised colour		
Wrought iron	Manufactured by smithing, giving a characteristic layered and fibrous appearance	Fibrous grey	Reddish-brown	Low – needs coating	Fastenings, small fittings e.g. locks, chains and hinges, railings and gates, beams and tie bars. 2500 BC to late 19 th century, large components from 18 th century onwards.
Cast iron: common or grey	Contains flakes of graphite: broken surfaces appear greyish, and form planes of weakness	Granular grey	Reddish-brown	Much more resistant than steel	Fireplaces, railings, load-bearing structures (panels, columns, beams). 15 th century to present. Can be cast into intricate shapes.
Cast iron: Spheroidal graphite or ductile	Malleable metal produced by melting grey cast iron with Mg: graphite forms spheres rather than flakes	Granular grey	Reddish-brown	Much more resistant than steel	Water pipes, grids, and other types of fittings at risk of breakage. 20 th century to present. Can be the same strength as grey cast iron for half of the weight.
Cast iron: white	Extremely hard and resistant to abrasion, but very brittle	Grey-white	Reddish-brown	Much more resistant than steel	Crankshafts. 20 th century to present. Extremely hard and abrasion-resistant
Cast iron: malleable	Produced by heating and treating white cast iron	Grey	Reddish-brown	Much more resistant than steel	Locks and other fittings, small components for water systems. 20 th century to present. Good ductility.
Pure iron (Swedish iron, butter iron, Armco iron)	Workability and strength similar to wrought iron, but homogeneous			Poor – needs coating	Early 20 th century and up to present.
Steel: carbon steel	Contains carbon (C), Mn and Si, and possibly other elements. Strong, malleable, easy to weld, excellent rigidity. Can be cast, machined and extruded.	Granular shiny grey	Reddish-brown	Poor – needs coating	Used extensively for structural applications 1880 to present Most important commercial form of Fe. Different qualities available: rimming steel fully-killed and semi-killed steel (deoxidised with elements such as aluminium (Al) or Si, so there is less gas evolution during solidification).
Steel: low alloy	Alloying improves tensile strength, but also resistance to corrosion.	Grey	Fine and sandy, darkens with time.	Poor – needs coating	Cladding, roofing. Early 19 th century to present. Can be cast into intricate shapes.
Steel: stainless	Many different alloys. May be cast or machined.	Grey	Reddish-brown	Good to very good	Cladding, roofing, decorative finishes. Early 20 th century to present. Stronger than carbon steel. Ferritic SS is alloyed with Cr (11-27%). Austenitic SS is alloyed with Cr (17 to 19%) and Ni (8 to 12%).

Table 26 Concentration limits of elements for classification as base or alloy metal (Schauwinhold et al., 2003)

Element		Limiting concentration %
Symbol	Name	
Al	Aluminium	0.10
B	Boron	0.0008
Bi	Bismuth	0.10
Co	Cobalt	0.10
Cr	Chromium*	0.30
Cu	Copper*	0.40
La	Lanthanides (assessed separately)	0.05
Mn	Manganese	1.65***
Mo	Molybdenum*	0.08
Nb	Niobium**	0.06
Ni	Nickel*	0.30
Pb	Lead	0.40
Se	Selenium	0.10
Si	Silicon	0.50
Te	Tellurium	0.10
Ti	Titanium**	0.05
V	Vanadium**	0.10
W	Tungsten	0.10
Zr	Zirconium**	0.05
Others (except C, N, O, S), each		0.05

* If two, three or four of these elements are present in concentrations less than the maximum permitted, their total concentration must not exceed 70% of the sum of the maxima.

** The same rules apply to these elements.

*** If the manganese content is quoted as minimum, this value applies.

Steels are divided further by the standard EN 10 020 into quality groups table 27.

Carbon steels and low-alloy steels are relatively inexpensive alloys of iron, with ~0.05 to 1% carbon (Jones, 2013) they are the most widely used construction material (Schweitzer, 2010). Low alloy steels usually contain < 2% other alloying elements that are added mainly for improved mechanical properties. Even in relatively non-corrosive conditions, carbon and low-alloy steels often require protective coatings as they have relatively low corrosion resistance (Jones, 2013). Greater resistance is conferred to them by small amounts of Ni, Cr, Al and molybdenum (Mo) often in combination with Cu, than mild steel with the addition of

Cu. Low alloy steel containing 0.5% Cu, 1.0% Cr, 0.16% phosphorus (P) and 0.8% Si corrodes at about one-third of the rate of ordinary mild steel in the atmosphere and with time the corrosion rate of low-alloy steels tends to fall off. A class of low-alloy structural steels that develop an adherent, protective rust layer during atmospheric exposure are described by the term ‘weathering steels’ (Townsend, 2001) and these do not require painting.

Table 27 Quality groups used to divide steel further in the standard EN 10 020 (Schauwinhold et al., 2003)

Quality group	Comments
Base steels	No special processing required during manufacture. Generally unsuitable for heat treatment.
High-grade unalloyed steels	No consistent response to heat treatment. No purity requirements specified. Stricter/more numerous requirements in terms of fracture toughness, grain size control, and formability, compared to base steels due to stresses that arise in use so their manufacture requires special care.
High-grade alloy steels	Generally unsuitable for quenching and tempering or surface hardening. Contain levels of alloying elements to give the special properties but are used for similar applications as high-grade unalloyed steels.
Special carbon steels	Contain fewer inclusions and are of a higher purity than high-grade steels. Show a consistent response to treatments such as quenching and tempering or surface hardening for which they are mostly intended. By precise control of chemical composition and special care in manufacture and process control procedures a wide range of working and application properties are achieved e.g. high-strength, or hardening properties within closely controlled limits, together with high specifications for toughness, forming and welding properties.
Alloy special steels	There is precise control of their chemical composition, special methods of manufacture and process control. They are able to have an extremely wide range of working and application properties. Steel for structural engineering, pressure vessels, mechanical engineering steel, stainless and heat-resistant, creep-resistant, bearing and machine tools steels, as well as steels with physical properties etc. are all included in this group of steels.

Townsend (2001) presented previously unpublished test results of research by Bethlehem Steel carried out during the initial development of their weathering steel, compiled from data and reports in the research files. This data was used to determine values for each elements’ contribution to the development of protective rust at 3 sites (figure 48). P had the largest beneficial effect on corrosion resistance and while Si, Cr, Cu, and Ni, are well known for their beneficial effects, the beneficial effects shown for tin (Sn) and Mo were not well so known and were not included in the ASTM G101 guide. S promotes corrosion and was another element not

included in ASTM G101. S is kept as low as possible during alloying as it is also harmful to the mechanical properties of steel.

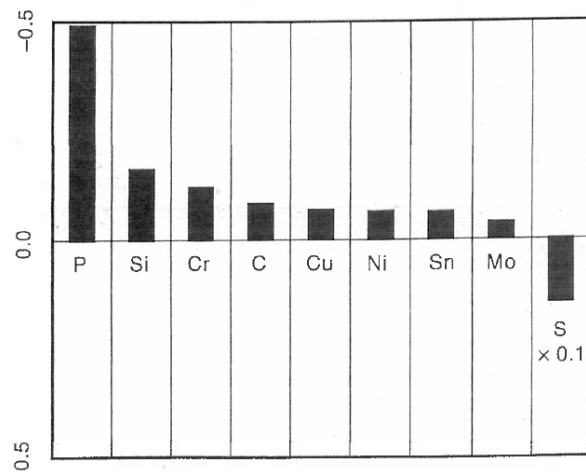


Figure 48 Effect of elements on corrosion based losses based on the value of b averaged over the test sites (higher negative values indicate less corrosion) (Townsend, 2001)

Stainless steels are Fe-based alloys containing at least 10.5% Cr. They are classified into groups, each with special characteristics: ferritic, austenitic, duplex, martensitic, and precipitation hardening (Jones, 2013). The formation of a bi-layer film consisting of outer iron oxide and inner Cr-rich oxide results from air oxidation of stainless steels (Hashimoto et al., 2007). Consisting of Cr and sometimes Mo alloyed with Fe, ferritic stainless steels are immune to Cl⁻ SCC.

Austenitic stainless steels, developed for use in mild and harsh corrosive conditions, are widely used in industry (Pardo et al., 2008a; Jones, 2013). The addition of Ni to Fe-Cr alloys leads to corrosion resistance, which primarily originates from a thin, hydrated, oxidised Cr-rich passive surface layer (Pardo et al., 2008a, b; Jones, 2013). Resistance to Cl⁻ pitting and SCC is improved by the addition of 3% Mo in Type 316 SS. Higher alloyed stainless steels are more resistant to pitting in Cl⁻ and higher acid concentrations. Austenitic stainless steels are attacked at intermediate concentrations of sulfuric acid but are resistant to very dilute and high concentrations. As passive films are attacked by HCl acid, no SS can be used with it. Cl⁻ and dissolved O₂ must be controlled to prevent SCC in boilers for the usual austenitic stainless steels.

Duplex stainless steels (DSS) are defined as 'a family of steels that have a two phase ferritic-austenitic micro-structure, where both components are stainless containing > 13% Cr (wt%)'. They are Cr-Mo alloys of Fe with Ni and N austenite

stabilisers in sufficient quantities to achieve a balance of ferrite and austenite (Jones, 2013). The ferrite provides resistance to SCC and the austenite ductility, Mo improves pitting resistance and strengthens the passive film, and carbides prevent the sensitisation to inter-granular corrosion by grain boundary precipitation as they tend to precipitate at the disperse austenite-ferrite interfaces (Jones, 2013). The advantages of DSS compared to austenite steels include:

- Higher mechanical strength,
- Superior resistance to corrosion,
- Lower price due to low Ni content.

Chosen primarily for mechanical strength, the martensitic and precipitation hardening stainless steels have lower corrosion resistance than other grades of stainless steel, thus limiting their applications to mild environments. They are also susceptible to hydrogen induced cracking because of the high-strength levels (Jones, 2013).

A summary of the effects of a wide variety of alloying elements on corrosion properties is displayed in table 28 and corrosion rates of different ferrous metals in marine, industrial and urban environments is shown in table 29 (Godfraind et al., 2012).

Table 28 Alloy elements and their effect on corrosion properties

Alloying element	Steel type researched	Effect on corrosion properties	Reference(s)
Cr	Weathering steels	Enhances compactness, densification and adhesion of corrosion layer, decreasing diffusion of O ₂ to the substrate. Forms stable oxyhydroxide films even in aggressive HCl acids.	(Chen et al., 2005a; Chen et al., 2005b)
	Fe-Cr and Fe-Ni-Cr steels	Pitting potential (U_p) increases with Cr content and as pitting occurs if the value of U_p is exceeded, increased content of Cr reduces the likelihood of pitting. In Cr-depleted zones pitting can start.	(Hougardy et al., 2003)
Ni	Low-alloy steels	Provides excellent corrosion resistance due to the formation of spinel double oxide in an inner layer. Mainly present as bivalent oxide in the spinel oxide. Not possible to differentiate from Fe ₃ O ₄ by X-ray diffraction (XRD). Ni-bearing steel has a low R_{rust}^* value in the early stages, but it increases considerably as the rust formation progresses. Improves the density of the inner rust layer.	(Nishimura et al., 2000; Nishimura and Kodama, 2003)
Cu	Weathering steels	Can accelerate the uniform dissolution of steel by segregating during dissolution of Fe and adsorbing on the surface of the steel. In the early stages promotes rust formation, but then enriches the layer resulting in enhanced protection and densification of the corrosion layer.	(Chen et al., 2005a; Chen et al., 2005b)
Si	Weathering steels	Should increase corrosion resistance as it enriches the rust layer and may enhance protection and densification of the rust layers.	(Chen et al., 2005a; Chen et al., 2005b)
	Austenitic steels	1-2% Si improves resistance to oxidation and especially carburisation, since an inner film of SiO ₂ below Cr ₂ O ₃ retards oxidation and carburisation.	(Hougardy et al., 2003)
Co (cobalt)	Low-alloy steels	Provides excellent corrosion resistance. Exists mainly as trivalent oxide in FeOOH. Co-bearing steel has a large R_{rust}^* value at the beginning of rust formation.	(Nishimura et al., 2000)
	Stainless steels	In the active regions of stainless steels Mo forms a passive MoO ₂ film, which decreases the active dissolution current. In the passive region of transition metals and valve metals Mo is usually dissolved and in the transpassive state. If the oxyhydroxide film is stable the inner MnO ₂ film acts as an effective barrier against diffusion of matter through the film as it is protected by the outer oxyhydroxide layer.	(Hashimoto et al., 2007)
Mo	Fe-Cr and Fe-Ni-Cr steels	U_p increases with Mo content, therefore increased content of Mo reduces the likelihood of pitting (Mo is more effective than Cr).	(Hougardy et al., 2003)
	Stainless steels	Shifts the cathodic polarisation curve to lower current densities reducing the corrosion rate.	(Pardo et al., 2006)

P	Low-alloy steels (weathering steels)	Has the largest beneficial effect on corrosion resistance, but due to its harmful effect in structural steel on toughness and weldability it is normally limited to a maximum of 0.04%. It is thought that the high corrosion resistance provided by small quantities, is as a result of PO_4 concentrating in the defect areas and not in the corrosion itself.	(Townsend, 2001; Nishimura and Kodama, 2003)
Ti (titanium)	Weathering steel	Lowers the strain energy when added in combination with some substitutional elements e.g. C and N	(Chen et al., 2005a; Chen et al., 2005b)
	SS	A stabilising element that can suppress inter-granular corrosion as it ties up carbon in a very stable carbide	(Hougardy et al., 2003)
Mn	Weathering steel	Believed to make no significant contribution to enhance the corrosion resistance of weathering steel.	(Chen et al., 2005a; Chen et al., 2005b)
	Stainless steels	Traditionally considered austenite former. Often added to increase the solubility of N. Reduces resistance to pitting corrosion as associated with the formation of MnS inclusions that are known to be precursor sites for pitting attack.	(Pardo et al., 2008b)
Al	Low-alloy steels	Provides high corrosion resistance due to the formation of spinel double oxide in an inner layer	(Nishimura and Kodama, 2003)
N	Duplex stainless steels	Replaces Ni for stabilising austenite, due to more rapid formation of austenite during welding and improved corrosion properties, specifically resistance to pitting corrosion. Increased N and reduced C content improves weldability.	(Nilsson, 1992)
	Fe-Cr and Fe-Ni-Cr steels	Has been found to be more effective at increasing U_p , than Cr and Mo and thus reduces the likelihood of pitting more effectively than Cr or Mo.	(Hougardy et al., 2003)
Nb (Niobium)	Stainless steels	Ties up C in a very stable carbide suppressing inter-granular corrosion as it is a stabilising element.	(Hougardy et al., 2003)

* R_{rust} – the high frequency resistance component obtained from alternating current impedance measurements.

Summary of references included within this table (Nilsson, 1992; Nishimura et al., 2000; Townsend, 2001; Hougardy et al., 2003; Nishimura and Kodama, 2003; Chen et al., 2005a; Chen et al., 2005b; Pardo et al., 2006; Hashimoto et al., 2007; Pardo et al., 2008b)

Table 29 Corrosion rates of ferrous metals in different environments (adapted from Metals from the English Heritage Practical Building Conservation Series (Godfraind et al., 2012).

Ferrous Metal	Environment			Corrosion product, coating type and comments
	Marine	Industrial	Rural	
Cast Iron (grey, white, ductile and malleable)	General corrosion Can suffer from graphitisation if fully or partly submerged in seawater. Typically loses 1 µm/yr	General corrosion above ground. General or pitting if buried in soil. Buried ductile iron is usually subject to pitting. Typically loses 0.7 µm/yr	General corrosion above ground. General or pitting if buried in soil. Buried ductile iron is usually subject to pitting. Typically loses 0.5 µm/yr	Corrosion product is hydrated iron oxide (rust) Frequently protected by paint coatings Very low corrosion rates in normal environments Corrosion rate decreases with exposure, as the corrosion products stiffen further attack.
	General corrosion	General corrosion	General corrosion	Corrosion product is delaminated layer of hydrated iron oxide (rust). Normally protected by paint or sometimes by Zn coatings Little corrosion rate data currently available. Corrosion products are non-protective; rates of loss remain constant with ongoing exposure. Can sometimes be subject to internal corrosion, resulting in delamination throughout body.
Wrought Iron	No available data on rates of loss but generally < mild steel. If exposed in damp stone (cramps, tie bars and restraints etc.), corrosion can be up to 100 µm/yr.	No available data on rates of loss but generally < mild steel. If exposed in damp stone (cramps, tie bars and restraints etc.), corrosion can be up to 100 µm/yr.	No available data on rates of loss but generally < mild steel. If exposed in damp stone (cramps, tie bars and restraints etc.), corrosion can be up to 100 µm/yr	
	General corrosion Sometimes pitting, especially if mill scale is present. Corrosion rates vary significantly depending on proximity to the sea; highest rates in tidal zone	General corrosion Sometimes pitting Corrosion rates increase sharply with pollution (especially SO ₂)	General corrosion Sometimes pitting	Steel containing between 0.25-0.5% C with ~ 2% of Mn and Si. Corrosion product is hydrated iron oxide (rust). Always protected by paint, Zn or other metallic coatings Corrosion products flake off and are therefore non-protective; rates of loss remain constant with ongoing exposure.
Carbon Steel / Mild Steel	Tidal zones: loss rate 250 to 620 µm/yr (depending upon exact situation and temperature) Submerged: loss rate 60 to 110 µm/yr	Typical loss rate 90 to 170 µm/yr, depending upon local pollution. Buried: loss rate 10 to 20 µm/yr Submerged: loss rate 10 to 70 µm/yr	Typical loss rate 50 to 70 µm/yr Buried: loss rate 10 to 20 µm/yr Submerged: loss rate 40 to 50 µm/yr	

Ferrous Metal	Environment			Corrosion product, coating type and comments
	Marine	Industrial	Rural	
Low-Alloy Steel	General corrosion, sometimes pitting that slows with time. Corrosion rate strongly dependent on location. Typical loss rate 150 µm/yr, decreasing to 15 µm/yr after 5 years	General corrosion, which slows with time. Corrosion rate typically about 50 µm/yr, decreasing to 5 µm/yr after 5 years	General corrosion, which slows with time. Corrosion rate typically about 30 µm/yr, decreasing to 3 µm/yr after 5 years	2-3% alloying elements, typically copper chromium and nickel. Typical examples for architectural applications are the weathering steels containing Cu and Cr. Weathering steels initially corrode to form a rust layer, but wetting and drying allows pores and cracks to fill; this layer becomes protective and corrosion slows. Not used where metal will be immersed or buried.
Ferritic Stainless Steel	Mainly localised corrosion e.g. pitting and crevicing in protected areas not washed by rainwater, where Cl ⁻ can build up. Rate of pitting may be up to 100 µm/yr depending on the situation	Localised pitting and crevicing in some conditions.	N/A	Contains at least 12% Cr. Relatively brittle. Cr-rich surfaces can depassivate in high Cl ⁻ concentrations, leading to a general brown staining of the surface. Super ferritic stainless steels with Cr contents > 25% were introduced in the 1970s for improved corrosion resistance.
Austenitic Stainless Steel	Occasionally some pitting and crevicing in protected areas not washed by rainwater. Normally corrosion resistant	N/A Normally corrosion resistant	N/A Normally corrosion resistant	Contains at least 18% Cr and 8% Ni; may also include Mo, Cu, Ti and Nb. Far more corrosion resistant than ferritic stainless steel. Introduced in the 1920s with the well-known 18Cr-8Ni; many hundreds of similar alloys now available.

3.3.2 Substrate Preparation

The service life of a coating is also governed by the level of surface preparation achieved (Bortak, 2002). The surface needs to be cleared of any contaminants such as local corrosion, old paint layers, mill-scale, grease and oil, dust and dirt, soluble salts and water. Guidance on surface preparation in the heritage sector is limited in scope, although well-intentioned, the methodologies are often difficult to translate into a practical context and the evidence is rarely quantified and frequently conflicting (Emmerson and Wakinson, 2013).

3.3.2.1 Cleaning Method

For the cleaning and stabilisation of iron, a considerable number of methods have been published in conservation literature but they are mostly based on mechanical stripping, chemical stripping, electrochemical stripping and electrolytic reduction (Blackshaw, 1982). Some of the stripping methods also double as stabilisation treatments as they are said to aid the removal of soluble chloride from rusted iron (table 30).

Grit blasting is employed at the Tank Museum and for standardisation purposes, samples in this project are being cleaned and prepared by air abrasion (air jet micromachining - AJMM). The parameters used for air abrasion must be standardised to achieve uniform surfaces on metal samples and include blasting pressure, angle, stand-off distance, grit size and type, which determine the roughness obtained, economy, efficiency and quality of the whole process (Momber, 2008; Poorna Chander et al., 2009). Cleaning process parameters can generally be divided as shown in figure 49 and for successful application, optimisation of the process is a prerequisite (Momber, 2008).

Paint layers erode layer by layer exhibiting behaviour consistent with ductile material (Parslow et al., 1997). The classic ductile erosion curve (figure 50) for metal surfaces has maximum erosion rate between the blasting angles of 20-30°, but the maximum erosion rate is shifted for paint layers to a blasting angle of 45-60° (Parslow et al., 1997). To achieve the best erosion rate of the remaining paint layers and clean the samples back to a fresh clean metal surface removing any corrosion products and/or mill scale present, a low blasting angle of 30-45° should be used.

Table 30 Cleaning Methods for Historic Ferrous Metalwork (Godfraind et al., 2012)

Cleaning Method	Type of ferrous metal			
	Wrought iron	Cast iron	Mild steel	Stainless Steel
Scapers Brushes	Relatively good control and visibility, but slow. Do NOT use steel brushes	Relatively good control and visibility, but slow. Do NOT use steel brushes	Relatively good control and visibility, but slow. Do NOT use steel brushes	Do NOT use steel brushes
Power brushes	If used with care	If used with care	If used with care	Depends on bristle material
Sanding Abrasive flap-wheels Angle grinders	Not recommended	Not recommended	Not recommended	Not recommended
Dry abrasive Blast cleaning	Not recommended	Not recommended for cast iron with fine decorative detail		Fine abrasives acceptable if used with care
Wet abrasive Blast cleaning	Slow but effective	Slow but effective	Slow but effective	Slow but effective
Needleguns Descaling chisels	Risk of surface damage	Risk of surface damage	Effective	
Flame cleaning	Considered particularly suitable, as loose mill-scale and rust only is removed	Do NOT use Risk of damage from thermal shock	Slow but effective	
Cold-water Pressure washing	Effective for salt removal	Effective for salt removal	Effective for salt removal	Effective for salt removal
Warm-water washing	Effective for salt removal	Effective for salt removal	Effective for salt removal	Effective for salt removal
High-pressure steam	Removes oil/waxes/grease	Removes oil/waxes/grease	Removes oil/waxes/grease	Removes oil/waxes/grease
Mild detergents	Removes oil/waxes/grease	Removes oil/waxes/grease	Removes oil/waxes/grease	Method normally used to remove surface stains
Releasing oil	N/A	N/A	N/A	Sometimes used on surface stains on cladding
Cream Polishes	Removing rust stains	Removing rust stains	Removing rust stains	Removing rust stains
Acid cleaners	2-5% phosphoric acid (pickling acid), useful for heavy rust-staining	2-5% phosphoric acid (pickling acid), useful for heavy rust-staining	2-5% phosphoric acid (pickling acid), useful for heavy rust-staining	Do NOT use materials containing hydrochloric acid or bleaches with sodium hypochlorite
Chemical dips and gels	Suitable only for dismantled work	Suitable only for dismantled work	Suitable only for dismantled work	Suitable only for dismantled work

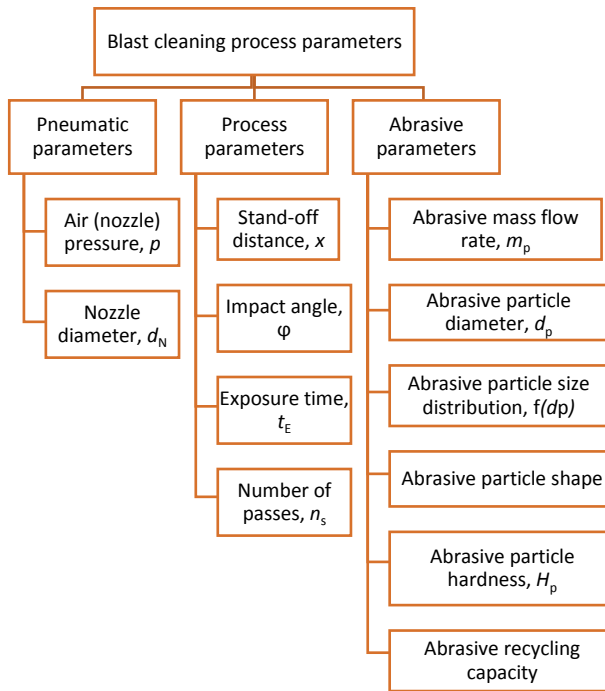


Figure 49 Parameters involved in the blast cleaning process, information taken from (Momber, 2008)

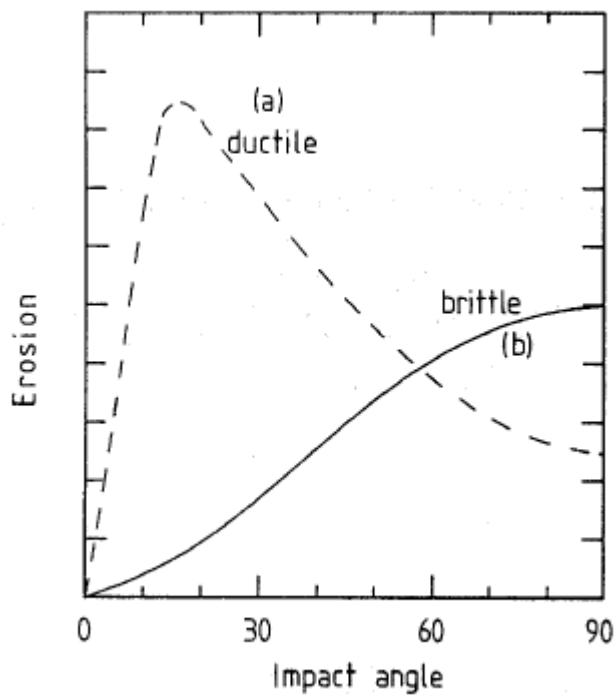


Figure 50 Angle dependent erosion rate for typical ductile and brittle material (Finnie, 1995; Wensink, 2002).

3.3.2.2 Surface Preparation

To encourage chemical and physical bonding between a coating and substrate, preparation of the substrate surface prior to coating is essential (Momber et al., 2002). Where physical bonding between coating and substrate is a concern, a rough surface finish is normally favoured and this also enhances the strength of adhesive joints (Harris and Beevers, 1999). Strong coating to metal adhesion can influence the corrosion process as it can reduce delamination and act to inhibit corrosion (Deflorian and Fedrizzi, 1999). Why adhesion is good or bad, which adhesion mechanism is operating and what the composition of the thin coating layer next to the substrate is, are rarely known. The perception is that loose contaminated layers are removed by the abrasive process and a degree of mechanical interlocking or “keying” with the adhesive is provided by the roughened surface (Harris and Beevers, 1999). Grit blasting is an economical and efficient method to provide a suitable surface profile and therefore it is widely used (Momber et al., 2002).

Angled blasting has two main effects: one is digging up or scratching and the other is indentation on the surfaces of the substrate (Amada and Hirose, 1998).

Scratching is dominant at the low blasting angle 45° , indentation is shallow, resulting in low adhesive strength due to a fairly smooth profile. High adhesive strength is generated using a blasting angle of 75° as the digging up mechanism mostly forms the profile, it also includes many hook shapes (Amada and Hirose, 1998). The indentation mechanism is dominant at a blasting angle of 90° and this profile does not include as many hook shapes as the profile formed by a blasting angle of 75° . Poorna Chander et al. (2009) found that with blasting angles up to 80° the roughness increased, however a decrease in roughness is caused by further increasing the blasting angle to 90° . Therefore, once the paint and corrosion has been eroded from samples using a low blasting angle a higher blasting angle of 75° - 80° should be employed to achieve the best adhesive surface in preparation for coating.

A side effect of grit blasting is embedded grit in the blasted surfaces (Griffiths et al., 1996; Amada et al., 1999) that is worst with a 90° blast angle. With embedded grit being worst at 90° , this supports the argument for employing a blasting angle of 75° - 80° , as adhesive strength of coatings decreases with residual grits. Removal of loose grit particles and dust after blasting, is not discussed with the exception of

Harris and Beevers (1999) who describe a jet of clean dry air being blown across the substrate surface.

Care has to be taken not to over-blast as craters begin to overlap as the erosion process continues. Adjacent craters form combined lips and create higher peaks, whereas strikes by following particles cause ductile tearing and result in some lips being detached (Griffiths et al., 1996). With continued impacts, the topography experiences further changes as some peaks become flattened, reducing the peak to valley height, which reduces adhesion of coatings to the surface (Griffiths et al., 1996). This data was used to devise surface preparation methodology for this project.

3.3.3 Coating Performance

The performance of a coating film is affected by its state after film formation, its chemistry, as well as its end-use and implies an estimate of the service life (Marrion, 2004). Fundamental mechanistic studies, long-term in-service or outdoor exposures and short-term, laboratory-based exposures, are three sources of data that can be used for generating service life predictions (figure 51), along with experience, specialist knowledge and published results (Martin et al., 1996).

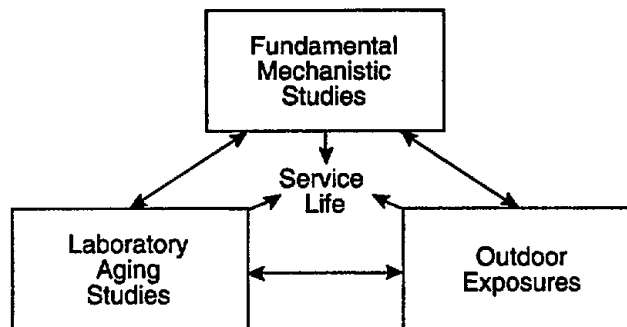


Figure 51 Quantitative service life data is available from three primary sources (Martin et al., 1996)

By using accelerated aging (short-term, laboratory-based aging) and fundamental mechanistic experiments, reproducible experimental results can be generated. Fundamental information about failure modes and mechanisms causing coating system degradation is derived, as it is possible to control the intensities of individual weathering factors (Martin et al., 1996). How well a coating is carrying out its function in service defines its performance (Marrion, 2004).

3.3.3.1 Causes and Nature of Failure

Failure of a coating can generally be linked to formulation deficiencies, application problems, inadequate surface preparation or external factors. There are many contributing factors to consider when evaluating breakdown mechanisms causing coating failure (Fitzsimons and Parry, 2010).

1. Those arising during application e.g. sagging and cissing
2. Those arising after application, prior to service entry e.g. blushing and wrinkling
3. Those appearing after entry to service e.g. chalking.

Especially in the industrial and marine coatings industry, application-related failures are common due to basic application faults e.g. inadequate film thickness, misses, lack of stripe coating, incorrect over coating times, and inadequate curing times and temperatures prior to entry into service, frequently leading to early coating failure (Fitzsimons and Parry, 2010).

Exposure to a variety of possible stresses produces irreversible changes that cause failure (Marrion, 2004). Tensile stress (effective perpendicularly to the interface) and shear stress (along the plane of contact) (figure 52) affect both the bulk material and the bond strength at the interface (Zorll, 2006). Paint becomes detached from the substrate by differences in the coefficient of expansion due to temperature variations and loss of adhesion can result from chemical absorption at the interface after penetrating through the coating (Zorll, 2006).

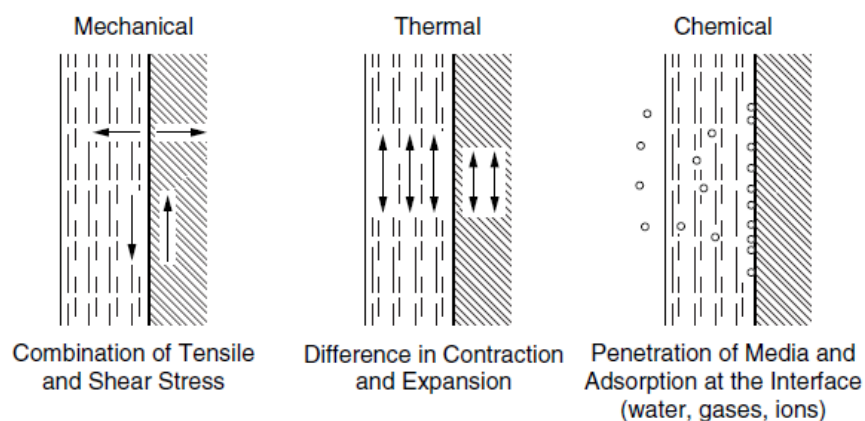


Figure 52 External factors putting the bond between coating and substrate under stress – potentially leading to failure (Zorll, 2006)

Common failure modes for architectural coatings include chalking, gloss loss, fading, dirt retention, blistering, corrosion, cracking and peeling (figure 53) (Martin et

al., 1996; Marrion, 2004). Decomposition of the binder by UV radiation causes the majority of cosmetic defects (Sorensen et al., 2009).

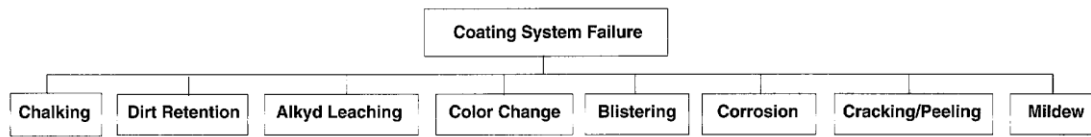


Figure 53 Architectural coatings common failure modes (Martin et al., 1996)

Reduced adhesion between the organic coating and the substrate is often the first sign that an organic coating is degrading, where there are no apparent defects and it is exposed to a high RH or constant immersion (Sorensen et al., 2009). Blistering and delamination (figure 54) are severe forms of visible failure. Blisters are generally a first sign of deterioration (Zorll, 2006) and result from the high water solubility of cathode reaction products producing an osmotic pressure, while the alkalinity of these products causes bonds to break at the coating-metal interface resulting in delamination (Sorensen et al., 2009).

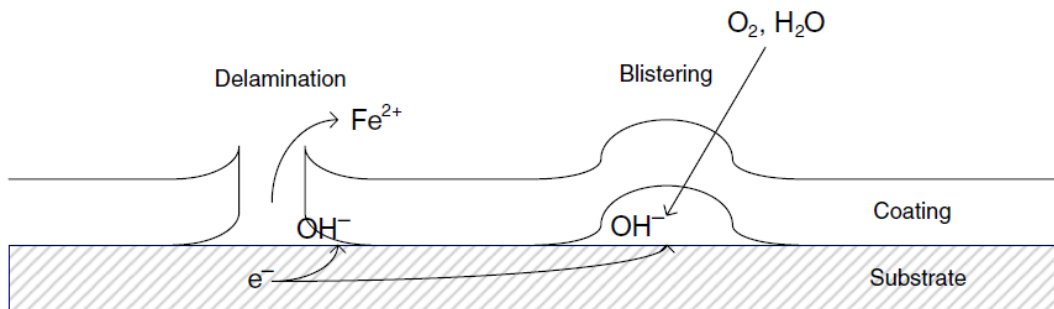


Figure 54 Idealised sketch of delamination and blistering (Sorensen et al., 2009)

The five root faults, partitioned into sub-faults in figure 55 are normally credited with failure of a coating system (Martin et al., 1996), and many of these basic faults have been discussed to some degree early in this chapter.

Table 31 lists many different types of coating failure or defect and the probable causes, but focuses on those more commonly seen on historic ferrous metal used for armoured vehicles and gates and railing. It is seldom that knowledge of underlying degradation mechanisms are complete. In fact, where coating systems fail by corrosion the underlying failure mechanism is poorly understood (figure 56) (Martin et al., 1996). The fault tree (figure 56) is a useful method for summarising and categorising the variables which could be the cause or a contributing factor for corrosion to occur, most of which have been discussed in this chapter or in chapter 2.

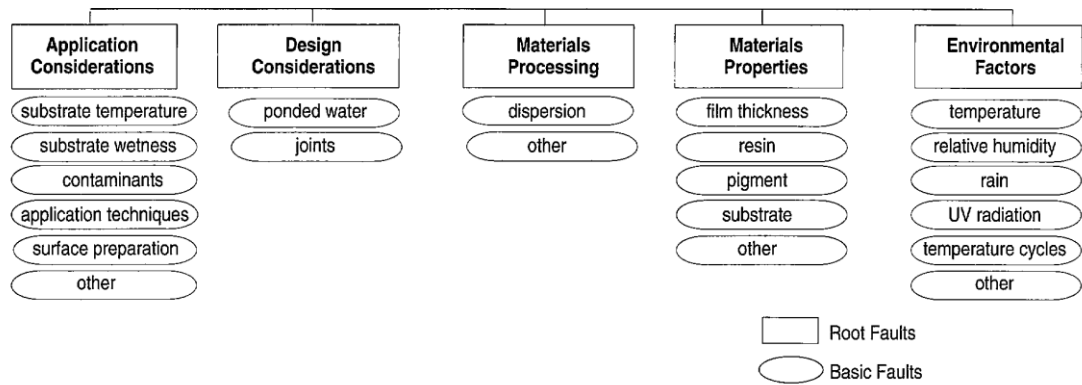


Figure 55 Common faults - root and basic associated with architectural and non-architectural coating system failures (Martin et al., 1996)

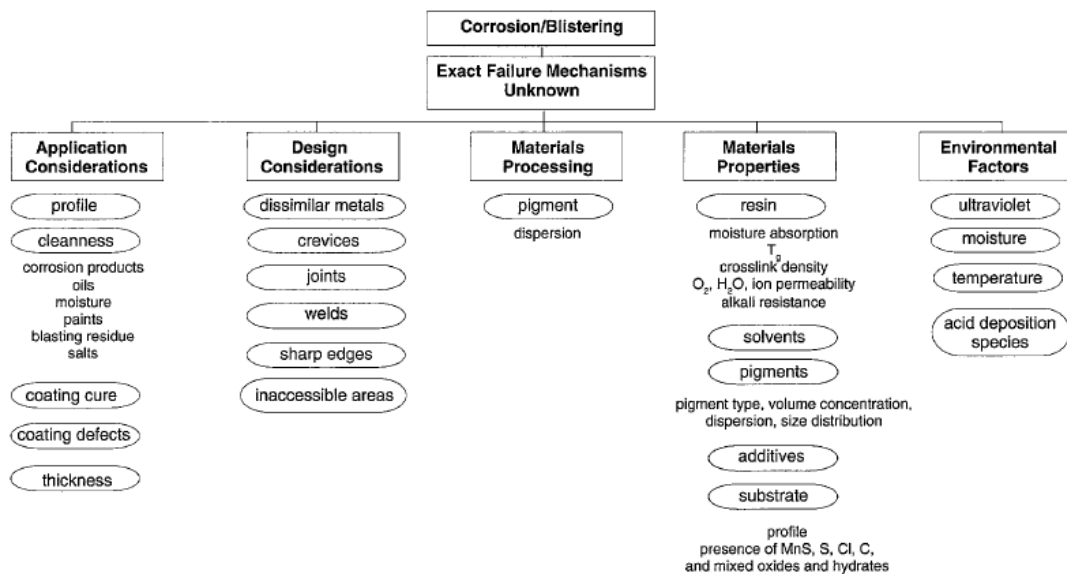


Figure 56 Fault tree - Underlying failure mechanisms are poorly understood where the loss of protection is due to corrosion (Martin et al., 1996)

3.3.3.2 Assessment of coating performance

This relies upon laboratory testing to a large degree and field trials to simulate in-service conditions (Fitzsimons and Parry, 2010). Monitoring changes in appearance and/or protection performance characteristics is used to evaluate the degradation of a coating system over time and its performance (Martin et al., 1996). Corrosion rates are often quantified by calculating the surface area (SA) of the sample that is covered with corrosion. This works well for uniform corrosion but not where corrosion is localised, where corrosion rates can be underestimated or filiform corrosion where corrosion is superficial but looks aggressive and corrosion rates are overestimated. Furthermore, this method cannot be applied to surfaces which are already corroded.

The traditional way to verify corrosion resistance of new materials and products, especially for testing new surface treatment systems or coatings for corrosion protection, was and still is field site exposure testing. Short-term/laboratory testing has to be of an accelerated nature and cannot cover all of the in-service variables; hence any formulation problems are only likely to come to light from long-term use of the product (Fitzsimons and Parry, 2010).

Table 31 Some of the most common types of failure or defect and probable causes, (information taken from Fitzsimons and Parry (2010))

Type of failure or defect		Description	Probable Cause
Adhesion failure	Adhesion failure	Where a coating has failed to adhere to the substrate or underlying paint.	Can be a result of internal stress or internal stress plus the exacerbating effect of one or more other factor. The contributory factor(s) could be related to formulation, inadequate surface profile, surface contamination, exceeding over-coating times, application to a glossy paint surface, amine bloom, incorrect surface preparation, and differential expansion/contraction of the paint coating and the substrate.
	Flaking	Detachment of the paint from the substrate. A form of adhesion failure where the paint flakes from the substrate and is a familiar sight on galvanising.	Incorrect paint system used. Either no pre-treatment or incorrect pre-treatment used for certain substrates e.g. non-ferrous or galvanised. Can be attributed to differential expansion and contraction of paint and substrate.
	De-lamination	Usually inter-coat detachment in a multi-coat system. Loss of adhesion between coats of paint.	Delamination defects are generally related to contamination between layers, including amine bloom, exceeding overcoat times, or application to a glossy surface, provided compatible paint materials have been used.
Bittiness		Contamination of the film by bits of paint skin, gel, flocculated material, or foreign matter, which project above the surface to give a rough appearance. When the particles are small and uniformly distributed the term peppery is used.	Paint skin, gelled particles, airborne sand and grit, or contamination from brushes or rollers causing contamination within or on the surface of the paint film is the main cause.
Blistering	Osmotic blistering	May contain liquid or gas, or may be dry. Local loss of adhesion from underlying surface, where dome-shaped projections form in the dry paint film.	Commonly associated with the presence of soluble salts, soluble pigments, retained solvents or the absorption and retention of low molecular weight water-miscible solvents, typically from the carriage of chemicals.
	Non-osmotic blistering		Often described as cathodic blistering and found as a circular pattern of blisters around a coating defect where the substrate is exposed. It can occur due to cold-wall effect producing condensation. H ₂ gas is possible where coatings are used with cathodic protection, and the resultant H ₂ vapour pressure could produce blisters.

Bloom (blush)	Loss of gloss and a dulling of the colour results from a hazy deposit on the surface of the paint film, resembling the bloom on grapes.	Exposure to condensation or moisture during curing (common phenomenon with amine-cured epoxies).
Bridging	Covering unfilled gaps e.g. cracks or corners, with a film of the coating material causes a weakness in the paint film, which can crack, blister, or flake off.	High-viscosity paint, poor application, or failure to brush paint into corners and over welds.
Brushmarks (laddering, ladders or ropiness)	After brush application where the paint film has not flowed out undesirable ridges and furrows that remain in a dry paint film. Where alternate coats have been applied in opposite directions it can be found as a cross-hatch (laddering). When the brush marks are pronounced they are known as ropiness.	For brush application the viscosity of the material may be too high, incorrect thinner used in the paint, poor application technique or inadequate mixing. The application pot-life may have exceeded if it is a two-pack paint.
Bubbles or bubbling	Should not be confused with blistering. Bubbles may be intact or broken to leave craters within a paint film and appear as small raised blisters. Found in excessively thick paint films, especially spray applied and also roller application.	Solvent/trapped air within the coating, which is not released before the surface dries. Also associated with factory-applied coating, applied by dipping, electrodeposition, or roller coating.
Cracking (alligatoring and checking)	Visible cracks in paint coatings, which generally penetrate to the substrate. Cracking can range from minor to severe cracking and comes in several forms.	Generally related to internal stress within the body of the coating. Formulation, high film thickness, thermal cycling, substrate geometry, substrate movement, ageing, absorption/de-sorption of water or chemicals, and inadequate surface profile are factors involved in cracking. The internal stress in the coating is exacerbated by one or more contributory factor(s).
Cratering	Small bowl-shaped depressions in the paint film, should not be confused with cissing	Burst trapped air bubbles that leave small craters as the coating dries and the coating has had insufficient time to flow out as a uniform film.
Erosion	Selective removal of paint films from areas of high spots.	More prominent on brush applied coatings due to uneven finish; it is the wearing away of the paint film by various elements e.g. rain, snow, wind, sand, etc.
Filiform (corrosion)	Random threads corrosion that develop beneath thin lacquers and other coating films from a growing head or point. Described in previous chapter.	Damage to the coating or contamination on the metallic substrate, allows a corrosion cell to develop and advance under the coating
Grit inclusions	Dust and grit particles adhering to or embedded within the coating system.	Prior to application of the paint – failure to remove used blast cleaning abrasive from the surface.
Growth (on the surface of paint film)	Attachment and growth of natural organisms to the surface of finished products - vary in form, size and lifespan e.g. algae, mosses, etc.	Natural organisms within moist, wet, or immersed conditions. After attachment growth may continue.
Impact damage (star cracking)	Cracks that radiate from a point of impact.	Damage to a relatively brittle coating due to impact. Often seen on glass fibre reinforced plastics.

Misses/skips/holidays	Exposed areas of previous coat or substrate when the intention was to coat the entire area. Could be restricted to one coat within a multi-coat system.	Lack of quality control, poor application or both.
Pinholes	Minute craters or holes, which form in wet paint during application and drying, due to air or gas bubbles that burst, but fail to coalesce before the film dries	A common problem when coating porous substrates such as zinc-filled primers, zinc silicates and metal-sprayed coatings, solvent or air becomes entrapped within the paint film.
Rust spotting (rash rusting)	Frequently starts as localised spotting but rapidly spreads over the surface – fine spots of rust that appear on a paint film, usually a thin primer.	Where the rust spotting originates from the substrate, probable causes are low film thickness, pinholes, and defects in the steel e.g. untreated laminations, or too high a surface profile causing penetration of peaks through the paint film. Where rust spotting does not originate from the substrate, ferrous grinding debris can probably be found within the coated surface as metallic contamination.
Solvent lifting	A weak surface and ultimate coating breakdown can be caused by eruption of the surface of the paint film by blistering and wrinkling.	Over-coating before the previous coat has adequately hardened or incompatible paint system used, topcoats with a strong solvent blend can attack underlying coatings with a weaker solvent blend.
Solvent popping	Soon after application solvent bubbles appear on the surface of the paint film.	Porous surfaces, incorrect solvent blends, or wrong environmental conditions
Undercutting	The paint film is lifted from the substrate as corrosion travels beneath the paint film and in severe cases it appears as flaking, cracks and exposed rust.	Rust creep from areas of mechanical damage and/or application of paint to a corroded substrate and/or missing primer coats. Possibly due to inadequate preparation and coating thickness applied or lack of maintenance to areas of poor design or access.

Industry Testing: Accelerated corrosion

In industry, testing utilises repeatable procedures and more often than not standards are used as guidelines. To obtain good correlation with service exposure, cyclic wetting and drying is believed to be important in providing more realistic simulations of the atmospheric corrosion environment with intermittent exposure to salt solution often included (Vera Cruz et al., 1996; LeBozec et al., 2008).

The corrosion rate of samples can be estimated from their O₂ consumption, a method that was employed by Shashoua and Matthiesen (2010). This method makes it possible to test corrosion rates of already corroded samples but it is not possible to incorporate cyclic corrosion testing (CCT) as samples are encapsulated in sealed glass jars. This O₂ monitoring system utilises chemical optical O₂ sensor spots (also called optodes, PSt3 type) from PreSens, which are adhered to the inner surface of transparent materials such as glass (figure 57) allow the O₂ concentration to be measured quantitatively through the glass wall, (Matthiesen, 2007).

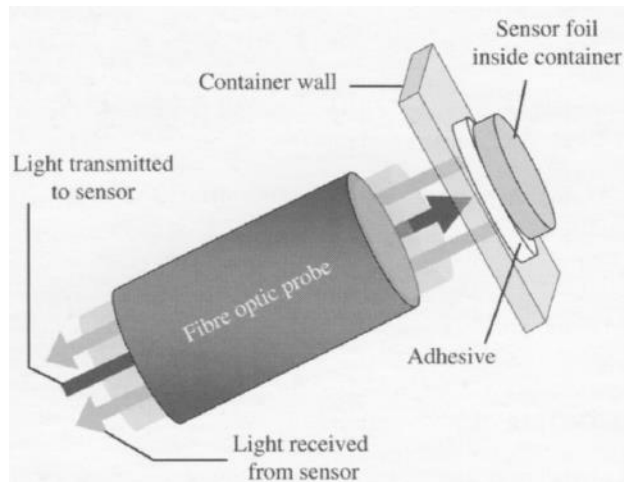


Figure 57 Oxygen-sensor spot glued inside the container, and light is transferred via fibre optic and measured through the transparent container wall (Matthiesen, 2007).

The fibre optic which is positioned against the outer surface of the transparent material, opposite the sensor spot emits light exciting luminescent dye in the sensor spot at one wavelength (figure 58). The sensor spot in response emits light at another wavelength. When O_2 is present, instead of emitting light, the energy of the excited molecule is transferred by collision with O_2 .

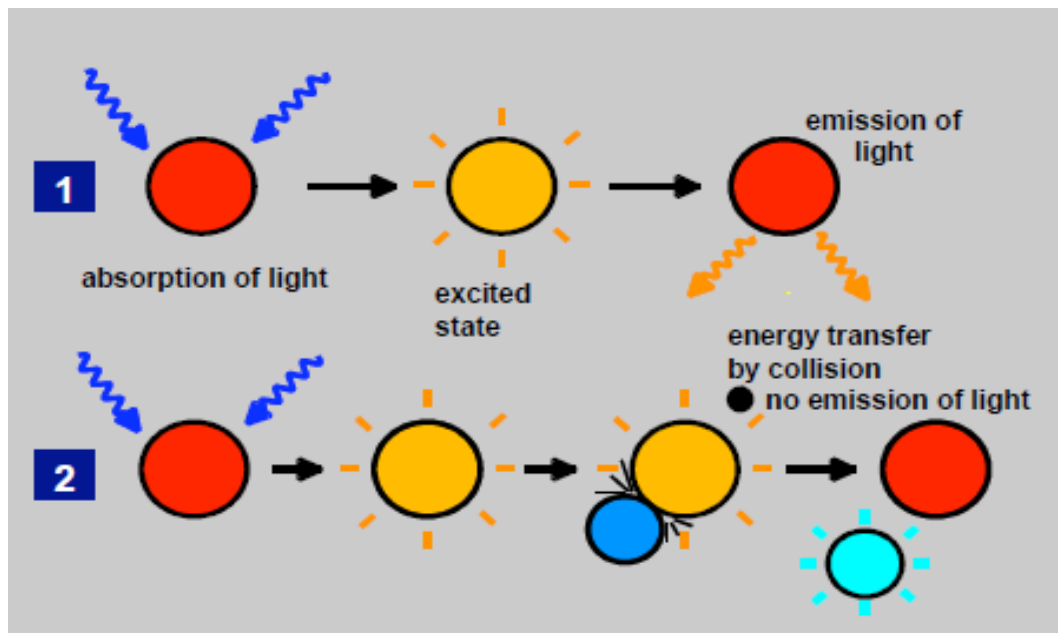


Figure 58 Working principle behind optical O_2 electrodes

1. The luminescent dye is excited by light at one wavelength and emits light at another wavelength.

2. When O_2 is present, the energy of the excited molecule is transferred by collision with O_2 instead of emission of light. Image taken from the appendix of the OxyMini Instruction Manual.

When testing the degradation of a coating it is often necessary to introduce artificial defects, as these initiate degradation of a coating system in a shorter time period. Industry commonly introduces a scribe in a coating before exposing it during accelerated corrosion tests. This kind of test is not only easier to set up, but also easier to interpret than tests such as electrochemical impedance, due to the complexity of the systems under study (Oliveira and Ferreira, 2003). Undercutting only occurs during alternate wetting and drying, not during continuous immersion, and is a result of the lifting action of compacted oxides. Although some observations summarised in figure 59 are possible, the mechanism is unclear (Jones, 2013)

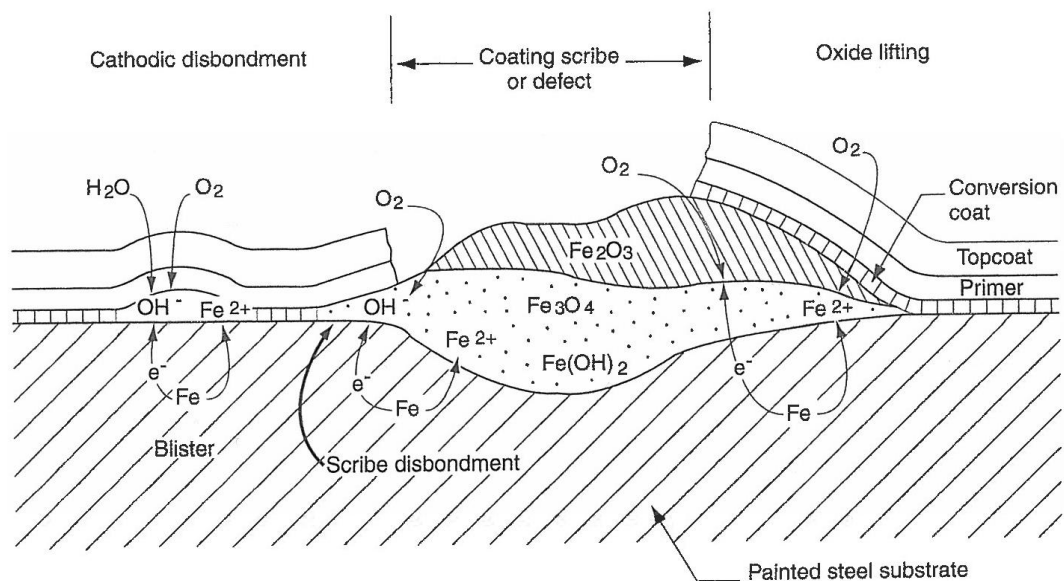


Figure 59 Representation of attack mechanisms at scribe in the coating (Jones, 2013)

A variety of compounds of various concentrations have been used for salt spray accelerated corrosion testing with varying degrees of comparability to in-service results. Dr J. B. Harrison and T.C. K. Tickle observed as early as 1962, that the performance of zinc phosphate primers was poor during accelerated salt spray testing, but they generally behaved excellently outdoors in an industrial environment (Cremer, 1989). Inconsistencies between real time and accelerated corrosion rate data and rankings have existed and been recorded for a long time. Harrison consequently used a mixture of the commonly occurring atmospheric salts ammonium sulfate ((NH₄)₂SO₄) and NaCl as a spray solution (table 32). The addition of sulfate represents to some extent an industrial atmosphere, but while the overall electrolyte solution is much more dilute than traditional salt spray (fog) in reality samples are cycled through a complete range of solution concentrations as

concentration increases with drying (Grossman, 1996). The commonly used test standard ISO 9227 (5% wt. NaCl) to calculate the durability of automotive products is not advised as it is now well known that it fails in replicating the type of degradation and ranking observed on automotive materials at natural weathering sites (LeBozec et al., 2008).

The standard neutral salt spray test e.g. ISO 9227 has been employed for decades to evaluate the corrosion performance of automotive materials (LeBozec et al., 2008). However, research by the Society of Automotive Engineers (SAE) Automotive Corrosion and Protection (ACAP) Committee, revealed the General Motors (GM) GM9540P Method B to be one of the preferred CCT methods for automotive cosmetic corrosion (painted or pre-coated metals) (Grossman, 1996). The salt solution used in this test includes components of typical road salt (table 32) (LeBozec et al., 2008) and the cyclic conditions involve short salt mist periods, room temperature dry-off, hot humid periods and hot dry-off (Grossman, 1996).

Table 32 Summary of salt solutions used for accelerated corrosion in the automotive industry (LeBozec et al. 2008), Harrison's salt solution and the prohesion test solution (Cremer, 1989; Grossmann, 1996)

Test Standard		Salt solution		Deposition rate in 80 cm ² mL/h
		Electrolyte (wt. %)	pH	
General Motors	GM9540P	NaCl - 0.9, CaCl ₂ - 0.1, NaHCO ₃ - 0.255	6.0-9.0	
Daimler Chrysler	KWT-DC	NaCl - 1	6.5-7.2	2
Renault	ECC1 D172028	NaCl - 1	4	5
Volvo VICT	VC 1027,149	NaCl - 1	4	120
VDA	VDA621-415	NaCl - 5	6.5-7.2	1.5
Volkswagen	PV1210	NaCl - 5	6.5-7.2	1.5
Neutral Salt Spray	ISO 9227	NaCl - 5	6.5-7.2	15
Harrison's salt solution		NaCl - 0.25, (NH ₄) ₂ SO ₄ – 3.25		
Prohesion (Protection is Adhesion)		NaCl - 0.05, (NH ₄) ₂ SO ₄ – 0.35-0.40	5.0-5.4	

Contradictions and misleading results are attached to salt spray testing.

Accelerated corrosion tests KWT-DC (Daimler Chrysler), GM9540P (GM), Renault ECC1 D172028 and Volvo VICT (Volvo indoor corrosion test) VC 1027,149 gave consistent life predictions of materials when comparing them to field data (LeBozec et al., 2008). This was not the case, however, for VDA621-415 (German

Association of the Automotive Industry -Verband der Automobilindustrie) and PV1210 (Volkswagen) tests that give quite similar results and ranking of materials; like the continuous neutral salt spray (NSS) test, these tests should not be used for the prediction of durability of steel based materials (LeBozec et al., 2008). However, Shashoua and Matthiesen (2010) employed the salt spray test DS/EN (Danish Standard/European Standard) ISO 9227 using a 5 % NaCl solution at 35°C for 504 hours for their research on heritage coatings. There is, therefore, a strong possibility that their results will not correspond to in-service results. The environment in which the coating is going to be exposed in practice should generally be the determining factor when choosing salts for accelerated corrosion testing (table 33).

Table 33 Extract from the summary by Bos (2008) of some standardized accelerated tests.

Test Method	Conditions
<i>Continuous salt spray tests</i>	
ASTM B117 ^a ISO 9227 (NSS) ^b DIN 50021 SS ^c JIS Z 2371 (NSS) ^d	Continuous, pH-neutral salt spray (5 % NaCl at 35 °C).
<i>Immersion test</i>	
ASTM D870 ^a	Coated specimens are partially or completely immersed in distilled or de-mineralized water at ambient or elevated temperatures.
<i>Humidity Tests</i>	
ASTM D2247 ^a ISO 6270 ^b	Coated specimens are exposed to atmosphere maintained at approximately 100 % relative humidity with the intention that condensation forms on the test specimens.

a – ASTM – American Society for Testing and Materials

b – ISO – International Organisation for Standardisation

c – DIN – Deutsches Institut für Normung e. V.

d – JIS – Japanese Standards Association

Since the TM is not situated in a marine environment and is in a rural location using NSS 5% NaCl solution would lead to unreliable results. The GM salt solution is more suited to this research project, since it is based on de-icing salt it is more likely to give life predictions consistent with real time atmospheric corrosion.

4 Conservation Approaches & Experimental Design

4.1 Guidance and specification in conservation of heritage ferrous metal

Conservation of heritage ironwork is often carried out by contractors and contracts are generally awarded to the lowest bidder (Topp, 2009), yet standards for delivering work programmes do not exist in heritage, unlike those offered by the International Standards Organisation (ISO). Conservation may employ some of these standards but they are often not suited to the heritage contexts. Reliance on qualitative data and the experiences of practitioners promoted by groups such as the National Heritage Ironwork Group (NHIG) and the Museums and Galleries Commission. Conservation requires research to generate data for producing evidence based standards to provide predictive performance and facilitate cost benefit calculations relative to ethical and aesthetic constraints within Heritage Conservation. Challenges exist here as well, as even in metal conservation research and testing of heritage materials the standards used to underpin methodology and interpret results are almost certainly going to be international standards such as ISO, BSI or DIN (Argyropoulos et al., 2013), rather than heritage specific standards.

As a minimum, the heritage sector requires qualitative data on the influence of different environments and treatment effectiveness (Williams, 2009a). The gold standard sought is quantitative assessment of treatment success set against treatment goals (Watkinson, 2010). This can be complex as quantitative data needs to be contextualised against resources, cost and object context, to assist in defining goals that can be used to create standards. Quantitative data that can be translated into hard currencies of object longevity, stability and survival is currently limited within metals conservation. Attainable and reproducible quantified outcomes allow the development of standards, thus, standardisation is key.

The study reported here seeks to standardise approaches to testing coatings by using a sensitive corrosion monitoring technique employed at Cardiff University (Rimmer et al., 2013; Watkinson and Rimmer, 2013; Emmerson and Watkinson, 2016) to assess coating performance by measuring corrosion rates in controlled conditions of temperature and RH. It is from such testing that a database for developing heritage specific standards can be built.

4.2 Approaches to Extending the Lifespan of Heritage Ferrous Metals

There are still many different approaches used to preserve ferrous metal and the approach chosen is largely dependent on where the object is or will be situated and whether it is still functioning. Thus, preservation approaches are largely influenced by the environment whether indoors or outdoors.

4.2.1 Indoor approaches

For ferrous metal objects housed inside a museum the two main threats are humidity and pollution (Museums Galleries Scotland, 2014). The approaches to indoor preservation include:

1) Environmental control

- a) **Air conditioning** - exerts influence over atmospheric pollutants and RH (Brimblecombe and Ramer, 1983)
- b) **Display cases** - create microclimates allowing RH to be controlled (Museums Galleries Scotland, 2014). Removal of air to prevent or stop corrosion is impractical as, as little as 3% O₂ in the gaseous environment can yield corrosion (Walker, 1982b). Display cases are a feasible option for museums unable to install air-conditioning systems for financial or structural reasons, especially if the ferrous metal objects are too delicate for open display (Brimblecombe and Ramer, 1983). RH within display cases is often controlled by moisture-absorbing desiccants e.g. silica gel, but an alternate option is to maintain a uniform temperature to prevent condensation or to keep objects warm (Walker, 1982b).
- c) **Storage** - often involves storing objects on open shelving, using boxes with lids, trays and dust covers. The best approach is the use of inert packing materials and storage furniture in well-sealed buildings. Use of dehumidifiers and heating larger spaces and silica gel in air-tight boxes for material such as archaeological iron should control RH to within desired levels as with display areas (Museums Galleries Scotland, 2014). However, air pollution is less easy to control as it is difficult to monitor.

- 2) **Protective coatings** - to mitigate corrosion of objects on open display (table 34).

Table 34 Coatings used by conservators in indoor environments in the UK

Coating	Comments	Organisation and Reference
Renaissance wax ²	Hot waxing is preferred as evidence suggests that hot waxing ³ is more protective than cold waxing (figure 60 a – hot waxed and figure 60 b – cold waxed) (Arnold, 2006; Schmuecker et al., 2010; Dalewicz-Kitto et al., 2013)	The Science Museum (Bird and Langfeldt, 2013)
Paraloid B72	5% solution in acetone used for objects such as the V2 rocket, classed as being too vulnerable to wax	
Paraloid B72	10-20% (w/v) solution in xylene/Shellsol A100 used. 48 hours is allowed to ensure layers were dry before additional layers were applied, which were thought to reactivate the layers below For large flatter surfaces.	Victoria and Albert Museum (V&A) (Thackray and Stevens, 2013)
Traditional Shellac		
TeCero-Wachs 30 201 microcrystalline wax	A 50:50 (w/w) mixture in white spirits Used in matte chased areas.	



Figure 60 (a) A hot-waxed lock after Hurricane Katrina; (b) A cold-waxed lock after Hurricane Katrina (Arnold, 2006)

² Renaissance wax is a mixture of 4 parts Cosmoloid H80 and 1 part polyethylene wax in a high flash point hydrocarbon solvent.

³ Hot waxing methods can vary; they involve heating the wax and/or object surface depending on whether a solid wax is being used or a wax liquefied by solvents.

4.2.2 Outdoor approaches

Outdoor historic ferrous metal can be found in many of forms:

- Monuments and sculptures
- Architectural ironwork e.g. gates or railings (figure 61),
- Industrial heritage
- Historic vehicles




Figure 61 South Gate of the Palace of Holyroodhouse

Coatings are the main approach used to preserve ferrous metal situated outdoors, with wax commonly used by conservation practitioners for monuments and sculptures, although other coatings are also used (table 35). Most historic ferrous metal such as gates and railings, historic vehicles and industrial machinery that are located outdoors have been protected by a multi-layer paint systems since being instated outdoors or since before leaving the manufacturers. A survey of outdoor paint layers detaching from historic ferrous metal around Scotland (table 36) emphasised modes of failure and maintenance regimes occurring.

Table 35 Coatings used outdoors by conservation practitioners

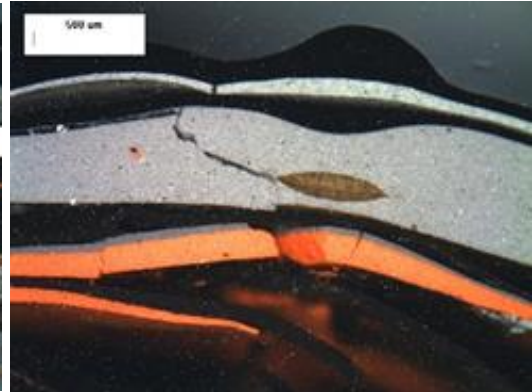
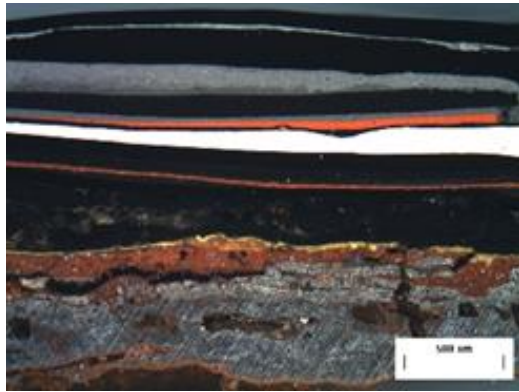
Coating	Application method	Museum/Company and reference
Renaissance wax - clear	Hot waxing – using a hot air gun to heat the metal surface. The wax is applied cold using a brush and again it melts on contact with the metal	The Barbara Hepworth Sculpture Garden (Lawson et al., 2013)
Renaissance wax – pigment used titanium white		
Bison wax		
Hammerite		
Incralac	Used on gold sections	
Carnauba and microcrystalline wax mixture - pigmented for surface patina.	Hot waxing - propane used for heating the metal surface and stippling wax on by brush. The wax melts on contact with the surface, allowing it to fill pores and cracks	Hall Conservation Ltd (Redman and Hall, 2013)

Table 36 Microscopy images of polished paint layer cross sections of samples collected around Scotland from historic ferrous metal at Historic Environment Scotland properties and one National Trust Scotland property with modes of failure and maintenance discussed



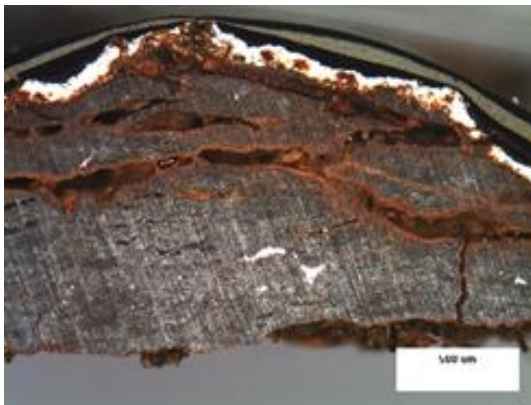
Broughty Castle

Cracking and lifting of paint layers in the 1st image. Multi-layer systems in both images and a visible attempt at maintenance. Possible application of primer over topcoat. Corrosion under paint in both images.



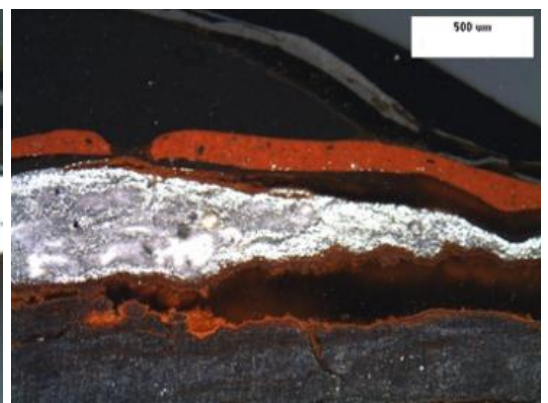
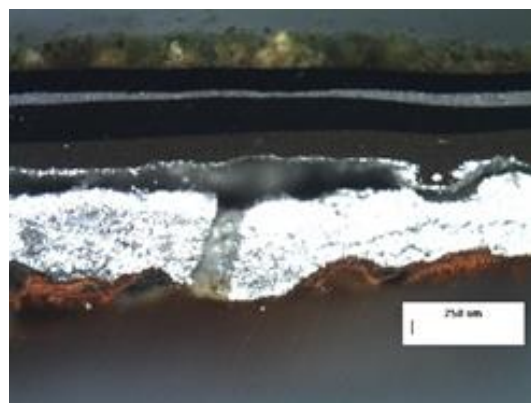
Dumbarton Castle

Under-layer and horizontal pitting corrosion are visible in image 1 in addition to delaminating paint layers. Image 2 shows cracking and air bubbles in the multi-layer coating system.



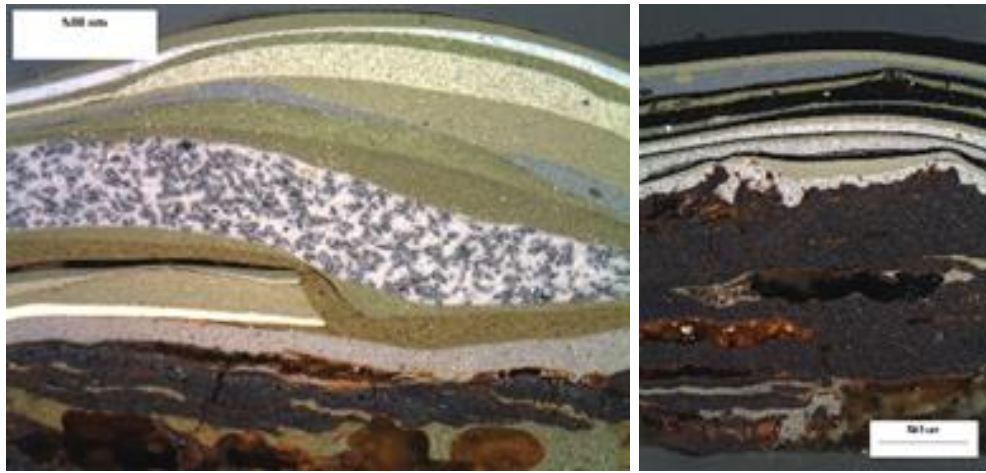
Dunstaffnage Castle & Chapel

Corrosion present at the paint-metal interface and within sub-surface cracks. Primer applied on top of past topcoats



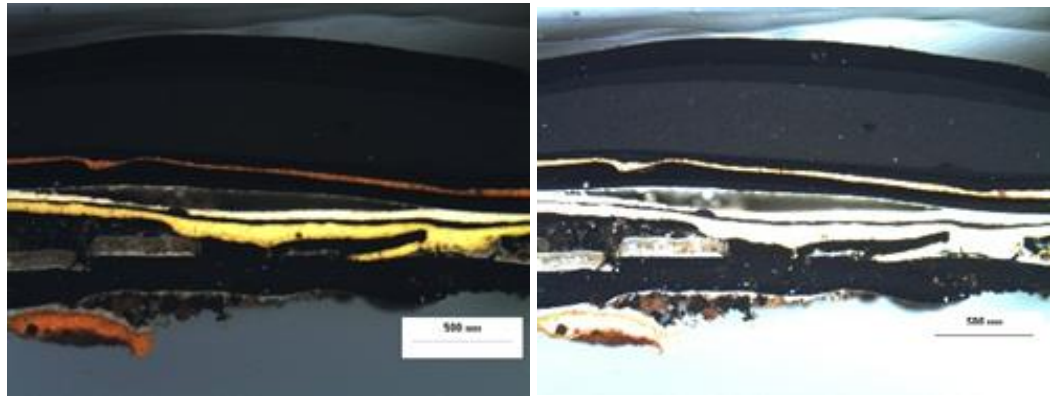
Fyvie Castle

Delamination caused by corrosion at the paint-metal interface. Separating paint layers with cracks and gaps. Biological matter on of the paint in the first image.



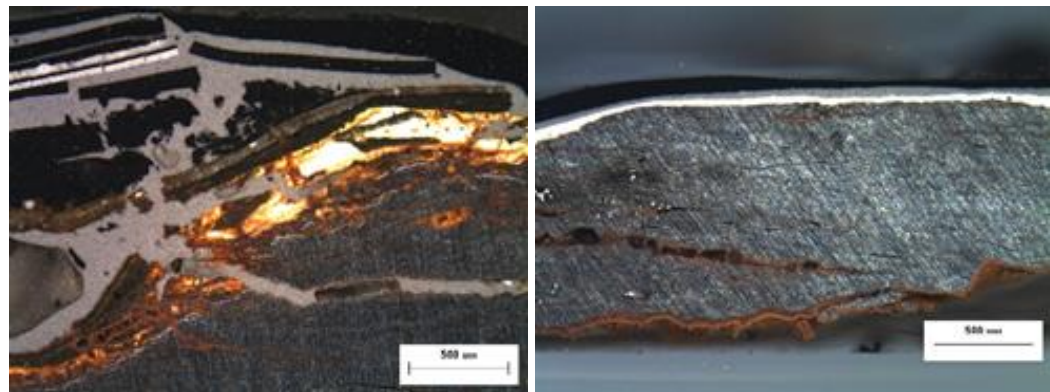
Fort George

Paint is applied around detaching metal. Corrosion is visible at the paint-metal interface and in cracks within the metal. Multiple layers of uneven thickness. Alternating between light and dark layers reveals missed areas image 2.



Palace of Holyrood House

Multi-layer system, with multiple black layers. Individual layers are more visible by varying the brightness, but this reduces the colour in the image. Delamination between layers. Corrosion under the paint.



St. Andrew's Cathedral

Corrosion at the paint-metal interface, image 1. Paint layers being used to consolidate detaching broken paint layers - evidence of maintenance. Newer thinner layers in image 2, with corrosion in the micro-cracks in the metal.

Causes and nature of coating failure was discussed in section 3.3.3.1, but these polished cross sections also reveal evidence of a variety of maintenance practices:

- Application of primer over old topcoat paint layers
- Multi-layer systems applied on top of multi-layer systems
- Consolidation of old broken layers with new

They also reinforce the need for standards for maintenance techniques, which provide answers to questions, such as:

- Should corrosion be cleaned off or coated over?
- Should old paint layers be cleaned off or consolidated and painted over?
- If coating over existing paint layers is recommended, how should it be done?
- Should a primer be used?

Primers containing metallic pigments e.g. zinc need to be applied to the ferrous metal surface to prevent electrochemical dissolution by acting sacrificially (3.2.2.3.2).

Much historic ferrous metal is at risk of being lost e.g. the 'Old Town Hall' in Dumfries (figure 62), which was completed in 1707, now referred to as the 'Midsteeple' (figure 63), narrowly avoided demolition in the early 1970s when the steeple was found to be leaning (Dumfries and Galloway Council, 2016). Thus regular maintenance is essential to prolong the life-span of outdoor historic ferrous metal.

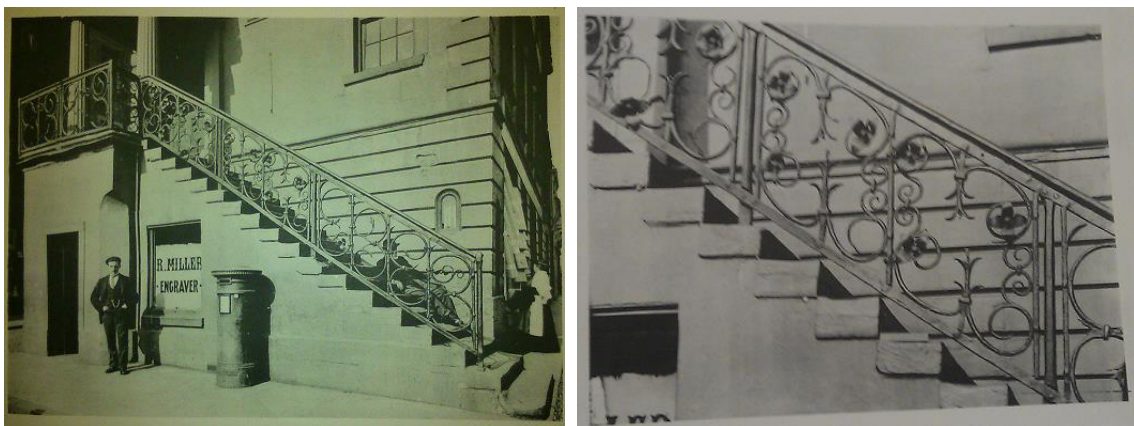


Figure 62 Dumfries Old Town Hall and stairway detail. Images of collotype reproductions of photographs taken from (Murphy, 1904)



Figure 63 Photograph of Dumfries Midsteeple ironwork taken March 2014

It is mainly external ironwork that suffers from atmospheric corrosion and is the subject of conservation work. Vehicle impact damage, missing components and the attentions of previous unskilled restorers are additional reasons why conservation might be required when dealing with architectural ironwork (NHIG, 2012).

In the absence of standards Historic Scotland created specialist inform guides e.g. 'The Maintenance of Iron Gates and Railings' (Davey, 2007) and the guide 'Boundary Ironwork - A guide to re-instatement' (Historic Scotland, 2005) to provide guidance and information for historic building owners. The message is clear, the most effective method of prolonging the life of ironwork is regular maintenance as decay and damage can be dealt with promptly if annual inspections are carried out.

As with other outdoor ferrous metalwork, historic vehicles and industrial machinery were originally coated with protective paint systems, which may now have suffered loss and require maintenance. Military and industry museums store large quantities of vehicles and equipment, which presents a major problem due to costs, maintenance and a lack of evidence based storage methods that would support predictive management.

The preservation processes vehicles and equipment undergo in museums are similar to the processes used by industry in "mothballing equipment" and by militaries who maintain prepositioned 'war reserves'. Mothballing is a relatively complete process and for vehicles or machines that are not being used for demonstration purposes in museums, a similar process is often carried out. Prepositioning entails only a 'partial preservation', but to deliver adequate corrosion protection, improved operational fluids or lubricating oil products had to be reformulated (Le Pera, 2004). For vehicles and equipment in museums, as with the vast majority of prepositioned vehicles and equipment, the RH should be maintained

at 40% and must remain within the range of 30 – 50%, with the temperature maintained between 15.6 and 26.7 °C (Le Pera, 2004). Provided the atmosphere is free of SO₂ and the vehicles and equipment have been cleaned of any salt contamination, maintaining the RH below 60%, a critical humidity level, should avoid corrosion (Syed, 2006). Trapped deionising salts may prove a problem in car underbodies. However, for vehicles and equipment on display outdoors the RH cannot be controlled, even indoors due to the large spaces required this is also unlikely in many museums.

The majority of vehicles and equipment within museums are stored, not displayed or demonstrated and so require a more complete preservation method like mothballing rather than the method used for prepositioned military vehicles and equipment. Therefore, new methods such those being tested by the Imperial War Museum, Duxford, need to be researched and trialled to find the best possible long-term storage method.

The Imperial War Museum (IWM), Duxford – Storage Trials

Only 5% of the historical military equipment at the IWM, Duxford is on show, the remainder of the equipment is either left to corrode outside or is housed in various types of hangers. The IWM and HITEK-nology Solutions Ltd are trialling a new storage system using a Matilda MK2 Tank and a Churchill Mk 7 tank (HITEK-nology Solutions, 2013). Inside and outside of the tanks VpCI 132 foam pads⁴ were positioned before they were wrapped in MilCorr and heat shrunk (figure 64).

To detect corrosion inside the bags low grade carbon steel plates were hung from the gun barrel and visually inspected via the MilCorr zip door. For comparison purposes additional plates were fitted in the areas surrounding the tanks (HITEK-nology Solutions, 2013). This storage solution is believed to protect the tank for a period of five years (Arkles, 2006; HITEK-nology Solutions, 2013).

Approximately seven and half months after positioning the plate within the 'bag' they showed no corrosion in contrast to the plate outside the bag (figure 65).

⁴ Cortec VpCI – 130 Series Foams are specially designed with vapour corrosion inhibitor impregnated throughout the foam's polymeric matrix. They provide excellent protection of ferrous, non-ferrous metals and alloys. They do not change critical chemical and/or physical properties of electronic components, and are suitable for protection of printed circuit boards. Cortec VpCI Foam Series conform to military standards MIL-PRF-81705D and NSN#6850-01-426-3539. Standard size - 10" x 10" x ¼" (25 cm x 25 cm x 0.64 cm). Protects up to 8 cubic feet (0.23 m³) per unit.



Figure 64 A “bagged up” tank in storage at the Imperial War Museum (IWM).



For large objects, this could be a feasible storage option. The cost for the IWM of ‘bagging’ a large item is in the range of £1500-£2000, with a significant discount. With the economy of ‘bagging up’ several vehicles at a time, prices could be reduced. To ‘bag up’ most of their items stored in 104 where the trial took place would cost in the region of £25k-£30k, which over a 20 year period could cost ~£150k (Delaney, 2015). Although not a small sum of money, it is considerably less than improving the building through major structural repairs or building new stores.



Figure 65 Front and back of two of the plates that were placed in position on the 1st October 2013 and were assessed on 19th May 2014. The plate from inside the bag (left-hand side of both images) suffered no corrosion, but the one in the area surrounding the tank has significant areas of corrosion (Delaney, 2015).

4.3 The Tank Museum, Bovington

The Tank Museum at Bovington, Dorset, one of the partners within this project, requires clarification of coating performance in a given context. The museum was set up in the 1920s but Bovington has been a base of military operations since the WW1 (Building Design Online, 2009). The collection held by the TM is designated as being of national importance. It is the most comprehensive vehicle collection of its kind in the world and receives over 1000 visitors per hour at peak times (King, 2006). The preservation of their vehicle collection is important and research into the best preservation strategies is vital.

4.3.1 The Environment

Of the 300 plus vehicles in their collection, approximately 140 were stored either in unheated, leaking sheds or outside (King, 2006; The Tank Museum, 2016). The VCC (figure 66) now houses a large proportion of these vehicles, removing the need for outside storage.



Figure 66 Vehicle Conservation Centre (VCC) - View from balcony open to the general public

Buildings at the TM do not have humidity control but their more recently constructed display hall employs overhead radiant heating panels to prevent condensation by raising the surface temperature of the tank hulls above dew point (Building Design Online, 2009). This provides an energy-efficient heating system. To carry the moisture in the air away quickly displacement ventilation is used, with large underground concrete ducts introducing fresh air (Building Design Online, 2009).

Within many of the vehicles the original leather and canvas fillings in their interior have already been removed for conservation and replaced with facsimiles (King, 2006). Desiccant gel is reportedly used for dehumidification within the tank's hull to conserve the interior with the electronics and instruments as with the hatches closed, this becomes a sealed environment (King, 2006). The exteriors of the

vehicles are largely resistant to decay except for corrosion, and it is the corrosion problem that is addressed in this study.

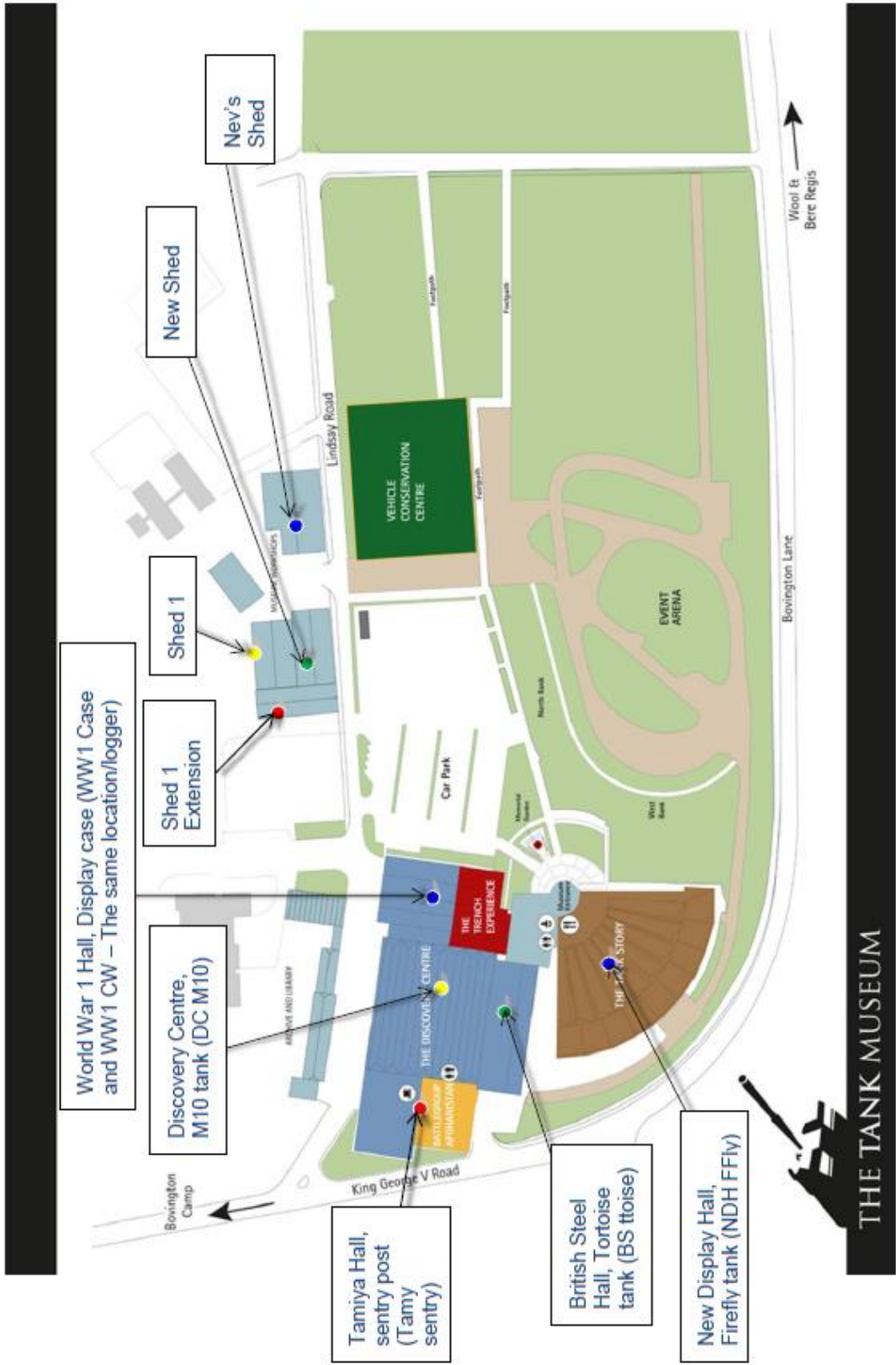
The TM monitors temperature and RH at various locations in the museum (figure 67). The map included indicates the locations of the data loggers placed around the museum. This offers insight into the ability of the environments to support corrosion but does not offer understanding of how these environments dictate the environment inside the vehicles, which may be crucial for preserving their heritage value.

4.3.2 Vehicle Preparation

The TM does not have a strict maintenance regime to which it adheres when preserving their vehicles. Where the historic paint layers have failed and the metal substrate is corroding, ethical implications have to be considered before a treatment plan can be decided upon. Minimal intervention is usually preferred, but questions need to be asked, such as:

- Where will the object be displayed or stored and will this environment prevent any further deterioration?
- Is intervention needed?
- Should the armoured vehicles be made to look as new or should the years of wear and tear be visible?
- Do the original coating layers have historical significance and need to be kept?
- Can they be removed or be only partially maintained?
- What type of coating is required?
- Do historic paints need to be used or are modern coatings more suitable?
- Are original paint layers safe for the general public?
- Is there a suitable colour match?
- Do modern coatings provide better corrosion protection?
- How many layers are required and how should it be applied?

The general methods used are described below.



THE TANK MUSEUM

Figure 67 Map of the Tank Museum site and locations of their data loggers monitoring the museum temperature and RH

4.3.2.1 Surface Cleaning and Preparation

Armoured vehicles are prepared for coating by removing large areas of original paint layers and corrosion by grit blasting (figure 68). Different grades of Guyson blast media (Saftigrit - aluminium oxide) are used by the TM for grit blasting.

4.3.2.2 Coating

Cromadex is one of many well-known brands in AkzoNobel's portfolio and their paints are used by the TM for coating armoured vehicles (table 37). When applying a new coating to one of their armoured vehicles, one coat of primer is used followed by one or two layers of topcoat depending on the final colour desired.

Paint at the TM is applied by brush, roller or spraying (see 3.2.2.1.1). The brushes and rollers (figure 69) used are disposable, reducing cross-contamination of the paints, the time and solvents needed for cleaning, and the cost as they are cheaper and possible obtain in bulk. Some products used at the TM are obtained by donations from local businesses.

Table 37 Cromadex paints used by the Tank Museum, Bovington

Cromadex Product Number	Topcoat or Primer?	Summarised Product Description	Application method and frequency of use
222	Topcoat	One pack fast air drying alkyd topcoat – semi synthetic – available in a range of colours and gloss levels including BS, RAL, metallic, sparkles and special matches – all lead chromate free	Brush application – used a lot
233	Topcoat	One pack air drying alkyd topcoat – semi synthetic – available in a range of colours and gloss levels including BS, RAL, metallic, sparkles and special matches – all lead chromate free	Normally sprayed
800	Topcoat	Two pack non-isocyanate acrylic topcoat – available in a range of colours and gloss levels including BS, RAL, metallic, sparkles and special matches – all lead chromate free	Generally not used, but when used, used with a hardener for use with trucks and vans
903	Primer	Two pack chromate-free etch primer - used to improve adhesion and corrosion resistance of all systems used over metal substrates - available in buff.	Generally not used, but when used, used with a hardener for use with trucks and vans
2100	Primer	One pack universal primer - available in white, grey, red oxide and buff as standard, it can also be tinted to ensure complete coverage even on difficult lead free colours.	Brush or spray application – red oxide version used a lot, sometimes toned down with matt black to imitate wartime primer that was much darker than modern red oxide/primer.



Figure 68 Machinery and safety equipment used by the Tank Museum for grit blasting armoured vehicles in preparation for painting (displayed by Mike Hayton, workshop manager at the TM).

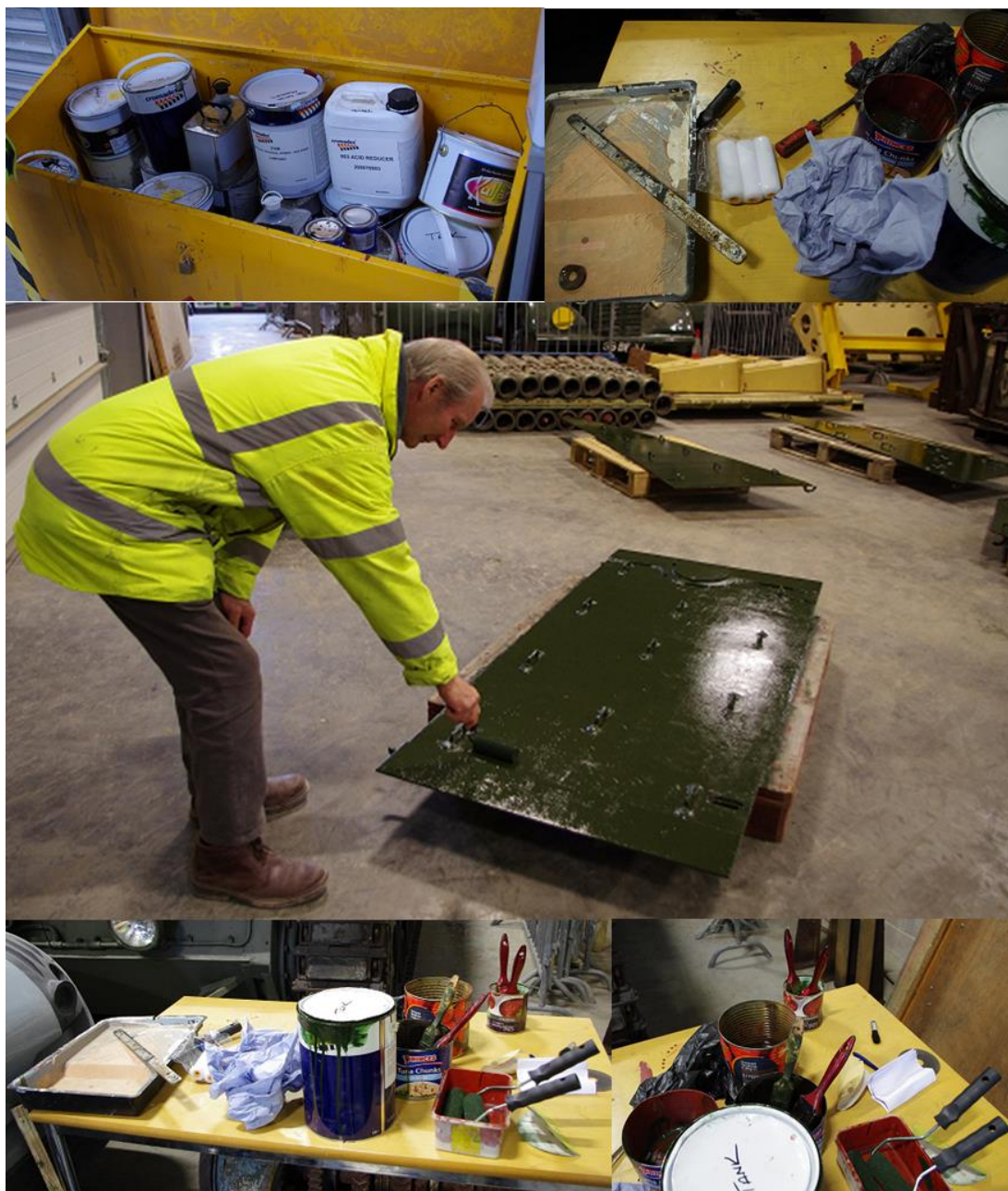


Figure 69 Paints and painting equipment used at the Tank Museum. Demonstrated by Mike Hayton, workshop manager at the TM.

Where there is original or later paintwork that offers either a record of the history of the object or milestones in its life, conservation ethics dictate that this should normally be preserved (Watkinson, 2010). Provided future interpretation of the object is not compromised there are instances where ethical arguments support the refinishing of the surfaces of cultural heritage objects (Watkinson, 2010). To offer the best opportunity for longevity, objects may be refinised to an improved standard rather than their original specification. In the case of the TM, a combination of refinishing and preservation of the original surfaces has been adopted, as can be seen in figure 70 with the refinised areas now painted dark grey and the black and

white cross at the centre of the photograph showing historic paint layers that have been left untouched. Areas like this cross left without intervention and only the damaged historic paint layers protecting the armoured steel from corrosion may be more susceptible to localised corrosion e.g. pitting and crevice corrosion.



Figure 70 A cleaned and painted armoured vehicle on display at the Tank Museum with historic paint detail left intact, but requiring additional protection, ideally a clear coating.

Original paint detail (figure 70) needs preserving. Whether clear coatings are the best method will require further research.

Coating areas of bare metal where original paint layers are detaching and using clear coatings as a touch-up coating between maintenance is the focus of this research. Standardised procedures to produce quantitative data to identify the most suitable coating for use on areas such as this are therefore required.

In addition to reducing corrosion any clear coating used should ideally have minimal impact on the paints already on the vehicle(s), whether it is the original paint or the refinishing paint. Although the visual impact of the clear coatings on the paints could be a concern as clear coatings frequently contain solvents, with the clear coatings reaching the edge of the paint residue and minimal overlap this should not be an issue.

4.4 Clear Coatings

4.4.1 Requirements

A recent study identified five properties that are required of coatings used to protect ferrous metal industrial objects:

- (1) Last three years or more without requiring further maintenance whether outdoors or indoors, without control of RH, temperature or light levels.
- (2) Allow the original appearance, function or cultural significance of objects to be retained.
- (3) Allow future retreatments or be removable.
- (4) Be a commercially available product.
- (5) Use of the treatment should not harm either the operator or the environment (Shashoua and Matthiesen, 2010).

Clear matte protective coatings that offer near invisibility for the viewer are an ethical goal in conservation. Many clear coatings are in use but gloss and aging that causes yellowing are major problems associated with them. A clear coating on an armoured vehicle may not have to be matte if the existing paint is gloss and yellowing may be too minor to concern the viewer. Thus these ageing changes that are normally important may not override the need for good protective properties that are long lived.

4.4.2 Coating-Solvent Combinations and Application Techniques

This project aims to specify coatings for use in real life scenarios, thus the application method must be commonly used for in situ coating. Shashoua and Matthiesen (2010) chose brush application for their research, as the thickness of the applied film can be readily controlled. Although brushing is a slow process, generally less health protection equipment is required than for spraying. Mottner et al. (2001) also applied transparent coatings to iron and steel outdoor industrial monuments by brush. Brush application is also one of the primary methods used at the TM (figure 69) and within conservation. The concentration (solid to solvent ratio) is key to producing a good coating finish.

When applying transparent coatings to iron and steel outdoor industrial monuments various numbers of layers or thicknesses and drying periods have been reported in research papers. Mottner et al. (2001) reported adding 3 to 5 layers with 3 to 4

hours drying period for each layer. Cano et al. (2010) applied 2 layers by brushing in criss-cross layers, and allowed 24 hours for drying between layers for a set of their samples. Shashoua and Matthiesen (2010) however, applied surface treatments so that they attained a dry film thickness of 20 to 25 μm , after drying horizontally for 7 days at 18 to 20 °C and 35 to 40% RH before evaluation.

Heating the substrate material is a practice used by conservation practitioners (4.3.2.1) when using wax to coat outdoor sculptures as the wax melts when in contact with the warmed surface, thus allowing it to be brushed on and fill pores and cracks. Coupons used in the PROMET project were also preheated in an oven at 50 °C for 1 hour as part of the short-term testing prior to immersion in Renaissance wax, Polyurethane varnish or Paraloid B72 (Argyropoulos, 2008). It is good practice to warm the samples prior to coating as surface moisture is removed.

A questionnaire distributed to Mediterranean Basin countries as part of the PROMET project received 54 responses, which revealed Paraloid B72 was the most popular clear coating for iron, followed by Cosmoloid H80 (Argyropoulos et al., 2007b).

4.4.2.1 Paraloid B72

Paraloid B72 is favoured by conservators due to its ability to remain clear, soluble and removable over time (Davidson and Brown, 2012). It is an ethyl methacrylate: methyl acrylate P(EMA-MA) copolymer with a molar ratio of 70:30 (Chapman and Mason, 2003). As a pure solid it has a relatively high glass transition temperature (T_g) of 40 °C (104 °F) and a refractive index of 1.49, it is versatile, resilient but rigid and has intermediate hardness (Chapman and Mason, 2003; Rohm and Haas, 2007). Paraloid B72 dries by solvent evaporation and can be re-dissolved repeatedly as needed or heat can be used for softening and reworking it (Davidson and Brown, 2012).

Data taken from the Argyropoulos et al. (2007b) paper was used to identify the different ways in which Paraloid B72 was mixed and used as a coating (figure 71) and which solvent is most associated with its use (figure 72). Acetone (48%) is the solvent most commonly associated with the use of Paraloid B72 as a coating, but toluene (28%), xylene (8%) and benzene (2%) are also used for dilutions. This is surprising as acetone is a volatile solvent and does not allow for as much levelling of the coating as other less volatile solvents may, but it is far less toxic and so is safer. As acetone is more volatile than these other solvents, less is likely to be retained by

the Paraloid B72 coating layers, reducing its possible impact on the O₂ sensor spots.

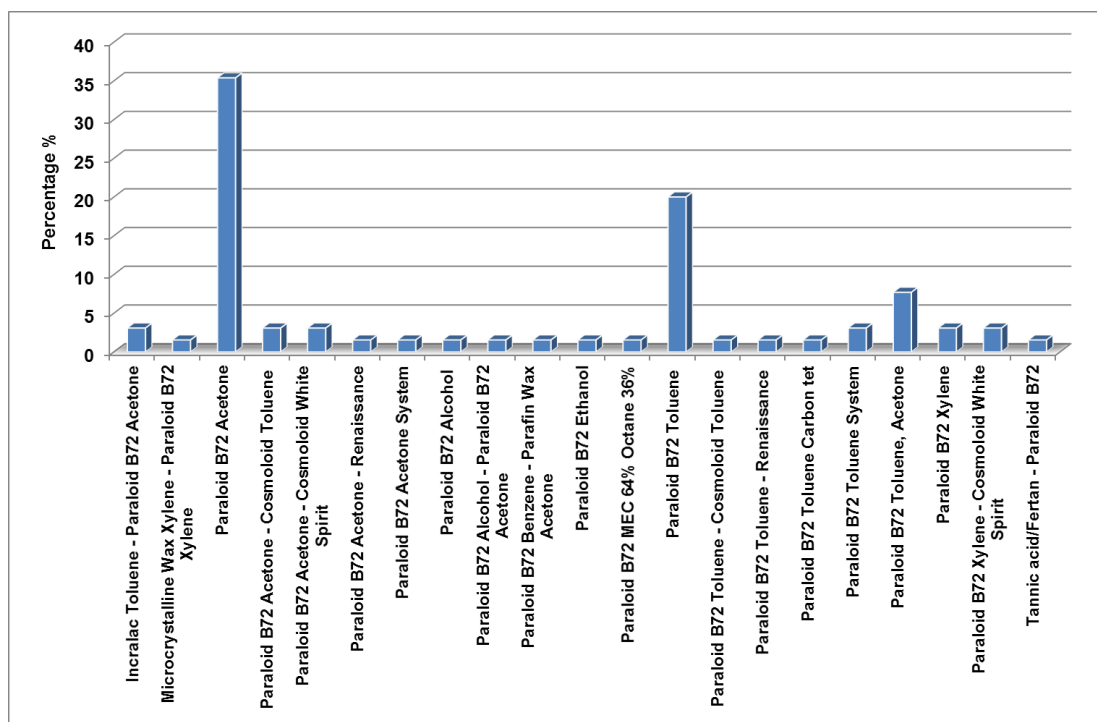


Figure 71 Uses of Paraloid B72 and method preferred (Argyropoulos et al., 2007b)

Paraloid B72 is commonly prepared as 10-15% w/v dilutions. Many studies have used 15% w/v in acetone (Argyropoulos et al., 2007a; Cano et al., 2007; Siatou et al., 2007; Degriigny, 2010), but Reedy et al. (1999) prepared a 10% w/v solution in 95% xylene and 5% butyl cellosolve. Butyl cellosolve (ethylene glycol monoethylene) is used in silver and brass conservation but is also sometimes added as a levelling agent to try to reproduce the levelling quality of Agateen⁵, as Paraloid B72 is difficult to apply without bumps appearing on the surface if it is not included in the solution (Reedy et al., 1999). Although optical properties of coatings are important, they are not as critical for the application to armoured vehicles. Xylene has a higher viscosity than both toluene and acetone (Horie, 2010), thus a lower percentage of Paraloid B72 in xylene is likely to create a surface finish with less brush marks. Although acetone produces a less viscous Paraloid B72 solution than xylene, it is more volatile and doesn't allow for as much levelling whilst the coating is drying. Research has also shown that Paraloid B72 films prepared in acetone and

⁵ Agateen Laquer no. 27 (cellulose nitrate, used with thinner no. 1) – due to levelling properties when applied by brush the coating is near invisible on the metal surface. The solvent system used with Agateen Laquer is very toxic. Perkins, B. N. 2003. The de-electrification and re-electrification of historic lighting fixtures at Winterthur Museum. *Journal of the American Institute for Conservation* 42 (3), p. 457 to 462..

to a lesser extent 1:1 acetone:ethanol are susceptible to water damage, which is apparent as the films become swollen and cloudy (Li, 2006).

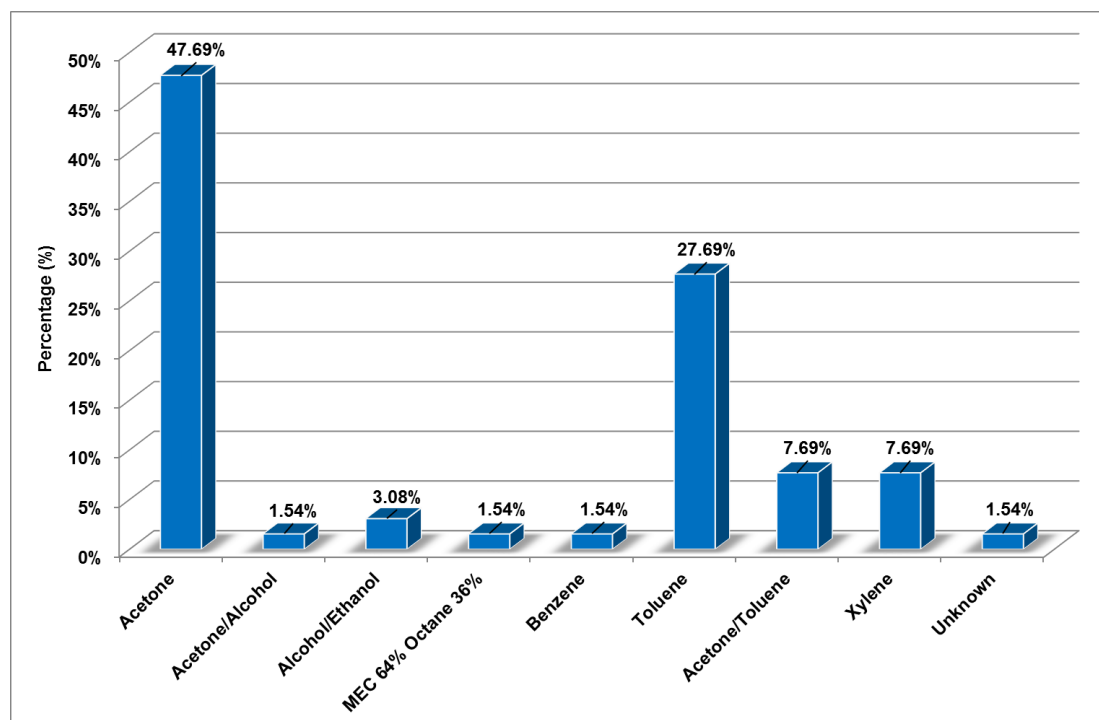


Figure 72 Preferred solvents associated with the use of Paraloid B72 calculated from the research done by Argyropoulos et al. (2007b)

4.4.2.2 *Cosmoloid H80*

Cosmoloid H80 is also popular with conservators (Argyropoulos et al., 2007b). It is supplied by Kremer Pigmente GmbH & Co. KG for application to ferrous metal, but the metal must if possible be paint free and acid-free. Before application, the metal must be degreased and although usage recommendations describe coating by immersion, it is possible to apply by brush. The research reported by Shashoua and Matthiesen (2010) using analogue sample material indicates that Cosmoloid H80 inhibits corrosion.

White spirit is the preferred solvent for Cosmoloid H80 within conservation practice (figures 73 and 74) (Argyropoulos et al., 2007b). Research by Wolfram et al. (2010) used a 10% (w/w) dispersion of Cosmoloid H80 in mineral spirit Shellsol T which, although free of aromatic compounds is highly flammable above 60 °C. The PROMET project used Cosmoloid H80 in additional research, but dissolved in toluene (13.33 g in 20 ml of toluene, a 66.65% w/v solution) (Argyropoulos, 2008). Both toluene and white spirit shall be trialled with Cosmoloid H80, toluene due to the solubility of Cosmoloid H80 dissolved in it and its use within the PROMET project and white spirit, due to its popularity with conservators generally. The survey

carried out by Argyropoulos et al. (2007b) showed the preferences of conservators, with 35% preferring to use white spirit with Cosmoloid H80 and 22% preferring to use toluene (figure 74).

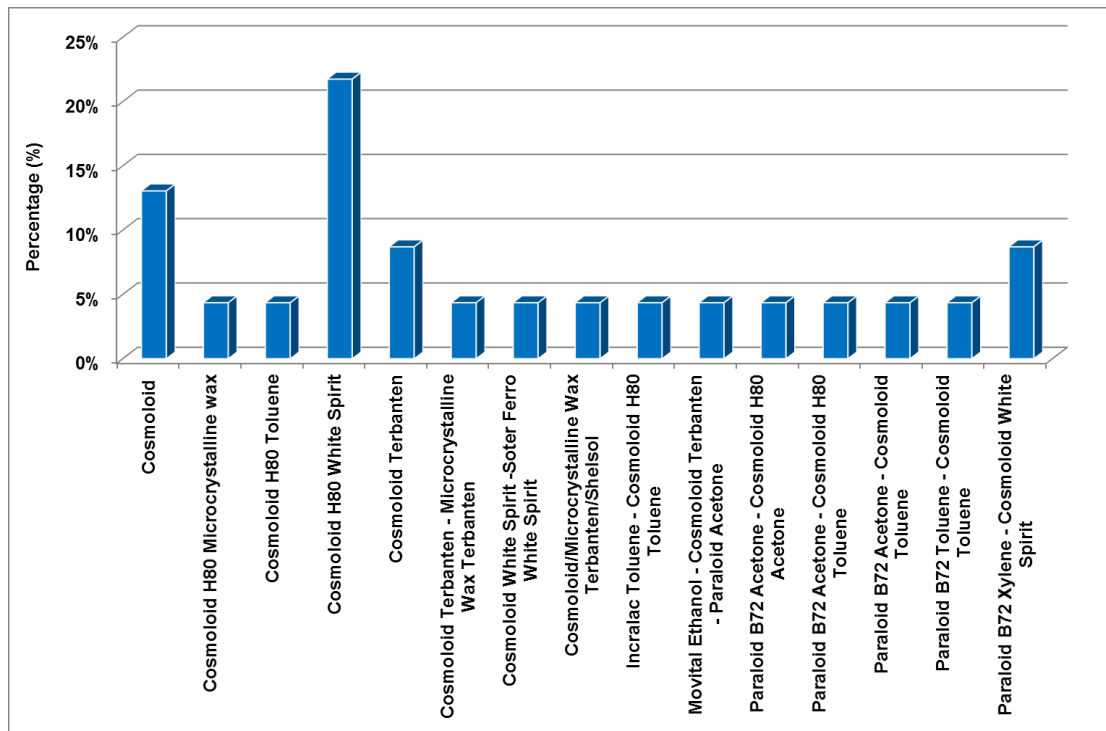


Figure 73 Uses of CH80 and preferred method (Argyropoulos et al., 2007b)

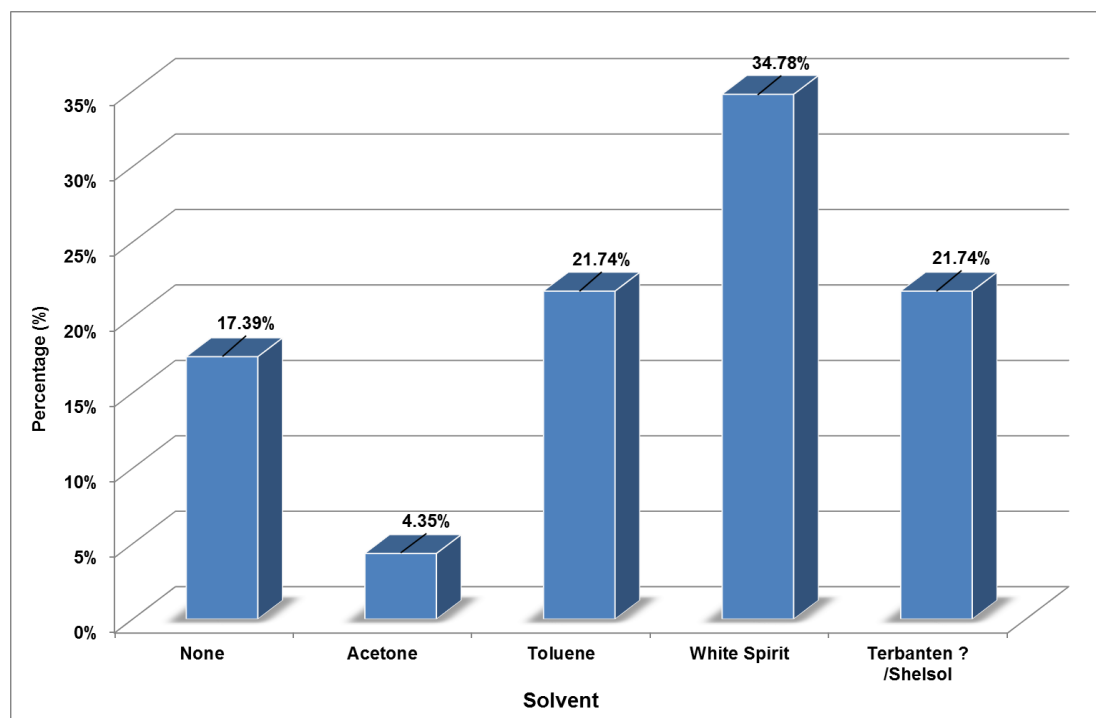


Figure 74 Preferred solvents associated with the use of CH80 calculated from Argyropoulos et al. (2007b)

4.4.2.3 Silanes, Polysiloxanes, Polysilazanes and Siliglide 10

To assist in conservation and supplement existing techniques, emerging technology, often from other subject areas, needs to be exploited (Williams, 2009a). One area for further development listed in the report on the 'Role of science in the management of UK's heritage' is research into new coatings particularly for outdoor metals e.g. super-hydrophobic materials (Williams, 2009a) and from time to time new materials do emerge.

In the early 90s, as an alternative to the carcinogenic chromium VI containing conversion treatments, silanes were introduced for adhesion promotion and corrosion protection of metals. Organic functional groups, e.g. methoxy (CH₃O-) or ethoxy (CH₃CH₂O-) groups, bonded to silicon atoms are the foundation of hybrid silane molecules, although some contain other functional groups, e.g. Cl, amine (NH₂), S or epoxy (De Graeve et al., 2007). Curing of the siloxane layer is deemed essential for corrosion protection purposes and is touched upon in 3.2.2.2.1. Effective barriers against corrosive attacks are formed due to the crosslinking and branching that produces a dense network, limiting electrolyte access to the underlying metal. Crosslinking between silane molecules in deposited films usually results from heating the coated substrates with -Si-O-Si- (poly)siloxane chains being produced by silanol groups (figure 75) that have not reacted with the metal surface (section 3.2.2.3.1, figures 43, 44 and 45).

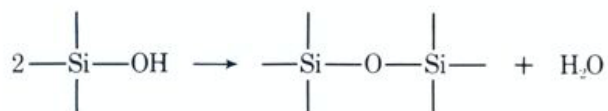


Figure 75 Condensation of silanol groups to form a siloxane chain taken from Arkles (1977)

The excellent bonding of silane/siloxane films to metal substrates is assumed to be a results of the Metal-O-Si and Si-O-Si covalent bonds that are formed (figure 76) (Palanivel et al., 2003).

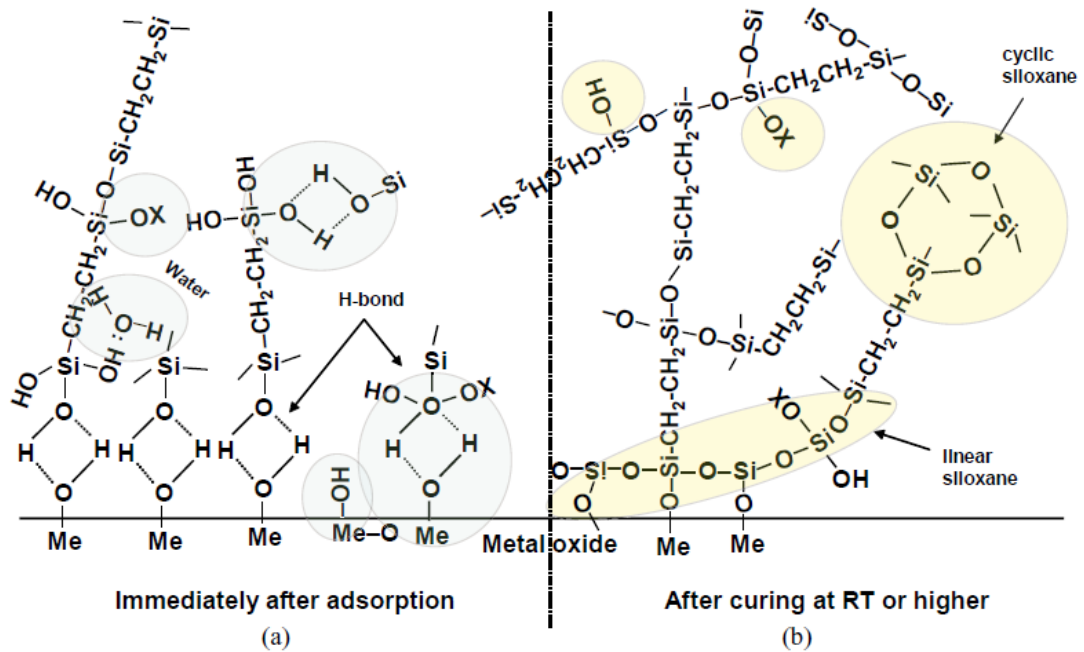


Figure 76 Simplified schematic of bonding mechanism between silane molecules and metal surface OH layer: (a) before condensation: H-bonded interface; (b) after condensation: covalent-bonded interface (Palanivel et al., 2003).

A high degree of permeability to water vapour is maintained by silane- and silicone-derived coatings although they are mostly hydrophobic. Reduced deterioration at the coating interface is linked to entrapped water and also allows the coatings to breathe. Protection is offered to composite structures ranging from pigmented coatings to rebar-reinforced concrete, as ions are not transported through non-polar silane and silicone coatings (Arkles, 2006).

Polydimethylsiloxane (PDMS) (figure 77), offers an example of a polysiloxane, many of which have excellent chemical, physical and electrical properties (Abe and Gunji, 2004). It is also the most common silicone material. Polysiloxanes have weak interactions between molecules affording them excellent physical properties, e.g. a low viscosity coefficient and a small contact angle. Modification or improvement of the polysiloxane structure could overcome its potential limitation for their use as coating films or fibers (Abe and Gunji, 2004).

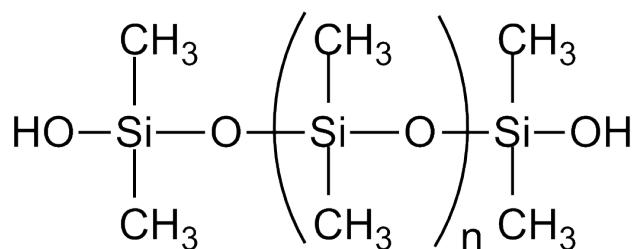


Figure 77 Silanol terminated polydimethylsiloxane

Within the conservation sector, silanes have already begun to be considered for surfaces such as bronze (Pilz and Römich, 1997; Mottner et al., 2001; Argyropoulos, 2008). A PROMET partner found that the combination they called silane A, which formed a copolymer at room temperature gave the best result, providing better protection with two layers and was reversible in 5M NaOH (Argyropoulos, 2008). Although polysiloxanes can have very high chemical resistance, alkalis are the exception as the Si-O-Si bond is not resistant to hydrolysis. Thus, silane based coatings could be potential coatings for the future for conservation of heritage ferrous metal and so are being considered within this project.

Discussions with coatings companies in the UK provided only one suggestion, Siliglide 10. Siliglide 10 is a product which is commercially available (from Fluorochem in the UK, a distributor for US based Gelest. Inc.). Although it is described as a release and slip coating for glass, ceramics and non-ferrous metals, it is being trialled with ferrous metal.

The chemical name for Siliglide 10 is polydimethylsilazane-polydimethylsiloxanes and silicones mixture in isoamyl acetate. Like Paraloid B72 and Cosmoloid H80, Siliglide 10 is a solvent-borne coating, with the flammable solvent isoamyl acetate (figure 78) making up > 85% of the ingredients (table 38). The dispersed polymer components make up roughly 15%, unlike Paraloid B72 and Cosmoloid H80 where they make up 10% w/v. Siliglide 10 has a very low viscosity of 1-2 cSt (centistokes) (Gelest Inc., 2007), similar to water with a kinematic viscosity of 1.01 cSt at 20 °C, and so can be used without further dilution.

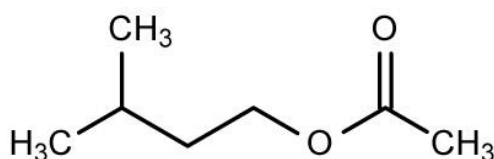


Figure 78 Chemical structure of isoamyl acetate

Table 38 Ingredients proportions in Siliglide 10 as stated on the MSDS

Identity	Percentage (%)
Poly(1,1-dimethylsilazane), telomer*	> 10
Poly(dimethylsiloxane) silanol terminated	5
Isoamyl acetate	> 85

*Telomer = an extremely short polymer with generally between 2 to 5 degrees of polymerisation

Siliglide 10 cures in 25 to 30 minutes at room temperature, where the RH is < 75%, as it is chemically similar to amine cure silicone RTV (room temperature vulcanizing). Small quantities of water normally found on the surfaces of substrates activate the curing process. During curing, the surface should be buffed or wiped with a soft rag to optimize release by ensuring a thin film covers surface imperfections.

Polyorganosilazanes, polymers with –Si-N- bonds in the main chain, have received little attention in comparison to polyorgano-siloxanes, mainly due to the shortage of suitable preparative methods for producing linear chains of high molar mass. But also partly due to the high chemical reactivity of poly(1,1-dimethylsilazane) (figure 79) with H₂O etc. (Soum, 2001). When in contact with water or moisture, the Si–N bond is cleaved by water molecules attacking the Si atom. Thus polysilazanes decompose more or less quickly depending on the rate of the reaction with water (or other OH containing materials like alcohols), which varies with the molecular structure of the polysilazanes and the substituents.

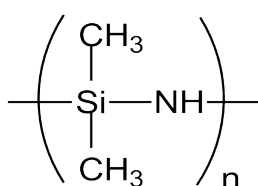
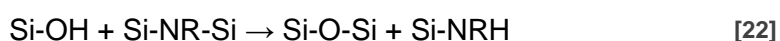
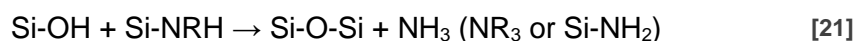


**Figure 79 Poly(1,1-dimethylsilazane)
telomer repeat unit**

Metals with –OH groups on the surface are often easily wetted by polysilazanes and good adhesion is promoted by the reaction in [20]. PDMS is rendered susceptible to condensation under mild acid and base conditions by the terminal silanol groups (Gelest Inc., 2013). Thus, the terminal silanol groups of PDMS in Siliglide 10, allow PDMS to react with silazane resulting in siloxane bond linkages and the liberation of either NH₃, an NH₂ or a Si-based radical comprising a terminal Si-NH₂ group [21]

(Knasiak et al., 2003; Lukacs and Knasiak, 2003). They also allow it to bond to substrate surfaces by reacting with –OH groups that will be present on ferrous metal surfaces (figure 80 also see 3.2.2.2.1). The Si-NRH formed by the reaction of the silanol group with polysilazane [22] can react further with additional –OH groups either by [20] or [21]. Thus, metal oxide surfaces reacts with Siliglide 10, a siloxane modified polysilazane and form a chemically bound polymethylsiloxane resin “siliconized” surface (Gelest Inc., 2007).



Where R = H, alkyl, substituted alkyl, cycloalkyl etc.

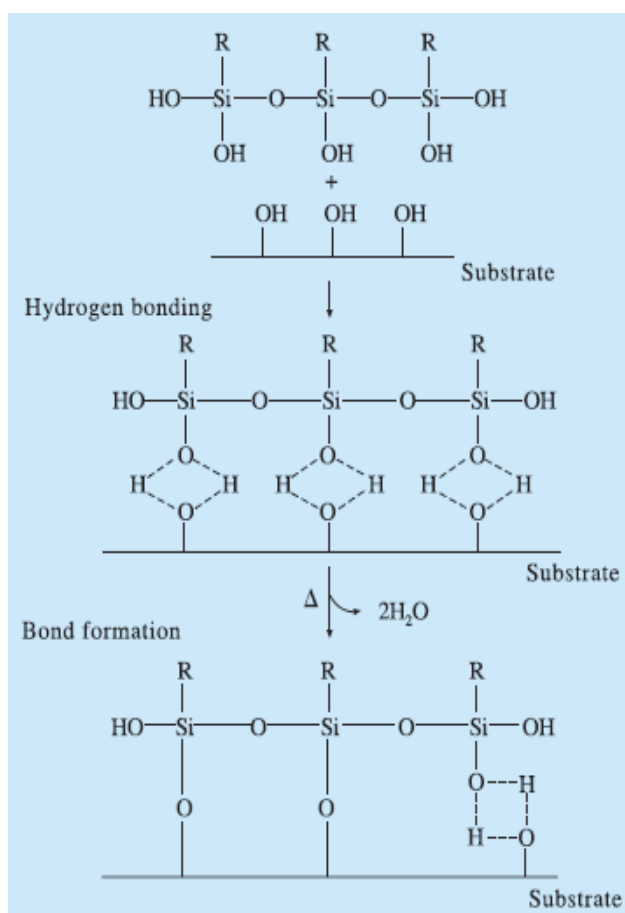


Figure 80 Silane hydrolytic deposition (Arkles, 1977)

Hydrophilicity and hydrophobicity are comparative terms frequently used when discussing silicone based polymers. The contact angle of a liquid droplet on a solid surface (figure 81, also see figure 40) however, is a simple, quantitative method

frequently used for defining the relative degree of interaction of a liquid with a solid surface. Young's equation provides the value for the contact angle (θ):

$$\gamma_{sv} - \gamma_{sl} = \gamma_{lv} \cdot \cos\theta_e$$

where γ_{sl} = interfacial surface tension and γ_{lv} = surface tension of liquid.

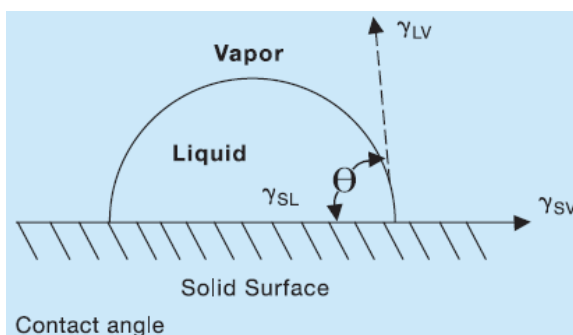


Figure 81 Wettability and contact angle (Arkles, 2006)

The contact angle of H₂O on a substrate is not a good indicator of wettability of a substrate by liquids other than H₂O, but it is a good indicator of the relative hydrophobicity or hydrophilicity of a substrate (table 39) (Arkles, 2006).

Table 39 Designation according to contact angle, information from Arkles (2006)

Angle (°) of the water, θ	Designation	Comments
< 10	Super-hydrophilic	Provided the H ₂ O is spreading over the surface and the surface is not absorbing, dissolving in or reacting with the H ₂ O.
< 30	Hydrophilic	Forces of interaction between the H ₂ O and the surface compared to the cohesive forces of the bulk H ₂ O are nearly equal – H ₂ O does not drain cleanly from the surface
> 90	Hydrophobic	H ₂ O forms distinct droplets – as the hydrophobicity increases, the contact angle also increases. On a smooth surface the theoretical maximum is 120°.
> 150	Super-hydrophobic	On micro-textured or micro-patterned surfaces which are severely hydrophobic

Within 3.2.2.1.2 surface tension of films was used to discuss edge and corner protection, and in 3.2.2.1.3 wetting was used to explain the adhesion of a coating to the substrate, but these terms were not used to discuss the impact of the coating on the surface properties of the coated substrate. Critical surface tension serves as a better predictor of behaviour of a solid with a range of liquids, and is therefore related to the wettability or release properties of a solid. The values stated for the properties of surfaces treated with Siliglide 10 are for glass slides dipped in 5%

solutions and cured for 30 minutes at room temperature. Untreated glass slides had a reported critical surface tension of 78 dynes/cm (Gelest Inc., 2007). Surfaces with critical surface tension > 45 dynes/cm are generally observed as having hydrophilic behaviour (Arkles, 2006). Usually surfaces with critical surface tensions < 35 dynes/cm display hydrophobic behaviour. Once treated with Siliglide 10, the glass slides exhibited hydrophobic behaviour and a critical surface tension of 25 dynes/cm (Gelest Inc., 2007). Surfaces are not considered oleophobic⁶ until the critical surface tensions decrease below 20 dynes/cm and the surfaces resist wetting by hydrocarbon oils (Arkles, 2006). Siliglide 10 can be applied to non-ferrous metals to provide a clear high water contact angle with excellent release properties and it is hoped that similar properties might be exhibited on ferrous metals.

The effectiveness of silanes on inorganic substrates varies (figure 82), and the hydroxyl (–OH) groups play a part in this. On substrates containing –OH groups both the type and concentration of –OH group present varies widely. Few –OHs are found on freshly made substrates stored under neutral conditions and considerable amounts of physically adsorbed H₂O can interfere with coupling where hydrolytically derived oxides have aged in moist air. Isolated or free –OHs react reluctantly, while H-bonded adjacent silanols react more readily with silane coupling agents.

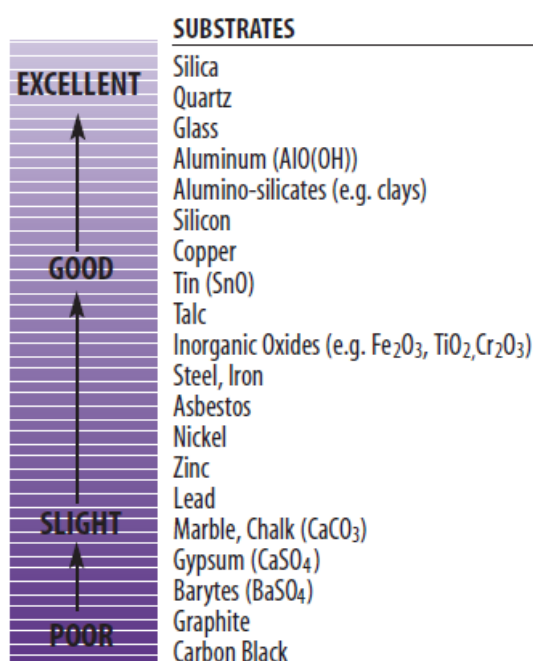


Figure 82 Effectiveness of silanes on inorganics

⁶ Oleophobic – Resistant to oil. Lacking an affinity for oil. Tending to repel oil. An oleophobic coating helps repel much of the natural oil from the fingers.

Siliglide 10 is frequently applied by dipping or wiping either in the solution as supplied or as a 1-2% solution in dry solvents such as white spirits or esters such as isobutyl acetate (Gelest Inc., 2007). As the dispersed polymer concentration is ~15% it will not be diluted to such an extent as Paraloid B72 and Cosmoloid H80 are being prepared as 10% w/v coatings.

5 Methodology

5.1 Aims and Objectives

5.1.1 Aims

- Determine the effectiveness of selected clear coatings for controlling the corrosion of modern historic steel in conservation contexts with specific reference to the needs of the TM and the occurrence of Cl⁻ contaminated surfaces.

5.1.2 Objectives

- Assess the environmental context for use of coatings within the Tank Museum.
- Survey the occurrence of Cl⁻ bearing corrosion products at historic sites in Scotland and contextualise this for heritage.
- Prepare samples of historic steel for testing the efficacy of three clear coatings: Paraloid B72, Cosmoloid H80 and Siliglide 10.
- Assess the ability of these coatings to prevent corrosion in high RH by monitoring the O₂ consumption of samples at 80% RH.
- Determine if standardised pre-corrosion of samples with de-icing salt solution prior to applying coatings impacts on the protective performance of the coating.

5.2 Field Testing and Data Collection

5.2.1 Sample Collection

Samples were collected from a variety of heritage site spread throughout main land Scotland and Orkney. The sampling sites were identified by research and staff working for heritage bodies and their locations are shown in figure 83. The site names and total number of samples collected at each site are listed in table 40. Where possible 10 corrosion samples and 2 detaching paint layer samples were collected throughout each site. Intact paint layers were not damaged. Corrosion layers were detached using a scalpel (figure 84), although a large proportion were already detaching from the metal. Samples were collected in dry, sterile sample bags. The size of sample collected was dependent on the amount of corrosion present, consequently it varied greatly. Cross sections of the corrosion layers down

to the metal surface were collected where possible, but the proximity of the corrosion products collected to the metal surface was dependent on how corroded the metal was and how easy they were to remove.

Table 40 Sites and numbers of samples collected

Site code	Site	Total no. of samples
AA	Arbroath Abbey	12
BC	Broughty Castle, Dundee	12
BG	Biggar Gasworks	1
CP	Claypotts Castle, Dundee	12
DB	Dunbar Castle	6
DBT	Dumbarton Castle	12
DC	Dunkeld Cathedral	12
DF	Dumfries, Midsteeple	8
DG	Dunglass Collegiate Church	12
DS	Dunstaffnage Castle & Chapel	12
FC	Fyvie Castle	12
FG	Fort George	12
GC	Glasgow Cathedral	8
KH	Kinnaird Head, Fraserburgh	12
LBE _d	Lindsay Burial Aisle, Edzell	5
NH	Newhailes House	12
PHR	Palace of Holyrood House	13
PW	Priorwood Garden, Melrose	12
SA	St. Andrew's Cathedral	12
SK	Skelmorlie Aisle, Larg	12
SL	Summerlee Museum, Coatbridge	12
SM	Stanley Mills	5
TQ	Traquair House	10
Total number of samples collected		236

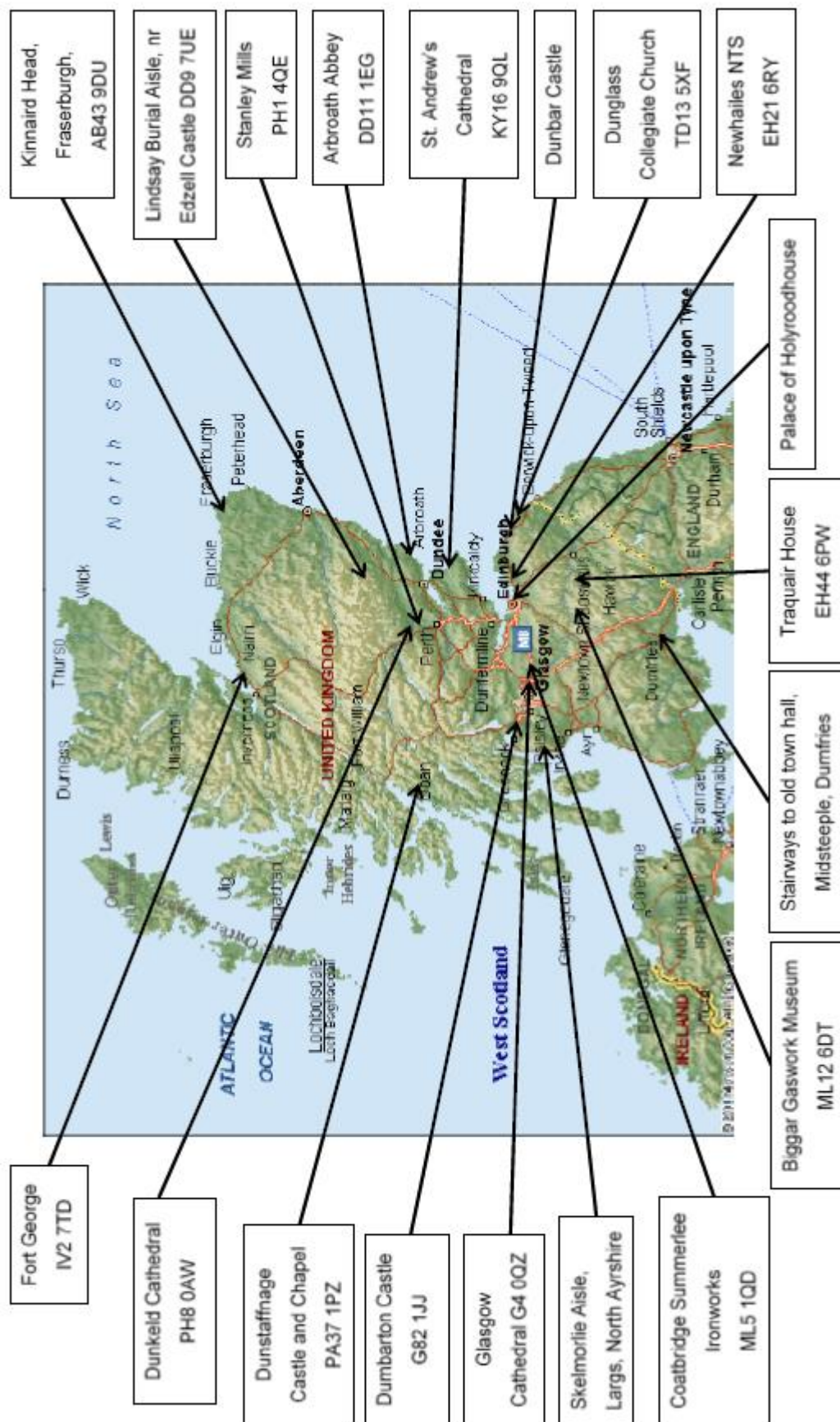


Figure 83 Sampling locations not including Stromness Ness Battery or the Scapa Flow Visitor Centre and Museum, both in Orkney

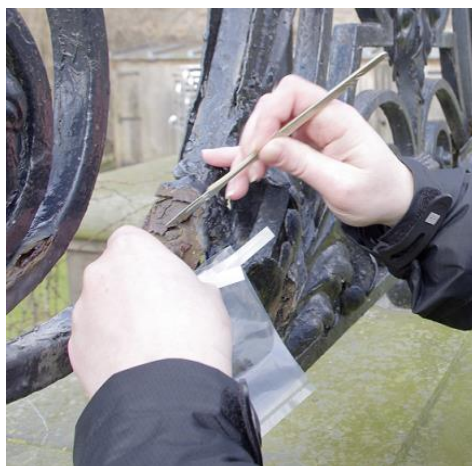


Figure 84 Collection of corrosion products

5.2.2 Sample Analysis

5.2.2.1 Powder X-ray Diffraction (XRD)

XRD was used for analysing the corrosion products semi-quantitatively. Three corrosion product samples per site were chosen for XRD analysis. Small amounts (0.012 - 0.500 g) of these samples were ground into a powder using a small pestle and mortar. Acetone was added to the powder to assist with further grinding. Additional acetone was added to transfer the powder to a glass disc by pipette. The acetone was allowed to evaporate leaving a thin layer of corrosion products on the glass disc. Cross contamination between corrosion samples ground in the pestle and mortar was avoided by grinding sandstone grit and detergent in the pestle and mortar before rinsing it with distilled water.

All samples were applied to glass discs, which were placed in labelled sample holders before positioning them in the sample changer in the ARL X'TRA XRD (Thermo Scientific). XRD analysis was carried out using Cu-K α radiation, scanning the 2θ range 5-80°, using 0.02° steps and 1 second/step counting time and these parameters are within the range used by other researchers investigating corrosion products (Balasubramaniam and Ramesh Kumar, 2000; Santana Rodríguez et al., 2002; Ståhl et al., 2003; Castaño et al., 2010; Antunes et al., 2014). Scanning between the 2θ range 5-80° allows for the major peaks of akaganéite and Lepidocrocite to be detected just past 10°, if present and not hidden in the initial short downward slope. By continuing up to 80° all the major corrosion product peaks are covered. Scanning with 0.02° steps and 1 second/step counting time will balance the need for a quality scan and the need to scan a large number of samples.

5.2.3 The Tank Museum – Environment data

5.2.3.1 Environmental Data Collection

Four data loggers were placed inside two tanks situated in different locations within the museum. The calibration of the loggers was checked within the environment chamber 5 days prior to their use within the the two tanks. The four MadgeTech RHTemp101A, humidity and temperature data-loggers (specifications table 41) were set to record the temperature and RH every 10 minutes (table 42, figure 85 and figure 86). To support this, environmental data collected by TM staff from different locations around the museum was obtained (figure 67).

Table 41 MadgeTech RHTemp101A data-logger sensor, range, resolution and accuracy specifications as set out by the manufacturer

Specifications	Temperature	Humidity
Sensor	Precision RTD Element	Internal Semiconductor
Range	-40 °C to 80 °C (-40 °F to 176 °F)	0 to 95% RH
Resolution	0.01 °C (0.018 °F)	0.1% RH
Calibrated Accuracy	±0.5 °C (±0.9 °F)	±3.0% RH (±2% RH typical at 25 °C/77 °F)
Specified Accuracy Range	+10 °C to +40 °C (50 °F to 104 °F); 10% RH to 80% RH	

Table 42 Location and environment of vehicles and location of the data loggers within the vehicle, which they were placed inside for approximately 27 months

Room	Environment	Vehicle	Logger	Location within vehicle
The Tank Story, new display hall	Radiant heated room	Inside the Sherman Firefly (figure 85)	N77402	Inside close to the turret roof
			N77403	Inside on the driver's seat
The Discovery Centre	Unheated, insulated room	Inside the Sherman V Crab - flail attached (figure 86)	N77404	Inside close to the turret roof
			N77409	Inside on the driver's seat



Figure 85 The Sherman Firefly inside the New Display Hall – Image on the left taken prior to monitoring internal temperature and RH conditions; image on the right at collection of data-loggers.

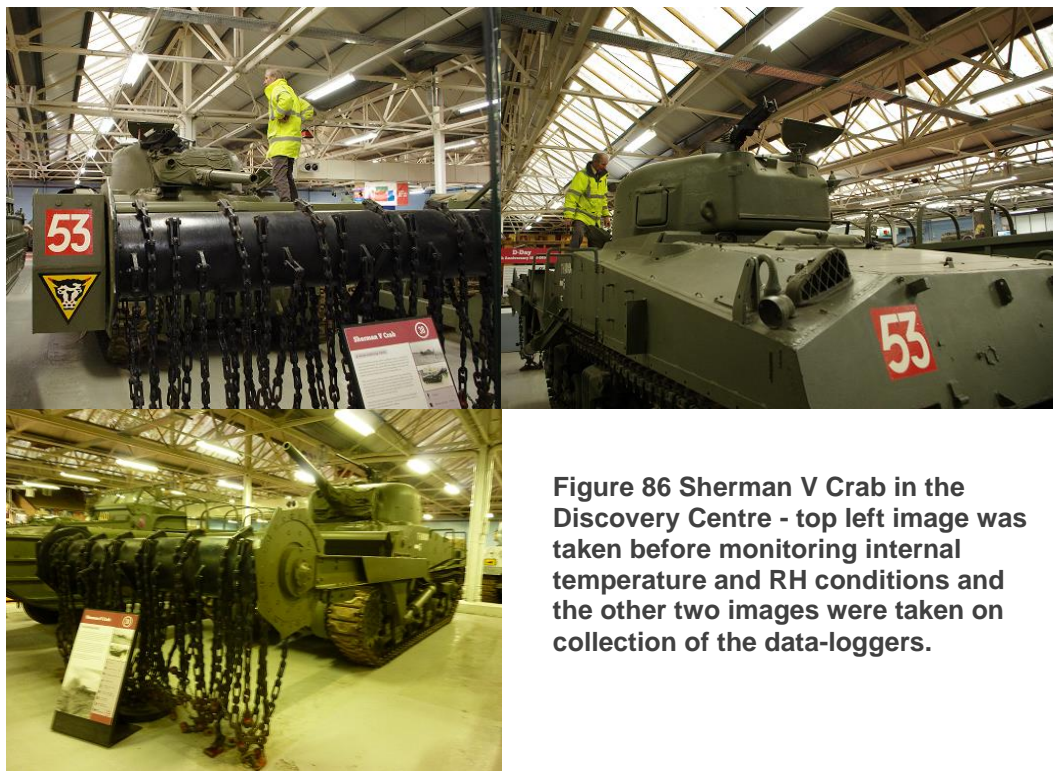


Figure 86 Sherman V Crab in the Discovery Centre - top left image was taken before monitoring internal temperature and RH conditions and the other two images were taken on collection of the data-loggers.

5.3 Laboratory testing

5.3.1 Standardisation – Reliability and Validity of Research

5.3.1.1 *Sample Preparation*

5.3.1.1.1 Material selection and sampling cutting

The sample material for this research was determined by the TM, who donated a ‘Saracen APV door’ (armoured personnel vehicle door). Their decision was largely based on what was considered acceptable to be cut up for sample material and availability. The sample material (the armoured steel and the paint on the door) is not representative of the whole collection held at the Tank Museum and is only representative of the armoured steel used for armoured vehicles in the Saracen series constructed during the same time period (1950’s to early 1960’s).

Samples 38 mm in diameter x 12 mm in depth were stamped out of a Saracen APV door (figure 87). Sample size was determined by the thickness of the door and the diameter of the reaction jar mouth, used for O₂ monitoring (figure 91). Other methods for cutting samples out of the armoured steel door were discarded due either to cost or the heat production likely during cutting.



Figure 87 Both sides of the Saracen APV door – laid flat and photographed from above

5.3.1.1.2 Metallography

A corner section was cut off the Saracen APV door (figure 88) using a hack saw prior to samples being stamped out. A small piece with welds was cut from the edge section of this corner piece using the Struers minitom diamond wheel saw. Tap water (235 ml) with 'Corrozip' (15 ml) added was used for lubricating the blade. The metal was held using an adapted clamp and due to its size, mass and thickness the saw was set running at \approx 100 rpm, slowly increased initially up to 200 rpm and then further to 400 rpm.

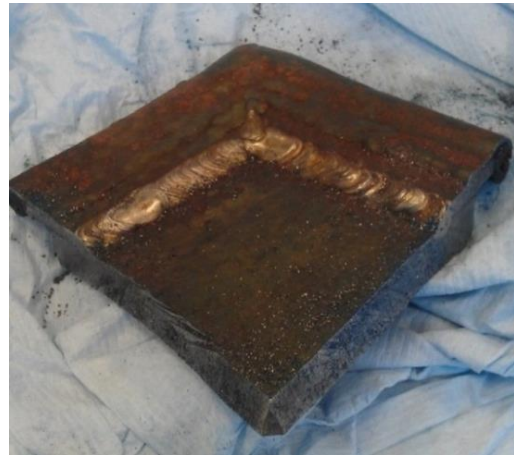


Figure 88 Corner section cut off the Saracen APV door using a hack saw.

The cross-section piece with welds was polished using the Struers LaboPol - 5 at 100 rpm. The grades of silicon carbide (SiC) grit papers used are listed in table 43 with the liquid used.

Table 43 Summary of the grades of abrasive and liquid used for grinding and polishing

Grades of SiC grit paper	Liquid used with the abrasive
180, 360, 600, 1200, 2500 and 4000	Water
6 μm , 3 μm and 1 μm	Oil based diamond suspensions

A 2% v/v solution of nital, nitric acid (2 ml) in ethanol (98 ml) was mixed up for etching. Nital (\approx 3 ml) was added via pipette to a 10 ml beaker. The cross-section sample was added to the solution for 30 seconds to etch and was then immediately washed in deionised water and dried to prevent further etching.

The etched cross-section was examined microscopically using the Nikon Eclipse ME 600 microscope with a Spot 25.4 digital camera and software attached. For each area examined several images with varying focal points were taken and then using Struers' Scenitis imaging software the images were aligned, sharpened and layered to produce images with the best focus throughout the whole image.

5.3.1.1.3 Surface preparation

Air abrasion with aluminium oxide is used for surface preparation of the samples to create a similar surface finish to that of the armoured vehicles prior to coating, as they are grit blasted with Guyson blast media (Saftigrit). Sample surfaces were prepared using a two-step air abrasion process. A Texas Airsonics Model AJ-1 abrasive unit was used for removing all the paint and corrosion from all the samples, except those which were left untreated to provide baseline data. To achieve the best results, different blasting angles are required (section 3.3.2.2):

- **Step 1** - 30-40° blasting angle for surface cleaning - removal of paint and oxide layers to near white metal (Sa 2.5).
- **Step 2** - 75-85° blasting angle to create an adhesive surface.

The stand-off distance used for step 1 (approx. 5 mm) was less than for step 2, due to the sample size and low angle blasting angle. Step 2 used a stand-off distance of approximately 10 mm. The blasting angle and stand-off distance were controlled by visual observation. Other standardised parameters employed were:

- Blasting pressure, 80 psi;
- Powder flow intensity, 6;
- Nozzle size, 1.0 mm (0.040") (this will be affected by the abrasive media);
- Aluminium oxide (Al_2O_3), grade 3 (53 microns, hardness 8-9 Mohs)

5.3.1.1.4 Examination of Surfaces

The surfaces of a selection of samples were compared before and after air abrasion. Macroscopic comparisons were recorded photographically. Microscopic comparisons were recorded by SEM (a CamScan Maxim 2040 variable pressure scanning electron microscope equipped with Oxford Instruments energy and wavelength dispersive X-ray spectrometers for chemical analysis). Microscopic surface profiles were imaged using secondary electron imaging (SEI). Electron backscattered diffraction (EBSD) images were used for further analysis of the substrate material by point and area analysis.

5.3.1.2 *Coatings: Concentrations, Solvents, Application and Oxygen Impact*

5.3.1.2.1 Coating Application, Concentrations and Solvent Tests

Paraloid B72 and Cosmoloid H80 coatings were prepared in the fume cupboard. The solid granules were placed in a Netlon bag and hung from supporting bars over

the beakers into the solvents. The solvent levels were marked and the beakers were covered with foil. The solvents were stirred continuously while the granules dissolved. Paraloid B72 required stirring overnight. Cosmoloid H80 with white spirit dissolved after a few hours, but the solvent was heated on a low setting whilst stirring. Solvent loss from the beakers by evaporation was made good and the resulting solutions were stored in sealed bottles. The coatings were all prepared as 100 ml solution:

- 10% w/v Paraloid B72 granules (10 g) dissolved in xylene (100 ml);
- 15% w/v solution Paraloid B72 (15 g) in xylene (100 ml);
- 10% w/v Paraloid B72 granules (10 g) dissolved in acetone (100 ml);
- 15% w/v solution Paraloid B72 (15 g) in acetone (100 ml);
- 10% w/v Cosmoloid H80 (10g) dissolved in white spirit (100 ml);

The 15% w/v Paraloid B72 solutions were made for comparisons to the 10% solutions, so the brush marks and film finish on glass slides could be compared. Xylene, which has a low volatility and thus good levelling of the coating, was later rejected as it interfered with the O₂ measurements.

5.3.1.2.2 Number of Coating Layers and Mass Applied

Prior to coating glass microscope slides, they were degreased by immersing them in industrial methylated spirit (IMS) for 20 minutes and brushed both sides and all edges, top to bottom 10 times. IMS was used as research by Lee (2010) showed IMS to be more effective at removing grease than white spirit and acetone. Once degreased the slides were air dried on cocktail sticks to allow air circulation underneath them. Their masses were measured using a Mettler Toledo AX504 balance (reads to 0.1 mg, has a maximum load of 510 g, repeatability is 0.1 mg).

Prior to application small amounts of the coatings were decanted into beakers. A soft bristled ½" brush was used for applying the coatings, dipping it into the coating mixture once, wiping the excess off on the edge of the beaker once and applying two strokes over the surface of the glass slides. The mass of the slides and coating were measured shortly after the coating was applied and at intervals over a 48 hour period before applying a second coating layer. The mass of the slide and coating was used as a guide for the drying time and extra time was allowed. Lee (2010) previously found that when Paraloid B72 in xylene was sprayed onto glass slides there was either no change or 0.0001 g change in mass between 120 minutes and

100 hours. The mass of the slides with two coating layers were measured shortly after the second layer had been applied and at intervals over a 48 hour period before applying the final layer. The procedure of measuring the mass of the slide and coating was repeated for the third layer, until approximately 48 hours after it was applied. The mass of each layer applied was considered separately to see if their addition added extra mass or dissolved and reapplied the existing coating. The mass increased with each of the 3 layers, thus 3 layers of the clear coating are used throughout this research. Applying 3 layers ensures defects in the initial layers are covered, it is also consistent with conservation practise described in section 4.4.2.

The mass of coating applied to the samples was recorded in a similar manner for 15 samples for each coating type. The thicknesses of the coatings were not measured in part due to the thinness of the Siliglide 10 coating layers making it impossible to measure with the equipment available and also owing to the uneven nature of the Paraloid B72 coating due to the brushmarks left behind.

5.3.1.2.3 Solvent Choice and Impact on the Oxygen Measurements

As O₂ consumption measurements are used to quantify the corrosion rate of ferrous metal, any impact of the coatings and/or solvent choice needs to be quantified or eliminated prior to testing them on the steel samples. The coated glass slides were placed in the reaction jars once dried. The reaction jars (250 ml Ball Mason jars) have PSt3 O₂ sensor spots (detection limit 0.03% O₂, 0-100% O₂) adhered to the interior walls using silicon adhesive (Radio Spares RTV silicone rubber compound) (figure 57, section 3.3.3.2). Xylene and water, which were tested separately were added directly to the reaction jars or to cotton wool which was then placed in the reaction jar. Two piece metal coated lids were used with the Ball Mason jars as the metal coated discs with an integral rubber ring on the underside form a hermetic seal when screwed down with a separate screw thread metal ring. Leakage of these jars was tested by Watkinson and Rimmer (2013) by filling a control reaction jar with nitrogen that showed negligible ingress of O₂ over a two year period.

The reaction jars containing coated glass slides or solvents were loosely sealed and stored in the Binder KBF240 climate chamber (0 °C to 70 °C, 10% to 80% RH). All the jars were left to equilibrate with the atmospheric conditions inside the climate chamber for an hour (temperature and RH within the laboratory are different to those within the climate chamber and may vary from day to day). The jars were opened and resealed tightly before the initial O₂ levels were measured using the Fibox4 fibre

optic O₂ transmitter (using a LED peak wavelength of 505 nm, and has an error < 3%, rel. between 4 to 50% O₂) connected to a polymer optical fiber (POF). The fibre optic which is positioned against the outer surface of the jar, opposite the sensor spot emits light exciting the luminescent dye in the sensor spot at one wavelength (figure 58, section 3.3.3.2). The sensor spot in response emits light at another wavelength. When O₂ is present, instead of emitting light, the energy of the excited molecule is transferred by collision with O₂. The Fibox4 works up to 80% RH and has an accuracy of 1% air saturation (± 2.07 hPa). Measurements were recorded every 10 seconds for 5 minutes for each jar. Following the initial measurements all jars were then assessed once approximately 24 hours later and again another 24-48 hours later, after which more time was left between measurements. The coating and solvent tests run are listed in table 44 along with the number of slides/jars tested, the number of days they were monitored and additional information e.g. number of days the coating were de-gassed prior to O₂ monitoring.

Paraloid B72

Xylene and acetone were both trialled with Paraloid B72. Xylene was trialled largely due to being less volatile than acetone, allowing the coating more time to level. Acetone was trialled due to its popularity with practicing conservators. The 10% w/v Paraloid B72 solution in xylene was compared to the 15% w/v solution in xylene by observing their appearances on glass slides. A Schott KL1500LED cold fibre optic light source with a 2-branch goose-neck light-guide (4.5 mm dia/600 mm long), was used to provide the lighting to photograph and enhance the visibility of the brush marks of these clear coatings on the glass slides.

Fresh slides were coated with the Paraloid B72 and stored at 20 °C, 40% RH on a tray in the climate chamber after drying (table 44), as both the 10% w/v Paraloid B72 coatings (one in xylene and one in acetone) affected the O₂ sensor spots. This should allow the coatings more time to de-gas as Paraloid B72 is known for its solvent retention properties (Podany et al., 2001; Horie, 2010; Davidson and Brown, 2012). These conditions will not promote corrosion of stored clean ferrous metal samples. The additional slides tested with Paraloid B72 in xylene were found to still affect the O₂ levels, but less significantly. Using acetone as the solvent in the coating had less of an effect on the O₂ sensor spot than xylene in the coating originally. Therefore storing slides coated 10% w/v Paraloid B72 solution in acetone for 21 days at 20 °C 40% RH after drying should allow for solvent evaporation, and eliminate the impact on the O₂ sensor spot. This was tested and these slides were

assessed for 84 days to confirm fluctuations were within the error of the O₂ meter (± 2 hPa).

Cosmoloid H80

Cosmoloid H80 was also prepared as a 10% w/v concentration solution. Cosmoloid H80 was initially trialled with toluene due to its solubility in toluene and the slower evaporation of toluene than many other solvents, but Cosmoloid H80 in toluene did not produce an evenly distributed coating on glass slides. Despite the uneven coverage of the coating on glass slides not being visually suitable, the effect of the coating on the O₂ concentration was still tested, and resulted in no impact on the O₂ partial pressure measurements. An uneven coating is only likely to affect the O₂ partial pressure measurements if solvent is being retained within the coating.

Table 44 Coating and solvent tests run to test the impact on the O₂ sensor spot

Solvent	Coating	No. of jars/slides monitored	No. of days of monitored	Comments
Acetone	PB72	5	39	
Acetone	PB72	5	84	21 days de-gassing at 20°C, 40% RH prior to O ₂ monitoring
White Spirits	CH80	3	14	
Isoamyl Acetate	S10	5	30	

White spirit a popular solvent for use with Cosmoloid H80 (4.5.2.2) was trialled, applying the wax coating to air abraded, warmed glass slides (4.3.2.1). Air abrasion was used to key the surface making it more adhesive for the coating, promoting good surface coverage on the slides. Only the slides were warmed, similar to conservation practise where wax is applied to warmed sculptures. Three 10% w/v Cosmoloid H80 in white spirit slides were tested to confirm there was no effect on the O₂ sensor spots and fluctuations are within the error margins.

Siliglide 10

Five Siliglide 10 coated slides were set up and tested for their impact on the O₂ sensor spots as was done with the other coatings. Although guidance for application is to dip or wipe articles, for continued standardisation of the coatings it was applied by brush undiluted. Prior to coating the slides were not air abraded or

warmed, but the coating was buffed approximately 10 minutes after application, before it was completely cured.

The concentrations and solvent/coating combinations for use with the ferrous metal samples are as summarised in table 45.

Table 45 Coating concentrations and solvents used

Coating	Concentration	Solvent
Paraloid B72	10% w/v	Acetone
Cosmoloid H80	10% w/v	White spirit
Siliglide 10	As sold > 10% poly(1,1-dimethylsilazane), 5% poly(dimethylsiloxane), silanol terminated	Isoamyl acetate (isopentyl acetate)

5.3.1.3 Accelerated Corrosion: Chloride Deposition and Testing

A 100 ml of the GM9540P 1.25% salt solution was prepared using 0.9% w/v NaCl (0.9 g), 0.1% w/v CaCl₂ (0.1 g) and 0.25% w/v sodium hydrogen carbonate (NaHCO₃) (0.25 g). The NaHCO₃ was dissolved separately in 25 ml of the distilled water before combining it with the other two dissolved components to avoid precipitation.

Application of the salt solution was trialled by pipette and spray. Both application methods were tested for the chloride deposition and uniformity of corrosion formation.

The chloride (Cl⁻) meter, a Radiometer Analytical PHM250 specific ion meter with a mercury/mercury sulfate reference electrode (REF621) and a chloride-specific electrode (ISE25Cl) (detection limit approximately 0.5 ppm, error c. 10%), was calibrated prior to treating the samples. Five dilutions were made from the calibration standard 0.1M NaCl aliquot (3544 ppm Cl⁻) for the preliminary tests 354.40, 177.20, 70.88, 35.44 and 7.09 ppm Cl⁻. Of the four lower concentrations 10 ml were added to separate small plastic beakers along with magnetic stirrer bars and 1 ml buffer (0.5M acetic acid/0.5M ammonium acetate in deionised water). Adding the ionic adjustment buffer adjusts the sample and standard solutions to the same ionic strength and pH, allowing the concentration rather than the activity to be measured and read directly off the meter. Addition of the buffer diluted the solutions further, thus Cl⁻ concentrations for calibrating the specific ion analyser were: 161.10, 64.44, 32.22 and 6.44 ppm.

The amount of Cl^- deposited by 10 drops of the salt water was tested using five samples. Samples were placed corrosion side down in separate beakers containing 15 ml de-ionised water and agitated gently for 30 seconds, before removing and drying the samples. As with the calibration tests 10 ml of the solution was placed into a small plastic beaker with a small magnetic stirrer and 1 ml buffer, diluting the solution and creating a total volume of 11 ml. These solutions were then tested for Cl^- concentrations.

The five samples used for drop application were re-used to determine the reproducibility and uniformity of Cl^- applied by spray application, after rinsing with de-ionised water, and cleaning by air abrasion. The samples were prepared one at a time, with the sides of the samples blanked off using masking tape (figure 89) and 1-2 mm of the masking tape overlapping the edge of smoother of the two surfaces. The spray bottle containing the salt solution was held in a stand and clamp (figure 90) with the nozzle 20 cm above the sample surface. The sample placement was determined by the distribution of salt solution after an initial spray with no sample present. Fresh dry paper was placed under each sample before application of the salt solution by one press of the spray bottle (figure 90).

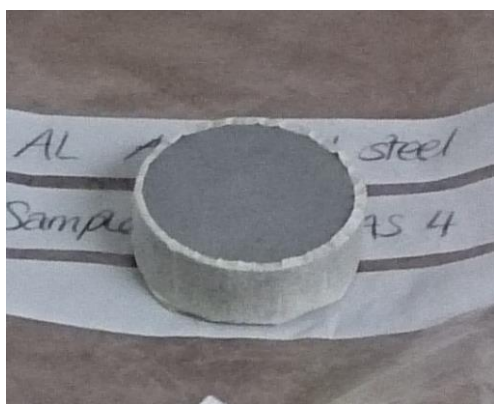


Figure 89 Sample with sides blanked-off



Figure 90 Spray bottle/sample set up.

Once sprayed with salt solution the masking tape was removed from the sample immediately and the sample was placed, sprayed side down in 15 ml de-ionised water. The water was agitated gently for 30 seconds, immediately after which the sample was removed and dried. As with the tests above 10 ml of the solution was placed into a small plastic beaker with a small magnetic stirrer and 1 ml buffer, before testing the Cl^- concentrations by direct measurement, which gives accurate and repeatable readings ($\pm 10\%$) with only one calibration.

The five samples were rinsed off by applying excess de-ionised water to both sides of the samples, dried with tissue-paper, cleaned by air abrasion, blanked with masking tape, and re-sprayed twice more. The first time the samples were again tested for Cl⁻ ions. The second time the samples were left to corrode at c. 19 °C, 50% RH without testing for Cl⁻ to observe the dried surface and the uniformity of the corrosion formation.

5.3.2 Preparation and Testing of Coating Performance

This section focuses on testing the sample material prepared in a variety of ways. The sample names, numbers, surface condition and coatings that were used for O₂ consumption testing are listed in table 46.

5.3.2.1 Sample Material Corrosion Rates Uncoated

To collect baseline data of the steel corroding without protection provided by fresh coatings the armoured steel was treated in the following 3 ways before testing:

1. Untreated – old damaged paint layers, corrosion and mill scale still present
2. Surfaces cleaned – samples air abraded to grade Sa2.5 finish (very thorough blast cleaning to achieve near white metal)
3. Partially corroded – samples cleaned as described above and corroded on one side using the standardised spray accelerated corrosion method above.

To test each of these treatments, 15 samples, 5 for each treatment method were tested for their influence on the O₂ partial pressure. The jars were set up as shown in figure 91 and figure 92 containing the items listed in table 47 for each jar. One jar was also set up as a control with no sample to reveal any fluctuations experienced that are not caused by the ferrous metal samples. Internal jar temperature was allowed to equilibrate with the temperature within the climatic chamber before the jars were sealed tightly. The O₂ partial pressure measurements were recorded as described above for the coated glass slides, with measurements made every 10 seconds for 5 minutes for each jar after it was tightly sealed. The jars were then assessed again 24 hours later recording data for 5 minutes for each jar and again 24 to 48 hours later, after which measurements were gradually spaced further apart, but each time recording measurements every 10 seconds for 5 minutes. The number of days the O₂ partial pressure in the jars was assessed (table 46), was influenced by rate of reduction in the O₂ partial pressure.



Figure 91 Jar setup - pink O₂ sensor spot adhered inside the jar, conditioned silica gel, data logger and sample.



Figure 92 Sealed jar containing content listed in table 47 and table 48.

Table 46 Sample names, numbers, surface condition, coating and no. of days of O₂ monitoring

Sample group names	No. of samples tested	Surface condition	Coating used (% as weight per volume)	No. of days O ₂ consumption was monitored
NS* Control	0	N/A	None	Run alongside different testing groups 163/65/341/218
UT*	5	Old paint and corrosion layers present	No additional coating added	163
	1			342
CS*	5	Cleaned by air abrasion	None	65
	1			341
PC*	5	Cleaned and partially corroded (corroded on one side only)	None	48
PB72CS	5	Cleaned surface and coated	10% Paraloid B72 in acetone	341
CH80CS	5		10% Cosmoloid H80 in WS	
S10CS	5		Siliglide 10 as sold	
PB72PC	10	Cleaned, partially corroded (de-icing salt corroded) and coated	10% Paraloid B72 in acetone	342
CH80PC	10		10% Cosmoloid H80 in WS	
S10PC	10		Siliglide 10 as sold	
PB72SC	10	Cleaned, coated, coating scribed and scribed area painted with salt solution	10% Paraloid B72 in acetone	70 + 148 = <u>218</u>
CH80SC	10		10% Cosmoloid H80 in WS	
S10SC	10		Siliglide 10 as sold	

*NS = No sample; UT = Untreated; CS = Cleaned sample; PC = Partially pre-corroded;

SC = Scribe creep test

PB72 = Paraloid B72; CH80 = Cosmoloid H80; S10 = Siliglide 10; WS = White spirit

Table 47 Content of different sample jars

Content of jars	NS (no sample)	UT (untreated samples)	CS (cleaned samples)	PC (partially pre-corroded samples)
Conditioned silica gel 159 g ~80% RH	✓	✓	✓	✓
SEM tripod clip stand	✓	✓	✓	✓
Data-logger (in 1 jar of each sample group)	✓	✓	✓	✓
Sample		✓	✓	✓

5.3.2.2 Coating Application Methodology

Paraloid B72 and Cosmoloid H80 coatings were prepared within the fume cupboard as described above, but Siliglide 10 was used as supplied.

With the exception of the untreated control group, all the armoured steel samples were air abraded with aluminium oxide (section 5.3.1.1.3). All the samples were photographed before treatment and after each stage of preparation.

Thirty samples were left to partially corrode for 8 days before coating, after using the spray accelerated method described above. Prior to coating the samples they were photographed and their masses were recorded using the Mettler Toledo AX504 balance. The samples were heated at 50 °C (in a SNOL 60/300 LFN laboratory oven) for a minimum of 1 hour before coating to ensure they were warmed through and eliminate any surface moisture. Samples were also heated at 50 °C prior to the application of the second and third layers.

As with the application of the coatings to the glass slides a small amount of the coating being applied was decanted into a beaker. The number of samples, surface condition and coating used are listed in table 46. Clean samples were coated first followed by the corroded samples to prevent contamination of the clean samples. A soft bristled ½” brush was used dipping it into the coating mixture once and wiping the excess on the edge of the beaker once. Three strokes were used to apply the coatings across the surface of the sample. The edges of the samples were coated by brushing in an upward direction, dipping the brush into the coating mixture twice to coat the full 360°.

The samples coated with Siliglide 10 were buffed using Kimberly-Clark® Professional KIMCARE® medical wipes 10 minutes into the curing time. All samples

were allowed to dry for a minimum of 1 hour to allow for the majority of the solvent to evaporate at a speed, similar to in situ application before being re-heated at 50 °C for a further hour. Samples were then turned over and the uncoated surface was coated with three strokes of fresh coating.

Once touch-dry the samples and coating masses were recorded. The masses were monitored over 48 hours, after which the second coating was applied. The drying time was largely based on the tests carried out on glass slides. The masses were monitored and the third coating layer was applied after a further 48 hours. Following the application of the 3rd coating layer the mass was monitored and the samples were left to dry for a further 48 hours. Samples were stored in the climatic chamber at 20 °C, between 30 to 40% RH for 3 weeks to allow them to de-gas (due to the solvent retention of Paraloid B72).

Scribe creep testing discussed in chapter 3 as a method industry uses to test adhesion of coatings to the substrate surface was also trialled with 30 samples, 10 for each clear coating. Samples were coated and stored as described above for the clean coated samples but after the 3 weeks the samples were then scribed using a scalpel to cut a 2 cm line through the coating into the steel underneath. The samples were held still using adhesive putty and a metal ruler was used to guide the scalpel cut through the coating. To accelerate any corrosion that may occur at these cuts, the previously prepared de-icing salt solution was painted down the cut in the coating using a very thin soft bristled brush. The samples were then allowed to begin corroding within the laboratory (18 to 20 °C, 40 to 50% RH). All samples were photographed prior to assessing the reduction in O₂ partial pressure and at all stages throughout this research.

5.3.2.3 Oxygen Partial Pressure Measurements of Coated Steel Samples

Frequently within conservation and industry corrosion rates are quantified by calculating the surface area of the sample that is covered with corrosion. This works well for uniform corrosion but not where corrosion is localised, for example for pitting corrosion, corrosion rates can be underestimated or for filiform corrosion where corrosion is superficial but looks aggressive, corrosion rates are overestimated. This method cannot be applied to surfaces which are already corroded and as coatings within conservation are often used on surfaces which are already corroded pre-corroded surfaces will also be utilised in testing the coatings. Therefore, the reduction in the O₂ partial pressure within the jars caused by the samples has been

used to compare the corrosion rate of the samples. This method was also employed by Shashoua and Matthiesen (2010), however, in this project small samples are used and the temperature and RH are controlled. Historic steel samples are used within this project rather than Q panels (analogues).

The sample group names, number of samples and treatment of samples being tested are listed in table 46. Larger sample numbers provide more reliable results with greater precision and power, reducing uncertainty, but sample numbers and time limits restricted numbers. Five samples were therefore used for each coating type used on the cleaned surface coated sample. Ten samples were used for each coating type used on the partially pre-corroded samples and for each coating type used on the scribed coated samples.

After photographing the surfaces of the samples, they were placed in jars containing O₂ sensor spots and the content as listed in table 48 before being sealed and placed in the climate chamber as described for the uncoated samples.

Table 48 Content of jars containing samples

Content of jars	PB72 CS	CH80 CS	S10 CS	PB72 PC	CH80 PC	S10 PC	PB72 SC	CH80 SC	S10 SC
Conditioned silica gel 159 g ≈80% RH	✓	✓	✓	✓	✓	✓	✓	✓	✓
SEM tripod clip stand	✓	✓	✓	✓	✓	✓	✓	✓	✓
Datalogger (in 1 jar of each sample group)	✓	✓	✓	✓	✓	✓	✓	✓	✓
Sample	✓	✓	✓	✓	✓	✓	✓	✓	✓

The jars remain sealed and O₂ levels in the jar were measured on a regular basis for the number of days listed in table 46. Although, the scribed samples were removed after 70 days of O₂ monitoring, photographed and returned to the chamber for a further 148 days, making a total 218 days of assessing the change in O₂ partial pressure.

All of the coated samples were returned to their jars, after being taken out to photograph at the end of the measurements made for this thesis and an initial measurement was made on them being returned to the chamber. All of the coated

samples are still running within the chamber, with the O₂ consumption being monitored so that long term degradation of the coating can be considered.

5.3.3 Compatability of the Clear Coatings with Cromadex Paint

5.3.3.1 Effect of Cromadex Paint on the Oxygen Sensor Spots

As with the clear coatings, the Cromadex paints used by the TM were also tested for their effect on the O₂ sensor spots. Degreased glass slides were coated and then placed into the climate chamber in Ball Mason jars. The number of layers added to the glass slides, finish and layer within a paint system, colour, and the number of slides coated/number of jars monitored for the effect on the O₂ sensor spots are listed in table 49.

Table 49 Cromadex paint colour, finish and numbers involved in monitoring

Finish and layer within paint system	Cromadex Code for tested paints	Colour	No. of coating layers added to glass slides	No. of slides coated/ No. of jars for O ₂ monitoring	No. of jars with data loggers included
No glass slide - control	N/A	N/A	N/A	1	1
Cleaned glass slide - control	N/A	N/A	N/A	1	1
Primer – Red Oxide – base layer	2100	Red	1	3	1
Matt – top coat	222	Green	2	3	1
		Panzer grey	2	1	1
Gloss – top coat	222	Green	2	1	1
Semi-gloss – top coat	222	Black	2	1	1
		Olive green	2	3	1

5.3.3.2 Compatibility of Cromadex Paint and the Clear Coatings

Cromadex paint on glass slides affected the O₂ sensor spots and so the compatibility was only tested visually on glass slides. Future work may establish the length of time these paint need for solvent evaporation or paint controls will need to be run alongside sample tests.

Glass slides were degreased and air dried, before Kimberly-Clark® Professional KIMCARE® medical wipes were used to remove drying marks. These glass slides were then all half coated with Cromadex paint, 3 slides for each of the Cromadex paint variations (colour and finish) and left for a minimum of 24 hours to dry. The drying and over-coating times specified on the datasheets for the coatings are listed below in table 50.

Table 50 Drying and over-coating times for Cromadex 2100 Primer and Cromadex 222 Topcoat as specified by manufacturer's datasheets

	Drying times				Over-coating times			
	Touch dry (minutes)		Through dry (hours)		Minimum (minutes)		maximum	
	20 °C	35 °C	20 °C	35 °C	20 °C	35 °C	20 °C	35 °C
Cromadex 2100 red oxide primer	25	15	6	5	25	15	Unlimited	Unlimited
Cromadex 222 top coat paint	25	15	16	12	60	40	Indefinite	Indefinite

The clear coatings (PB72, CH80 and S10) were added to the slides half coated in each of the different paints, overlapping approximately half of the paint already on the slide. This made it possible to see if the solvent used in the clear coatings affected the paint, possibly dissolving some of it and dragging it over the rest of the glass slide. Three layers of the clear coatings were added as with all the other stages within this research. Each layer was given at least 24 hours to dry. The glass slides were photographed using the LED lighting system and the fibre optic lights normally used with the microscopes, to enhance the visibility of the brush strokes of clear coatings on the glass slides.

At all stages of this methodology every effort was made to control variables and create a reproducible method.

6 Results and Analysis

6.1 Field Test Results

6.1.1 Corrosion Products From Around Scotland - X-Ray Diffraction

From the samples collected from the 22 different sites around Scotland, 72 samples were analysed by XRD and table 51 summarises the frequency with which different corrosion products were detected. The summary has been produced from the data in table 52, which summarises the corrosion products detected in the spectra and other components when they were detected, in addition to the atmospheric environment from which they were collected.

The short summary in table 51 shows that magnetite/maghemite, which cannot be distinguished between by XRD are the most frequent major component of the samples tested. Goethite and lepidocrocite have very similar occurrence frequencies.

Table 51 Summary of the corrosion products detected around Scotland. (Major components $\geq 75\%$, $50 \leq \text{moderate} < 75\%$, $10\% \leq \text{minor} < 50\%$, trace $< 10\%$ of the major peak intensity)

Corrosion products detected	Number of times detected in corrosion samples				
	Major	Moderate	Minor	Trace	Total
Magnetite/Maghemite	47	10	10	1	68
Goethite	36	20	10	2	68
Lepidocrocite	35	24	8	2	69
Akaganéite	6	13	27	16?	62?

NB. The '?' used in the table above indicates a level of uncertainty with the number of times trace amounts of akaganéite was detected – 6 samples included trace amounts of akaganéite, on a further 10 samples a trace may have been present but the XRD spectra was not sufficiently clear to be certain.

Analyses of the spectra also detected some paint and stone components in several of the corrosion product samples:

- **Barium sulfate** (BaSO_4) was detected in samples from Arbroath Abbey (3), Dunkeld Cathedral (8), Edzell (1), Newhailes House (2) and Priorwood Gardens (5). It is used as a component of white pigment in paint or in oil paint it is used as a filler or to modify consistency.

- **Hydrocerussite** ($\text{Pb}_3(\text{CO}_3)_2(\text{OH})_2$) was detected at Arbroath Abbey (3), Newhailes House (2) and Priorwood Gardens (5). Hydrocerussite is the name of naturally occurring white lead ($2\text{PbCO}_3 \cdot \text{Pb}(\text{OH})_2$), but what is detected here is most likely white lead which used to be used in paint, but is now banned in most countries as it tends to cause lead poisoning.
- **Quartz** was detected at Dumfries Midsteeple, and in this case it is likely to be a component from the sandstone of the building rather than the paint, quartz is also a very common dust component.

The spectra produced from the powder XRD of the corrosion samples were analysed and a summary of the location information and data obtained from the XRD spectra is shown in table 52.

The data collected from the XRD spectra is only semi-quantitative. Many of the spectra have low count rates as shown by the counts per second (CPS) values in table 52, and this increases the difficulty of identifying the corrosion products from the back ground noise. Thus trace components are ignored in further analyses. Attempts to plot the occurrence of akaganéite against the distance from the coastline failed to highlight a clear trend (figure 93) and further highlights the complexity of the corrosion mechanisms and the interaction with the environment.

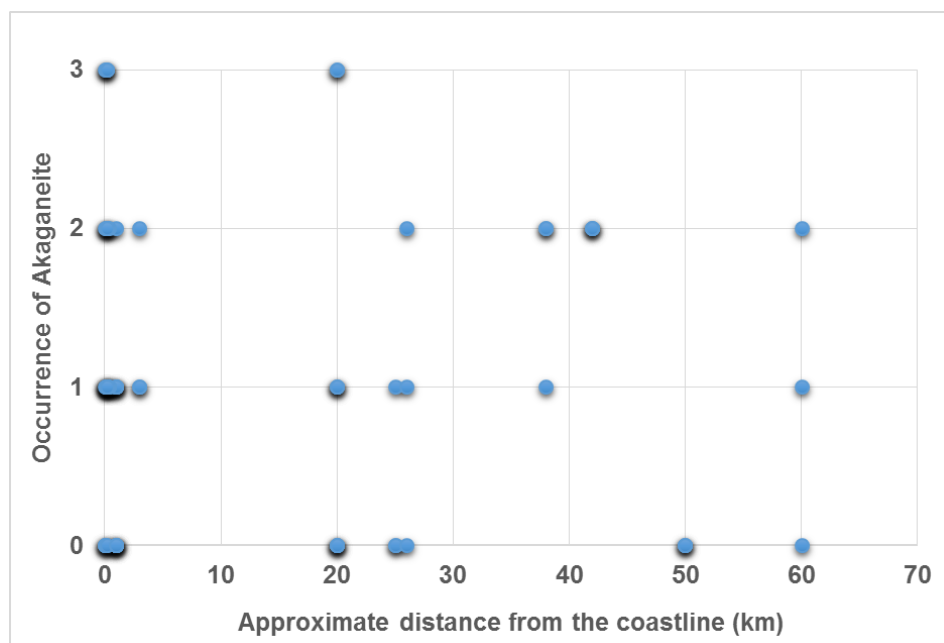


Figure 93 Distance vs occurrence of akaganéite (minor = 1; moderate = 2; major = 3) – higher intensity shadows imply multiple points plotted at the same location.

Table 52 Corrosion products found on historic wrought iron and mild steel around Scotland; (I = industrial, M = marine, R = rural, U = urban atmospheres);
(Major components $\geq 75\%$, 50 \leq moderate component $< 75\%$, 10% \leq minor component $< 50\%$, trace components $< 10\%$ of the major peak intensity); (A = Akaganéite, G = Goethite, H = Hematite, L = Lepidocrocite, M = Magnetite/Maghemite)

Site	Sample No.	Approximate description of location in Scotland			Highest peak values from XRD scan		Corrosion Product Identified				Paint components identified
		Compass description	Distance from the coast	Atmospheric description	Angle	CPS	Major Components	Moderate Components	Minor Components	Trace Components	
Arbroath Abbey	3				42.68	479.17	-	-	-	A, L	Barium Sulphate & Hydrocerussite
	9	East	~ 1 km	U/M	35.58	631.67	M	G, L	-	A	-
	10				35.52	495.83	M	G, L	A	-	-
Broughty Castle, Dundee	3				35.64	397.5	G, M	L	-	A	-
	6	East	~ 5 m	M	35.56	306.67	G, M	L	-	A	-
	10				35.62	197.5	M	L	G	A	-
Clay Potts Castle, Dundee	3				35.58	685	M	L	G	A?	-
	8	East	< 1 km	U/M	35.62	103.33	M	G, L	-	A?	-
	12				36.46	372.5	G, L, M	-	-	-	-
Dunbar Castle	1				36.72	144.17	A, G, L	M	-	-	-
	2	East	< 5 m	M	36.62	387.5	G, L	A	M	-	-
	5				35.6	231.67	M	L	A, G	-	-

Dumbarton Castle on the River Clyde	6	West	<200m from the River Clyde	U/M	35.62	95	M, L	A, G	-	
	9				36.32	151.67	G, L, M			A?
	11				36.38	296.67	G, L, M			A
Dunkeld Cathedral	3	Central	<100 m to the River Tay	R	36.26	550	G, L, M	Barium Sulphate	-	
	8				35.56	543.33	G, L, M			
	9				35.58	581.67	M			G, L
Dumfries, Midsteepie	1	West	<300 m from the River Nith	U	26.68	765	A	G, L	M	
	2				21.16	573.33	A, G	L	M	
	4				26.66	3033.33			G, L, M	Quartz –main component
	2				35.58	619.17	M		A, G, L	
Dunglass Collegiate Church	7	East - coastal	~ 1 km	MR	35.54	487.5	M	A, G, L	-	
	11				35.52	558.33	M	G	A, L	-
	4				36.38	413.33	G, L	M		A?
Dunstaffnage Castle & Chapel	9	West	~ 100 m	R/M	36.32	330.83	G, L, M	A	-	
	11				35.6	563.33	M	G, L	A	-
	1				25.94	482.5	L	G	A, M	Barium Sulphate
Edzell	4	East	< 20 km	R	36.34	403.33	G, L	M	A?	
	5				36.52	446.67	G, L	M	A?	
	4				36.58	557.5	G, L, M	A		
Fyvie Castle	8	North East	~ 25 km	R	35.58	644.17	M	G, L	A	
	12				36.3	575	G, L, M		A?	
	2				35.56	475.83	M	G, L	A	
Fort George	4	North	~ 100-200 m	M	35.18	411.67	A, G,	L, M		
	8				35.58	320	M	G, L	A?	

Glasgow Cathedral	2	West	< 2 km from the River Clyde	U	35.54	582.5	G, L, M			A?	
	4				35.52	439.17	G, L, M		A		
	5				35.48	571.67	M	G, L	A		
Kinnaird Head, Fraserburgh	3	North East	< 100 m	M	36.6	390	A, G, L	M			
	6				36.2	396.67	G, L, M		A		
	12				35.56	323.33	G, L, M	A			
Newhailes House	2	East	< 1 km	U/R/M	27.14	791.67		L		G	Barium Sulphate & Hydrocerussite
	7				35.56	380.83	G, L, M		A		
	12				36.34	417.5	G, L	A, M			
Palace of Holyrood House	4	East	< 3 km	U/R	35.58	540	M	G, L	A		
	6				35.52	504.17	M		A, G, L		
	9				35.7	499.17	G, M	L	A		
Priorwood Garden, Melrose	1	South East	~ 42 km	U/R	36.42	465	G, L	A	M		
	5				26.74	425.83		G, L, A	M	Barium Sulphate & Hydrocerussite	
	8				36.46	370	G, L	A, M			
St. Andrew's Cathedral	2	East - Coastal	~ 325 m	M/R/U	35.66	433.33	L, M	A, G			
	8				35.66	374.17	G, L, M		A		
	10				35.64	461.67	M	G, L	A		
Skelmorlie Aisle, Largs	3	West - Coastal	~ 160 m	M/U	35.6	315.83	M	G, L	A		
	6				36.62	405	G, L	M	A		
	10				35.54	440	M	G, L	A		

Stromness, Ness Battery, Orkney	1	North of Scotland, SW of Orkney Mainland	~ 220 m	MR	36.24	360.83	G, L		A, M	
	4				35.68	215	L, M	A, G		
	11				35.56	402.5	M	G, L	A	
Summerlee Museum, Coatbridge	1	Central	> 26 km	U	35.52	1041.67	M		G, L	A
	5				35.58	264.17	G, M	L	A	
	9				35.58	425.83	M	G	A, L	
Traquair House	3	East/ Central	> 38 km	R	36.4	321.67	G, L	M	A	
	8				36.38	416.67	G, L, M	A		
	9				36.5	424.17	G, L	A, M		
Scapa Flow Visitor Centre and Museum - samples not collected in person	1	North of Scotland, East of Hoy Orkney	~ 200 m	M	35.32	161.67	A, G, L, M			
	5				35.52	303.33	L, M	A, G		
	7				35.6	427.5	G, L	A, M		

SW = South West

6.1.2 Internal Environment Data - The Tank Museum

The large volume of data received from and collected at the Tank Museum has been reduced considerably, to help draw out any patterns. Without summarising the large volume of data key pieces of information would be lost within the mass of data points on a graph. By considering the range in the environmental data it reveals the potential for wetting and drying to occur on metal surfaces and initiate corrosion.

6.1.2.1 Data collected by the Tank Museum (TM)

Summary tables of data collected and supplied by the TM from Oct 2011 to Aug 2012 are included in the appendix 10.1. The maximum, average and minimum temperatures (figure 94) and RHs (figure 95) experienced in the visitor areas of the museum during this time period are shown below in the bar charts.

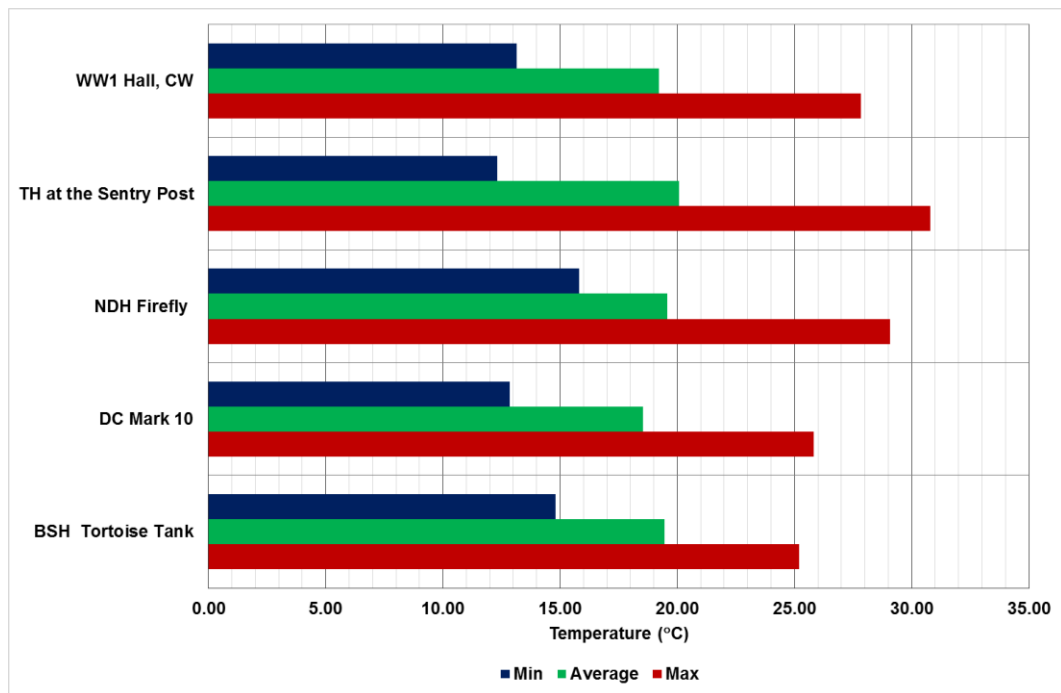


Figure 94 Range in temperature experienced around the Tank Museum between Oct 2011 and Aug 2012. The data logging locations are shown in figure 67 - TH = Tamiya Hall; NDH = New Display Hall; DC = Discovery Centre; BSH = British Steel Hall.

The temperature and RH in the Discovery Centre (DC) logged from Oct 2011 to Aug 2012 with the logger located on the Mark 10 tank had a range of 12.9 °C from 12.9 to 25.8 °C and 63% from 19 to 82% (table 53). Table 53 has been included for comparison as data was also collected from within the Sherman V Crab also within the DC. Although the average RH over this monitoring period is approximately 53% RH, table 53 clearly shows there are periods of time where the RH is above 60% a critical humidity level.

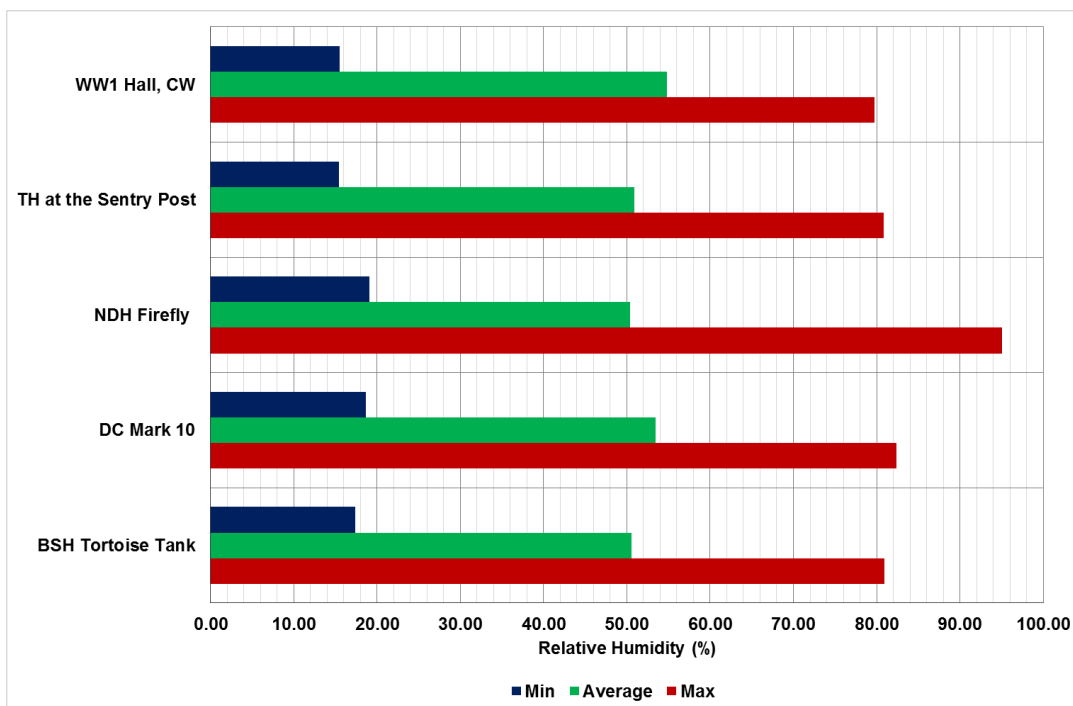


Figure 95 Range in RH experienced around the Tank Museum between Oct 2011 and Aug 2012

Table 53 Data summary collected in the Discovery Centre on the Mark 10

Monitoring period	Start date	End Date	Temperature (°C)			Relative Humidity (%)		
			Min	Ave	Max	Min	Ave	Max
Oct - Nov '11	24/10/2011	16/11/2011	16.8	17.8	25.7	47	67	80
Nov '11 – Jan '12	16/11/2011	19/01/2012	14.2	17.4	22.8	29	51	70
Jan – Mar '12	19/01/2012	05/03/2012	12.9	17.4	23.0	19	41	62
Mar – May '12	05/03/2012	01/05/2012	17.1	18.1	23.0	26	43	60
May – Jun '12	01/05/2012	22/06/2012	17.1	19.7	25.0	33	54	79
Jun – Aug '12	22/06/2012	29/08/2012	18.0	20.8	25.8	41	65	82

On top of the Firefly in the NDH the temperature range 13.3 °C fell between 15.8 and 29.1 °C and the RH range 76% fell between 19 and 95%, (table 54).

Table 54 Summarised data collected in the New Display Hall on the Firefly

Monitoring period	Start date	End Date	Temperature (°C)			Relative Humidity (%)		
			Min	Ave	Max	Min	Ave	Max
Oct - Nov '11	24/10/2011	16/11/2011	18.0	19.5	22.9	46	60	72
Nov '11 – Jan '12	16/11/2011	19/01/2012	15.8	18.8	22.9	26	46	64
Jan – Mar '12	19/01/2012	05/03/2012	17.3	18.8	23.5	19	38	73
Mar – May '12	05/03/2012	02/05/2012	16.0	18.6	29.1	25	42	95
May – Jun '12	02/05/2012	22/06/2012	16.2	20.0	24.3	34	54	93
Jun – Aug '12	22/06/2012	29/08/2012	19.3	21.8	25.4	41	62	77

Between 17th November 2011 and 22nd June 2012 a logger that was placed inside the Firefly in the New Display Hall recorded temperatures ranging from 16.4 to 25.4 °C (9.0 °C) and relative humidities between 17 and 87% (70%) (table 55). Tables 54 and 55 have been included as data was also collected inside the Sherman Firefly in the NDH over approximately 27 months during this project.

Table 55 Summary of data by the TM in the New Display Hall inside the Firefly

Monitoring period	Start date	End Date	Temperature (°C)			Relative Humidity (%)		
			Min	Ave	Max	Min	Ave	Max
Nov '11 – Jan '12	17/11/2011	19/01/2012	16.9	18.8	23.1	28	46	62
Jan – Mar '12	19/01/2012	05/03/2012	16.4	18.9	23.0	17	37	57
Mar – May '12	05/03/2012	01/05/2012	16.6	18.7	25.4	28	42	87
May – Jun '12	01/05/2012	22/06/2012	16.9	20.0	23.5	40	53	68

The data collected in the various sheds at the TM have been considered separately from the data collected in the visitor areas as the data collected covers a more extreme range. The minimum temperatures measured in the sheds all fell below zero except the new shed (indicated by the yellow lines). The maximum value for shed 1 extension reached above 40 °C (figure 96).

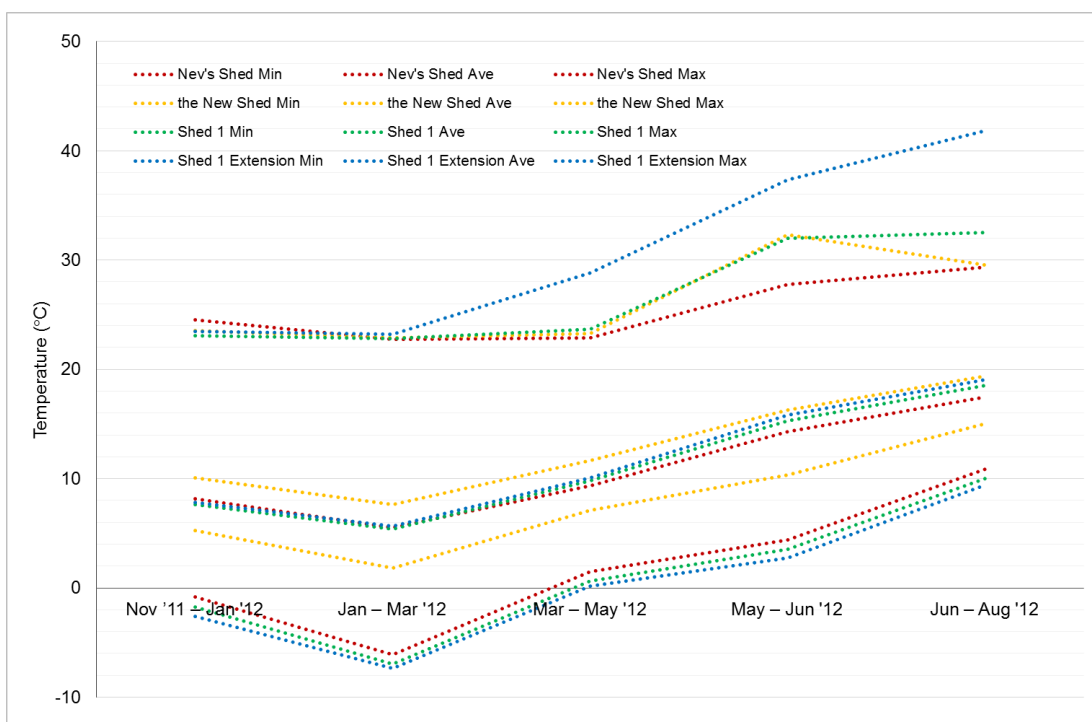


Figure 96 Temperature ranges for the sheds at the TM between Nov 2011 and Aug 2012

The maximum RH measurements for all of the sheds reached 100% and the average values were all above 70% between Nov 2011 and Aug 2012 (figure 97). The minimum values all fall below 50% RH.

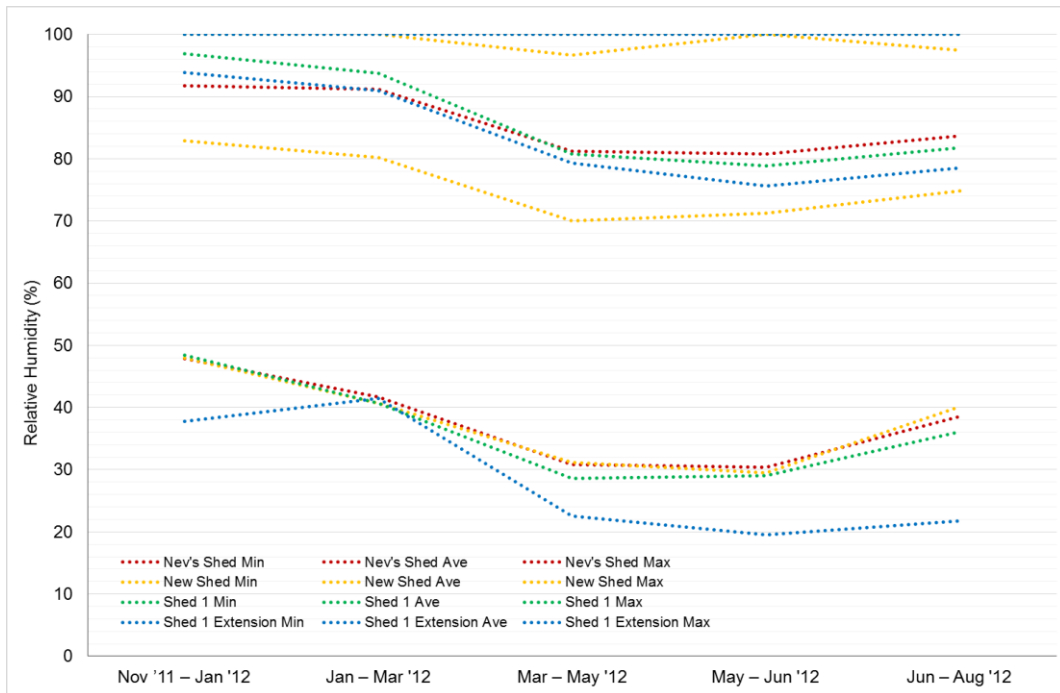


Figure 97 Range of RH measured within the sheds at the Tank Museum between Nov 2011 and Aug 2012

6.1.2.2 Data collect inside tanks

The interiors of the Sherman Firefly in the NDH with radiant heating and the Sherman V Crab in the unheated DC were monitored for ~27 months. Figures 98 and 101 presents the average daily temperatures and RHs of the two data loggers in each vehicle combined. Figures 99 and 102 shows the temperature cycles in the two vehicles over the 27 month period and include the maximum and minimum values along with the average. The RH cycle in the two vehicles are shown in figures 100 and 103, again the daily maximum and minimum values are included with the average. Horizontal lines are included on the RH graphs to highlight 60, 75 and 80% RH, important RH values when considering corrosion.

The average daily data from within the two vehicles differ according to the building the vehicles were located in. The temperature data is compared in figure 104 and the RH data is compared in figure 105.

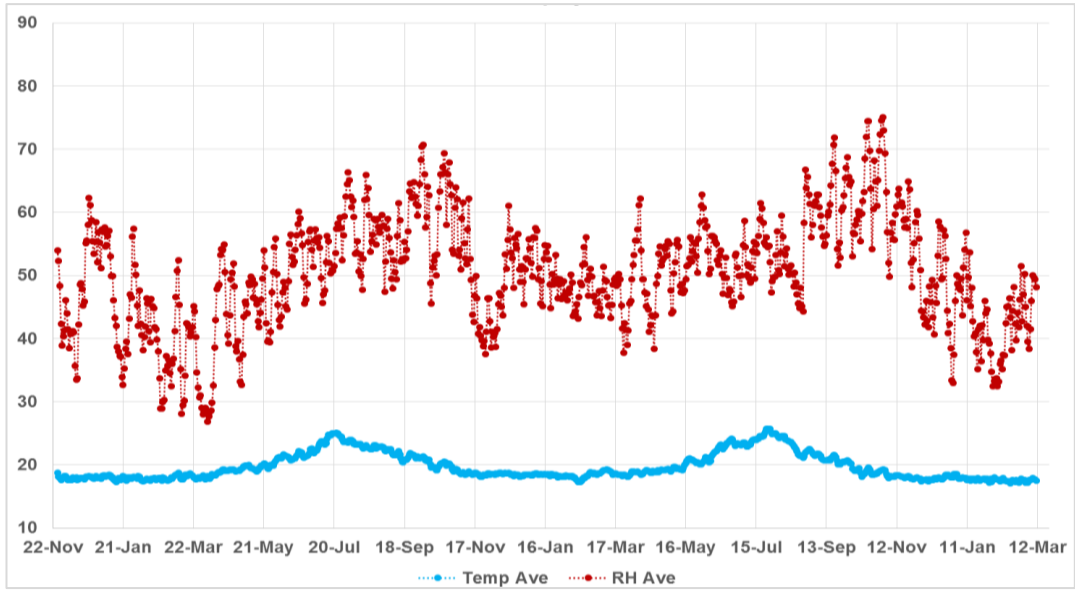


Figure 98 Average daily temperature and RH data from the two data loggers stored inside the Sherman Firefly in the NDH

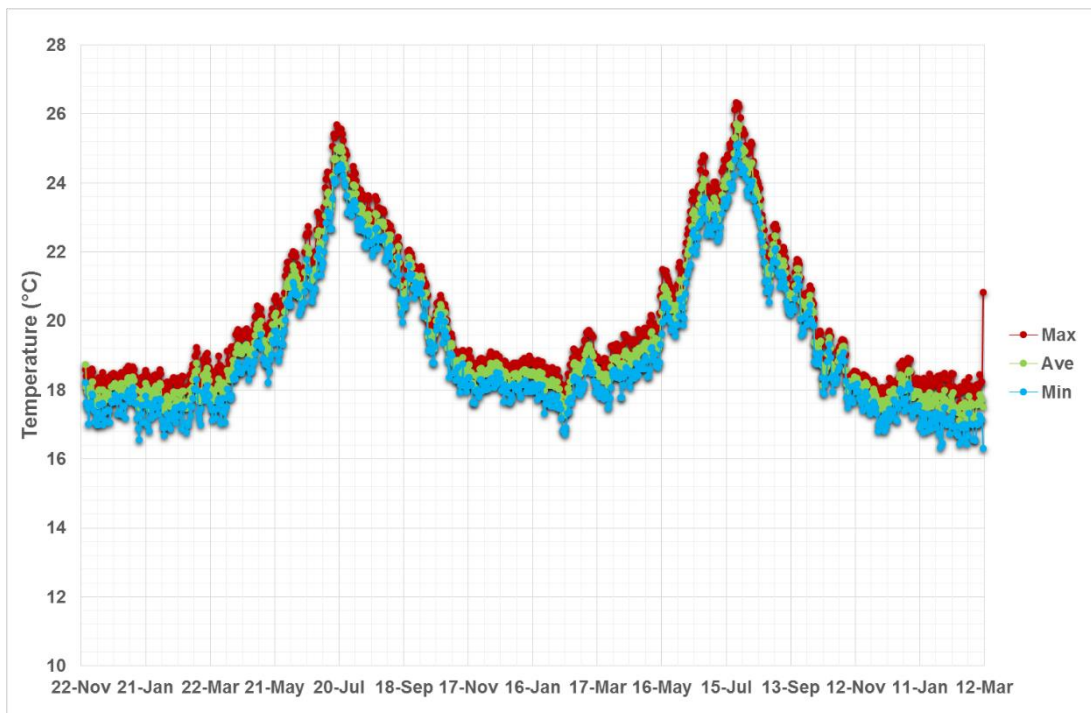


Figure 99 Summary of the temperature data collected by two data loggers stored inside the Sherman Firefly in the NDH

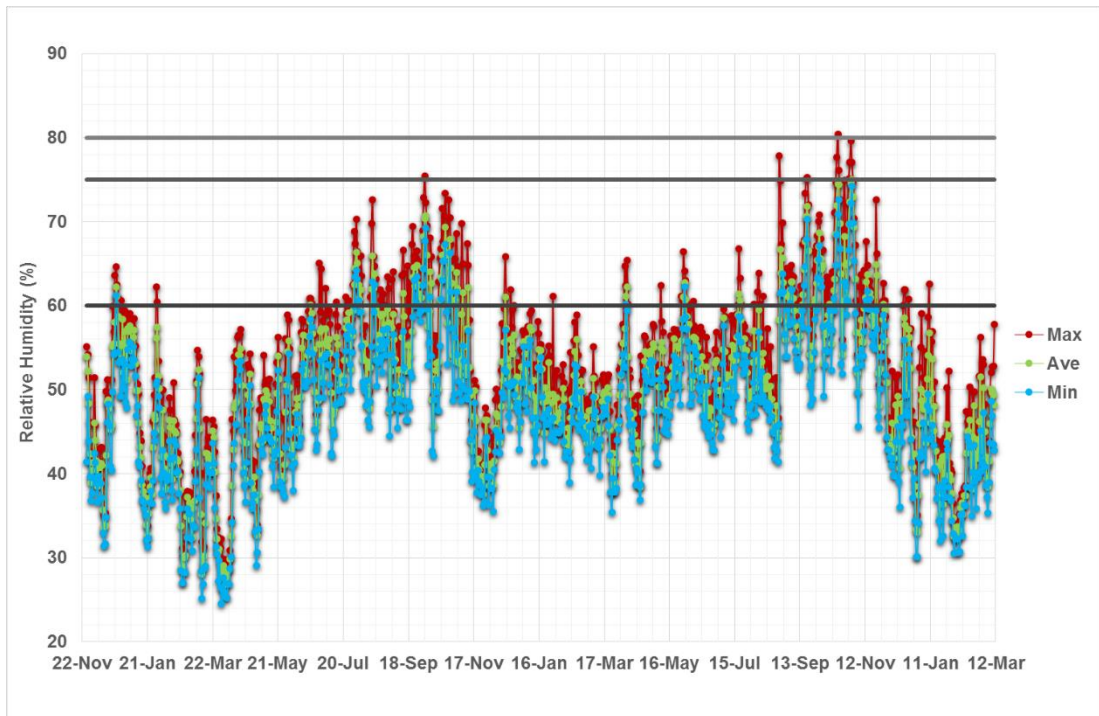


Figure 100 Summary of the RH data collected by two data loggers stored inside the Sherman Firefly in the NDH

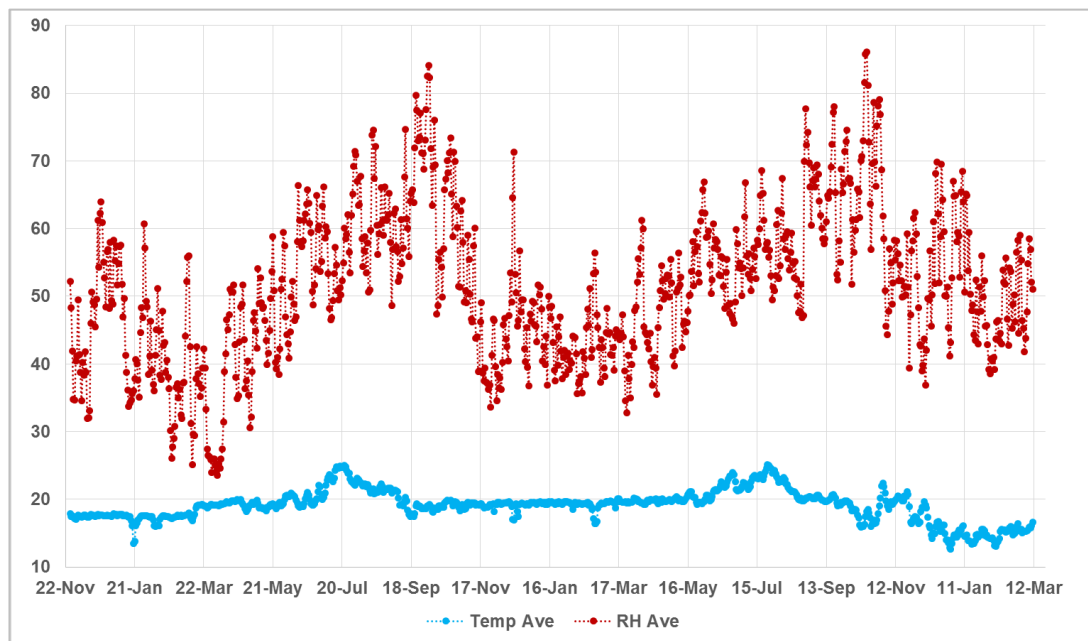


Figure 101 Average daily temperature and RH data from the two data loggers stored inside the Sherman V Crab in the DC

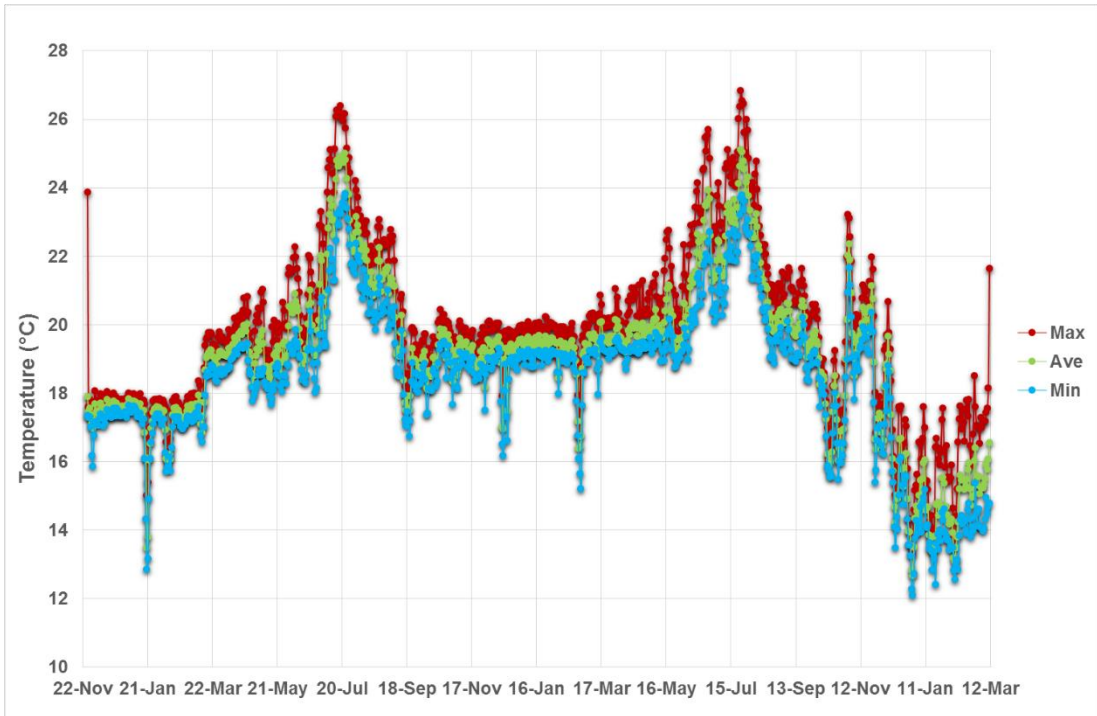


Figure 102 Summary of the temperature data collected by data loggers stored inside the Sherman V Crab in the DC

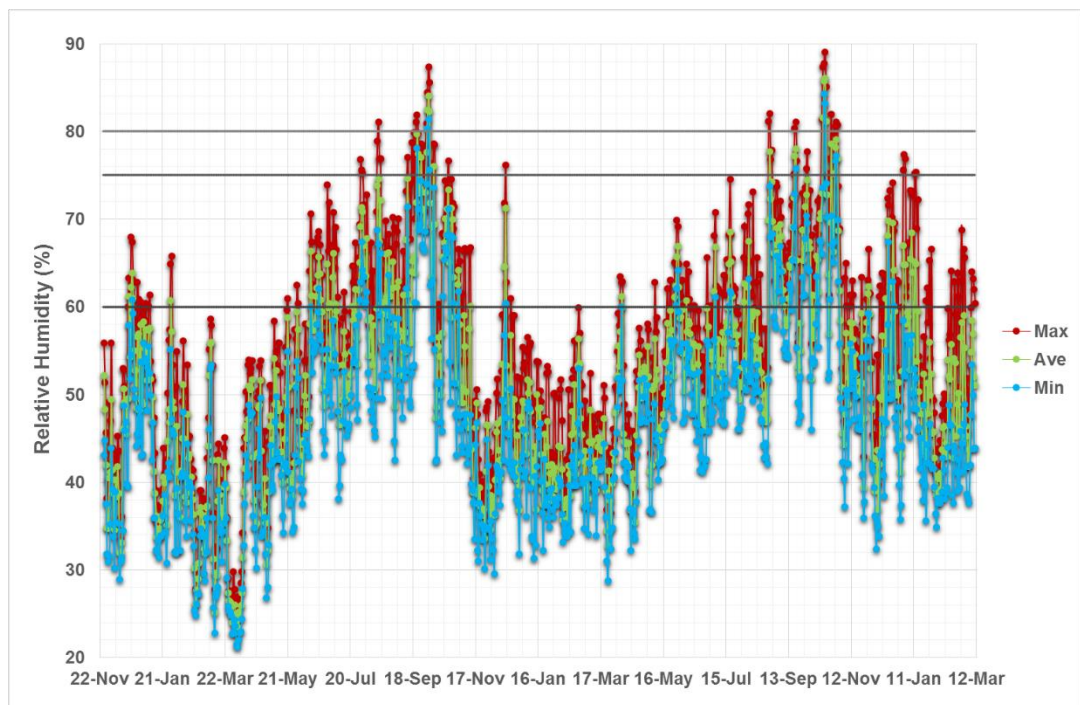


Figure 103 Summary of the RH data collected by data loggers stored inside the Sherman V Crab in the DC

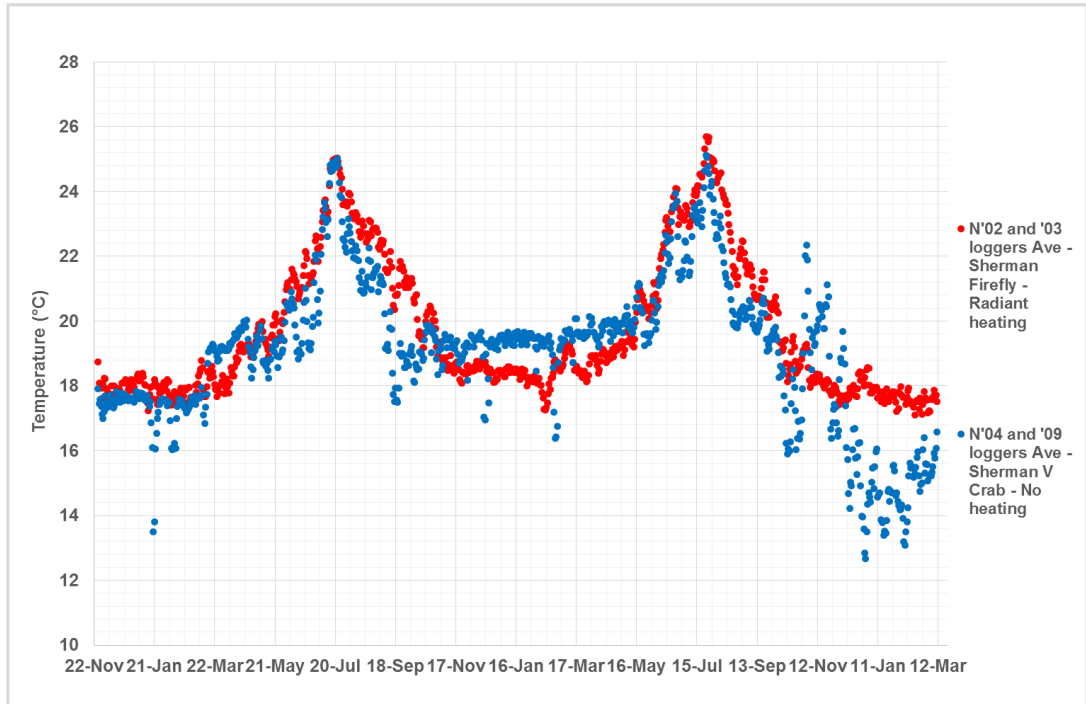


Figure 104 Comparison of the average temperature data collected within the two different vehicles in different rooms.

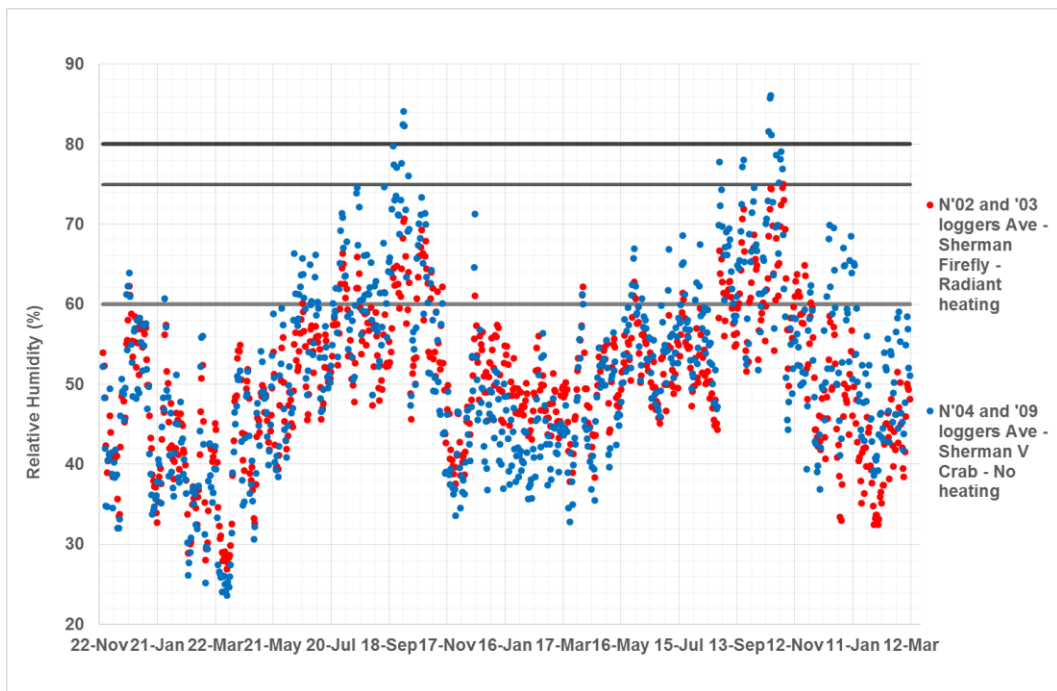


Figure 105 Comparison of the average RH data collected within the two different vehicles in different rooms.

6.2 Laboratory Results

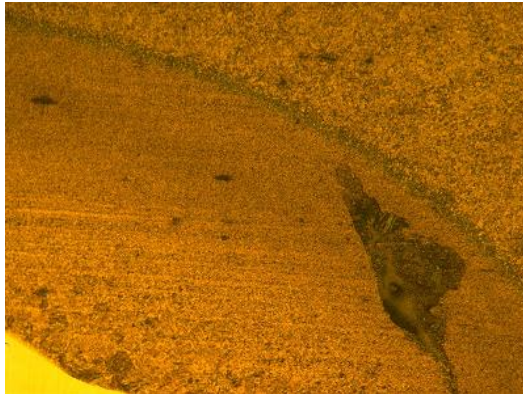
6.2.1 Samples Material and Preparation

6.2.1.1 Metallography

Microscope images of a small sample cut from the corner of Saracen Armoured Personnel Vehicle (APV), which was polished and etched are included in table 56. At x50 magnification several images were taken of each area examined, varying the focal point for each one, then using Struers' Scentis imaging software the images were aligned, sharpened and layered to produce images with the best focus throughout the whole image.

Table 56 Images of etched steel sample from a Saracen APV – at x5 and x50 magnification (layered images have been used and where necessary they have been aligned, focused and sharpened)

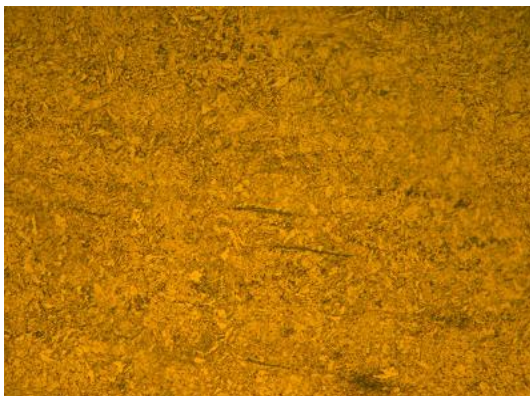
X5 Magnification - Cross-section near weld



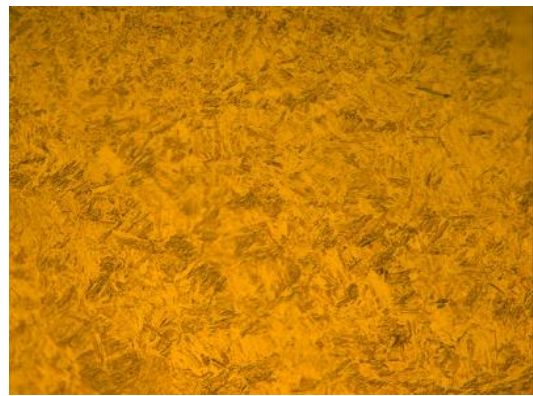
X50 Magnification - Etched edge metal



X50 Magnification - Etched metal



X50 Magnification - Etched weld area



A summary of the data collected of a sample analysed using SEM elemental analysis is presented in table 57.

Table 57 SEM analysis of Saracen APV Steel (x500) – 3 sites included, results are normalised and reported as weight %

Spectrum No.	C	Si	Cr	Mn	Fe	Ni
1	2.97	0.43	1.83	0.8	93.13	0.85
2	2.48	0.39	1.93	0.64	93.67	0.89
3	2.36	0.39	1.9	0.66	93.84	0.86
4	2.11	0.4	1.89	0.74	93.93	0.94
5	1.94	0.4	1.87	0.58	94.15	1.06
6	1.84	0.45	1.89	0.71	94.07	1.05
7	2.3	0.41	1.83	0.65	93.86	0.95
8	2.31	0.39	1.94	0.79	93.61	0.96
9	2.37	0.42	1.96	0.62	93.63	1
Mean	2.3	0.41	1.89	0.69	93.77	0.95
Std. deviation	0.33	0.02	0.05	0.08	0.3	0.08
Max.	2.97	0.45	1.96	0.8	94.15	1.06
Min.	1.84	0.39	1.83	0.58	93.13	0.85

6.2.1.2 Prepared Samples

Substrate Sample Mass

The cut metal samples were not exact replicas of each other. A survey of 15 samples showed each one had a different mass (table 58). From the average value of 107.19 g all of the other masses were within $\pm 0.94\%$. Eight of the masses measured fell between 106.5 g and 107.5 g, four were > 107.5 g and three were < 106.5 g.

Table 58 Masses and sample labels of 15 samples before treatment

Sample	Mass (g)	Sample	Mass (g)	Sample	Mass (g)	For all 15 samples measured	
NT 1	107.31	SC 1	107.55	CAS 1	106.32		
NT 2	108.20	SC 2	106.70	CAS 2	107.39		
NT 3	106.81	SC 3	107.04	CAS 3	108.03		
NT 4	107.95	SC 4	107.04	CAS 4	107.45		
NT 5	107.01	SC 5	106.98	CAS 5	106.16		
Average	107.46	Average	107.06	Average	107.07	Average	107.19
Std. Dev	0.60	Std. Dev	0.31	Std. Dev	0.80	Std. Dev	0.59
Max	108.20	Max	107.55	Max	108.03	Max	108.20
Min	106.81	Min	106.70	Min	106.16	Min	106.16
Range	1.39	Range	0.85	Range	1.87	Range	2.04

Surface area

For the purpose of analysing corrosion rates surface area (SA) is a more important measurement to consider. As each sample should have a diameter of 38 mm, (radius of 19 mm) and a thickness of 12 mm (figure 106), the SA of both sides can be calculated using the equation for the SA of a circle and the overall SA area of a sample can be calculated using the equation for the SA of a cylinder. However, due to the variations in the surface profile and indentations at the edges it was not possible to measure the SA of the sides or the overall cylinder accurately for each sample or work out the error range.

Therefore, each side of the sample has the following SA:

$$SA = \pi r^2 = 1134.11 \text{ mm}^2 = \underline{11.34 \text{ cm}^2}$$

The overall SA of the cylinder samples are:

$$SA = 2\pi rh + 2\pi r^2 = 3700.8 \text{ mm}^2 = \underline{37.01 \text{ cm}^2}$$

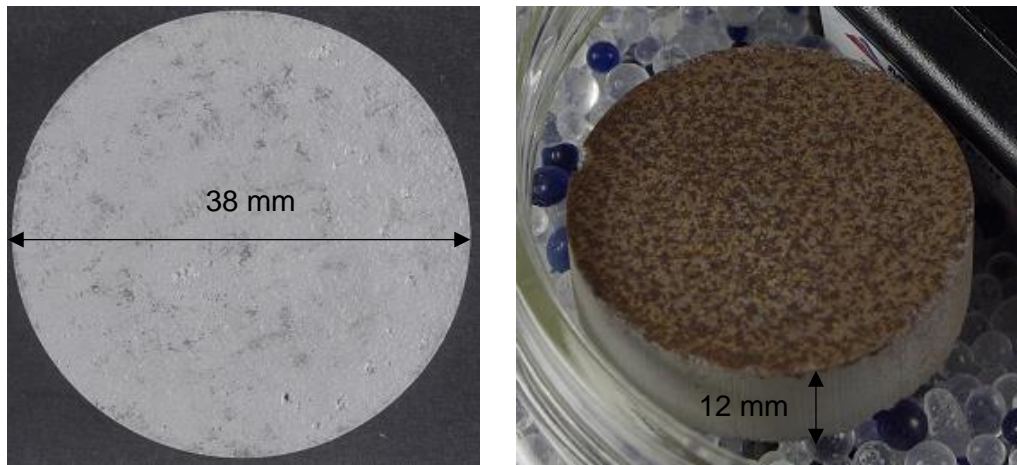


Figure 106 Sample dimensions

Surface Profile

Imaging using the scanning electron microscope (SEM) reveals the impact of surface cleaning and preparation by air abrasion, including the impact on SA (figure 107).

Before cleaning



After cleaning

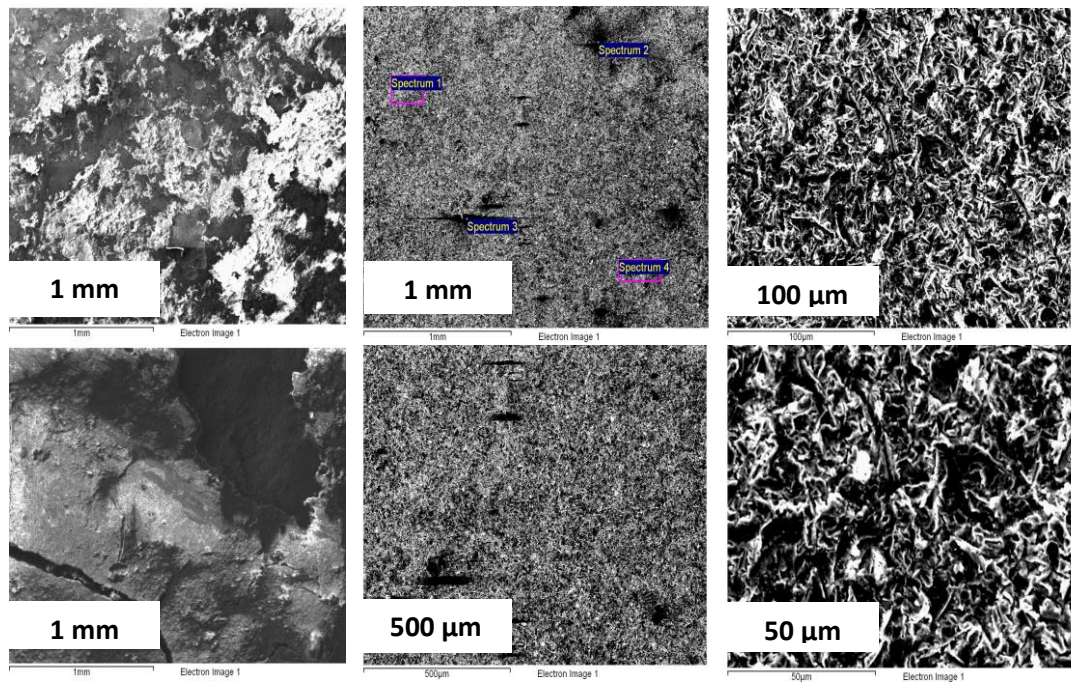


Figure 107 SEM SEI images summarising the changes to the surface profile during preparation

6.2.1.3 Accelerated Corrosion and Chloride Deposition

Accelerated corrosion was trialled as a method of accelerated aging and producing a corrosion layer similar to one which may be produced in situ and in some circumstances coated over.

Appearance

Drop application of Cl^- solution did not produce a uniform corrosion layer, as the droplets did not spread/flow out over the prepared metal surface. Post-evaporation rust patches surrounded by a ring of salt crystals remained (figure 108).

Spray application produced a more uniform corrosion (figures 109 and 110). The sides and bottoms of the samples were blanked-off with masking tape and remained corrosion free 11 days after the spray application (table 59).



Figure 108 Sample corroded by salt solution applied by pipette

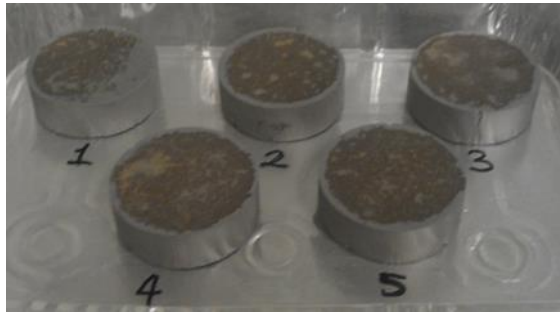


Figure 109 Trial 1-5 11 days after being sprayed with salt solution.

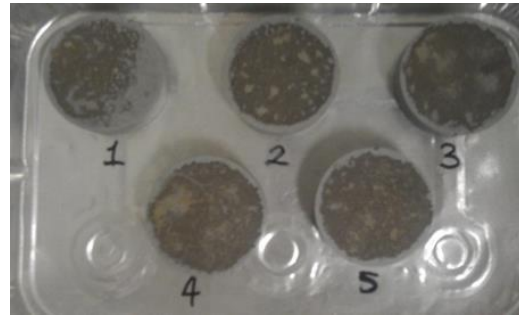
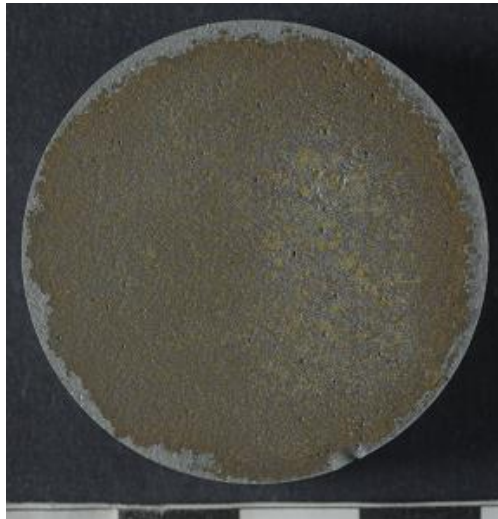


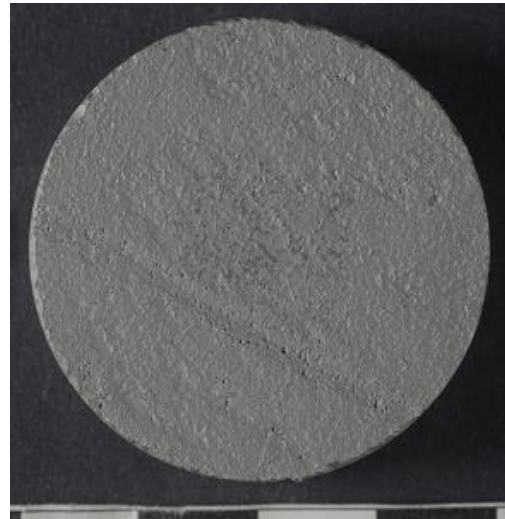
Figure 110 Trial 1-5 after being allowed to corrode for 11 days in the laboratory.

Post-corrosion the limit of the masking tape around the edge of each sample is evident from the appearance of an uncorroded edge.

Table 59 Samples PC1-5 after being sprayed with salt solution and allowed to corrode.



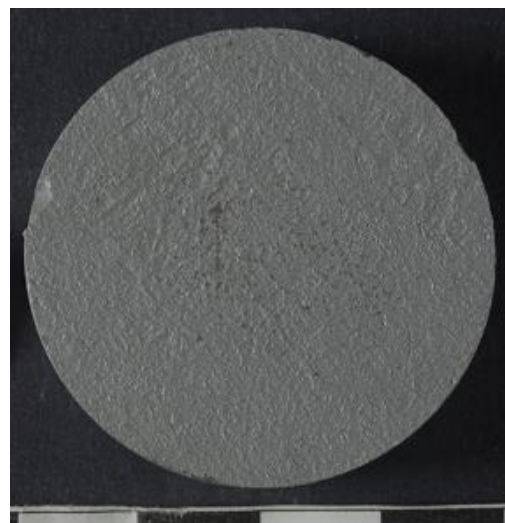
Sprayed side of sample PC1



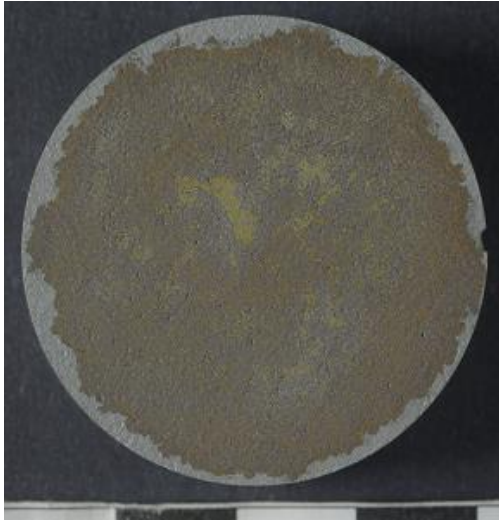
Blanked off side of sample PC1



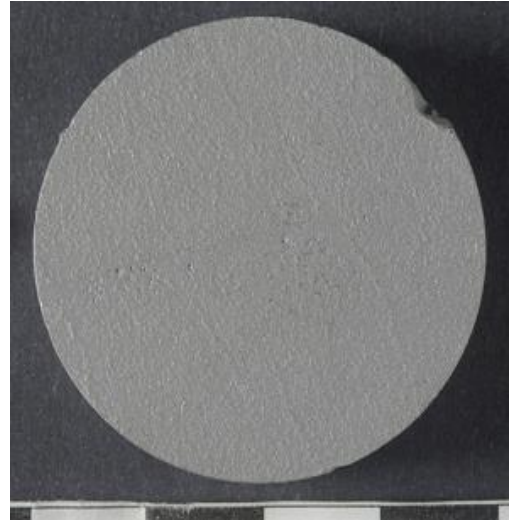
Sprayed side of sample PC2



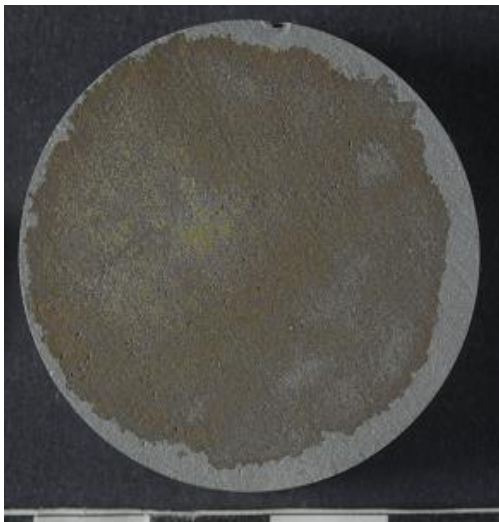
Blanked off side of sample PC2



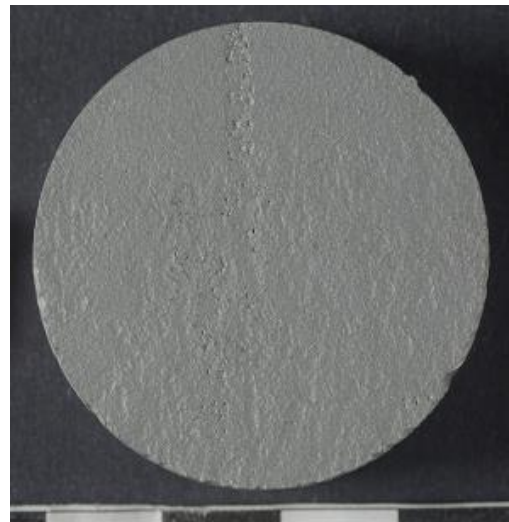
Sprayed side of sample PC3



Blanked off side of sample PC3



Sprayed side of sample PC4



Blanked off side of sample PC4



Sprayed side of sample PC5



Blanked off side of sample PC5

6.2.1.3.1 Chloride Deposited

Drop application

The Cl⁻ deposited by 10 drops of deicing salt solution were measured and recorded. This method showed some consistency across the samples (figure 111 and table 60).

Table 60 Chloride deposited by pipette drop application

Sample	Chloride added by 10 drops (µg)	Average chloride deposited for 1 drop (µg)
1	1483	148
2	2506	251
3	2300	230
4	2521	252
5	2140	214
Average	2190	2194

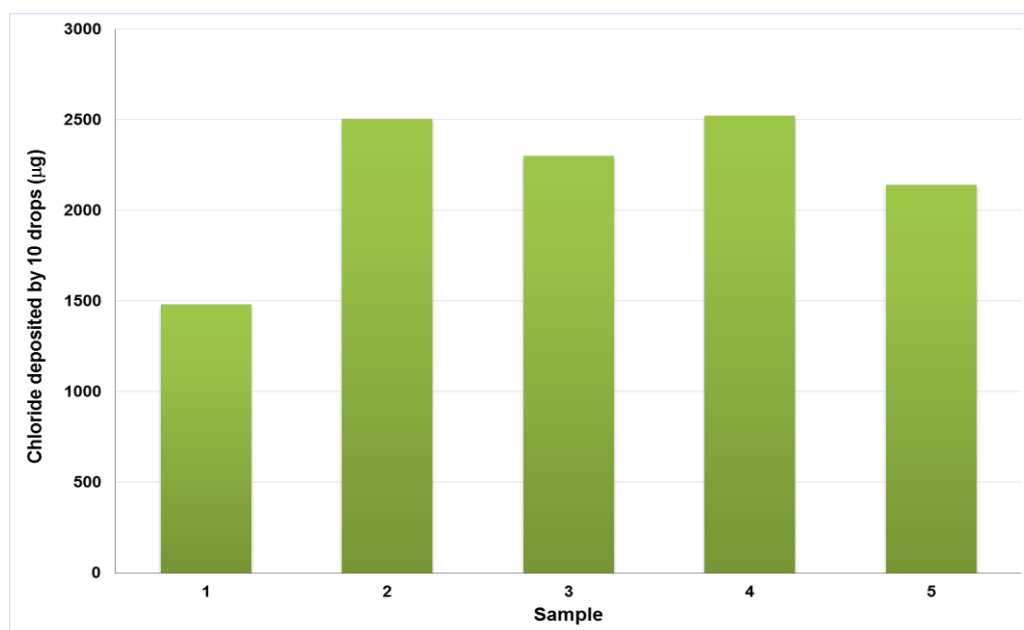


Figure 111 Chloride deposited by 10 drops of de-icing salt solution

Spray application results

Spray application resulted in overall average of 145 µg of Cl⁻ deposited for the 10 repetitions and a standard deviation of 46.4 µg. The range in the mass of chloride deposited per spray is visible in figure 112 and table 61.

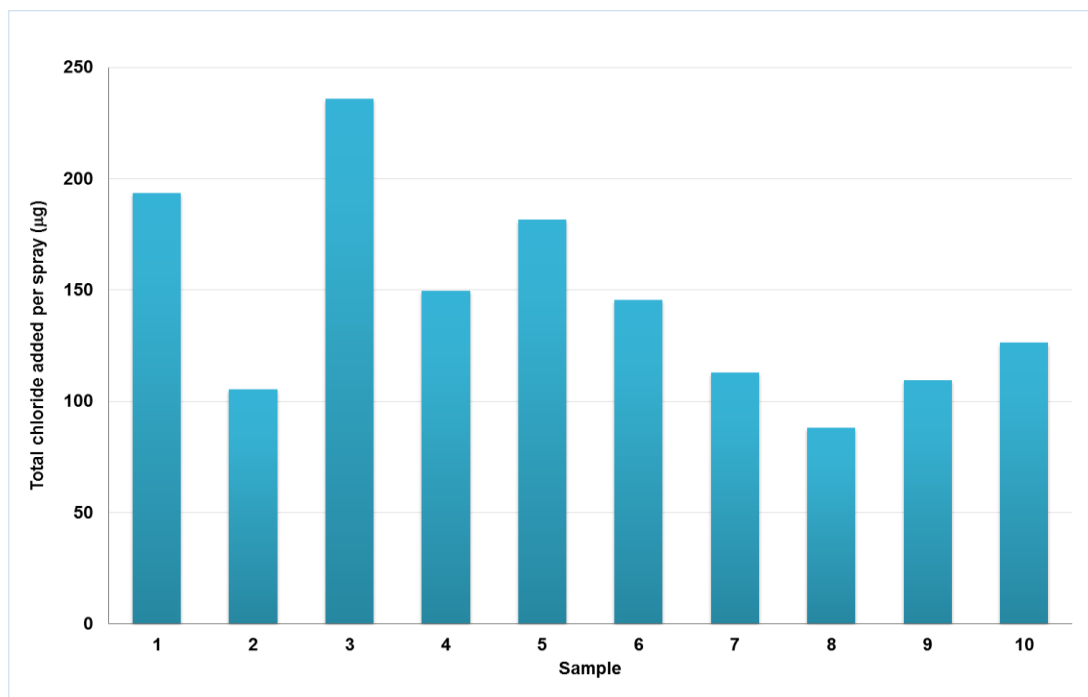


Figure 112 Mass of chloride per spray of de-icing salt solution on a sample

Table 61 Chloride deposition by spray application converted to µg

Sample	Chloride (ppm) in 11 ml (10 ml of wash solution and 1 ml of buffer)	Total mass of chloride in test solution (µg)	Total mass of chloride in 15 ml wash solution (µg)
1	12	129	193
2	6	70	105
3	14	157	236
4	9	100	150
5	11	121	182
6	9	97	146
7	7	75	114
8	5	59	88
9	7	73	110
10	8	84	126
Average	8.8	96.5	145
Standard deviation	2.8	31	46.4
Maximum	14	157	236
Minimum	5	59	88
Range	9	98	148

6.2.2 Oxygen Consumption of Armoured Steel Samples

The results for O₂ consumption of armoured steel samples prior to using the clear coatings are presented in figures 113-119.

6.2.2.1 Untreated Samples

Untreated samples produced a baseline for the corrosion rate of the samples without intervention. These showed a slow rate of corrosion after 163 days (figure 113).

Fluctuations in O₂ partial pressure in the control jar containing no sample were subtracted from samples data points recorded on the same day. The initial trial of the untreated samples included 5 samples, but another untreated sample (UT6) was monitored alongside the coated samples in tests and has been included in figure 114. UT6 had other control fluctuations subtracted from its data set than UT1-5.

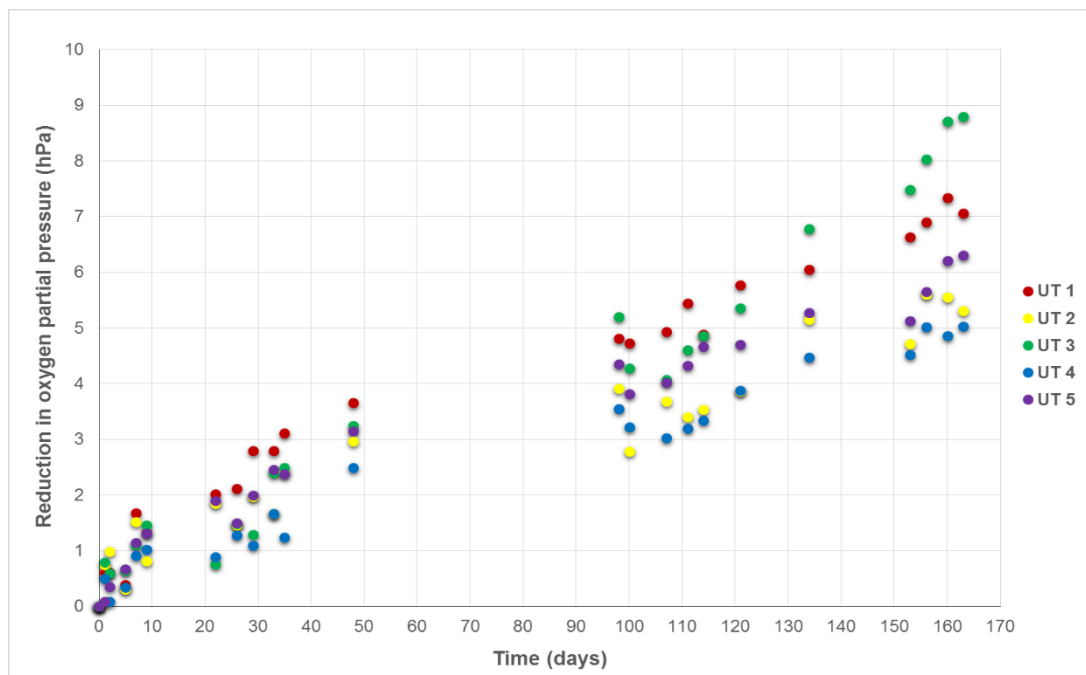


Figure 113 Reduction in O₂ partial pressure over 163 days caused by untreated samples with damaged paint layers etc left on at ≈ 20 °C, 80% RH.

Analysis of figure 114 was carried out using linear trendlines (table 62) to produce rate values for the reduction in O₂ partial pressure per day.

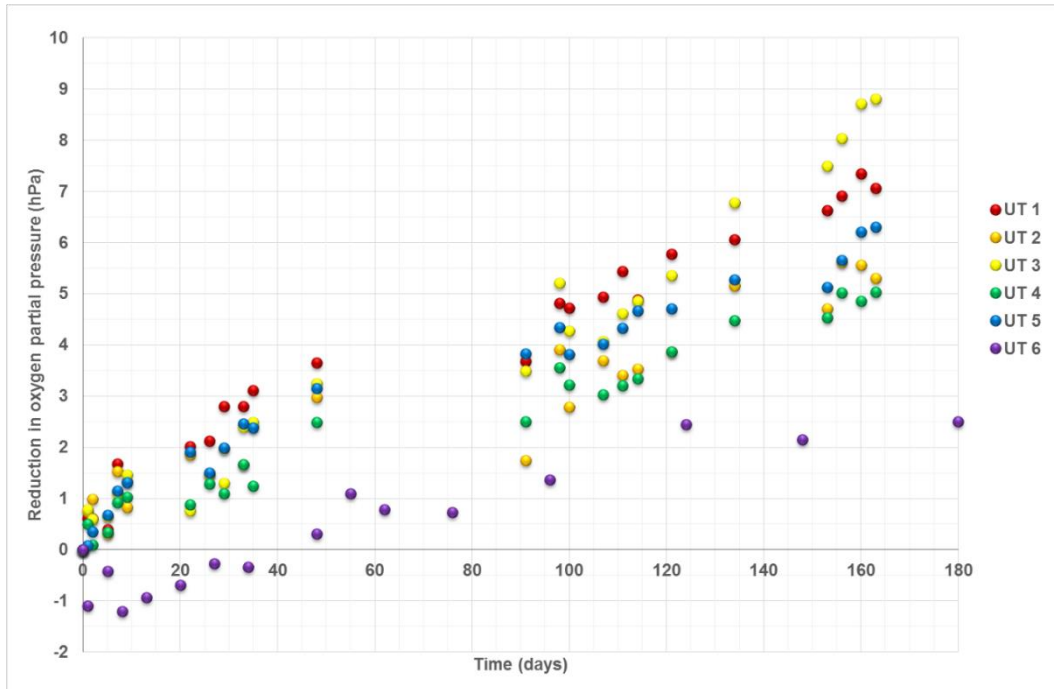


Figure 114 Reduction in O₂ partial pressure caused by untreated samples cut from the Saracen APV door with damaged paint layers left on at 20 °C, 80% RH with the fluctuations experienced by the control jar subtracted from each of the sample jars. Samples UT1 to 5 were part of the original trial, but sample 6 was tested later and run along side some of the coatings test.

Table 62 Linear trendline analysis of figure 114 - approximation of O₂ consumption rate

UT Samples	Linear Trend-Line Equation	Rate of reduction in O ₂ partial pressure per day (hPa/day)
1	$y = 0.0382x + 0.9747$	0.0382
2	$y = 0.0275x + 0.7675$	0.0275
3	$y = 0.0458x + 0.3729$	0.0458
4	$y = 0.028x + 0.4096$	0.028
5	$y = 0.0329x + 0.7662$	0.0329
6	$y = 0.0209x - 0.7669$	0.0209
Average		0.03222
Maximum		0.0458
Minimum		0.0209

6.2.2.2 Cleaned and uncoated samples

The five samples that were cleaned by air abrasion and left uncoated, produced a baseline for the corrosion rate of the cleaned but unprotected samples (figure 115).

The initial trial of the cleaned samples included CS1-5, CS6 was monitored

alongside the coated samples in tests and therefore, CS6 had different control fluctuations subtracted from its data set than CS1-5 (figure 116).

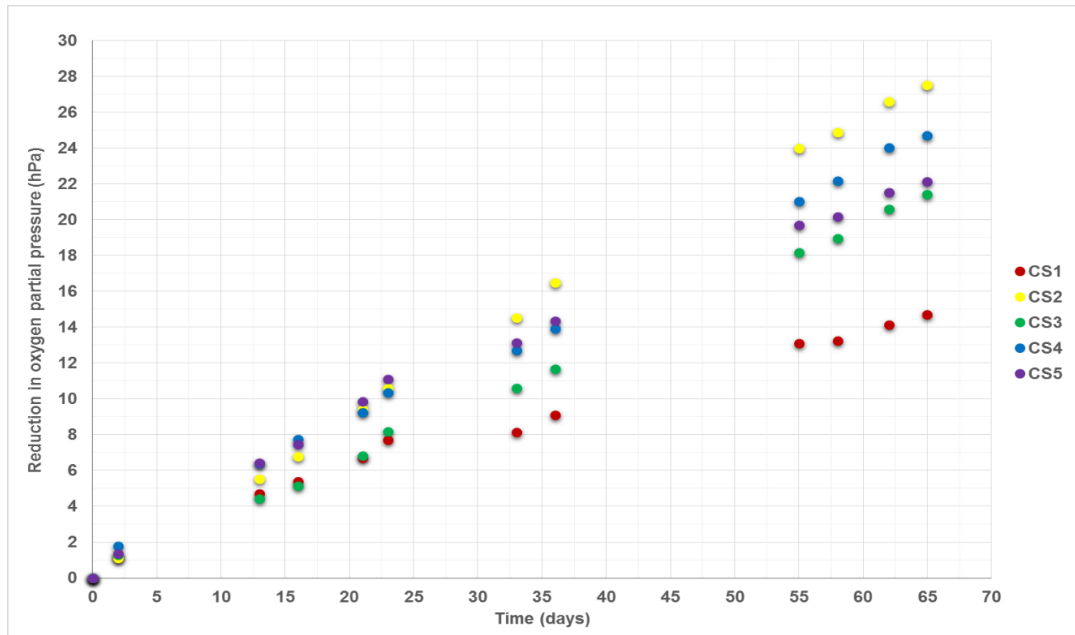


Figure 115 Reduction in O₂ partial pressure at 20 °C, 80% RH, caused by samples air abraded clean. Fluctuations experienced by the control jar have been subtracted from the data for each sample.

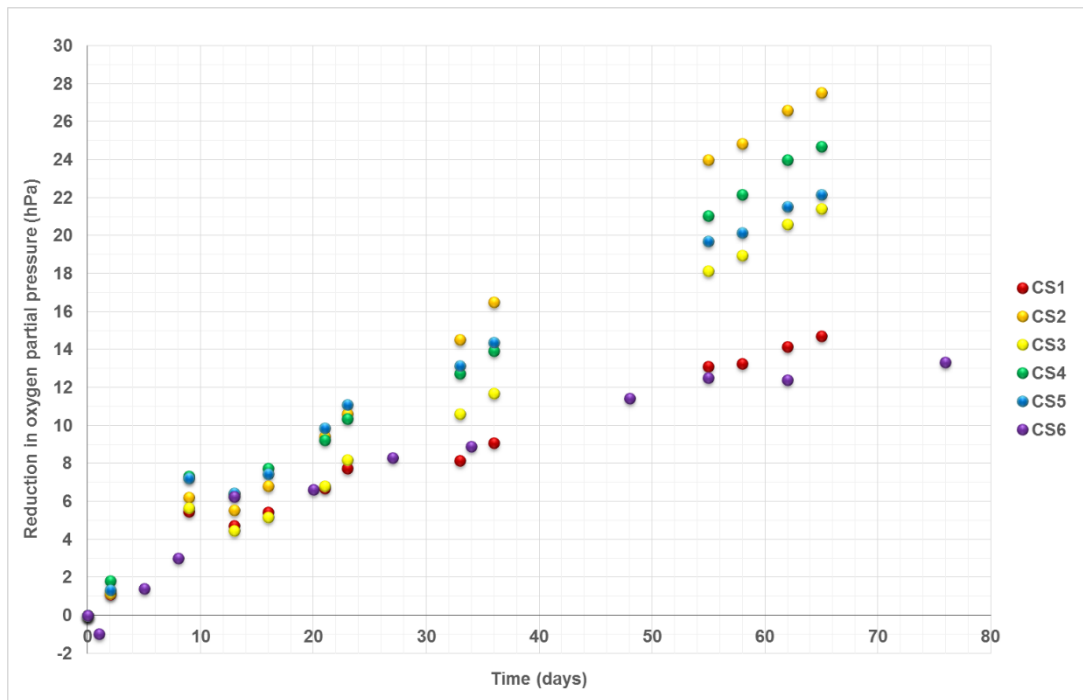


Figure 116 Reduction in O₂ partial pressure at 20 °C, 80% RH, caused by samples air abraded clean. The fluctuations experienced by the control jar have been subtracted from the results for each of the jars. Samples CS1 to 5 were part of the original trial, but sample 6 was tested later and run along side some of the coatings test.

Analysis of figure 116 was carried out using linear trend-lines (table 63), but quadratic polynomial trend-lines may be more suitable, as a few of the CS samples are slightly curved especially sample CS6. Thus using linear trendline analysis is slightly problematic for the CS samples. For most of the CS samples the majority of the data will fit a linear trendline, but the initial 10 days show a faster rate than the next 50 days as can be seen in figure 116, this leads to the lines intercepting the y axis higher than zero. Therefore, if CS6 and the other CS samples' trendlines are considered in two parts you can see there is a short-term fast rate of corrosion at the start and then a long-term slightly slower rate of corrosion. As corrosion rates over longer time periods are being considered linear trendlines are still useful. Slowing of reaction rates is typical for corrosion as after an initial oxide layer is formed it restricts the access to the metal substrate slowing the reduction in O₂ concentration.

Table 63 Linear trendline analyses of figure 116 - approximation of O₂ consumption rate

CS Samples	Linear Trend-Line Equation	Rate of reduction in O ₂ partial pressure per day (hPa/day)
1	$y = 0.2026x + 1.8381$	0.2026
2	$y = 0.4193x + 0.6788$	0.4193
3	$y = 0.3173x + 0.6327$	0.3173
4	$y = 0.3549x + 1.6894$	0.3549
5	$y = 0.3169x + 2.2937$	0.3169
6	$y = 0.1866x + 1.5008$	0.1866
Average		0.2996
Maximum		0.4193
Minimum		0.1866

6.2.2.3 *Partially pre-corroded uncoated samples*

The pre-corroded samples that were cleaned and subjected to accelerated corrosion using a de-icing salt solution, were monitored for 48 days (figure 117). Linear trend-lines were used to analyse figure 117 (table 64).

6.2.2.4 *Comparison of uncoated samples*

Figure 118 compares the results of the three treatment groups presented up to this point. The partially pre-corroded samples (red) corroded the fastest and have the largest range, air abraded cleaned samples are green and the untreated samples

(navy) corroded the slowest with the smallest range. Figure 119 compares the average O₂ partial pressure reduction per day over approximately two months. There are no overlaps between the treatment groups.

Table 64 Linear trendline analyses of figure 117 - approximation of O₂ consumption rate

PC Samples	Linear Trend-Line Equation	Rate of reduction in O ₂ partial pressure per day (hPa/day)
1	$y = 1.38x + 6.3371$	1.38
2	$y = 1.3661x + 5.6845$	1.3661
3	$y = 1.0589x + 3.1956$	1.0589
4	$y = 1.0189x + 2.7821$	1.0189
5	$y = 1.6599x + 5.9292$	1.6599
Average		1.29676
Maximum		1.6599
Minimum		1.0189

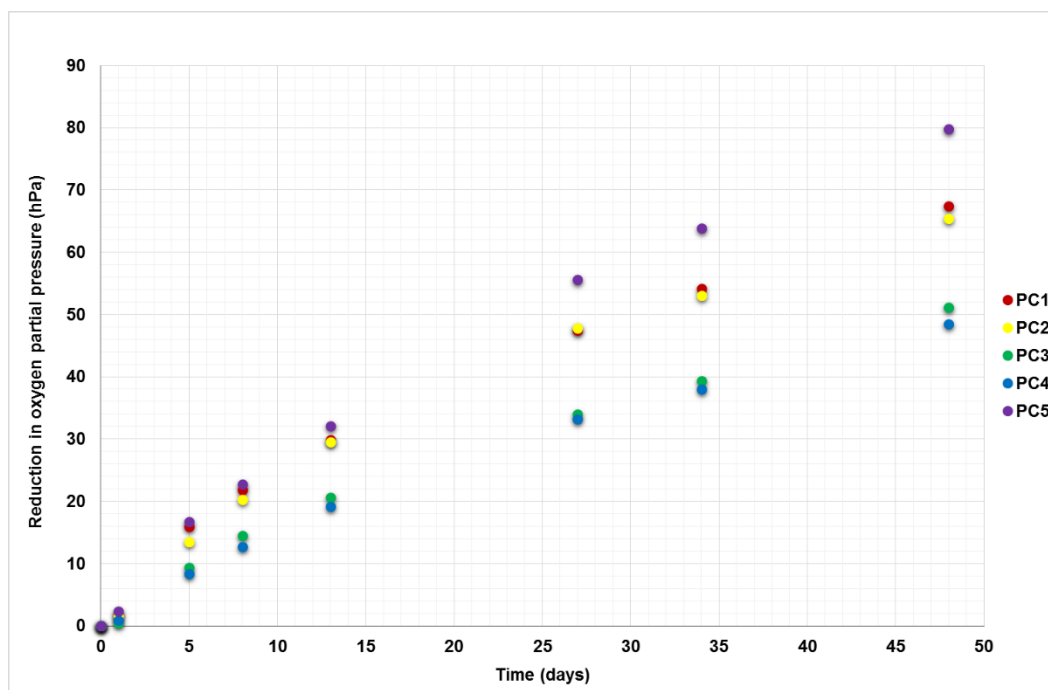


Figure 117 Reduction in O₂ partial pressure at 20 °C, 80% RH. Samples were air abraded clean and sprayed on one side with salt solution prior to measuring the O₂ levels. The control fluctuations have been subtracted from the results for each of the jars.

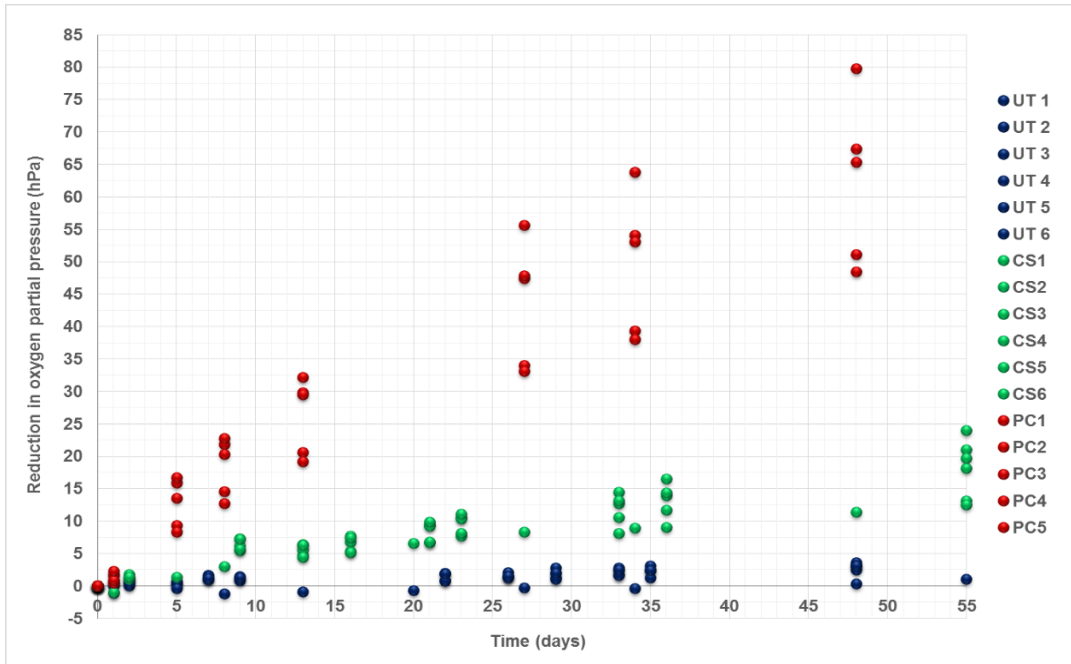


Figure 118 Comparison of the reduction in O₂ partial pressure caused by armoured steel samples over approximately the first 50 days of monitoring of the uncoated samples

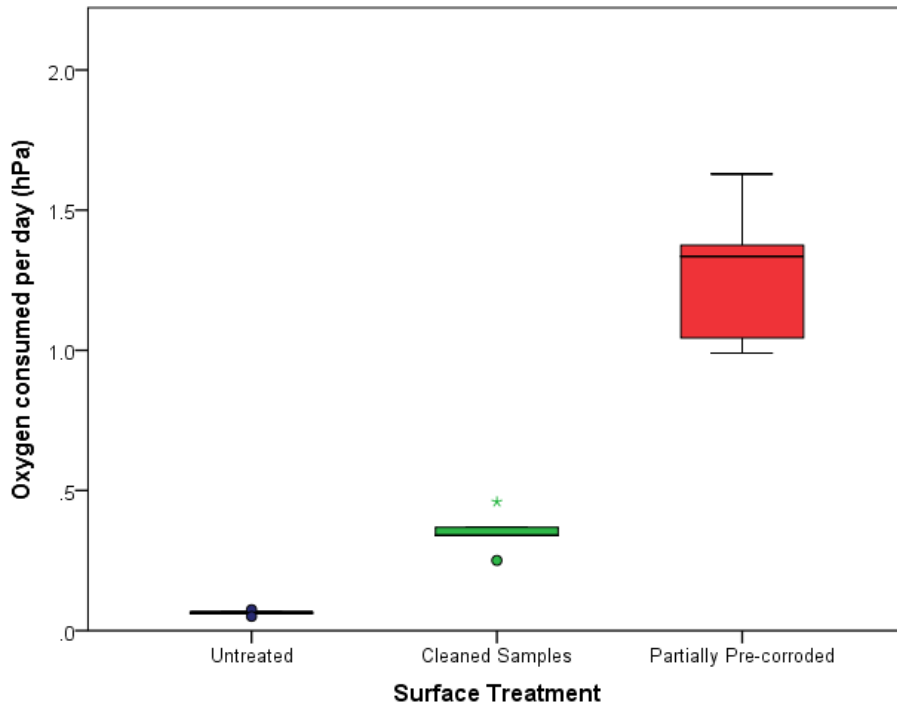


Figure 119 Boxplot comparison of the uncoated samples, comparing the O₂ consumed per day for each sample over the first 50-60 days of measuring. The median values are indicated by the dark line in the middle of the boxes. The top of the boxes indicates the third quartile (75th percentile) and the bottom of the boxes represent the first quartile (25th percentile). The T-bars extend from the boxes to 1.5 times the height of the box or if no case falls in that range they extend to the minimum or maximum value. Values which do not fall within the range indicated by the T-bars are indicated by circular points or in the case of extreme outliers (> 3 times the height of the box) by an asterisk or star.

6.2.3 Clear Coatings: Application and Effect on Oxygen Concentration Measurements

6.2.3.1 Physical Appearance of Coatings Applied to Glass Slides

All the photographs of Paraloid B72 on glass slides show clear brush marks (figures 120 - 127), although different solvents and concentrations of the coating were used. For the majority of the slides the more pronounced area of visible brush strokes is down the centre of the slides where there is a slight overlap of the brush strokes from the same coating layer. Highly visible brush strokes are apparent in figures 125 and 126 after being coated with 10% w/v Paraloid B72 in acetone.

Cleaned but otherwise untreated glass slides were used for most of the slides coated with Paraloid B72. Air abraded slides were trialled with Paraloid B72 in xylene and this reduced the visibility of the marks (figure 127).

Whether 10 or 15% w/v Paraloid B72 coatings in xylene or acetone they produce a gloss finish. Cosmoloid H80 however, produces a matt finish and in some areas small but visible crystals can be seen, creating opaque areas within the coating (figure 128). Brush marks are hardly visible within the coating layer when using Cosmoloid H80.

Images of Siliglide 10 applied to glass slides have not been included in this section because once the coating has been buffed during curing, it is invisible to the naked eye on a glass slide. Without buffing little circular droplet marks were formed on the glass slides.

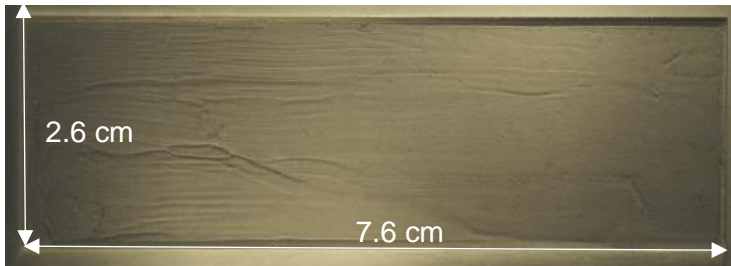


Figure 120 10% w/v Paraloid B72 in xylene on a glass slide using fibre optic lighting. All glass slides are 2.6 x 7.6 cm

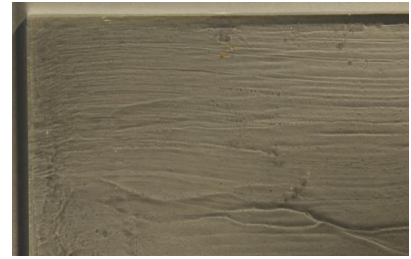


Figure 121 Zoomed area of figure 120



Figure 122 15% w/v Paraloid B72 in xylene



Figure 123 10% w/v Paraloid in acetone



Figure 124 Zoomed areas of figure 123

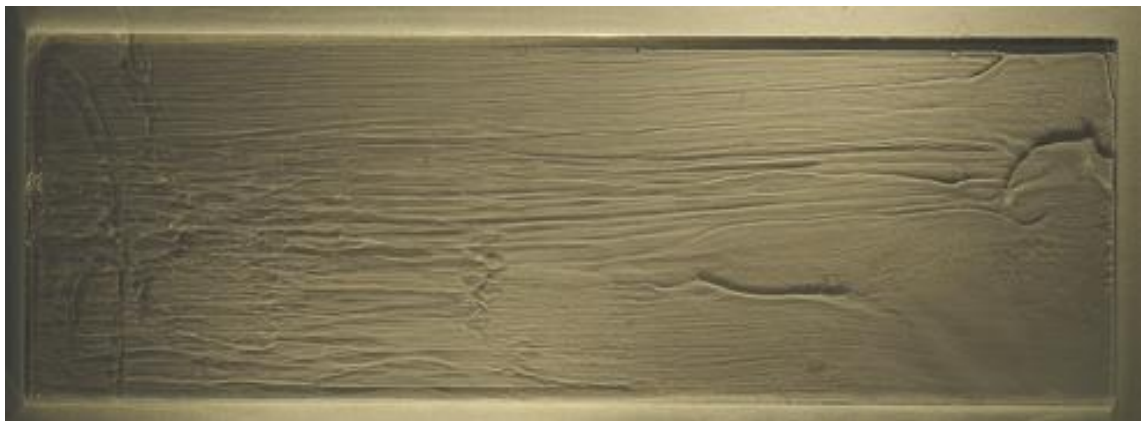


Figure 125 Coated with 10% w/v Paraloid in acetone

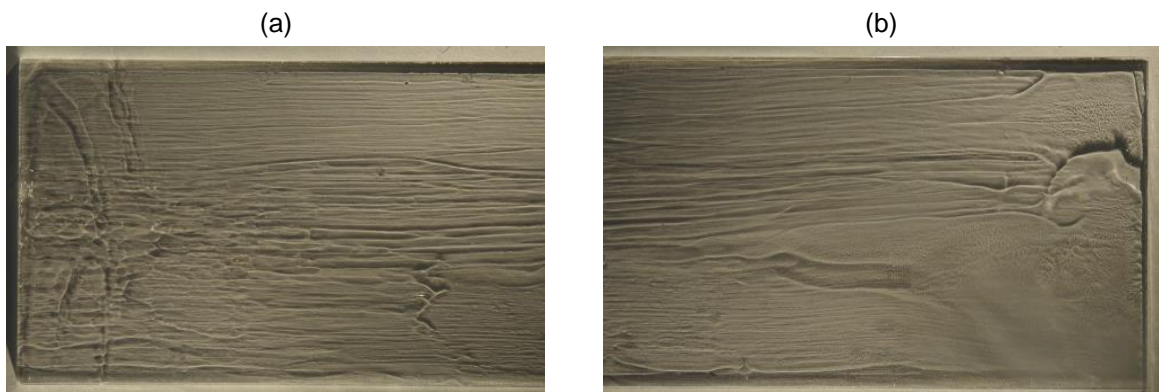


Figure 126 Zoomed areas of 10% w/v Paraloid B72 in acetone

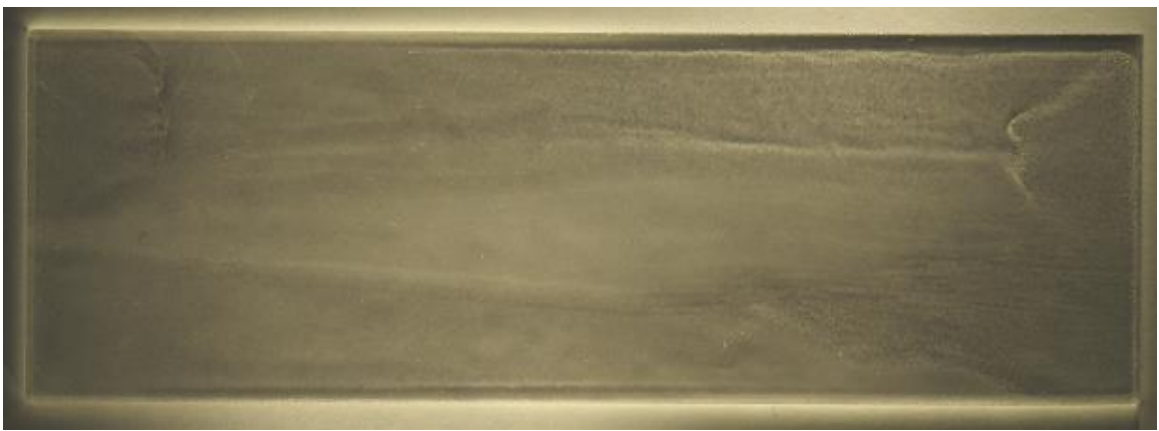


Figure 127 10% Paraloid B72 in xylene applied to an air abraded slide

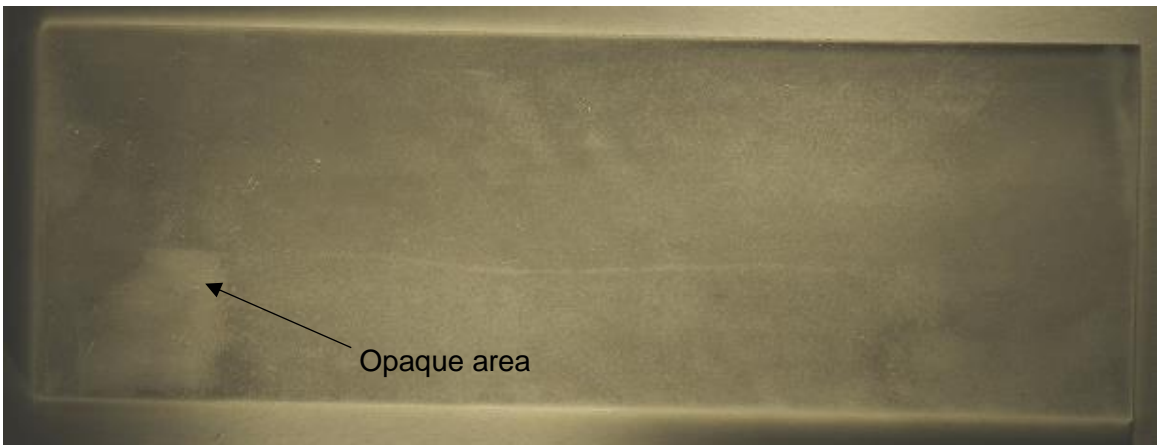


Figure 128 10% w/v Cosmoloid H80 in white spirit applied to an air abraded slide.

6.2.3.2 Mass of Coating Applied

6.2.3.2.1 Mass Applied on Glass Slides

10% w/v PB72 coating mass

After drying for 48 hours there were slight fluctuations in mass, less than ± 0.0002 g, this could be considered a significant error ($> 5\%$) due to the low mass of the individual coatings (tables 65 and 66).

Table 65 Mass of each layer of 10% Paraloid B72 in xylene coated on a glass slide

Paraloid in xylene coated slides	Mass of one coat (g)	Mass of second coats (g)	Mass of third coats (g)	Total mass of three coats (g)
1	0.0053	0.0039	0.0089	0.0181
2	0.0065	0.0052	0.0071	0.0188
3	0.0065	0.0058	0.0072	0.0195
4	0.0071	0.0064	0.0091	0.0226
5	0.0078	0.0096	0.0086	0.0260
Average	0.0066	0.0062	0.0082	0.0210

Table 66 Percentage difference of each layer of 10% w/v Paraloid B72 in xylene and the total mass in comparison to the highest mass.

Paraloid in xylene coated slides	Difference from coating layer with highest mass (%)	Difference from coating layer with highest mass (%)	Difference from coating layer with highest mass (%)	Difference in comparison to the highest total mass with 3 layers (%)
1	32.05	59.38	2.20	30.38
2	16.67	45.83	21.98	27.69
3	16.67	39.58	20.88	25.00
4	8.97	33.33	0.00	13.08
5	0.00	0.00	5.49	0.00
Average	15.4	35.4	9.9	19.2

Examining the percentage of the total coating applied in each layer shows there is a fairly even increases in the mass of the coating, indicating adding three layers rather than one or two of this coating is worthwhile (table 67).

Table 67 Percentage of the total coating mass contained in each layer of 10% w/v Paraloid B72 in xylene.

Paraloid in xylene coated slides	Percentage mass in 1 st coat (%)	Percentage mass in 2 nd coat (%)	Percentage mass in 3 rd coat (%)	Total percentage (%)
1	29.28	21.55	49.17	100.00
2	34.57	27.66	37.77	100.00
3	33.33	29.74	36.92	100.00
4	31.42	28.32	40.27	100.00
5	30.00	36.92	33.08	100.00
Average	31.43	29.52	39.05	100.00

The patterns of mass increase for three coats of 10% Paraloid B72 in acetone are shown in tables 68 and 69.

Table 68 Mass of each layer of 10% Paraloid B72 in acetone coated onto slides

Paraloid in acetone coated slides	Mass of 1 st coat (g)	Mass of 2 nd coat (g)	Mass of 3 rd coat (g)	Total mass of 3 coats (g)
1	0.0118	0.006	0.0144	0.0322
2	0.0097	0.0087	0.0153	0.0337
3	0.0108	0.008	0.0108	0.0296
4	0.0124	0.0099	0.0189	0.0412
5	0.012	0.008	0.0109	0.0309
Average	0.0113	0.0081	0.0141	0.0335

Table 69 Percentage difference of each layer of 10% w/v Paraloid B72 in acetone and the total mass in comparison to the highest mass.

Paraloid in acetone coated slides	Difference from coating layer with highest mass (%) for the 1 st layer	Difference from coating layer with highest mass (%) for the 2 nd layer	Difference from coating layer with highest mass (%) for the 3 rd layer	Difference in comparison to the highest total mass with 3 layers (%)
1	4.84	39.39	23.81	21.84
2	21.77	12.12	19.05	18.20
3	12.90	19.19	42.86	28.16
4	0.00	0.00	0.00	0.00
5	3.23	19.19	42.33	25.00
Average	8.87	18.18	25.40	18.69

Examining the percentage of the total coating applied in each layer shows approximately a third of the coating is deposited in the first layer, but there is a notable drop for the second layer (table 70). If the first layer was not thoroughly dried and the solvent in the second layer may redissolve part of the first layer, whilst also reducing how much is deposited. More is deposited in the third layer than the first or second layer, thus adding three layers rather than one or two layers of this coating is worthwhile. Provided the coating layers are thoroughly dried the unevenness of the surface after two layers may cause more of the coating to be pulled off the brush for the third layer than the first or second layers.

To compare the mass distribution of Paraloid B72 in the three layers when using the different solvents acetone and xylene a boxplot was produced (figure 129).

Table 70 Percentage of the total coating mass contained in each layer of 10% w/v Paraloid B72 in acetone.

Paraloid in acetone coated slides	Percentage mass in 1 st coat (%)	Percentage mass in 2 nd coat (%)	Percentage mass in 3 rd coat (%)	Total percentage (%)
1	36.65	18.63	44.72	100
2	28.78	25.82	45.40	100
3	36.49	27.03	36.49	100
4	30.10	24.03	45.87	100
5	38.83	25.89	35.28	100
Average	33.73	24.18	42.09	100

For each of the layers the average mass when acetone is used is higher than when xylene was used (table 71). Thus, the accumulated mass for all three layers is higher when acetone is used compared to when xylene is used (figure 129). The average total coating mass when acetone is used is 0.0125 g higher than the average total coating mass when xylene is used (table 71).

Table 71 Difference between using acetone and xylene as the solvent for the coating Paraloid B72: comparison of the average mass for each layer

	Acetone average mass (g) minus xylene average mass (g)
1 st layer	0.0047
2 nd layer	0.0019
3 rd layer	0.0059
Total coating	0.0125

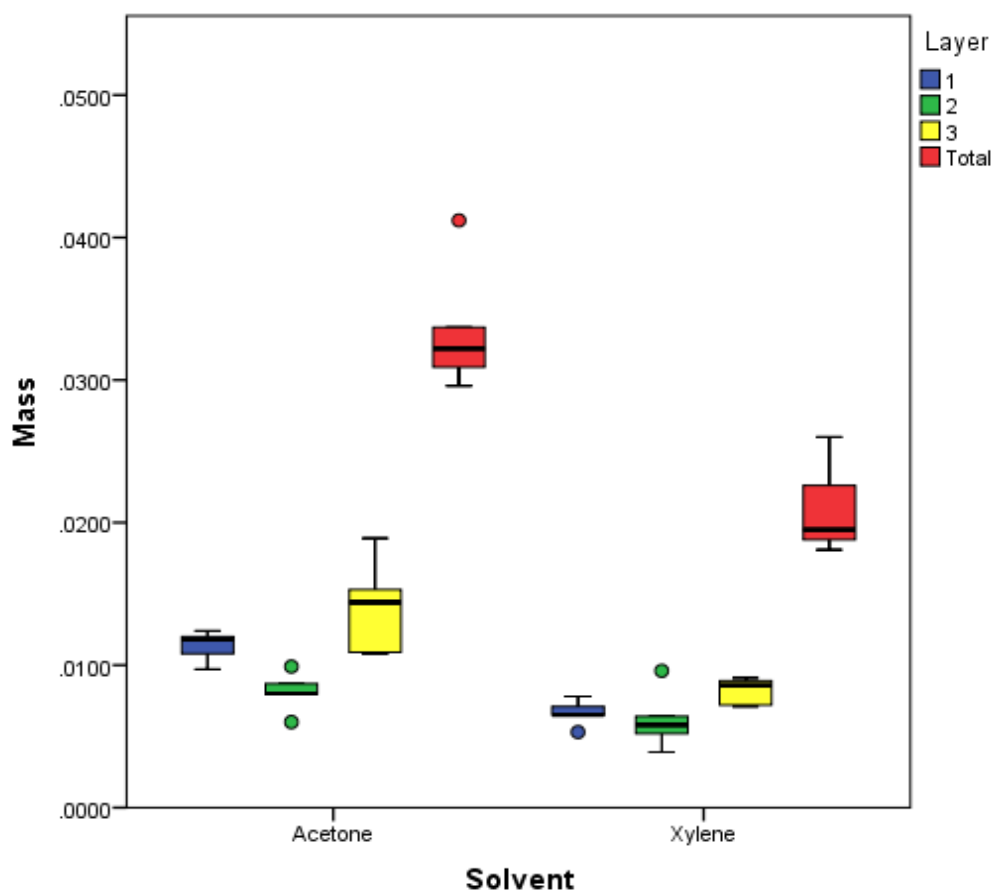


Figure 129 Boxplot to compare how the use of acetone and xylene solvents affect the average mass distribution of the 10% w/v Paraloid B72 coating over three layers and the overall totals of the three layers.

10% w/v Cosmoloid H80 coating mass

The mass and average of 3 coats of Cosmoloid H80 applied to 3 slides is recorded in tables 72 and 73. Without the anomalous value for the first layer for the first slide the range for the average total mass would be reduced showing the application method is fairly consistent in the mass of coating applied per layer.

Table 72 Mass of each layer of 10% Cosmoloid H80 in white spirit and slide used for coatings

Cosmoloid H80 in white spirit coated slides	Mass of 1 st coat (g)	Mass of 2 nd coat (g)	Mass of 3 rd coat (g)	Total mass of 3 coats (g)
1	0.0129	0.0053	0.0064	0.0246
2	0.0062	0.0086	0.0059	0.0207
3	0.0047	0.0056	0.0095	0.0198
Average	0.0079	0.0065	0.0073	0.0217
Range	0.0082	0.0033	0.0036	0.0048

Table 73 Percentage difference of each layer of 10% w/v Cosmoloid H80 in white spirit and the total mass in comparison to the highest mass.

Cosmoloid H80 in white spirit coated slides	Difference from coating layer with highest mass (%) for 1st layer	Difference from coating layer with highest mass (%) for 2nd layer	Difference from coating layer with highest mass (%) for 3rd layer	Difference in comparison to the highest total mass with 3 layers (%)
1	0.00	38.37	32.63	0.00
2	51.94	0.00	37.89	15.85
3	63.57	34.88	0.00	19.51
Average	38.76	24.42	23.16	11.79

Table 74 shows each of the 3 slides has a significant jump in % mass increase at one of their application stages.

Table 74 Percentage of the total coating mass contained in each layer of 10% w/v Cosmoloid H80 in white spirit.

Cosmoloid H80 in white spirit coated slides	Percentage mass in 1st coat (%)	Percentage mass in 2nd coat (%)	Percentage mass in 3rd coat (%)	Total percentage (%)
1	52.44	21.54	26.02	100
2	29.95	41.55	28.50	100
3	23.74	28.28	47.98	100
Average	36.41	29.95	33.64	100

The distribution of the mass of the coating, the range and median values are clearly illustrated in the boxplot in figure 130. The median mass for the three layers applied to the three slide are all fairly similar and shown by the thick black line within each of the boxes on the boxplot, the difference in the range of values for the first layer is also clearly visible.

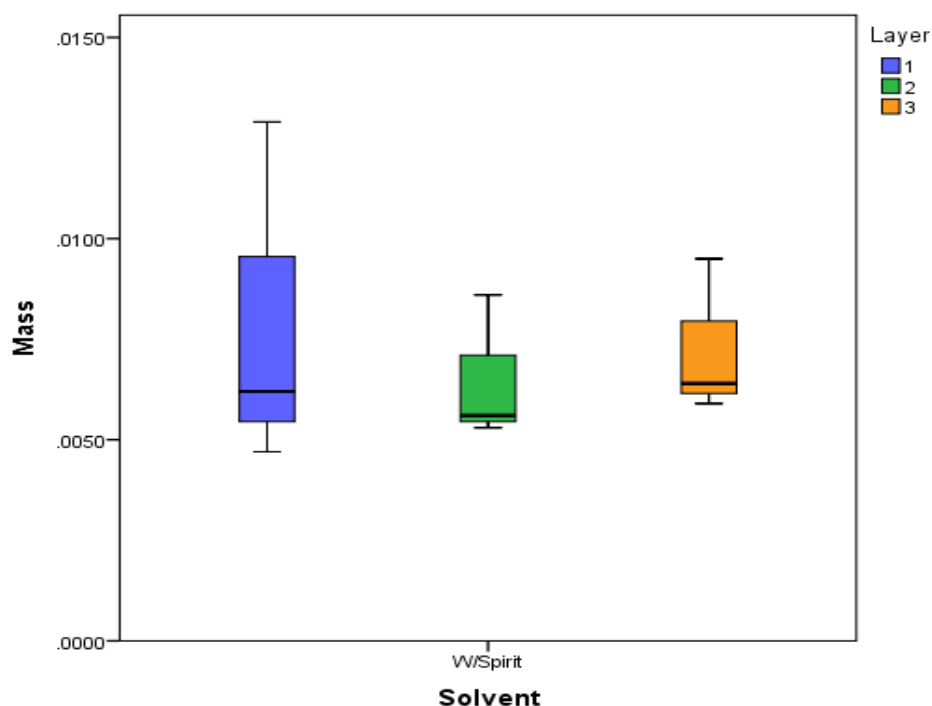


Figure 130 Boxplot to compare the average mass distribution of 10 % w/v Cosmoloid H80 in white spirit coating over the three layers applied

6.2.3.2.2 Mass Applied on Ferrous Metal Samples

Paraloid B72

The analysis of fifteen samples coated with Paraloid B72 revealed an increase in the mean mass of coating with each layer applied and in the standard deviation (table 75).

Table 75 Summarised distribution of Paraloid B72 over 3 layers on metal samples

	Layer 1	Layer 2	Layer 3	Total Coating
Mean mass (g)	0.0299	0.0314	0.0389	0.1002
Standard deviation	0.0033	0.0039	0.0104	0.0123
Percentage of total coating layer (%)	29.84	31.34	38.82	100
Range (g)	0.0125	0.0200	0.0500	0.0600

The results for the percentage of the total coating applied in each layer on the samples are in agreement with the results from the coatings applied to the glass slides, with the highest average percentage being applied in the third layer.

Cosmoloid H80

Analysis of fifteen samples coated with Cosmoloid H80 showed a fluctuating mean mass of coating with each layer applied (table 76).

Table 76 Summarised distribution of Cosmoloid H80 over 3 layers on metal samples

	Layer 1	Layer 2	Layer 3	Total Coating
Mean mass (g)	0.0140	0.0150	0.0128	0.0418
Standard Deviation	0.0016	0.0032	0.038	0.0050
Percentage of total coating layer (%)	33.49	35.89	30.62	100
Range (g)	0.0070	0.0125	0.0150	0.0300

The total masses of the coatings were distributed evenly around the mode with four above and four below.

Siliglide 10

Analysis of fifteen samples coated with Siliglide 10 showed the mean mass of coating layers 1 and 3 were close, but the mean mass for layer 2 was significantly lower (table 77).

The range for the masses of Siliglide 10 decreased for each layer, but the total coating masses have a bigger range than the first layer, the layer with the largest range. The total coating masses are distributed between 0.0060 and 0.0085 g. Six of the fifteen masses fell between 0.0070 and 0.0075 g, with 0.0072 g being the mean value for the total coating masses. The total masses of the coatings were not normally distributed as six lie above and four below the mode.

Table 77 Summarised distribution of Siliglide 10 over 3 layers on metal samples

	Layer 1	Layer 2	Layer 3	Total Coating
Mean mass (g)	0.0030	0.0013	0.0026	0.0072
Standard Deviation	0.00045	0.00037	0.00029	0.00057
Percentage of total coating mass* (%)	43.48	18.84	37.68	100
Range (g)	0.0020	0.0018	0.0014	0.0025

* Total coating mass used for percentage calculations was 0.0069 g.

Comparison of the layers and total masses of the three coatings

Boxplots have been used to compare the individual layers of the different coatings (figures 131-133) and the total coating masses of the different coatings (figure 134). There were no overlaps between the masses of the different clear coatings for the first and second layers (figures 131 and 132). However, figure 133 of the third layers shows an overlap in the masses of the Paraloid B72 and Cosmoloid H80 coatings. An overlap of the error bars or outliers indicates that there is not a statistically significant difference between the masses of the two types of coatings for the layer that overlaps.

When the total masses of the coatings are considered (figure 134) it is clear that a lot less mass is being applied for Siliglide 10 and therefore is likely to be a much thinner coating. Although the mass of Cosmoloid H80 applied is larger than that for Siliglide 10, it is notably smaller than that for Paraloid B72. It also has a slightly smaller range than Paraloid B72.

To confirm that the samples surfaces did not influence the coating mass a boxplot of the forty five coated samples discussed above is included where the samples are split according to surface preparation, cleaned or partially corroded, as well as the coating types (figure 135). For each coating type five samples had clean surfaces prior to coating and ten were partially corroded prior to coating. A difference that can be seen from this boxplot plot is that for the partially corroded samples coated with Paraloid B72, there is a much larger range in the coating mass applied to the samples.

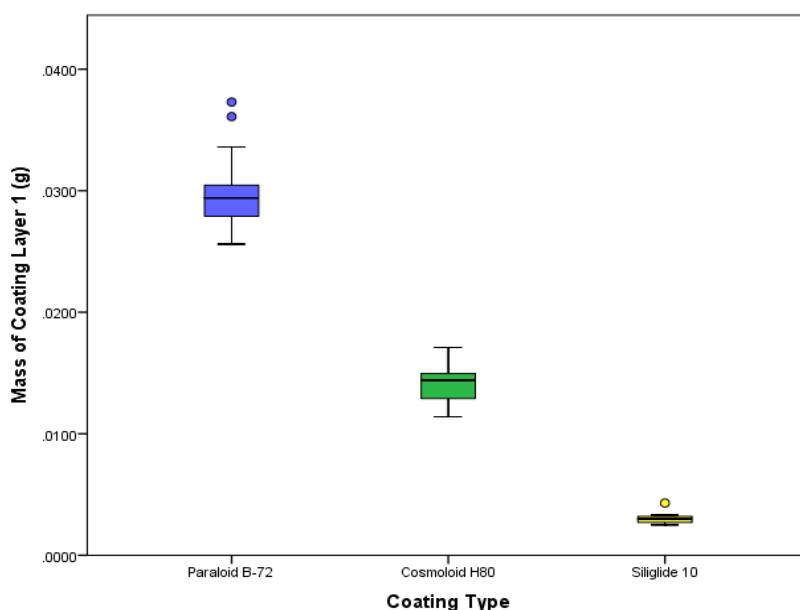


Figure 131
Comparison of
the masses of
the first layer
of coatings
Paraloid B72,
Cosmoloid H80
and Siliglide
10.

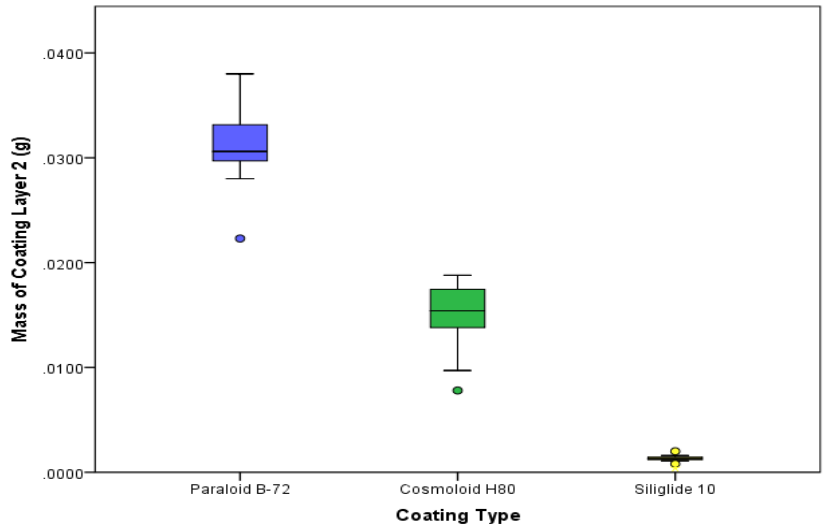


Figure 132
Comparison of the masses of the second layers of the clear coatings.

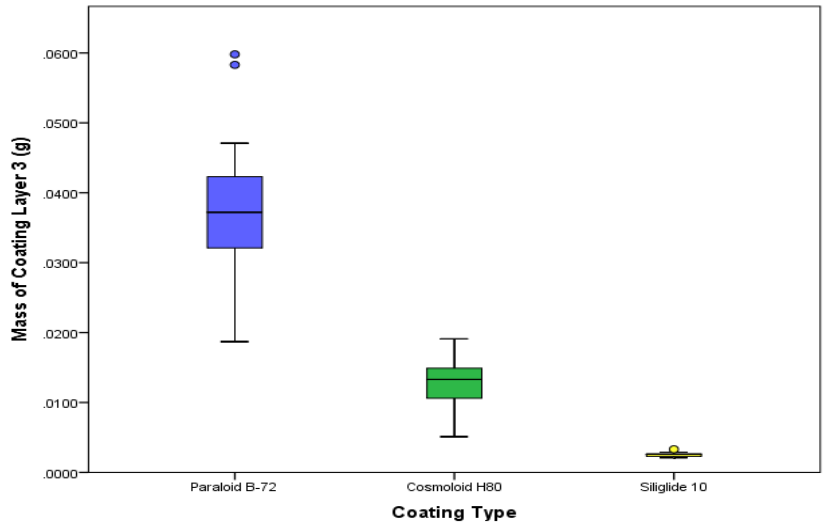


Figure 133
Comparison of the masses of the third layers of the clear coatings.

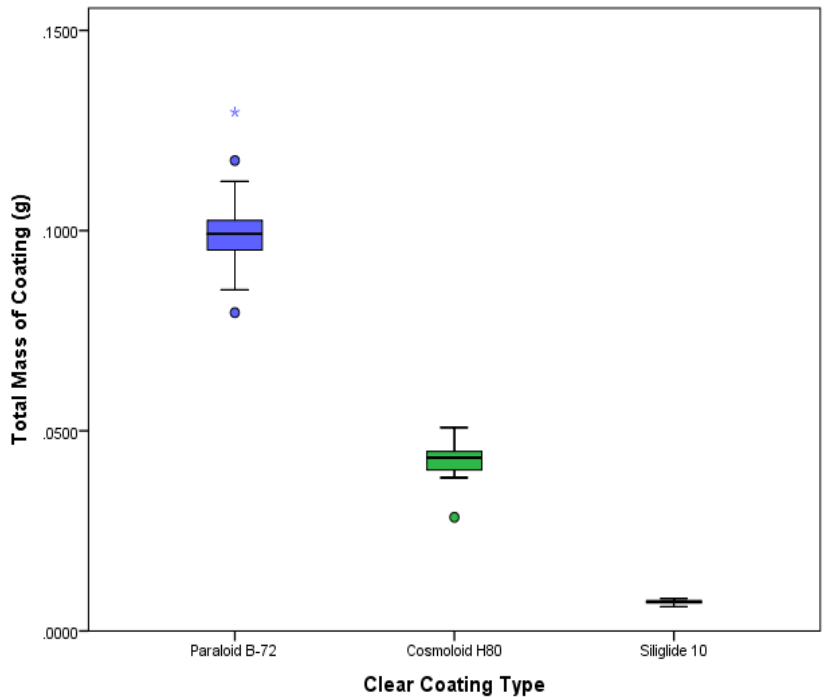


Figure 134
Comparison of the total masses of the Paraloïd B72, Cosmoloid H80 and Siliglide 10 coatings.

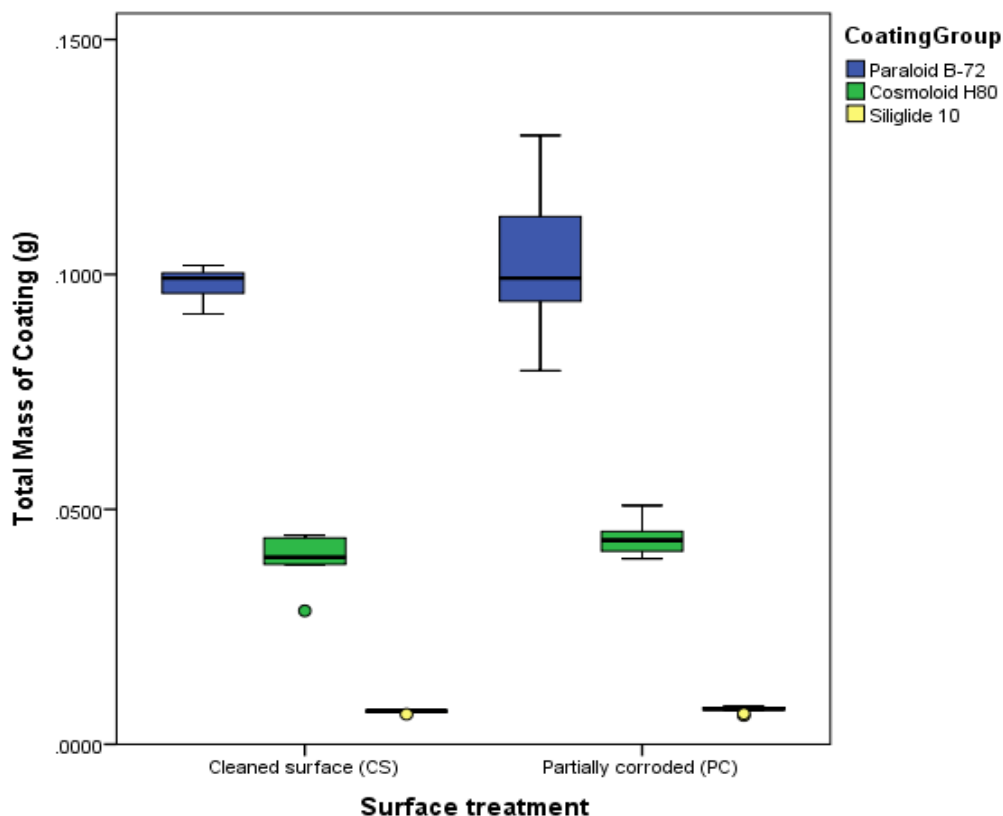


Figure 135 Comparison of the total masses of the Paraloid B72, Cosmoloid H80 and Siliglide 10 coatings separated into coatings that were applied to cleaned surfaces and those that were applied to partially corroded samples.

6.2.3.3 Impact of Coatings and Solvent Choice on Oxygen Sensors

The impact of the coating on the O₂ measurement system was evaluated by coating inert controls (glass slides) and measuring their effect on the O₂ partial pressure.

Paraloid B72

Xylene used with Paraloid B72 was found to affect the sensor spots performance.

Five glass slides coated with 10% w/v Paraloid B72 in acetone were tested to see the impact of acetone on the O₂ sensor spots performance (figure 136). The effect of acetone on the O₂ levels is significantly less than the effect xylene had as the solvent. The accuracy of the O₂ meter is ± 2 hPa, a systematic error of 1%, which leads to a ± 2 hPa level of uncertainty in the measurements made. The data points dipping below -2 hPa on figure 136 therefore indicates that more O₂ is getting into the jars and this may result from the solvent degassing and damaging the rubber seal on the lid of the jar.

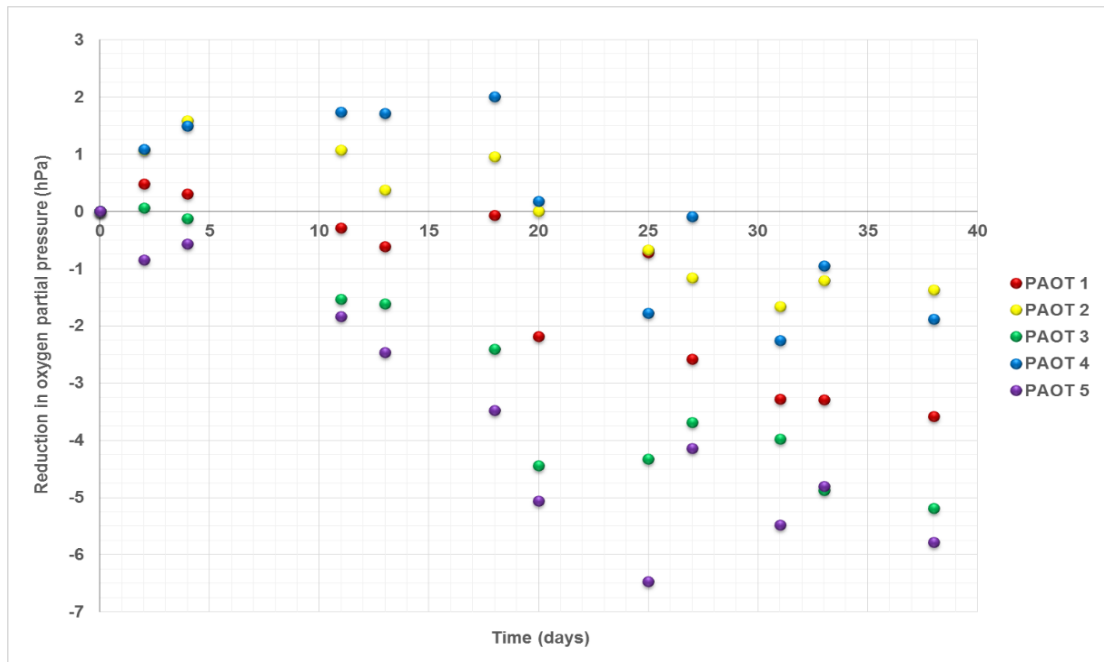


Figure 136 Reduction in P_{O_2} for 10% w/v Paraloid B72 in acetone not degassed – 3 layers of coating on glass slides at $\approx 20^\circ\text{C}$, 50% RH – monitored for more than 1 month

Fresh de-greased glass slides were coated with Paraloid B72 in acetone, de-gassed for 21 days before their influence on the O_2 levels was monitored and control fluctuations were removed from the coating data, which fluctuated within the ± 2 hPa error margins for the O_2 meter (figure 137). Therefore, after being allowed to de-gas this coating no longer influences the measurements of the O_2 concentration.

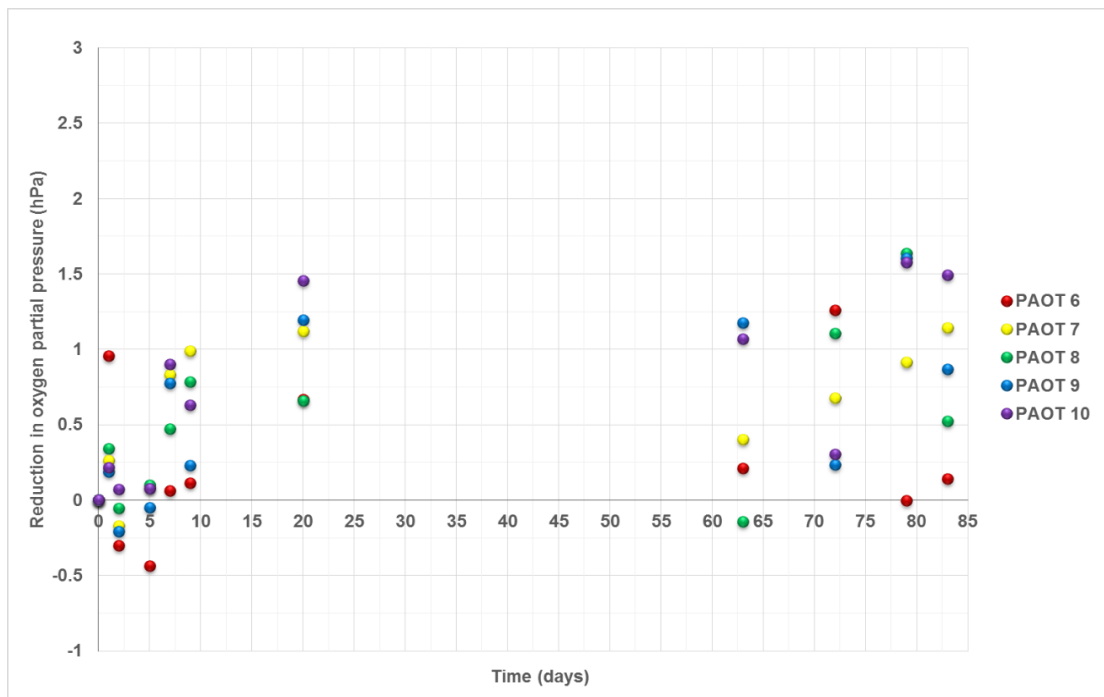


Figure 137 Reduction in P_{O_2} for 10% w/v Paraloid B72 in acetone – 3 layers on glass slides after de-gassing for 21 days monitored at 20°C , 50% RH over roughly 3 months

Cosmoloid H80 and Siliglide 10

Cosmoloid H80 in white spirit (figure 138) and Siliglide 10 (figure 139) coatings on degassed glass slides caused little change in the O_2 partial pressure with control fluctuations removed from the data. The data for Cosmoloid H80 (figure 138) clearly fluctuated within ± 2 hPa as the y-axis only extends from -2 hPa to +2 hPa. For Siliglide 10 (figure 139) although the data points all fall within 2 hPa of each other they do fluctuate below -2 hPa. This may not imply anything or it could suggest that the coating has affected the seal on the jar and may get worse with more time.

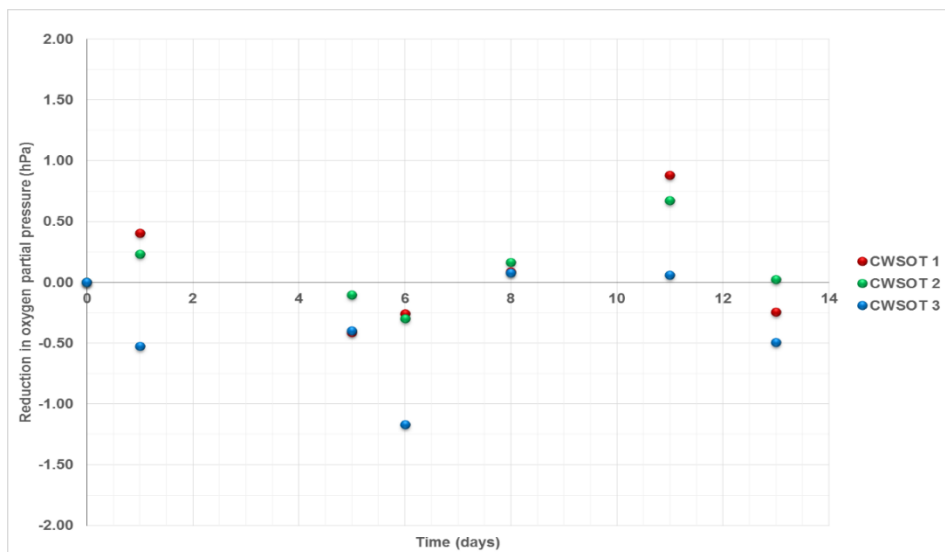


Figure 138 Reduction in P_{O_2} for 10% w/v Cosmoloid H80 in white spirit not degassed – 3 layers of coating on 3 glass slides monitored at 20 °C, 50% RH for over 2 weeks

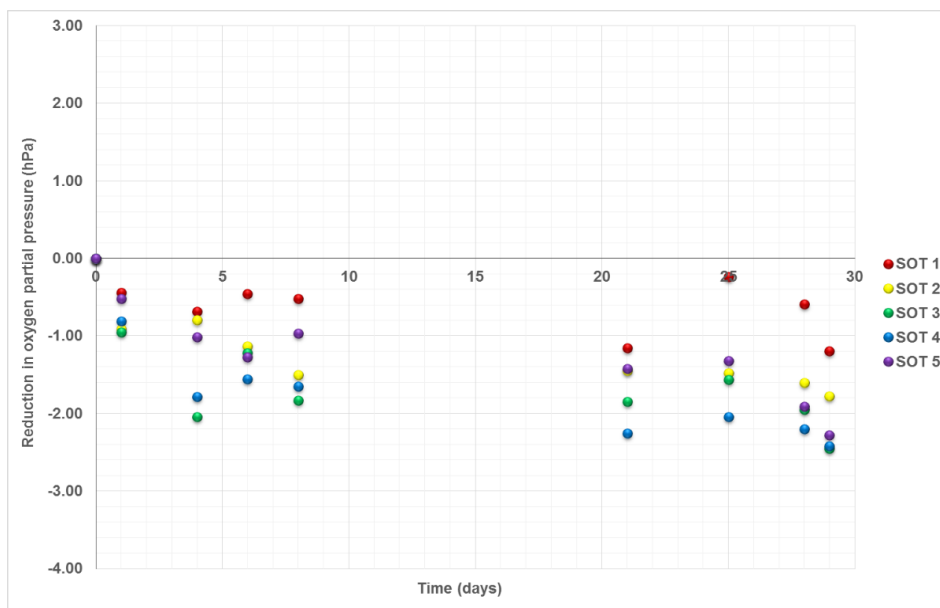


Figure 139 Reduction in P_{O_2} for Siliglide 10 not degassed – 3 layers of coating on glass slides at 20 °C, 50% RH for approximately 1 month

6.2.4 Oxygen Consumption of Cleaned Coated Samples

Paraloid B72

The sample data for the cleaned Paraloid B72 coated samples with control fluctuations removed is shown in figure 140. The data can be compared to visual results later in the chapter as photographs of an example from this treatment group is shown.

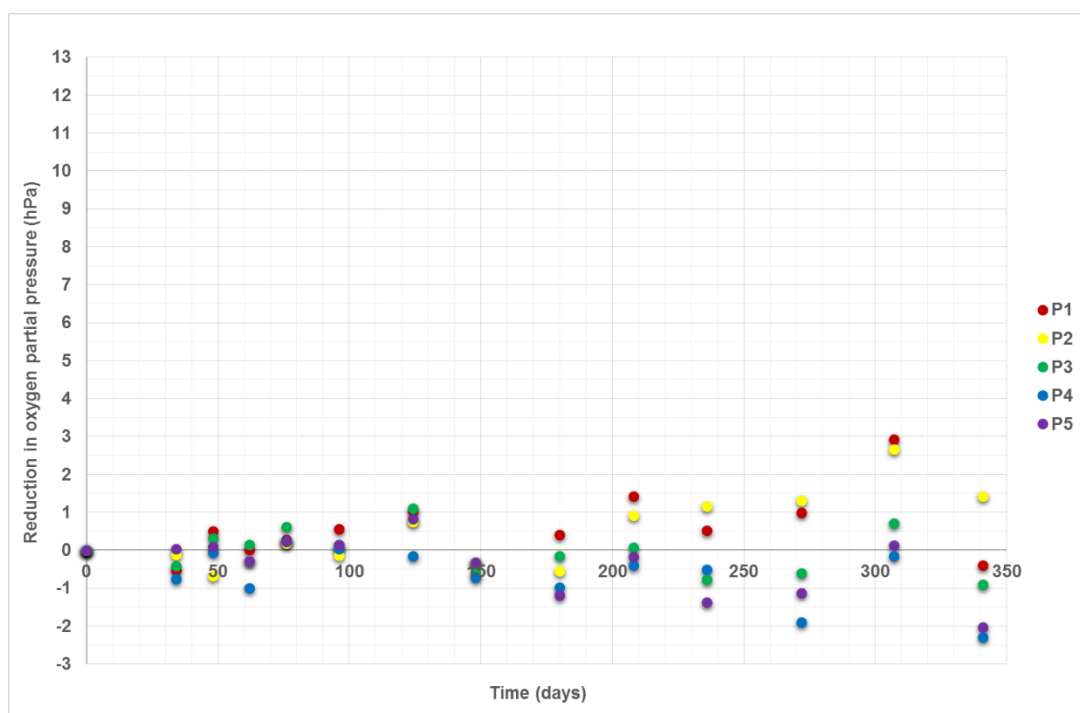


Figure 140 Reduction in O₂ partial pressure over 341 days at 20 °C, 80% RH for Paraloid B72 coated clean samples. Control jar fluctuations have been subtracted from the sample data.

Cosmoloid H80

Figure 141 displays the reduction in O₂ partial pressure of the jars containing the Cosmoloid H80 coated clean samples over the 341 days of exposure at 80% RH with the control fluctuations removed.

Siliglide 10

The reduction of O₂ partial pressure in the jars containing clean Siliglide 10 coated samples with control fluctuations subtracted are shown in figure 142 for the 341 days of exposure at 80% RH.

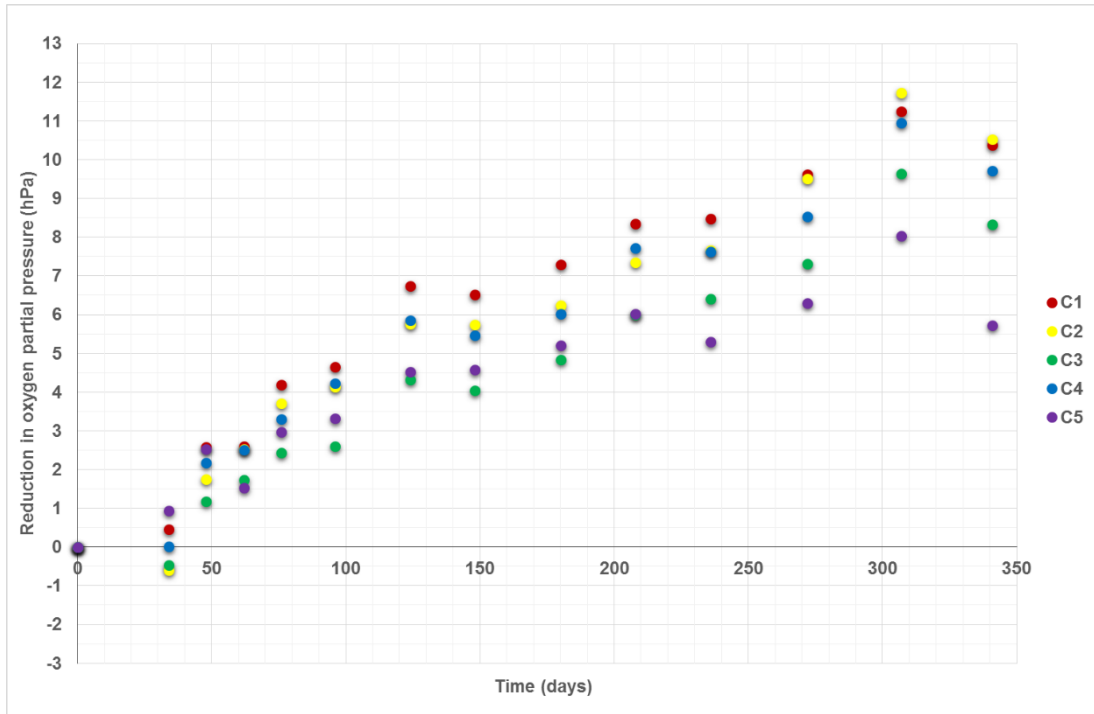


Figure 141 Reduction in O₂ partial pressure over 341 days at 20 °C, 80% RH for Cosmoloid H80 coated cleaned samples. Control jar fluctuations have been removed from sample data.

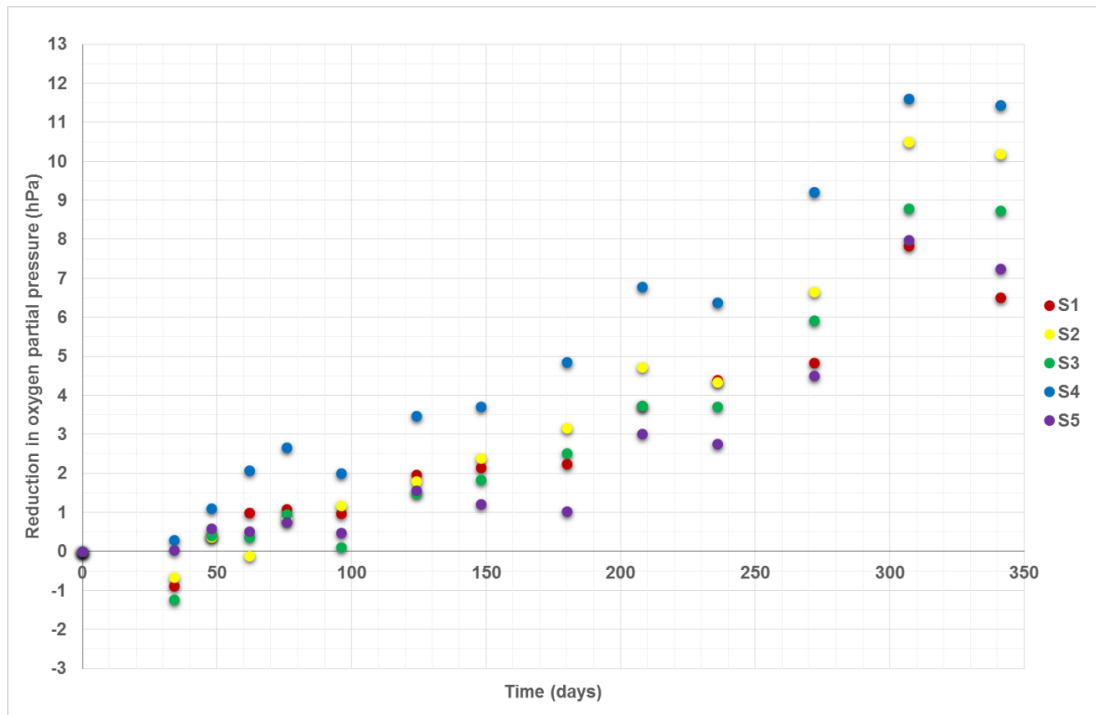


Figure 142 Reduction in O₂ partial pressure over 341 days at 20 °C, 80% RH for Siliglide 10 coated cleaned samples. Control jar data fluctuations have been subtracted from the sample data.

Comparison of the Coatings on Cleaned Sample

Figure 143 displays the data collected for all three coatings on cleaned samples as well as the data for samples UT6 and CS6; all the data points have the control fluctuations subtracted.

Faint dotted lines are included on figure 143 for samples CS6 (cleaned uncoated) and UT6 (untreated), as the data points for UT6 are largely hidden under the coated sample data points. Again it is clear that the trend for sample CS6 is not linear, but in the case of figure 143 the lines have only been added to highlight the data for the untreated and cleaned uncoated samples compared to the samples that have been cleaned and coated.

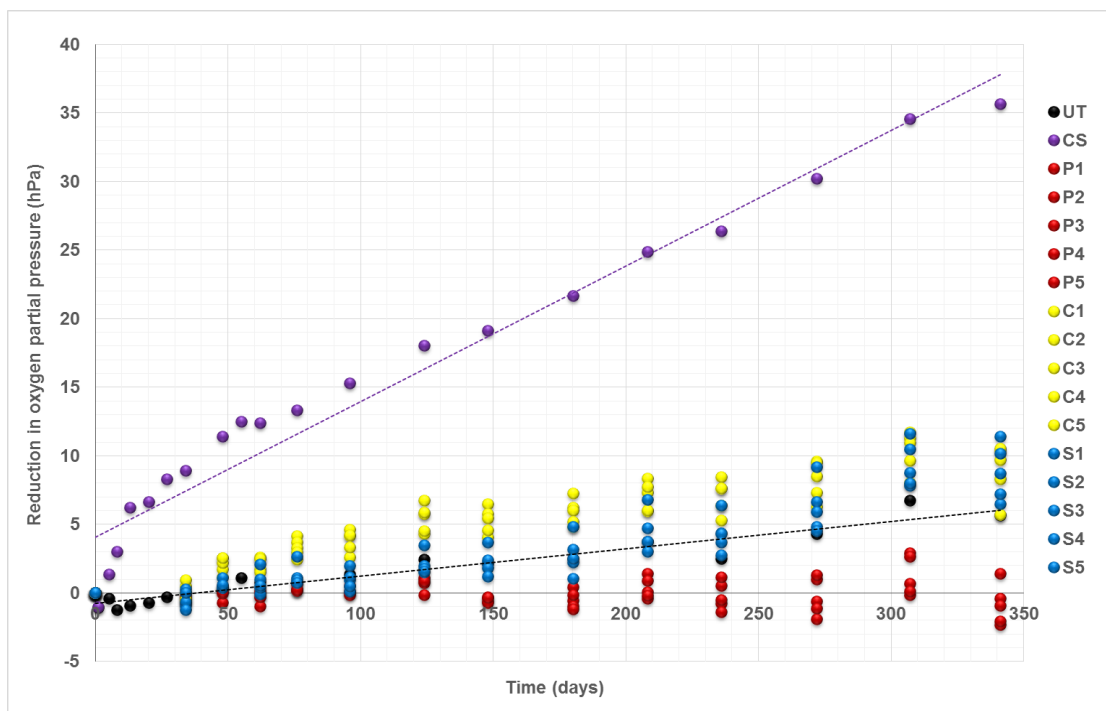


Figure 143 Comparison of the reduction in O₂ partial pressure over 341 days at 20 °C, 80% RH of 15 cleaned and coated samples – 5 coated with each of the 3 different coatings – Paraloid B72 (red), Cosmoloid H80 (yellow) and Siliglide 10 (blue). Untreated sample (UT6 – black) and cleaned uncoated sample (CS6 – purple) are included for comparison. Control jar fluctuations are subtracted from all the data points

The boxplot in figure 144 summarises the statistical data the O₂ partial pressure reduction - the range, maximum, minimum and median values and these values are presented in table 78. The boxplot in figure 145 compares the data for the cleaned coated samples to the cleaned uncoated samples to show the impact of coatings on reduction in O₂ partial pressure.

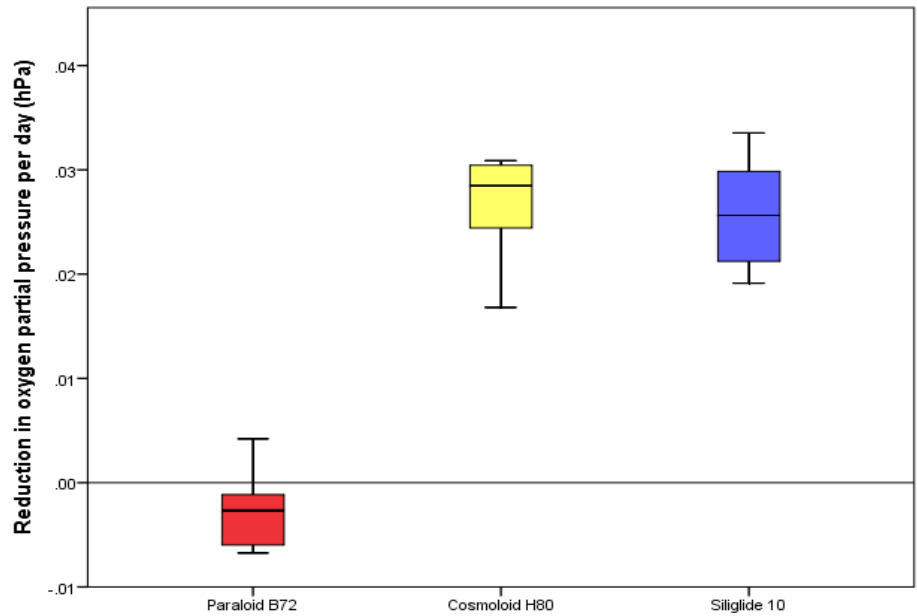


Figure 144 Boxplot summarising statistical data for the reduction in O₂ partial pressure for each coating type on cleaned samples after 341 days.

Table 78 Comparison of the clean coated samples with control data substracted

	PB72CS	CH80CS	S10CS
Maximum	1.43	10.53	11.44
Minimum	-2.30	5.73	6.52
Range value	3.73	4.80	4.92
Median	-0.91	9.71	8.74

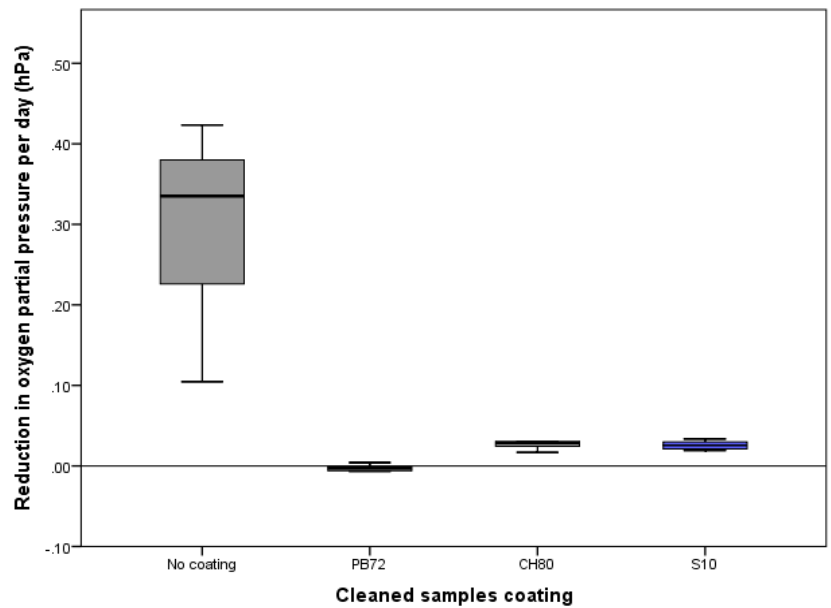


Figure 145 Boxplot comparing the reduction in O₂ partial pressure per day for all of the cleaned samples including those not coated

6.2.5 Oxygen Consumption of Partially Pre-Corroded Coated Samples

The cleaned partially corroded samples coated with the clear coating used a larger number of samples (10 rather than 5) with each coating as increased variability is introduced by spray application of the salt solution. The control data for these samples has not been subtracted from the data points as it was not measured on exactly the same day, but it has been included on the graphs. The data displayed for the different coatings can be compared to visual changes later in the chapter as photographs of examples of the different treatment groups are shown.

Paraloid B72

Figure 146 displays the reduction in O₂ partial pressure for the cleaned partially pre-corroded Paraloid B72 coated samples exposed to 80% RH for 342 days.

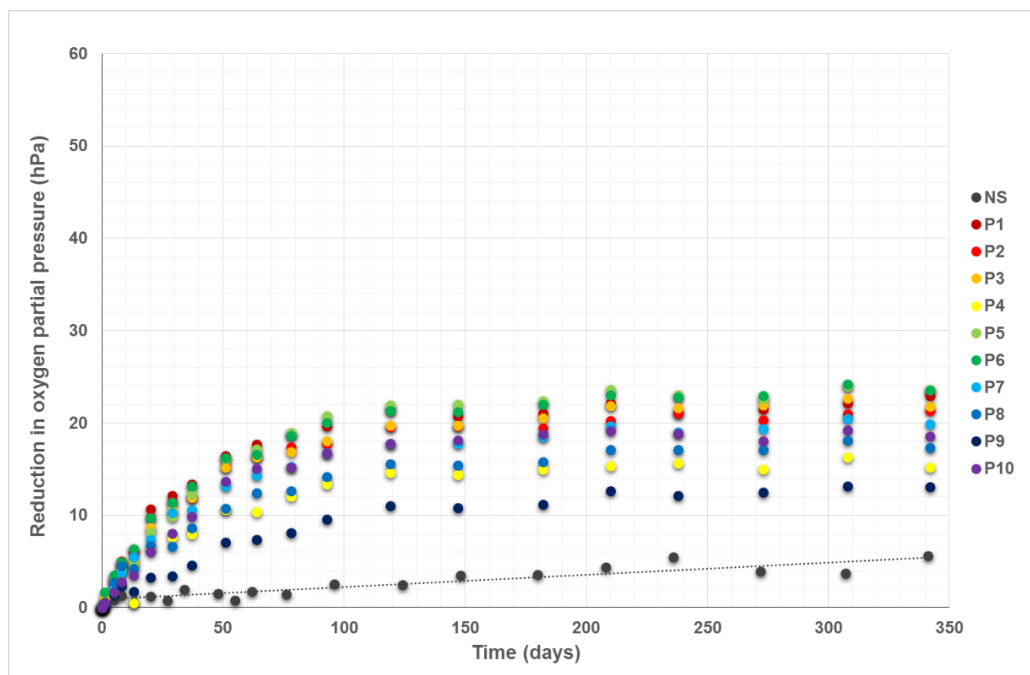


Figure 146 Reduction in O₂ partial pressure over 342 days at 20 °C, 80% RH for Paraloid B72 coated partially pre-corroded samples. The control jar (NS) has also been included in this graph to compare the background fluctuations to those of jars with samples included.

Cosmoloid H80

The data for the reduction in O₂ partial pressure for the Cosmoloid H80 coated partially pre-corroded samples exposed to 80% RH 342 days is displayed in figure 147 along with the control data, measured during the same period but not on the same days.

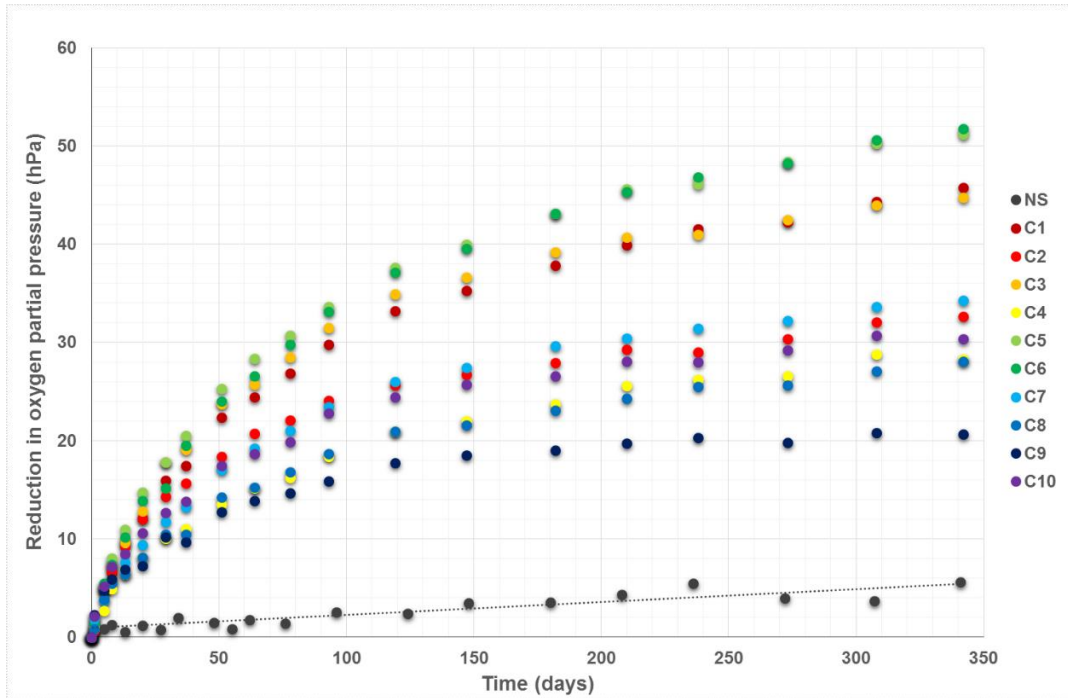


Figure 147 Reduction in O₂ partial pressure over 342 days at 20 °C, 80% RH for Cosmoloid H80 coated partially pre-corroded samples. The control jar (NS) has been included in this graph to compare the fluctuations to those of jars with samples included.

Siliglide 10

Figure 148 displays the reduction in O₂ partial pressure for the jars containing Siliglide 10 coated partially pre-corroded samples exposed to 80% RH for 342 day and the control fluctuations

Comparison of the Coatings on Partially Corroded Samples

The statistical data for the final data points collected for the 30 partially pre-corroded coated samples (10 of each coating) is summarised in the boxplots displayed in figure 149. Table 79 summarises much of the statistical data shown in figure 149 providing quick access to the numerical values.

A graph containing the data collected for all 30 samples over the 342 days has not been included. Graphs comparing the average data for each coating, the data for samples CS6, UT6 and control fluctuations have all been included (figures 150 and 151). The average data for the partially corroded uncoated samples has also been included for comparison.

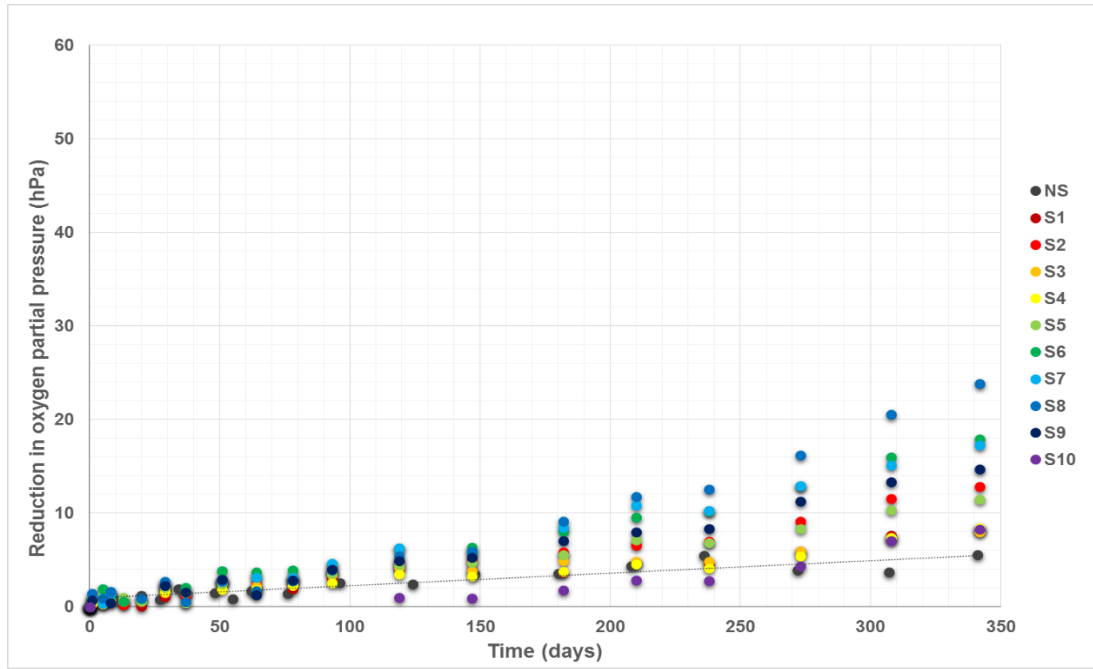


Figure 148 Reduction in O₂ partial pressure over 342 days at 20 °C, 80% RH for Siliglide 10 coated partially pre-corroded samples. The control jar (NS) has also been included in this graph to compare the fluctuations to those of jars with samples included.

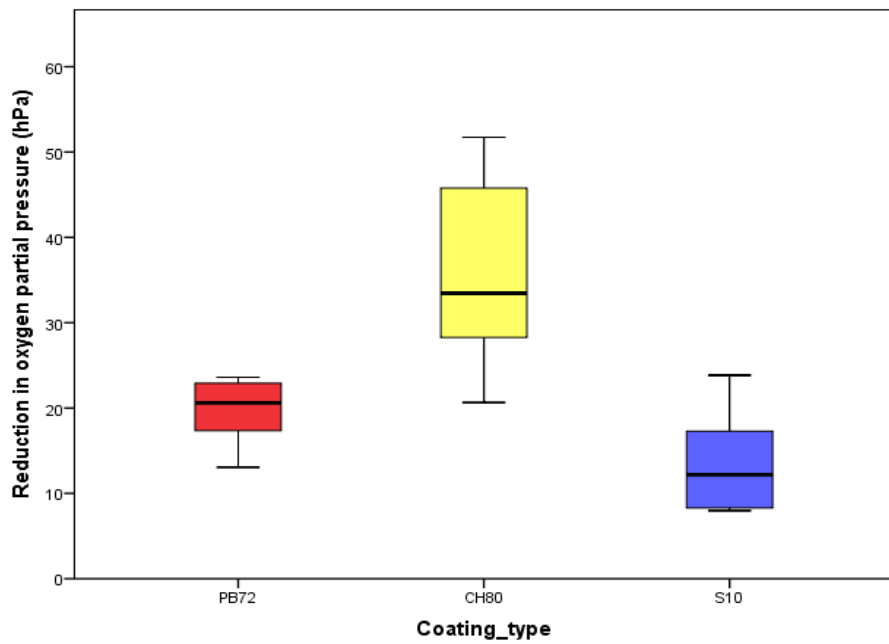


Figure 149 Boxplot summarising statistical data of the reduction in O₂ partial pressure by partially pre-corroded samples after 342 days, divided up into the types of coatings used.

Table 79 Comparison of partially pre-corroded coated samples – control data not subtracted from data

	PB72PC	CH80PC	S10PC
Maximum	23.61	51.73	23.84
Minimum	13.05	20.64	7.97
Range value	10.55	31.09	15.87
Median	20.60	33.45	12.18

Of the two graphs comparing the average trends one focuses on the first 50 days (figure 150) due to the speed of the reduction in O₂ partial pressure by the partially pre-corroded uncoated samples and the other displays the whole 342 days that they were exposed to 80% RH (figure 151).

A further boxplot has been included (figures 152) comparing the reduction in oxygen partial pressure per day, the effect of the coating used (or not used), and split according to the surface treatment.

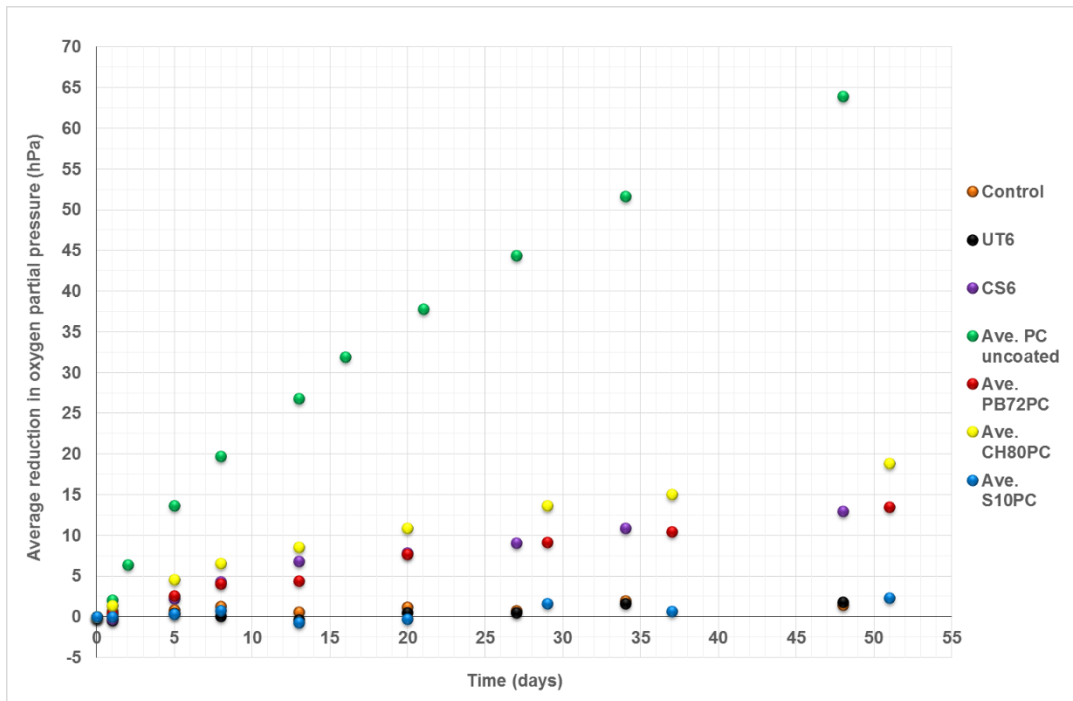


Figure 150 Comparison of the average reduction in O₂ partial pressure of the partially corroded samples coated and uncoated over approximately 50 days. The control jar fluctuations, the untreated sample (UT6), and the cleaned uncoated sample (CS6) have been included on this graph for comparison.

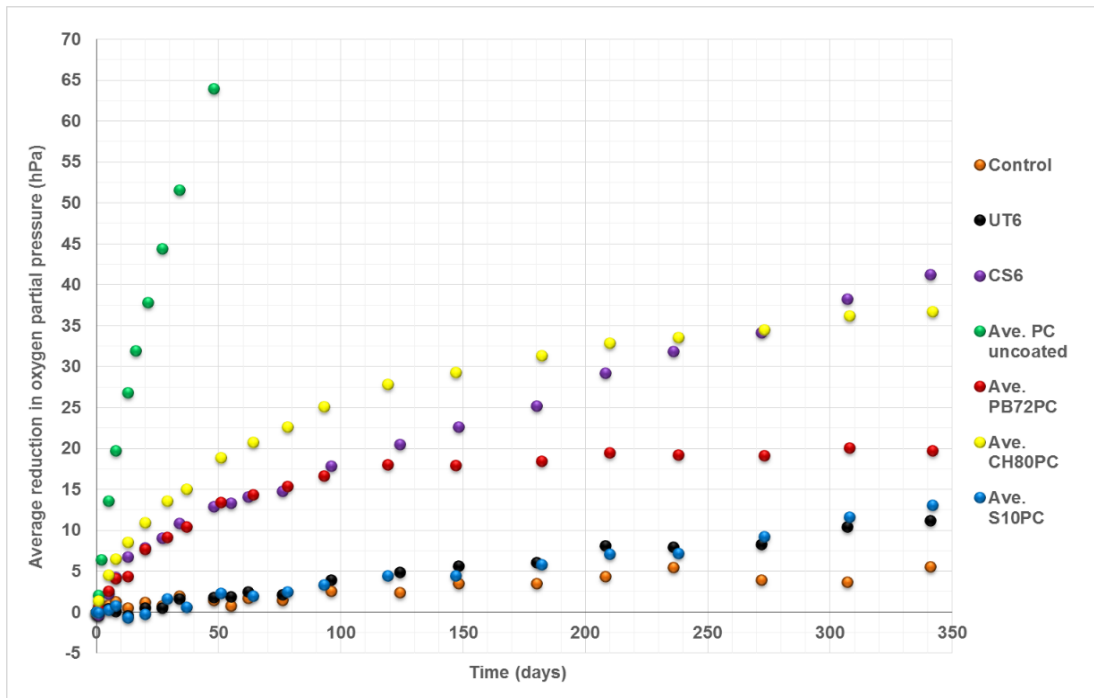


Figure 151 Comparison of the average reduction in O₂ partial pressure of the partially corroded samples coated and uncoated over approximately 340 days. Measuring for the partially corroded uncoated samples was stopped after 48 days. The control jar fluctuations, the untreated sample (UT6), and the cleaned uncoated sample (CS6) have been included on this graph for comparison.

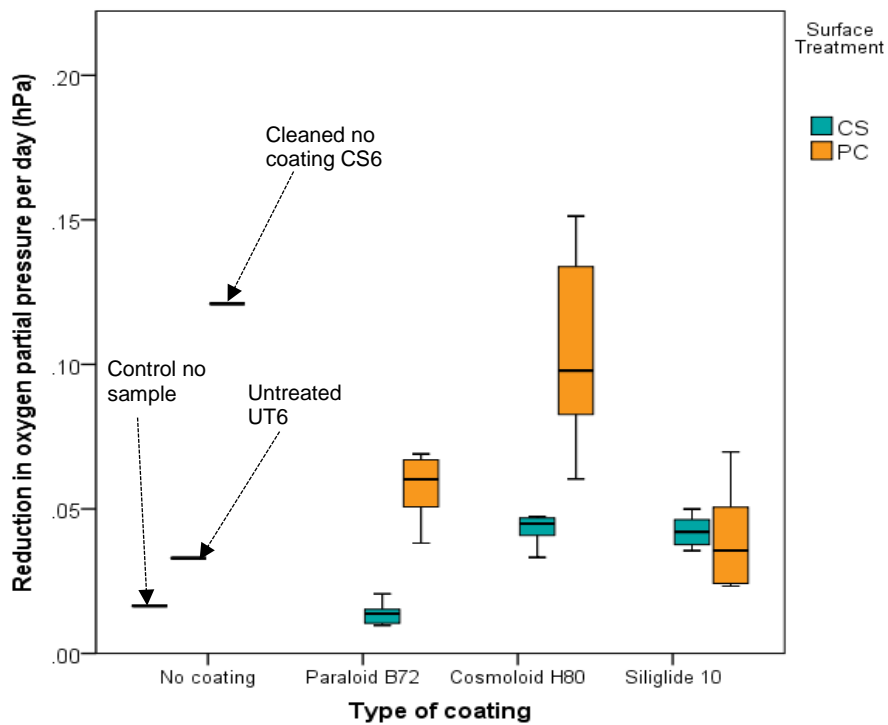


Figure 152 Comparison of the reduction in O₂ partial pressure per day for the different types of coating on different surfaces, the control data, and samples UT6 and CS6 have also been included.

6.2.6 Accelerated Corrosion at a Scribe through the Coatings

Due to the low rate of reduction in O_2 partial pressure all of these samples were removed from the chamber after 70 days, photographed and returned to the chamber for further monitoring. Control data has been subtracted from all the sample data in this section.

Paraloid B72

The first 70 days of monitoring the reduction O_2 partial pressure are shown in figure 153 for the scribed Paraloid B72 coated samples. The additional 148 days are shown separately in figure 154 and combined with the initial 70 days in figure 155.

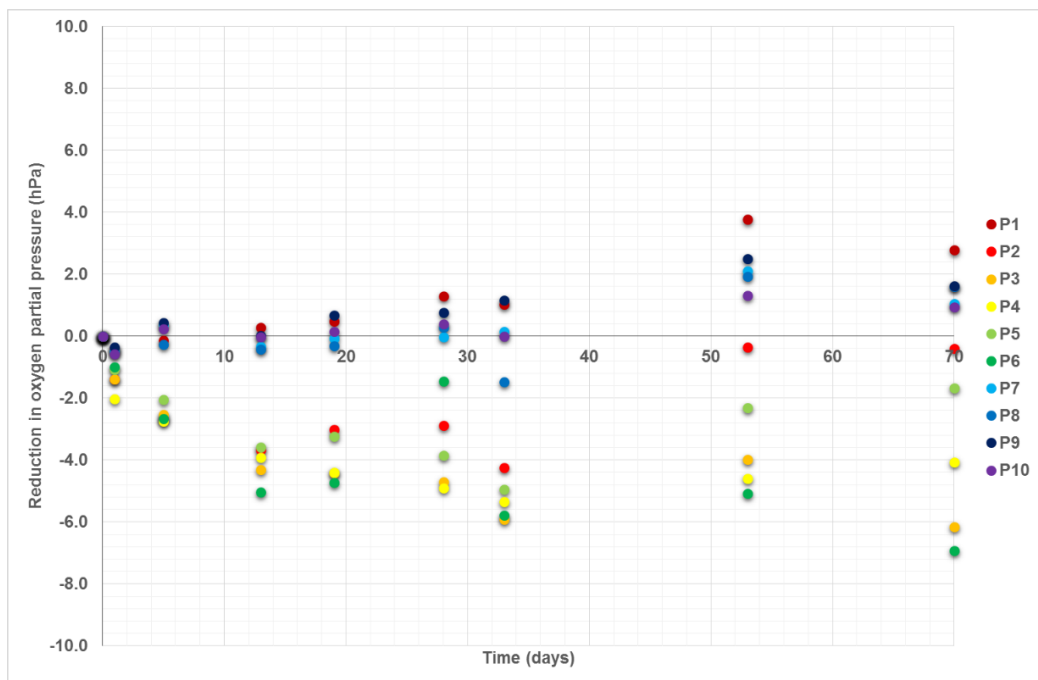


Figure 153 Reduction in O_2 partial pressure for clean coated samples with salt solution applied to a scribe in the Paraloid B72 coating initially monitored for 70 days at 20 °C, 80% RH.

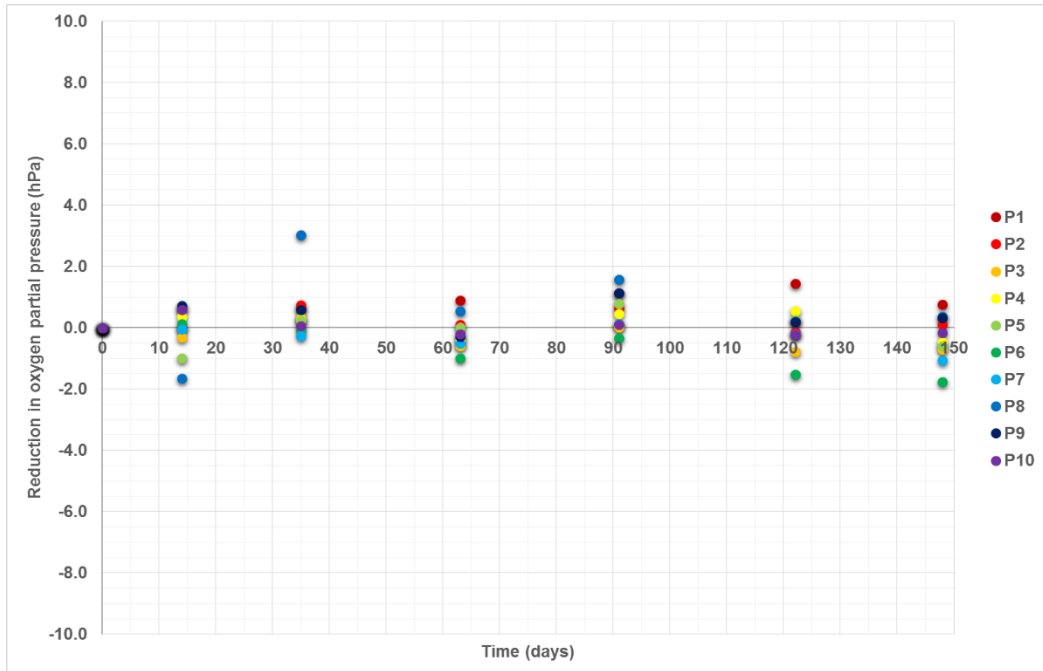


Figure 154 Reduction in O₂ partial pressure for clean coated samples with salt solution applied to a scribe in the Paraloid B72 coating after returning to the chamber for a further 148 days at 20 °C, 80% RH.

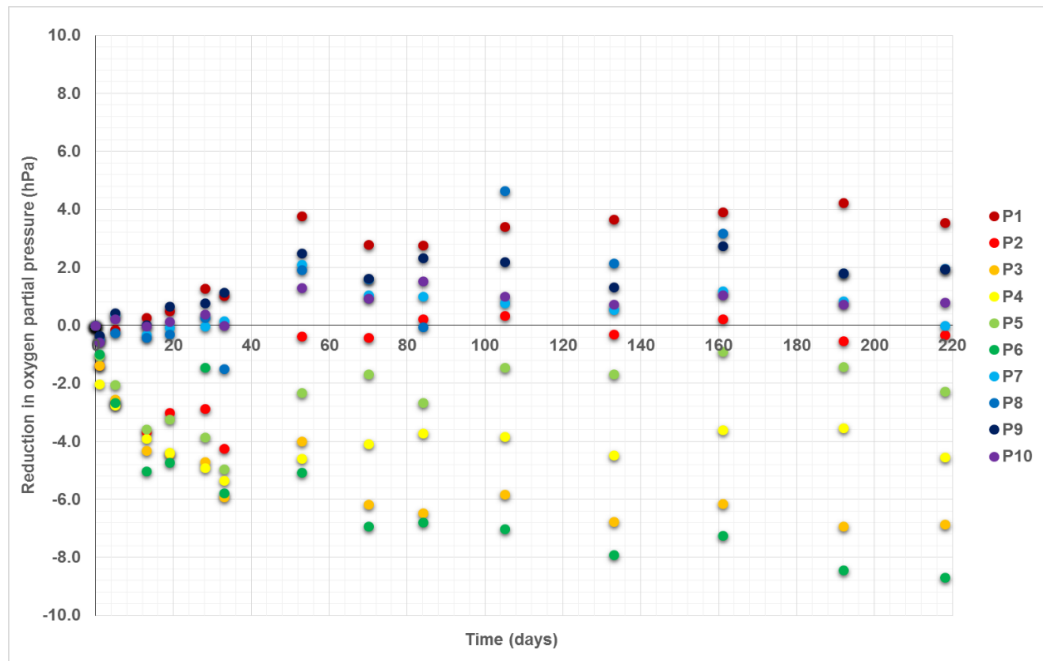


Figure 155 Combined data for the reduction in O₂ partial pressure for clean coated samples with salt solution applied to a scribe in the Paraloid B72 coating monitored for a total of 218 days at 20 °C, 80% RH.

Cosmoloid H80

The first 70 days of monitoring the reduction in partial pressure O₂ of the scribed Cosmoloid H80 coated samples is shown in figure 156. Figure 157 shows the data collected on returning the samples to the chamber and for figure 158 the data has been combined.

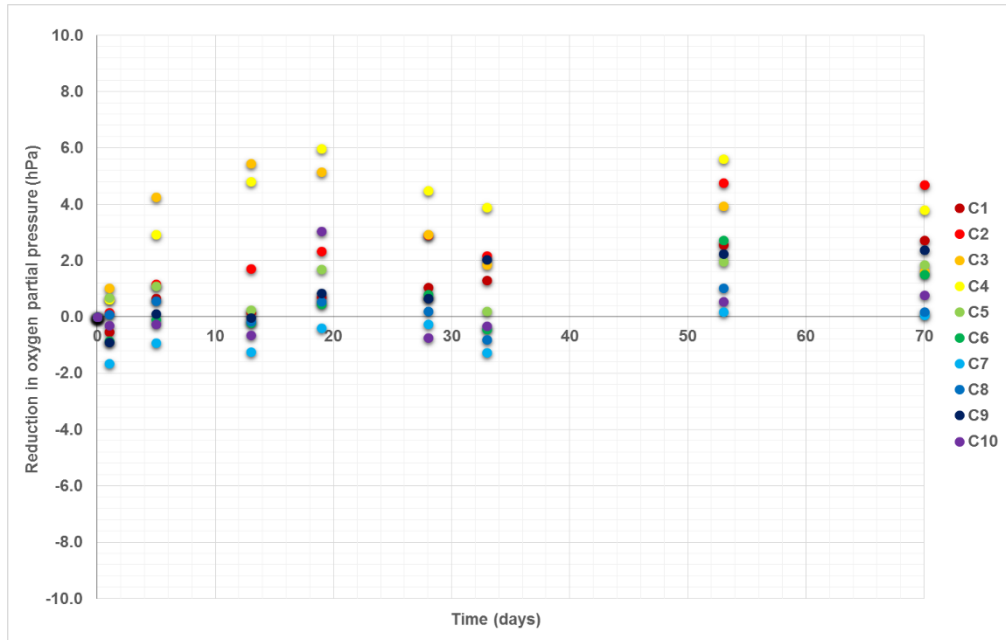


Figure 156 Reduction in O₂ partial pressure for clean coated samples with salt solution applied to a scribe in the Cosmoloid H80 coating initially monitored for 70 days at 20 °C, 80% RH.

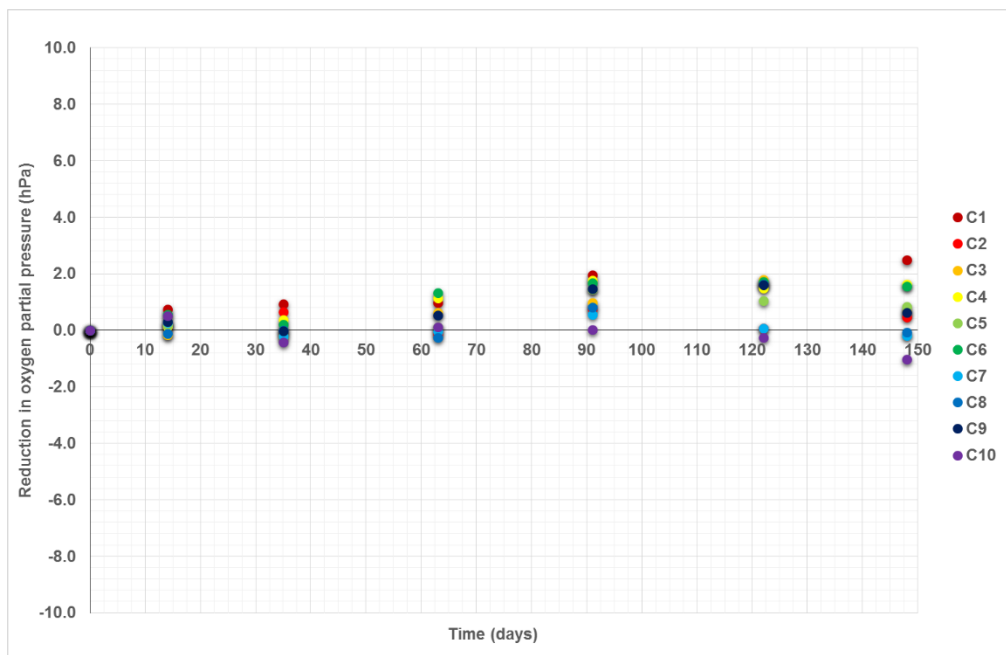


Figure 157 Reduction in O₂ partial pressure for clean coated samples with salt solution applied to a scribe in the Cosmoloid H80 coating after returning to the chamber for a further 148 days at 20 °C, 80% RH.

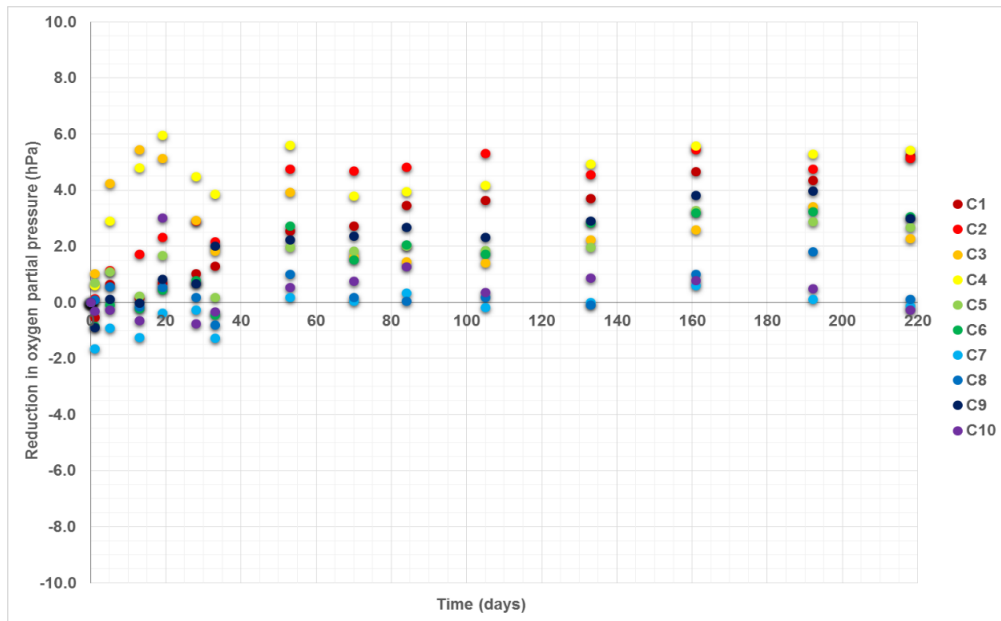


Figure 158 Combined data for the reduction in O₂ partial pressure for clean coated samples with salt solution applied to a scribe in the Cosmoloid H80 coating monitored for a total of 218 days at 20 °C, 80% RH.

Siliglide 10

The first 70 days of exposure to 80% RH for the scribed Siliglide 10 coated samples are displayed in figure 159, followed by another 148 days (figure 160) after photographing the samples and returning them to the same exposure conditions. The combined data for the 218 days of exposure is displayed in figure 161.

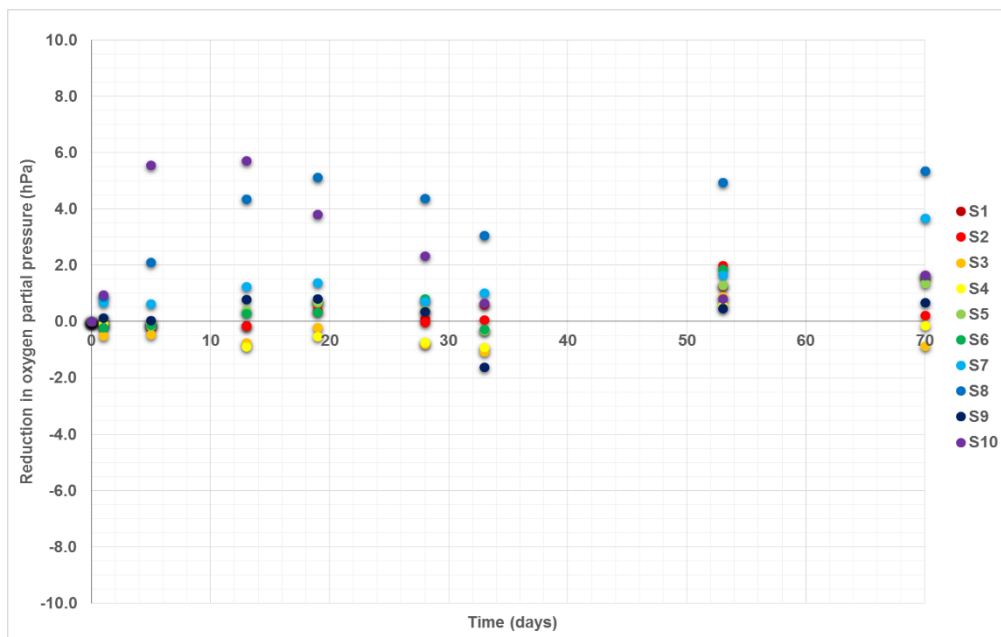


Figure 159 Reduction in O₂ partial pressure for clean coated samples with salt solution applied to a scribe in the Siliglide 10 coating initially monitored for 70 days at 20 °C, 80% RH.

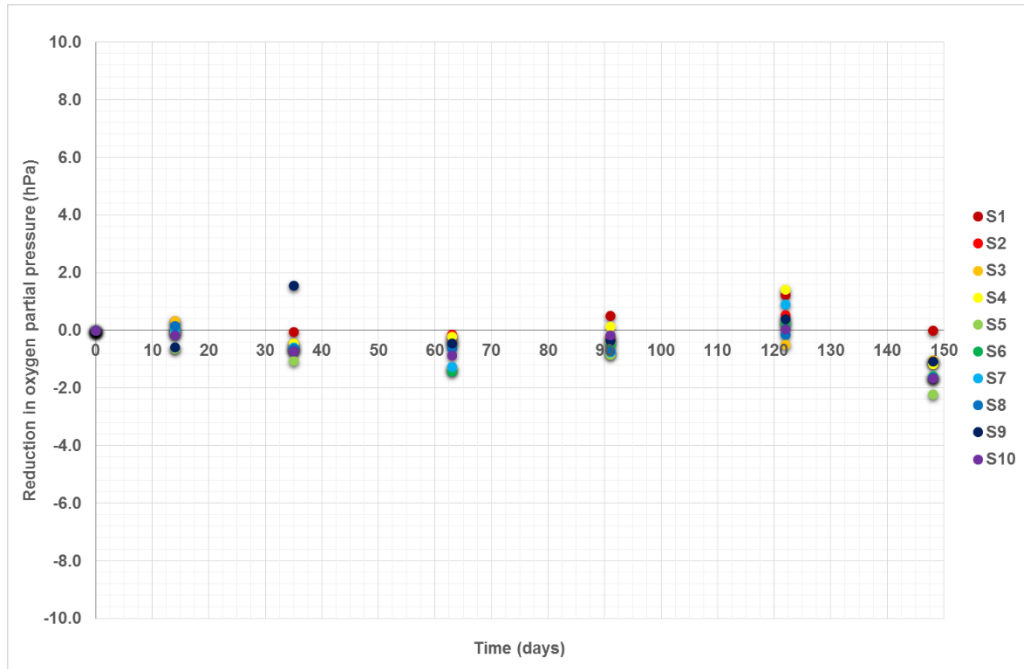


Figure 160 Reduction in O₂ partial pressure for clean coated samples with salt solution applied to a scribe in the Siliglide 10 coating after returning to the chamber for a further 148 days at 20 °C, 80% RH.

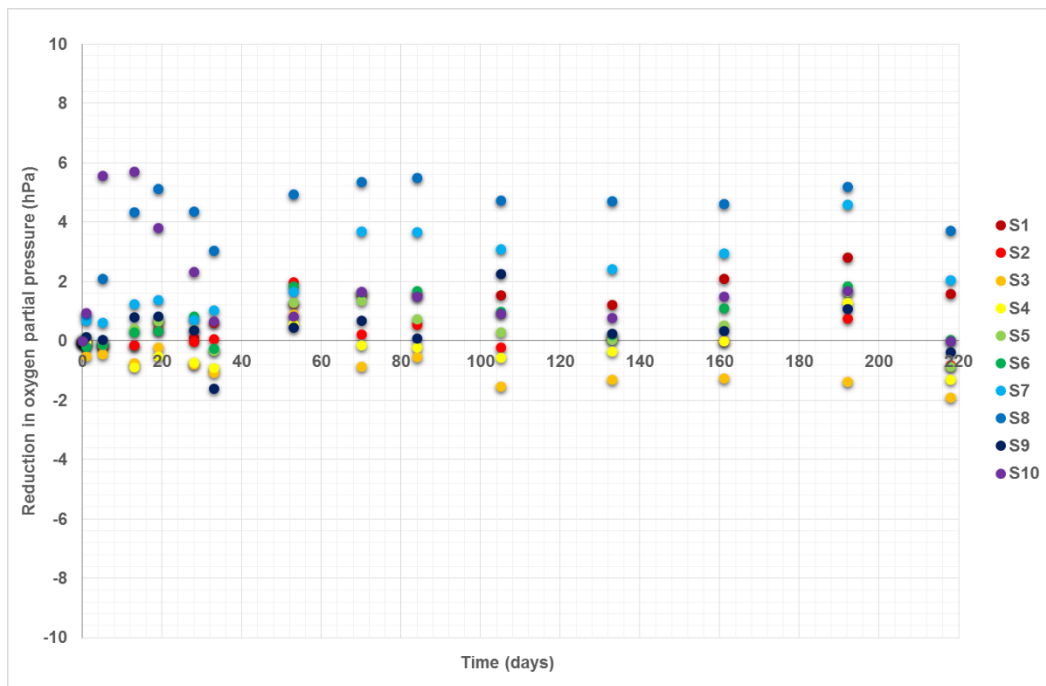


Figure 161 Combined data for the reduction in O₂ partial pressure for clean coated samples with salt solution applied to a scribe in the Siliglide 10 coating monitored for a total of 218 days at 20 °C, 80% RH.

6.2.7 Images of samples

Untreated samples

Prior to the experiment the two sides of the untreated sample UT1 (figures 162 and 163) have a different appearance as a small area of green paint is left on side B (figure 163). Figures 164 and 165 show there are no major visual differences to the sample after monitoring O₂ consumption for 163 days. Corrosion is light (figures 166 and 167).

Cleaned samples

Prior to cleaning the two sides of the untreated sample CS3 (figures 168 and 169) have a different appearance, side A (figure 168) has more of the old paint layers present than side B (figure 169) that appears to have a surface cover of primer and mill scale. Samples cleaned to bare white-silver metal were left with a few darker areas (figures 170 and 171). Figures 172 and 173 show the differences in the corrosion coverage after 65 days exposure at 80% RH. Higher magnification images reveal filiform corrosion is present (figures 174 and 175).

Partially accelerated corroded samples

The two sides of sample PC1 prior to cleaning (figures 176 and 177) looked much the same as those discussed above ahead of cleaning. Samples were cleaned to silver white metal, revealing pits and grooves in the surface (figures 178 and 179). Figures 180 and 181 show the sample one week after the application de-icing salt solution pre-corroding one side (figure 181).

After monitoring the O₂ consumption of these samples for 48 days both sides of the samples had visibly changed (figures 182 and 183). The corrosion appears widespread but more localised than in figure 181. Higher magnification images of both sides of sample PC1 (figures 184 and 185) show the presence of corrosion filaments.

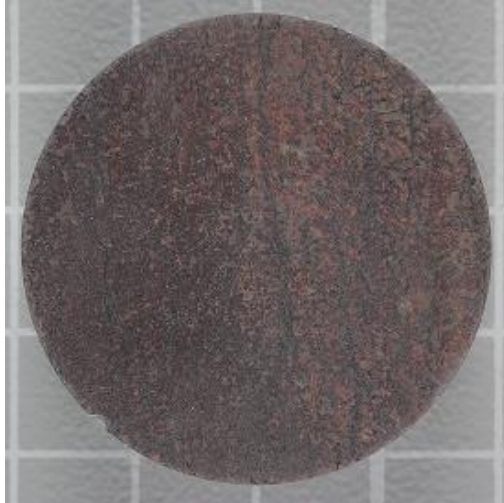


Figure 162 Untreated (UT) sample 1 side A prior to exposure at 80% RH



Figure 163 UT1B prior exposure at 80% RH



Figure 164 UT1A after 163 days exposed to 80% RH



Figure 165 UT1B after 163 days exposed to 80% RH



Figure 166 Zoomed area of UT1A after 163 days exposed to 80% RH



Figure 167 Zoomed area of UT1B after 163 days exposed to 80% RH



Figure 168 Sample CS3A prior to air abrading clean

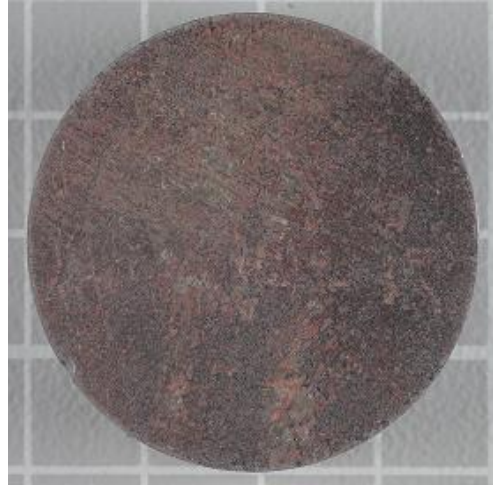


Figure 169 Sample CS3B prior to air abrading clean



Figure 170 CS3A after air abrading before exposure at 80% RH

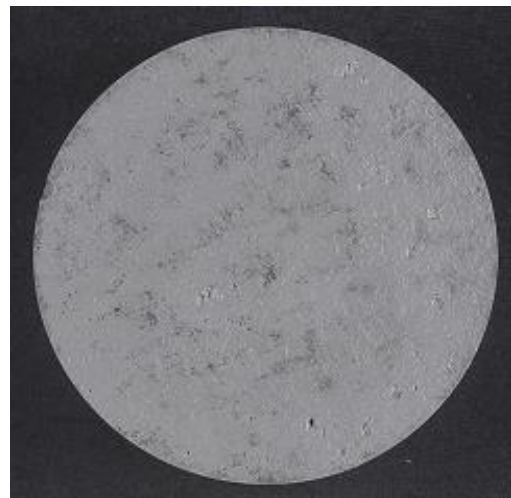


Figure 171 CS3B after air abrading before exposure at 80% RH



Figure 172 CS3A after exposure at 80% RH for 65 days



Figure 173 CS3B after exposure at 80% RH for 65 days



Figure 174 Zoomed area of CS3B showing the effect of surface profile on the corrosion pattern



Figure 175 Zoomed areas of CS3B showing a mix of filiform and general corrosion



Figure 176 Sample PC1A before air abrading clean

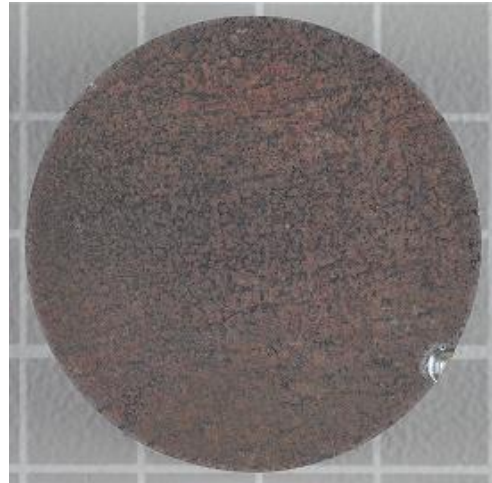


Figure 177 PC1B prior to air abrading clean

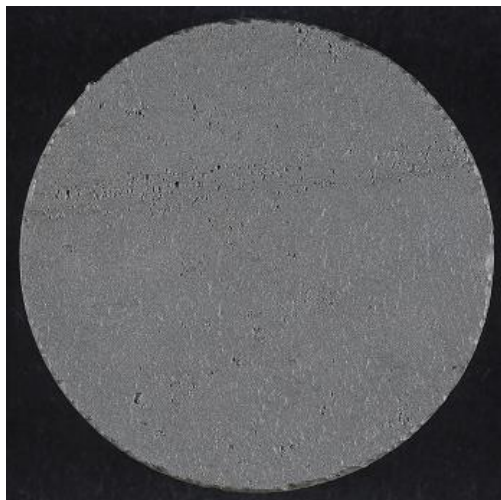


Figure 178 PC1A after cleaning by air abrasion

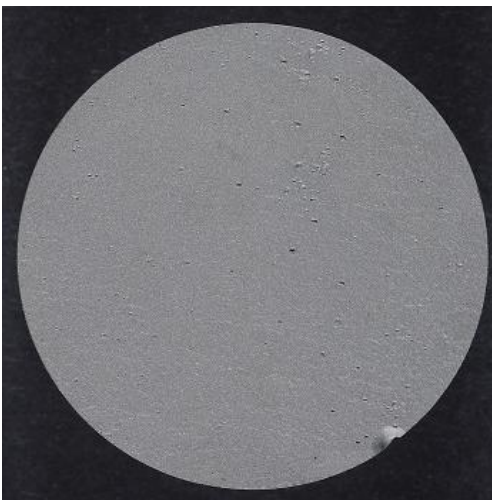


Figure 179 PC1B after cleaning by air abrasion



Figure 180 PC1A prior to exposure at 80% RH

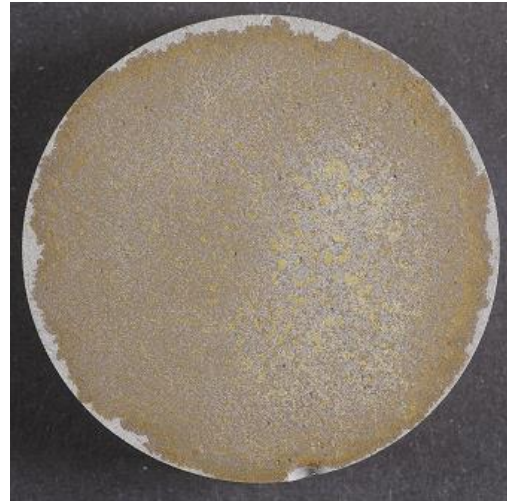


Figure 181 PC1B after partially corroding with salt spray prior to exposure at 80% RH



Figure 182 PC1A after exposure at 80% RH for 48 days



Figure 183 PC1B change in corrosion after exposure at 80% RH for 48 days



Figure 184 Zoomed area of corrosion on PC1A showing filiform corrosion and a small area of light coloured general corrosion



Figure 185 Zoomed area of PC1B salt-spray corroded side – clear variations in the colour of the corrosion products formed

6.2.8 Images of cleaned, coated samples

Coated with Paraloid B72

Prior to treatment all samples including sample PB72CS5 looked similar to the samples above, thus photographs prior to cleaning are no longer included. After cleaning to the bare metal pits and grooves were visible in the smooth surfaces (figures 186 and 187).

After application of Paraloid B72 there is a darkening in the colour of the sample and a gloss finish results with bubble formation (figures 188 and 189). After 341 days at 80% RH the sample appears unchanged (figures 190 and 191). Higher magnification images (figures 192 and 193) reveal very limited corrosion located at the edges.

Coated with Cosmoloid H80

After cleaning by air abrasion samples including sample CH80CS5 looked similar to those previously cleaned by air abrasion (figures 194 and 195). Cosmoloid H80 darkened the surface (figures 196 and 197) and the collection of wax in pits or next to ridges produces opaqueness (white and waxy). Exposure at 80% RH for 341 days caused large areas of orange-brown corrosion (figures 198 and 199). Higher magnification images of the corrosion are shown in figures 200 and 201.

Coated with Siliglide 10

After air abrading the samples (figures 202 and 203) bare white-silver metal was revealed. Siliglide 10 darkened the surfaces fractionally (figures 204 and 205), producing a sheen and slight rubbery feel. Exposure to 80% RH for 341 days produced yellow/orange-brown corrosion focused on one-side (figures 206 and 207). Higher magnification images (figures 208 and 209) revealed darker powdery areas of corrosion protruding through the coating.

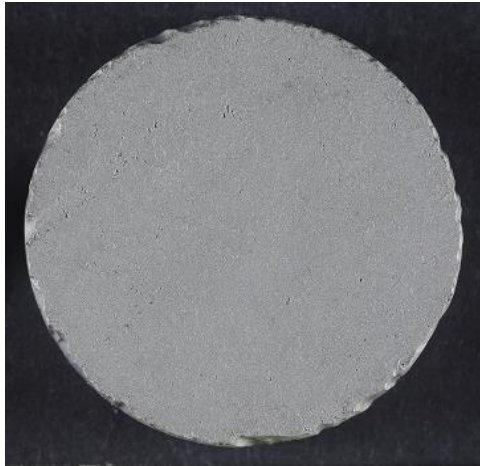


Figure 186 PB72CS5A cleaned by air abrasion

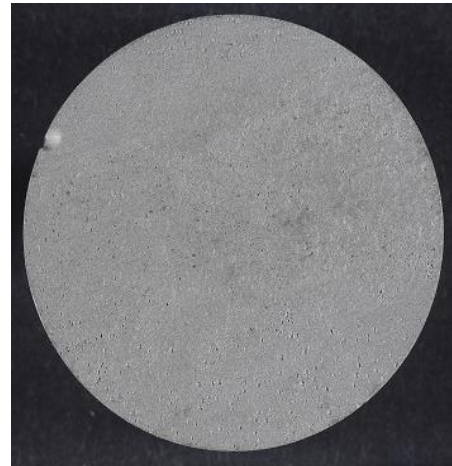


Figure 187 PB72CS5B cleaned by air abrasion



Figure 188 PB72CS5A after coating with 3 layers of 10% w/v Paraloid B72 in acetone before O₂ monitoring



Figure 189 PB72CS5B after coating with 3 layers of 10% w/v Paraloid B72 in acetone before O₂ monitoring



Figure 190 PB72CS5A after O₂ monitoring for 341 days – minimal corrosion visible



Figure 191 PB72CS5B after O₂ monitoring for 341 days – minimal corrosion visible



Figure 192 Zoomed area of PB72CS5A showing the corrosion formed and the gloss of the coating



Figure 193 Zoomed area of PB72CS5B highlighting corrosion patches and bubbles within the coating.

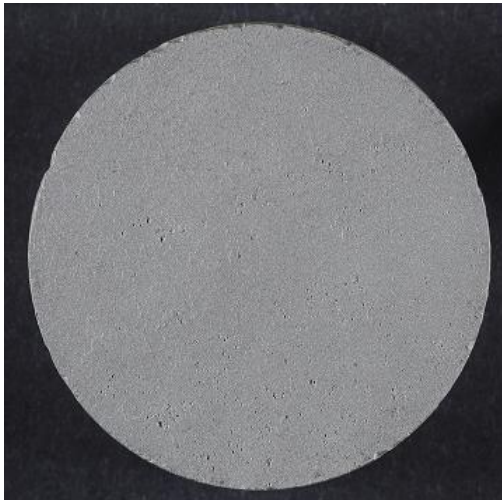


Figure 194 CH80CS5A cleaned by air abrasion

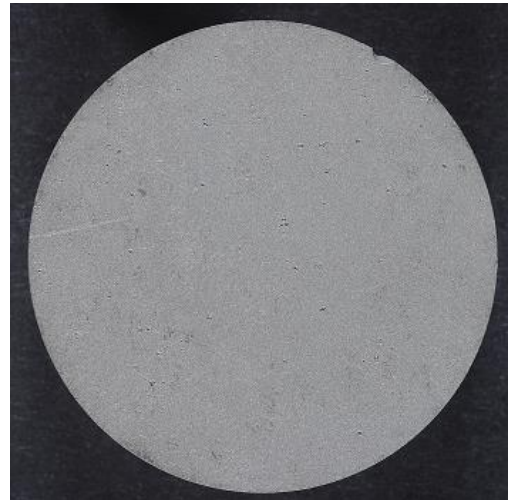


Figure 195 CH80CS5B cleaned by air abrasion



Figure 196 CH80CS5A after coating with 3 layers of 10% w/v Cosmoloid H80 in white spirit before O₂ monitoring



Figure 197 CH80CS5B after coating with 3 layers of 10% w/v Cosmoloid H80 in white spirit before O₂ monitoring



Figure 198 CH80CS5A after monitoring O₂ levels for 341 days



Figure 199 CH80CS5A after monitoring O₂ levels for 341 days

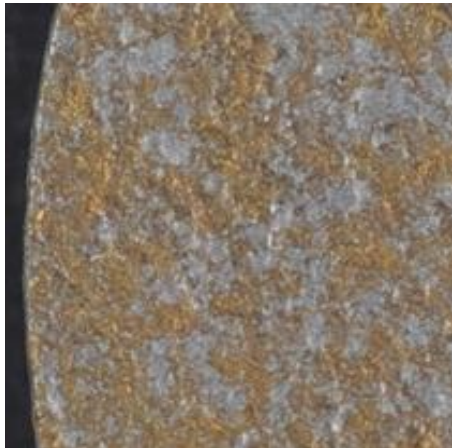


Figure 200 Zoomed area of general corrosion on sample CH80CS5A

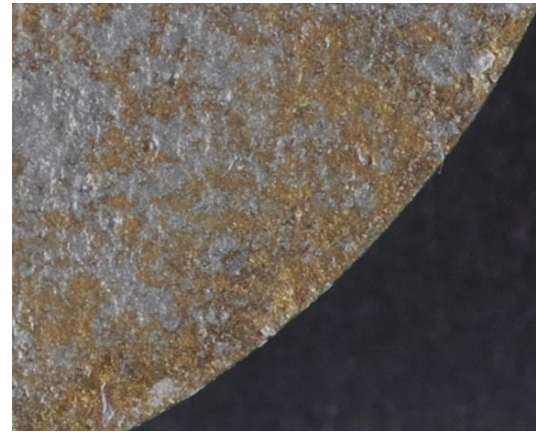


Figure 201 Zoomed area of general corrosion yellow-brown in colour on sample CH80CS5B

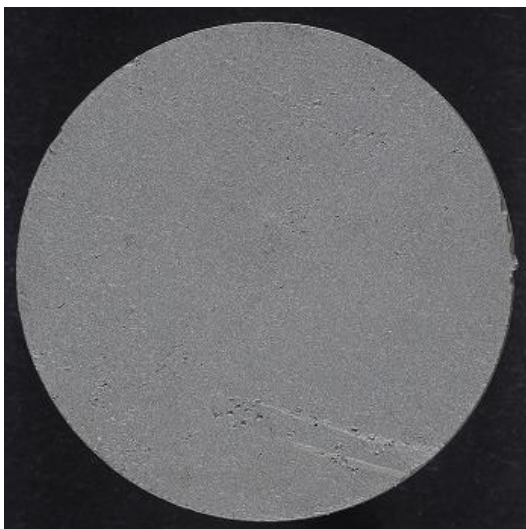


Figure 202 S10CS5A cleaned by air abrasion

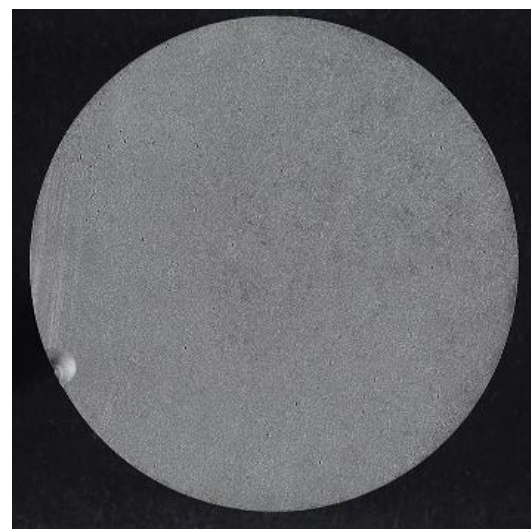


Figure 203 S10CS5B cleaned by air abrasion

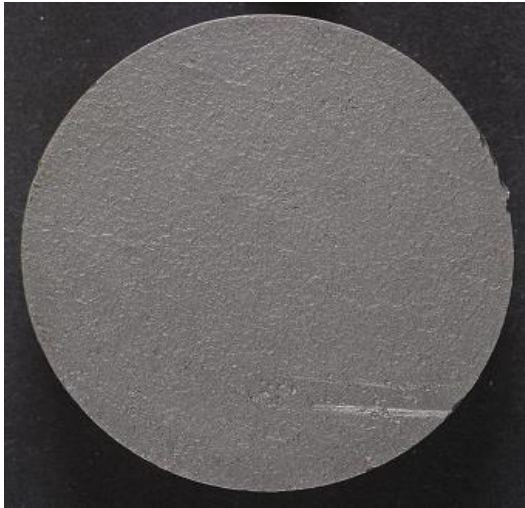


Figure 204 S10CS5A after being coated with Siliglide 10 prior to monitoring O₂ consumption

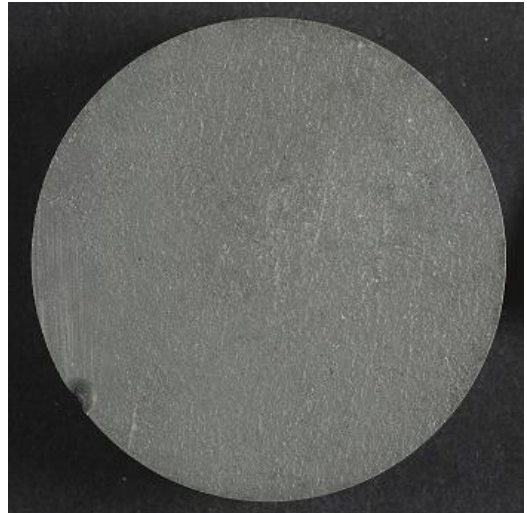


Figure 205 S10CS5B after being coated with Siliglide 10 prior to monitoring O₂ consumption

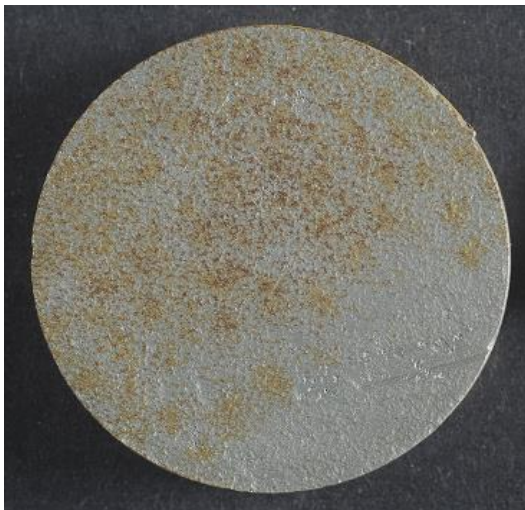


Figure 206 S10CS5A after monitoring O₂ levels for 341 days



Figure 207 S10CS5B after monitoring O₂ levels for 341 days



Figure 208 Zoomed area of S10CS5A displaying mainly yellow-brown corrosion



Figure 209 Zoomed area of corrosion on sample S10CS5B

6.2.9 Images of partially pre-corroded coated samples

For all further analysis of visual changes of the samples only the surface which is subject to additional treatments shall be focused on below, starting with the image of the sample post air abrasion preparation.

Coated with Paraloid B72

Cleaning by air abrasion to the silver metal reveals small pits in sample PB72PC1B (figure 210). Uniform orange-brown corrosion developed over the pre-corroded surface after exposure at 50% RH for 8 days (figure 211). Application of Paraloid B72 darkened the colour of the sample and the corrosion on the surface and a gloss finish resulted. The coating was de-gassed (figure 212) prior to exposure at 80% RH for 342 days. After the exposure at high RH the corrosion had spread (figure 213). A higher magnification image (figure 214) revealed filiform corrosion at the edge of the metal sample, uneven corrosion and bubbles in the coating.

Coated with Cosmoloid H80

Only a few small pits were visible in the surface of the bare silver metal after cleaning sample CH80PC2B by air abrasion (figure 215). Uniform brown corrosion developed over the sprayed surface after the sample had been exposed to 50% RH for 8 days (figure 216). Application of Cosmoloid H80 and allowing it to de-gas resulted in a matt-greayed surface finish (figure 217). After 342 days exposure at 80% RH the corrosion had spread (figure 218). The higher magnification image (figure 219) revealed the powdery corrosion and a few small flakes of loose wax coating.

Coated with Siliglide 10

Once air abraded small pits were visible in the surface sample S10PC6 side B (figure 220). Uniform brown corrosion developed on the sprayed surface over 8 days (figure 221). After Siliglide 10 was applied the corrosion colour was less intense (figure 222). The corrosion whilst exposed to 80% RH for 342 days (figure 223). A higher magnification image (figure 224) revealed powdery corrosion on the surface.

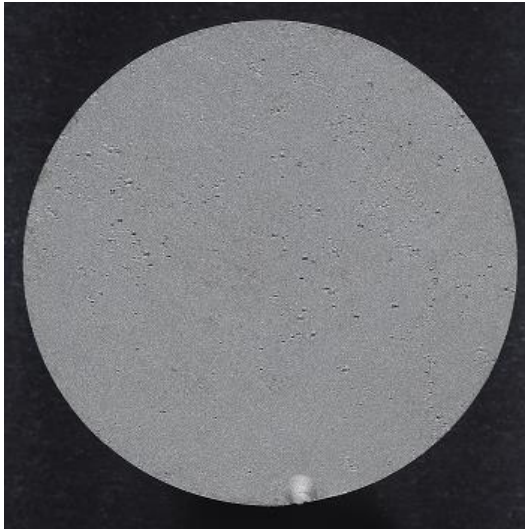


Figure 210 PB72PC1B – top side after cleaning by air abrasion

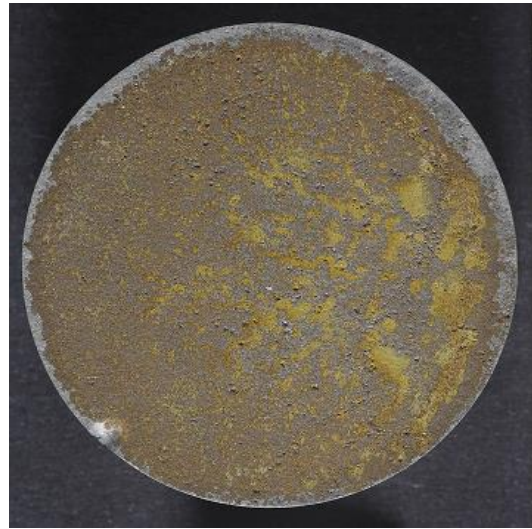


Figure 211 PB72PC1B – top side sprayed with salt solution, after corroding for 8 days



Figure 212 PB72PC1B – top side cleaned, corroded and coated



Figure 213 PB72PC1B after exposure at 80% RH for 342 days



Figure 214 Zoomed area of PB72PC1B - filiform corrosion at the edge and bubbles in the coating.

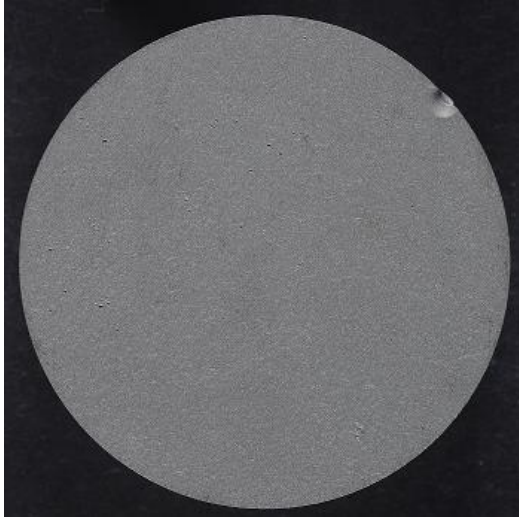


Figure 215 CH80PC sample 2 side B – top side after cleaning by air abrasion



Figure 216 CH80PC2B – top side sprayed with salt solution and allowed to corrode for 8 days



Figure 217 CH80PC2B – top side cleaned, accelerated corroded and then coated



Figure 218 CH80PC2B after monitoring O₂ levels for 342 days



Figure 219 Zoomed area of CH80PC2B with loose corrosion and small fragments of detaching coating

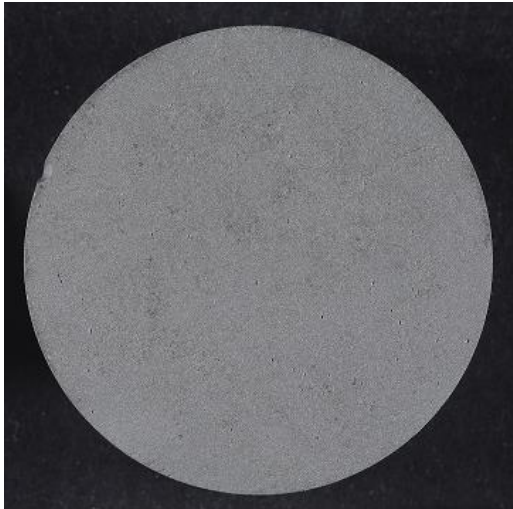


Figure 220 S10PC6B – top side after cleaning by air abrasion



Figure 221 S10PC6B – top side sprayed with salt solution, after corroding for 8 days



Figure 222 S10PC6B – coating applied over the corrosion caused by sprayed salt solution



Figure 223 S10PC6B after exposure at 80% RH for 342 days



Figure 224 Zoomed area of S10PC6B revealing powdery corrosion

6.2.10 Images of accelerated corroded scribed coated samples

The images in this section start with the clean coated samples once they have had a 2 cm scribe and salt water solution applied, and the scribe has been allowed to begin corroding.

Coated with Paraloid B72

In addition to the sample appearing darker with the clear gloss coating applied, bubbles were also trapped in the coating layers on sample PB72SC1B (figure 225). Prior to exposing the sample to 80% RH only a faint hint of yellow/orange-brown corrosion was visible at one end of the scribe. After exposure at 80% RH for 70 days, filaments of corrosion largely originating from the scribe were visible (figure 226). Following a further 148 days exposure at 80% RH (figure 227), small changes between figure 226 and figure 227 are visible. A higher magnification image of the scribed area (figure 228), shows aggressive filiform corrosion, with filaments which appear to collide and pass over other filaments in some areas.

Coated with Cosmoloid H80

Sample CH80SC5A with the coating applied has a clear matt finish with small opaque areas (figure 229). Prior to exposure at 80% RH there was only a hint of yellow-brown corrosion in the scribe. After exposure at 80% RH for 70 days, orange-brown corrosion was focused but not limited to the area around the scribe (figure 230). Exposure at 80% RH for a further 148 days (figure 231) resulted in minimal change. A higher magnification image (figure 232) of the scribed area reveals uniform corrosion with friable corrosion products forming at one end.

Coated with Siliglide 10

The coating on sample S10SC4B (figure 233) with the exception of the slight sheen it provides, is hard to detect. Prior to exposing the sample to 80% RH the corrosion in the scribe is hardly detectable. After 70 days of exposure to 80% RH corrosion can clearly be seen in the scribe but not in other areas of the sample (figure 234). Following a further 148 days of exposure to 80% RH (figure 235), the amount of powdery corrosion product at one end of the scribe had increased. The higher magnification image of the scribed area (figure 236) focuses on this powdery corrosion product formed at one end of the scribe.



Figure 225 PB72 coated, scribed sample 1 side B with salt solution painted down the scribe in the coating to accelerate corrosion



Figure 226 PB72SC1B after monitoring O₂ levels for 70 days, clearly showing filiform corrosion

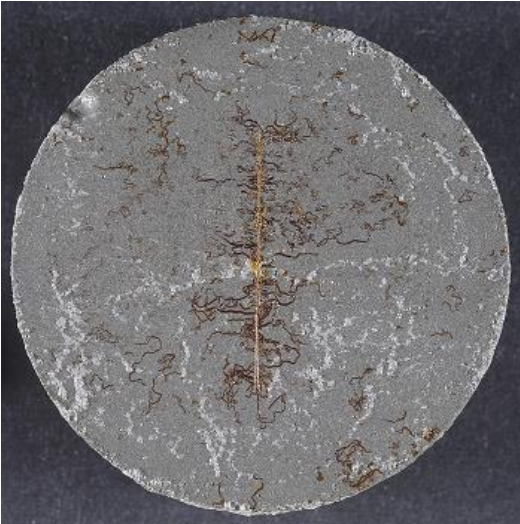


Figure 227 PB72SC1B after monitoring O₂ levels for a further 148 days – 218 days in total

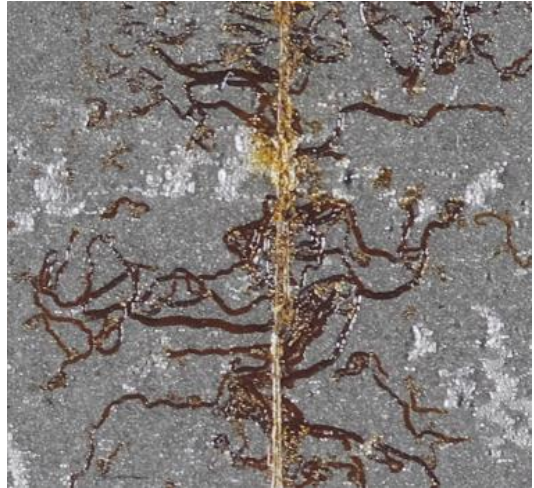


Figure 228 Zoomed area around the scribe on PB72SC1B



Figure 229 CH80 coated, scribed sample 5 side A with salt solution painted down the scribe in the coating to accelerate corrosion



Figure 230 CH80SC5A after monitoring O₂ levels for 70 days, showing yellow-brown general corrosion



Figure 231 CH80SC5A after monitoring O₂ levels for a further 148 days – 218 days in total

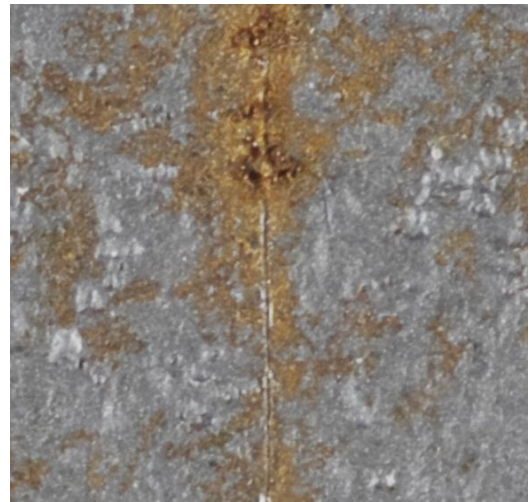


Figure 232 Zoomed area around the scribe on CH80SC5A

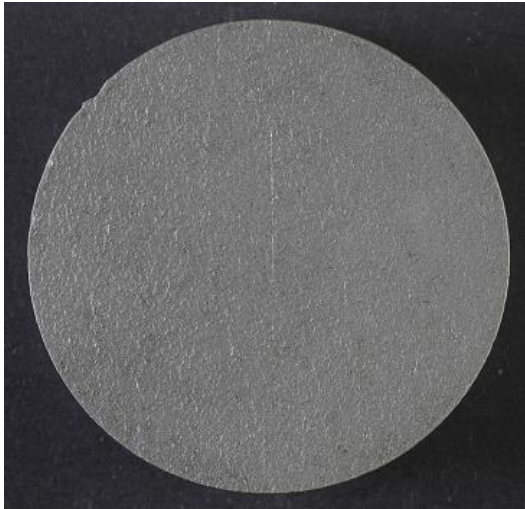


Figure 233 S10 coated, scribed sample 4 side A with salt solution painted down the scribe in the coating to accelerate corrosion

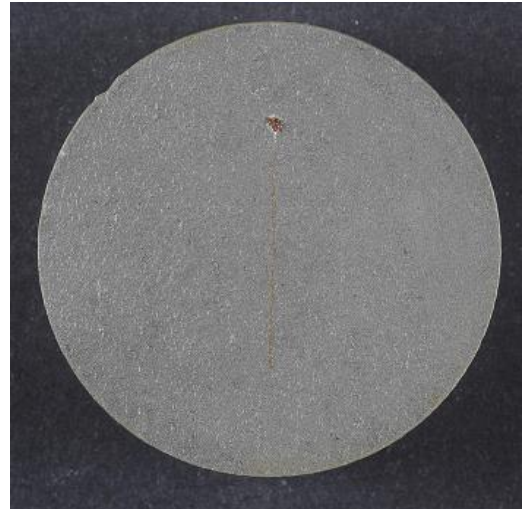


Figure 234 S10SC4A after monitoring O₂ levels for 70 days, with corrosion mainly focused in the scribe area.



Figure 235 S10SC4A after monitoring O₂ levels for a further 148 days – 218 days in total

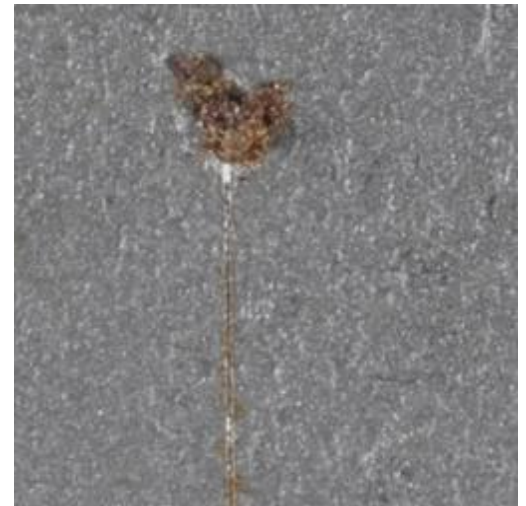


Figure 236 Zoomed area around the scribe on S10SC4A

6.2.11 Compatability of Coatings with Cromadex Paints

The crude initial compatibility tests carried out on glass slides are included below (figures 237 to 242). The clear coatings do not all behave in exactly the same with each of the paints. For the different Cromadex paint samples tested Paraloid B72 caused the most change to the dried paint layers. Siliglide 10 also causes some change to the different paints, but Cosmoloid H80 did not appear to change the paint itself.

Paraloid B72 causes lifting of the Cromadex paints in figures 237, 238 and 242 due to solvent attack. Cosmoloid H80 leaves behind a wax layer, with visible microcrystalline particles in most cases where it has been used. These microcrystalline particles cause a greying effect where they overlap the paint layers which is visible in figure 237b. Siliglide 10 causes some lifting of the paint layers in figures 238c and 239c.

Siliglide 10 damaged a little more of the red oxide primer coating than Paraloid B72 when the coatings were applied. Cosmoloid H80's only impact appears to be the slightly visible thin wax layer (figure 238). The most severe attack by one of the clear coatings is seen in figure 239a.

Of the three slides painted with matt green paint (figure 240), Siliglide 10 has the neatest appearance but a small amount of paint was removed. Paraloid B72 in acetone caused lifting of the paint and left visible brush marks. Cosmoloid H80 left a hazy wax film over both the paint it overlaps and on the glass slide in this case.

The semi-gloss green paint received very little damage from any of the clear coatings (figure 241). However, brush marks are visible under fibre optic lighting for Paraloid B72 (figure 241 aii), pale wax layers were visible with Cosmoloid H80 (figure 241b) and faint markings where the brush strokes were started when applying Siliglide 10 are also visible (figure 241c).

Dust particles adhered to the paint layers for all three slides coated with green gloss paint (figure 242). Although dust particles trapped in the other paint samples used the most noticeable, other than the green gloss is the semi-gloss green paint slides (figure 241).



i) Main LED lights

ii) Fibre optic lights

a) Overlapped with 10% w/v Paraloid B72 in acetone



i) Main LED lights

ii) Fibre optic lights

b) Overlapped with 10% w/v Cosmoloid H80 in white spirit

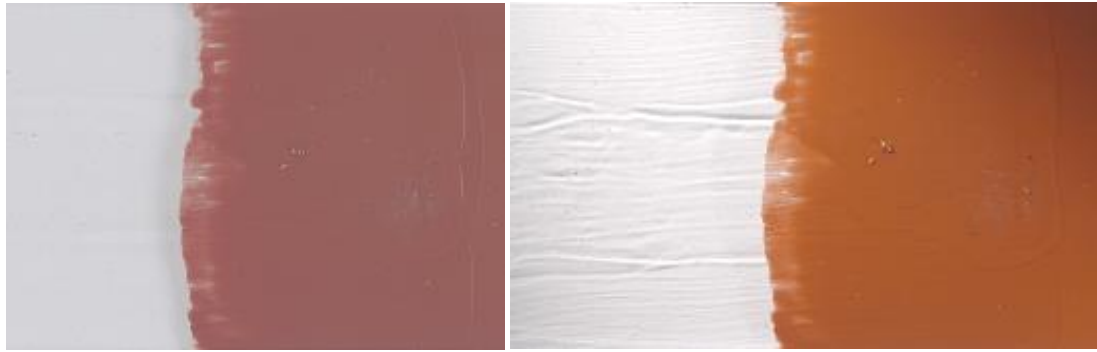


i) Main LED lights

ii) Fibre optic lights

c) Overlapped with Siliglide 10

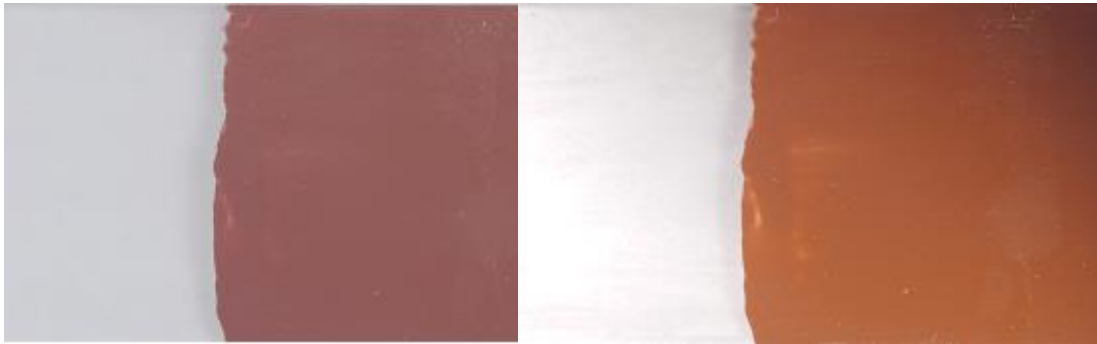
Figure 237 Panzer grey - Cromadex paint



i) Main LED lights

ii) Fibre optic lights

a) Overlapped with 10% w/v Paraloid B72 in acetone



i) Main LED lights

ii) Fibre optic lights

b) Overlapped with 10% w/v Cosmoloid H80 in white spirit



i) Main LED lights

ii) Fibre optic lights

c) Overlapped with Siliglide 10

Figure 238 Red oxide - Cromadex paint



i) Main LED lights

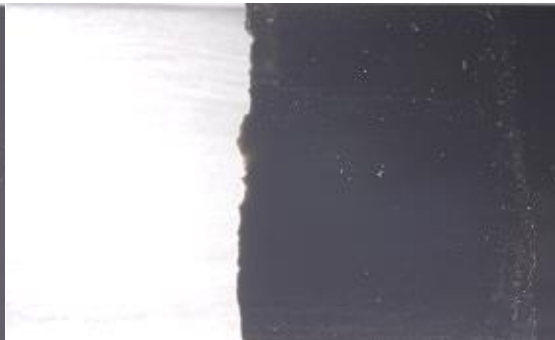


ii) Fibre optic lights

a) Overlapped with 10% w/v Paraloid B72 in acetone



i) Main LED lights



ii) Fibre optic lights

b) Overlapped with 10% w/v Cosmoloid H80 in white spirit



i) Main LED lights



ii) Fibre optic lights

c) Overlapped with Siliglide 10

Figure 239 Semi-gloss black - Cromadex paint



i) Main LED lights

ii) Fibre optic lights

a) Overlapped with 10% w/v Paraloid B72 in acetone



i) Main LED lights

ii) Fibre optic lights

b) Overlapped with 10% w/v Cosmoloid H80 in white spirit



i) Main LED lights

ii) Fibre optic lights

c) Overlapped with Siliglide 10

Figure 240 Matt green - Cromadex paint



i) Main LED lights

ii) Fibre optic lights

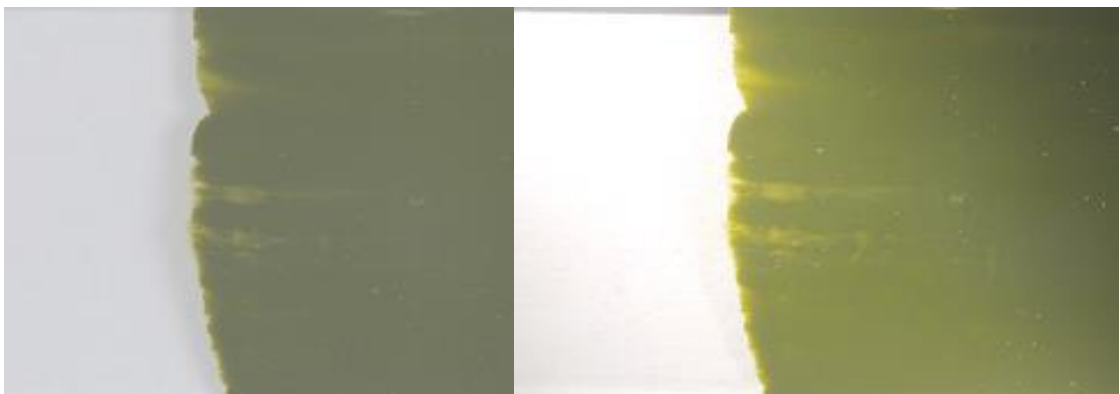
a) Overlapped with 10% w/v Paraloid B72 in acetone



i) Main LED lights

ii) Fibre optic lights

b) Overlapped with 10% w/v Cosmoloid H80 in white spirit



i) Main LED lights

ii) Fibre optic lights

c) Overlapped with Siliglide 10

Figure 241 Semi-gloss green - Cromadex paint



i) Main LED lights

ii) Fibre optic lights

a) Overlapped with 10% w/v Paraloid B72 in acetone



i) Main LED lights

ii) Fibre optic lights

b) Overlapped with 10% w/v Cosmoloid H80 in white spirit



i) Main LED lights

ii) Fibre optic lights

c) Overlapped with Siliglide 10

Figure 242 Green gloss - Cromadex paint

7 Discussion

7.1 Background field testing

7.1.1 Corrosion products

Analyses of the corrosion samples collected from historic sites around Scotland show agreement with data from Nasu et al. (2002), Dillmann et al. (2004) and Høerlé et al. (2004). The main phases constituting the corrosion layers formed on the wrought iron or mild steel exposed to atmospheric corrosion are either amorphous or crystallised iron oxyhydroxides (γ -FeOOH, α -FeOOH, β -FeOOH (linked to Cl⁻ in the environment)) and iron oxides (Fe₃O₄).

As the samples of corrosion were collected from historic sites the high percentage of magnetite detected is unsurprising. The older the rust the more magnetite and/or goethite are expected to be formed to the detriment of lepidocrocite. This is in agreement with the electrochemical processes connected to the wet-dry cycles as lepidocrocite is an electrochemically active phase in the atmospheric corrosion process and semi-conducting (Dillmann et al., 2004). Magnetite is mainly characterised by its high density and thermodynamic stability and is considered protective despite being a good conductor (Dillmann et al., 2004; Høerlé et al., 2004).

The layers within the corrosion samples have not been examined as cross-sections, but assumptions and observations can be made about the locations of the corrosion products within the corrosion layers. As discussed in 2.4 table 5 magnetite is usually detected in the inner dense part of the corrosion adhering to steel surfaces; lepidocrocite is found in the outer loose crystalline mass; goethite has been reported in both the inner and outer layers; and akaganéite although generally distributed in the surface region of the rust also appears in the inner layers where water deposits containing Cl⁻ ions penetrate through cracks (Dillmann et al., 2004; Ma et al., 2009; de la Fuente et al., 2011; Morcillo et al., 2011).

Asami and Kikuchi (2003) found that the formation of magnetite (or Fe_{3-x}O₄) and akaganéite are in competition with each other, with akaganéite preferentially formed where Cl⁻ ions are present. They found akaganéite to be scarce at thin parts of rust layers, usually existing in the thick parts of rust layers. In support of this model, where akaganéite was a major component in the samples tested magnetite dropped to either a moderate or smaller component of the sample, with the exception of a

sample collected and donated by the Scapa Flow Visitor Centre and Museum (SFVCM). Where akaganéite was a moderate component, magnetite frequently remained a major component or was found as a moderate component, with the exception of Dunbar castle where it was a minor component in sample 2.

Akaganéite was not a common major component of the samples tested, as it was a major component in only 6 out of the 72 samples tested (tables 51 and 52). Four of these samples with akaganéite as the major component are located ≤ 200 m from the coastline, but two of the samples are located in a pedestrian area in a town centre (figure 93). Although the samples collected from the town centre are close to a river (< 300 m) they are over 20 km from the coast. A more likely cause for the Cl^- ions promoting the formation of akaganéite is de-icing salt, most likely used for health and safety reasons on the pedestrian area of the town centre. This fits with Cook (2005) in the US, who confirmed that NaCl is more prevalent in the environment from the use of road de-icing salt, even though it is usually associated with marine environments. At the coastal site of Broughty Castle there was a surprising lack of akaganéite, appearing only as a possible trace component. This may be due to the sheltered position of the ferrous metal, with the majority of the Cl^- ions getting blown into the walls of the castle and the smaller particles getting lifted up by the wind and being carried further inland. Similar reasons can be used to account for akaganéite only being a minor component at Dunstaffnage castle and chapel. The metal work at the castle was inside the outer walls and the chapel is hidden within woodland and medium to large salt aerosols are known to get deposited on trees and man-made structures (Cole et al., 2003b), sheltering the metal work from the most of the Cl^- ions.

These results indicate that with the large variation in terrain (shelter) and the use of de-icing salt, predicting the range of corrosion products and mechanisms is difficult. Within the UK this is an area which may require further work, perhaps similar to the model outlined by Cole and summarised in 2.5 figure 14 but this is used for quantitative corrosion rates prediction and not complex corrosion mechanisms and predicting which corrosion products may be formed. However, with more consideration it may be possible in the future to quantify the influences environment factors deliver and predict which corrosion products might be present. In the data here where Cl^- was expected to occur due to maritime contexts, it was often absent.

7.1.2 Environments at the Tank Museum

The data supplied by the TM and summarised in the results section highlights the vast range in the temperature and RH experienced in different areas of the site.

Internal and sheltered environments

The data in the results section has been considered in terms of areas accessed by the general public and shed/workshop areas.

In the public areas the temperature averaged between 17.5 and 20 °C, but the Tamiya Hall experienced the largest temperature range, ≥ 18 °C (12 to > 30 °C). The RH average was roughly 49 – 54%, below the first critical humidity level for ferrous metal corrosion. The maximum RH values experienced were all > 75 -80%, the second critical humidity level for ferrous metal corrosion that leads to a rapid increase in the corrosion rates. The maximum RH in the NDH was the highest experienced at $> 90\%$. The radiant heating employed in this hall prevents metal corrosion by keeping the metal temperature above its dew point, stopping condensation forming on its surface. However, other materials within the vehicles are not safe at this RH, even with the radiant heating, thus additional methods of reducing the RH should be employed.

The sheds experienced a wider range of conditions over the year, and except for the new shed, minimum temperatures dropped below -5 °C during the winter. The maximum (> 40 °C) and minimum temperatures were recorded in the shed extension. The minimum RHs were sufficiently low that they would not likely initiate corrosion. The average RHs were $> 70\%$ throughout out the year (mostly $> 75\%$) so corrosion was likely to be fast as the RHs are around the second critical humidity level. The maximum RHs for the sheds are maintained at 100% RH or close. Although vehicles are not likely to be stored in the sheds for long periods, being moved into the sheds only for maintenance and repair, these conditions are still not ideal for ferrous metal. Any metal that has the paint layers removed, should be coated soon after. They should not be left uncoated in these conditions for a long period of time.

The highest and lowest temperatures over the period of the data supplied by the TM were recorded in Shed 1 extension. The lowest RH was recorded in the Tamiya Hall at the Sentry Post, but the highest RH 100% was experienced in all the sheds over the year analysed. With the large range of temperature and RH conditions experienced throughout the TM it is highly likely that atmospheric wet-dry cyclic

corrosion takes place and so it is essential that the vehicles are coated for protection. No data has been analysed for the VCC (Vehicle Conservation Centre) at the TM, so it has not been discussed, but a large number of the TM's vehicles are now stored in here and the conditions should be evaluated.

Both the NDH and VCC are beneficial additions to the Tank Museum in terms of protection against corrosion. The NDH employs radiant heating stopping condensation forming on the metal surfaces and the VCC houses a lot of vehicles which were previously outdoors significantly reducing the TOW the vehicles experience. In both of these cases the initiation of corrosion on vehicles will have been reduced. Housing the vehicles indoors in the VCC also makes it almost impossible for Cl⁻ ions to induce corrosion.

Environments within armoured vehicles

The temperature and RH data logged for the internal environments of the two armoured vehicles show annual cycles. The cycles of the temperature and humidity did not directly coincide with each other. The temperature peaked at the end of July, but RH peaked at the start of October. RH is known to change when the temperature changes as warm air can hold more water vapour than cool air, thus RH decreases when temperature rises. This relationship was not reflected in the graphs illustrating the data collected (figures 98 and 101). The fluctuations in RH were much larger than those apparent in the temperature data, thus the two trends are not easily compared.

A rise in temperature would normally reduce the RH unless more moisture was added to the atmosphere. As the rise in temperature begins in June and peaks at the end of July when schools often put on trips and the school holidays begin, the number of visitors to the museum is also likely to increase. With each visitor exhaling moisture into the atmosphere the RH does not drop but instead as the temperature begins to fall the RH increases as the air is now holding more moisture than before the temperature rise. This may explain the temperature and RH relationship experienced within the armoured vehicles at the museum. Also the external climate was not recorded and may have been unduly wet. Summer RH can be very high.

The annual cycles in temperature are very clear, but the daily maximum and minimum values may result from daily fluctuations due to the number of staff and

tourists present or the diurnal cycle. The same might be said for the RH annual and diurnal cycles, although they are less defined than for the temperature.

The baseline temperature inside the Firefly in the NDH appears to be approximately 17 °C, which rises to approximately 26 °C once a year. The RH however shows a lot more fluctuation, with the lowest RH falling between 20 and 30% and the highest reaching between 75 to 80%. Using a dew point calculator (www.dpcalc.org) it is clear that these temperature and RH ranges would normally lead to corrosion of steel. With radiant heating however, the metal should be kept at a temperature higher than the dew point temperature, preventing moisture from forming on the surface and initiating corrosion of the metal. The radiant heating does not prevent the other materials inside the hull from corroding.

The data loggers inside the Sherman V Crab in the DC showed larger variations in both the temperature and RH data collected compared to loggers in the Firefly in the NDH. In this case the baseline temperature is not so defined but roughly ranges between 17 and 20 °C, but drops as low as 12 °C at points and has yearly maximums of 26 to 27 °C. The RH in the Sherman V Crab fluctuates even more than in the Firefly, with the lowest almost reaching 20% and the highest almost reaching 90%. Without the radiant heating that is employed in the NDH it is clear from this data that the vehicles in the DC are likely to experience aggressive atmospheric corrosion at times. Condensation will form on the metal surfaces and wet-dry cyclic corrosion will take place. At several point during the 27 month period the corrosion rate will have increased as the RH reached well over the 75 to 80% critical humidity level (Syed, 2006).

The environmental data clearly shows the challenges faced by the TM in preventing or reducing corrosion taking place whilst displaying, storing or maintaining the vehicles for future generations.

7.2 Laboratory Data

7.2.1 Sample Material

Little is known about the sample material aside from the fact it was supplied by the TM and was once a back door of a Saracen APV. Frequently within the heritage sector there is limited information about the material being worked with. In this case it was possible to cut samples and analyse it further.

Metallography

Images of the metal etched particularly those in of the main body metal show that the microstructure can be described as martensitic. Martensite transformation is associated with high strains and so within austenite grains martensite forms in small plates or laths to provide an acicular structure (ASTM, 2009). There is a clear difference in the crystal structure of the metal in areas where the metal was welded. This is shown both in the first image at x5 magnification (table 56) and the last image shown for x50 magnification. The heat applied to many areas of the metal door to weld clearly affects the metallic structure.

Elemental analysis of a metal sample using the SEM revealed spectrum no. 7 listed in table 57 as close to the values for the mean weight percentage (%). The values for carbon and silicon are probably influenced by the use of silicon carbide paper for polishing, but this had a smaller impact than using Al_2O_3 for air abrasion, therefore the weight % for carbon is likely to be below 2%. The steel used for the Saracen APV is most likely a low-alloy steel as it contain < 2% alloying elements, which are often Cu, Cr, Al, Mo and Ni. In the case of this steel small amounts of Cr and Ni may have been used to improve mechanical properties and corrosion resistance.

Research into the steel used for the Saracen APV has had limited success, however the FV603 Saracen hull is described as being made of all-welded steel (Royal Airforce Museum, 2013) and fully-armoured, with Rolled Homogeneous Armour (RHA) (Military Factory, 2015).

7.2.2 Sample size and surface preparation

The samples stamped out of the Saracen APV door are clearly not uniform with slight variances $\pm 0.94\%$ in the mass of the individual samples from the mean value of 106.94 g. The mass of each sample is an easy method of testing how

comparable the samples are size wise. It does not provide much valuable information when considering the corrosion rates of the samples, but can be used to calculate the density of the steel combined with the size measurements. The density using the average mass and specified sample dimensions can be calculated as 7.8576 g/cm³. Although the density may not reveal the exact identity of the steel it can rule out other ferrous metals e.g. pure iron (7.87 g/cm³) (ASTM, 2009), wrought iron (7.7 g/cm³), grey cast iron (6.9 to 7.35 g/cm³), SS type 304 (7.9 g/cm³) and type 316 (8.0 g/cm³), but 1.25Cr-0.5Mo steel (7.86 g/cm³) (Bauccio and American Society for Metals, 1993) for example has a similar density.

The sample size measurements provide an easy method of calculating the surface areas of the samples, which is more relevant when considering corrosion rates of the samples per surface area (SA). The general SA however, does not take into account variations in the SA caused by pits and grooves in the surface of the metal or edges which were not cut cleanly by the stamping method or the peaks and troughs formed in the surface by air abrasion. Preparation of the surface by air abrasion ready for coating, providing a keyed surface (figure 107) clearly increases the SA of the samples but this is not easily calculated.

Accelerated corroded samples

Of the two methods trialled as accelerated corrosion methods, the spray application method produced a more evenly distributed corrosion layer. Excess salt was visible after the drop application method as a ring of salt crystals was left after the individual drops were applied and left to dry (figure 108).

Although blanking off the side and reverse of the samples kept the majority of the samples contamination free on the sides and the reverse surface this was not the case for all samples. The reverse side of sample PC5 (table 59) indicated that contamination with the salt solution was likely, thus accelerating the corrosion on the surface in selected areas.

Images of the reverse side of sample PC5 (figures 243 and 244) following exposure to 80% RH, do show darker more aggressive corrosion in the areas which appeared to have been contaminated, although corrosion was not limited to these areas.

The area of corrosion on the surfaces sprayed with salt solution was not identical for all samples. This is visible when comparing samples PC1 and PC4 (table 59). Both the variation in area of corrosion on the sprayed side and on the non-sprayed side due to contamination will have affected the O₂ consumed whilst corroding, leading to

larger variations and a bigger range in the data collected for the partially pre-corroded samples. Work in the future may seek to measure the area of accelerated corrosion prior to assessing the O₂ impact, and this can be compared to the resulting data to establish if there is a clear trend.

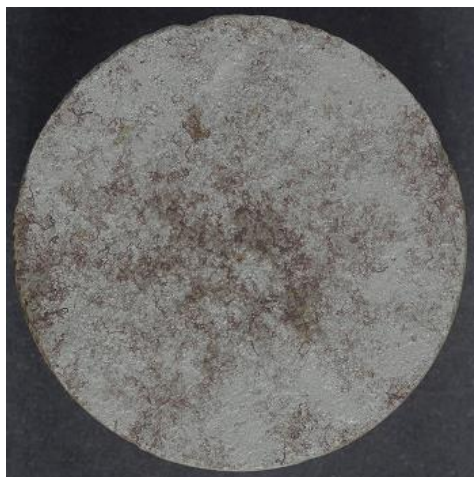


Figure 243 Reverse side of sample PC5 following exposure at 80% RH



Figure 244 Zoomed central area of sample PC5 after exposure at 80% RH

The average mass of Cl⁻ calculated as deposited by one drop of salt solution (219.01 μg) is approximately 1.5 times larger than the average mass of Cl⁻ one spray deposits on the surface of the sample (144.83 μg). Drop application also leaves the Cl⁻ focused in a small area of the sample. However, as 10 drops were applied the average amount applied was 15 times that applied by one spray application. Atmospheric corrosion accelerated by Cl⁻ deposition is generally more evenly distributed and involves a slow build-up of Cl⁻, thus spray application is much more suited for accelerated aging.

More testing of the spray application method does need to be carried out. The spray was not always consistent, especially as the spray bottle was held horizontally to spray down onto the samples. For the 10 sprayed samples tested the average mass of Cl⁻ deposited was 144.8 μg (standard deviation = 46.5), the range was 147.8 μg, distributed between 88.1 and 236.0 μg. Removing the anomalous result from the data reduces the values for the average, standard deviation, range and maximum in this case, but with the inconsistency of the spray, anomalous results which do not fit with the majority of other results may occur. If further testing was to be carried out using different spray bottles for spray application even larger variations of Cl⁻ deposited may result. This being said the spray application generally provided a fairly even coating of corrosion without salt crystals forming on

the surface and could easily be employed by others for conservation science research. Variations in the Cl^- deposited result in larger variations in the amount of corrosion forming and the amount of O_2 consumed. Thus it is important to standardise the Cl^- application technique so that differences in O_2 consumption are due to the performance of the coatings and not the quantity of Cl^- applied. This method offered a reasonable level of reproducibility for the coatings test in this study, as evidenced by the quality of the data produced.

7.2.3 Comparing the Oxygen Consumption of the Steel Samples

Untreated samples

A variety of factors may have influenced the reduction in O_2 partial pressure caused by the untreated samples, such as:

- Quantity of original paint layers left
- Presence of corrosion or mill scale
- SA of bare steel available for corrosion as well as the metallic structure
- Distribution of the alloying elements

One or more of these factors may have led to the variation in the data collected for these samples.

Over the 163 days of exposure to 80% RH, there was a slow but steady rate of corrosion taking place. The range between the samples for the reduction in the O_2 partial pressure gradually increases over the 163 days of measurements. After 163 days all the data falls between 5 and 9 hPa for the 5 samples within the error range of ± 2 hPa from each other (figure 113).

The untreated sample (UT6) run alongside the coated samples is included in figure 114. Due to different control data being subtracted from sample UT6 than UT1-5, the reduction in O_2 partial pressure drops below zero UT6. An increase in O_2 partial pressure for these samples is unlikely, thus indicating the fluctuations for this sample jar were mostly likely not in-line with those of the control jar. Apart for the first few data points the trend for UT6 matches that of samples UT1-5 until approximately 120 days after which the reduction in O_2 partial pressure for UT6 appears to level off.

Linear trend-line analysis has been used on figure 114 for all six untreated samples to produce approximate rates of change data (table 62). Sample UT6 had the

lowest rate of change (0.021 hPa/day) and sample UT3 had the highest rate of change (0.046 hPa/day), more than double that of UT6. The average rate of change for these samples was 0.032 hPa/day. These values can be compared to values achieved for the other uncoated metal samples.

Cleaned steel

The data collected for the cleaned steel samples CS1-5 (figure 115) ranged between approximately 14 – 28 hPa after 65 days of exposure at 80% RH. The range in data could result from the following variations between samples:

- SA due to air abrasion and stamping the samples out of the steel door
- Metallic crystal structure
- Distribution of the alloying elements

On figure 116 data for sample CS6 was also included and for the first 25 days it reduced the O₂ partial pressure at a similar rate to samples CS1-5. After the first 25 days the rate of reduction in O₂ partial pressure for both CS3 and CS6 slowed, indicated by slight curves in the data and resulting in the large range in the data points. Linear trend-lines on figure 116 provide approximate data for the rate of reduction in O₂ partial pressure (table 63). Sample CS6 had the lowest rate of change (0.1866 hPa/day) and CS2 had the fastest rate of change (0.4193 hPa/day), which is more than twice as fast. The average rate of change for the cleaned steel samples was 0.2996 hPa/day.

It is clear from figures 168 - 175 that these samples corrode producing a mixture of uniform and filiform corrosion whilst the data shows O₂ is being consumed. Although filiform corrosion is usually discussed when considering corrosion under a coating, it clearly also occurs on the surfaces of these cleaned, prepared steel samples. The surface preparation method produces a keyed surface and filiform corrosion is reported to be favoured by a highly rough surface (Bautista, 1996). Some embedded Al₂O₃ is to be expected in the surface of the steel after air abrasion and like sandblasted surfaces, air abrading surfaces prior to coating favours filiform corrosion. Both the images and O₂ data confirm that when exposed to 80% RH this steel corrodes, consuming O₂ at a steady rate, but with variances in the rates between samples treated in the same manor possibly due to the reasons mentioned above. For filiform corrosion to develop it is also widely accepted that the optimal RH range is 80-85% (Almeida et al., 1999).

Although the data for four of the six samples shown, show a positive straight line trend, two show a slowing trend with one appearing to flatten. This slowing with time is possibly due to a normal corrosion pattern where a protective layer begins to form over the surface. Normally porous rust, which has poor protective properties is formed in the during an initial period when corrosion rates are high (Kucera and Mattsson, 1987). To determine if the corrosion rate of all cleaned samples would slow given a longer measurement period further research is needed. In future research cleaned samples like these should be monitored for a longer time period to provide information on how long it takes for cleaned samples in high RH to become stable once corrosion has initiated.

Partially corroded steel

The partially pre-corroded samples reduced the O₂ partial pressure quickly while they were exposed to 80% RH for 48 days (figure 117). The range in the data (48 – 82 hPa) is high, mostly likely due to the variances in the quantity of Cl⁻ applied by the spray application of the salt solution, but a small amount is likely attributable to the variables mentioned for the cleaned samples.

Again linear trend-lines were used to analyse the graph (figure 117) and provide approximate data for the rate of reduction in O₂ partial pressure. Sample PC4 produced the slowest rate (1.02 hPa/day) and PC5 produced the highest rate (1.66 hPa/day). The average rate of reduction for the partially pre-corroded samples was 1.298 hPa/day.

The standardisation of the application procedure for accelerating the corrosion aimed to deliver a reproducible corrosion standard, which would consume the same volume of O₂ and develop similar corrosion coverage, profile and composition on the samples surfaces. These would then act as a platform for applying the three coatings to be tested in this study. Any corrosion detected when the coated samples are placed in 80% RH could then be attributed to differences in coating failure, rather than intrinsic differences in the corrosion rate of the samples.

Data for the 5 partially pre-corroded samples (figure 117) shows a wide range for O₂ consumption, with the maximum value (80 hPa) after 48 days 63% greater than the minimum (49 hPa). The standard produced is not reproducible and this should be considered when examining coating performance. A lack of reproducibility could relate to numerous variables. While sample composition is the same and surface preparation standardised there will still be some intrinsic differences in surface area.

Salt application was standardised but the quantity delivered to the sample varied for the 10 samples tested from 88 μg to 236 μg with an average of 145 μg (standard deviation = 46.4) (table 61, figure 112). For the 10 samples tested for Cl^- deposition the range of Cl^- delivered was almost 3 times (168%) greater on the maximum delivery compared to the minimum. However, the O_2 consumption data for the 5 samples sprayed but not tested for Cl^- deposition, showed significantly less variation with the maximum only 63% greater. While reproducibility was not possible, this method was used to pre-corrode samples and offered a much more reactive platform than the air abraded samples (figure 118).

Comparison

There was a much larger range in the data collected for the cleaned steel (CS) samples after 65 days than there was for the untreated (UT) samples after 163 days (table 80). The range in the data for the partially pre-corroded samples (PC) after 49 days was very high in comparison to both the CS and UT samples even though they were assessed for longer periods of time.

Table 80 Comparison of data ranges and rate of reduction values

Sample group	No. of days exposed 80% RH	Range (hPa)	Slowest rate (hPa/day)	Average rate (hPa/day)	Fastest rate (hPa/day)
Untreated	163	5 – 9	0.021	0.032	0.046
Cleaned steel	65	14 – 28	0.1866	0.2996	0.4193
Partially pre-corroded	48	48 – 82	1.019	1.298	1.66

The cleaned samples were consuming O_2 between 4 to 20 times faster than the untreated samples. The partially pre-corroded samples were consuming O_2 between 22 to 79 times faster than the untreated samples and between 2 to 9 times faster than the cleaned samples. Linear trend-lines oversimplify the trends which are slightly curved as the speed of O_2 consumption slows with time and does not continue at a steady rate.

Figure 118 compares the data visually for the first 50 days of exposure to 80% RH for these uncoated and untreated samples. The comparative rates of O_2 consumption are visible in both figures 118 and 119. For these samples treatment

increased the variation within the data in addition to increasing the size of reduction of O₂ partial pressure.

Including both the results for the uncleaned and the cleaned samples highlights the impact of cleaning materials and leaving them uncoated, open to the atmosphere. The cleaned steel consumed O₂ faster than the untreated steel with old coating layers and corrosion left intact, suggesting that it is better to leave damaged paint layers and stable corrosion layers intact and only remove them when the new coating is ready to be applied. If the material is located in a marine environment or in an area which requires application of de-icing salt, corrosion is likely to occur much faster. Coatings are clearly essential on cleaned steel surfaces where abrasion offers a large surface area for reaction.

7.2.4 Clear Coatings

7.2.4.1 Availability and cost

Paraloid B72 and Cosmoloid H80 are already widely used by conservators, indicating they are easily available and feasible cost wise.

Siliglide 10 has not been used for conservation before, but it is commercially available and in the UK it can be obtained from Fluorochem for £26.00 for 100 g or £196.00 for 1 kg. Gelest the parent company is an international company with distribution partners around the world, so availability is not be a problem. Siliglide 10 is a very thin coating, therefore 100 g will offer good coverage. This cost should be feasible even within the poorly funded conservation sector.

7.2.4.2 Concentration, solvents, aesthetics and practicalities

Three layers of Paraloid B72 in xylene applied to glass slides provided a fairly good clear coating whether it was the 10% and 15% w/v concentration. Although, brush marks were visible on the coated slides, they are had begun to flow and smooth out before drying. The brush marks are more noticeable down the centre of the slides where the two strokes down the slide overlapped and at the ends where the brush is first applied to the slide or removed from the slide. The brush marks for the 10 and 15% coatings were comparable, but the 15% coating contained many more trapped tiny bubbles. They were due to either solvent evaporation or trapped air and reduced the transparency of the 15% coating compared to the 10% coating. Thus, while using xylene as the solvent the 10% concentration was found to be more

suitable. When air abraded glass slides were used with the 10% w/v Paraloid B72 in xylene coating there was a reduction in the visible brush marks, which should also happen with air abraded samples.

The three layers of 10% w/v Paraloid B72 in acetone on glass slides produced clear coatings with more prominent brush strokes than when xylene was used as the solvent. With acetone being more volatile than xylene the coating has less time to flow out when it is used. When used on air abraded samples there should be a reduction in visible brush marks as there was for the 10% w/v Paraloid B72 in xylene on the air abraded glass slides.

Although xylene used as the solvent produces better visual coatings on glass slides, a survey carried out by Argyropoulos et al. (2007b) revealed that acetone was the most common choice for use with Paraloid B72. From a health and safety perspective acetone is also the preferred choice.

Once heat and air abraded slides were used with the 10% w/v Cosmoloid H80 in white spirit coating, it produced a good 3 layered coating. Cosmoloid H80 produced a matt coating unlike Paraloid B72 which produced a high gloss coating. Brush marks are not very visible in the Cosmoloid H80 microcrystalline wax coating, but where the crystals are visible or the coating collects the coating becomes opaque and almost white. From a conservation viewpoint, as treatments should allow the retention of the original appearance, the preferred appearance of a coating is clear, transparent and where possible invisible to the naked eye.

Photographs of Siliglide 10 coated slides have not been included as on glass slides the coating is invisible to the naked eye, if buffed whilst curing.

7.2.5 Mass of coating, number of layers and distribution between layers

On glass slides

The application of the coatings to glass slides recorded the build up of coatings.

When Paraloid B72 in xylene was applied to glass slides the mass of coating applied for the first two coating layers increased from slide 1 to slide 5, possibly due to loading within the brush, but this was not the case for the third layer. There was a fairly even distribution of the coating between the first (31%), second (30%) and third (39%) layers. If this build-up in mass of coating equates to a build-up in thickness, three layers should provide a thicker barrier layer between the substrate

surface and the atmosphere. Therefore, three layers should be beneficial in terms of the protection provided.

For Paraloid B72 in acetone like with xylene there was a build-up of the mass with each layer applied. However, when using acetone as the solvent the layers were not quite so evenly distributed with 34% applied in the first layer, 24% in the second and 42% in the third. The pattern does however, match that of the coating with xylene as the solvent. For both acetone and xylene Paraloid B72 coating there is a drop in the mass for the second layer compared to the first and an increase in mass applied for the third layer compared to the first and second layers. More coating may be dragged off the brush for the third layer as the surface it is being applied to is not as smooth as the glass slides surface or the glass slide with one layer of coating. The build-up of the coating over the three layers while using acetone as the solvent showed that it was worthwhile using three layers rather than two as explained above for Paraloid B72 with xylene as the solvent.

As well as being slightly more evenly distributed when xylene is used as the solvent each layer applied also has a slightly smaller mass, resulting in a smaller mass of the overall coating. If a thinner more discrete coating is what is required xylene would be the better solvent to use. If a higher mass coating equates to a thicker coating which equates to a thicker barrier layer providing better protection and better protection is the aim then acetone may be the better solvent to use.

Cosmoloid H80 in white spirit when applied to heated air abraded surfaces provides a fairly even build-up of the wax coating with 36% applied in the first layer, 30% in the second and 34% in the third. The average total masses of the coatings on glass slides were comparable for Cosmoloid H80 in white spirit (0.0217 g) and Paraloid B72 in xylene (0.0210 g), but Paraloid B72 in acetone (0.0335 g) was significantly larger.

This led to a decision to use Paraloid B72 in acetone as the standard application as well as its non-interference with the sensor spots for O₂ consumption.

The masses of Siliglide 10 layers on glass slides has not been analysed, but they have been analysed on the sample material and so will be discussed in the next section.

On the samples

Paraloid in xylene was not tested on the steel samples, but Paraloid B72 in acetone was, and was found to have more evenly distributed layers on the air abraded samples (1st layer = 30%, 2nd layer = 31% and 3rd layer = 39%) than on the glass slides. The percentage distribution was very similar to that of Paraloid B72 in xylene on glass slides, but is an improvement compared to Paraloid B72 in acetone on the slides. As the whole surface of the samples were coated ($SA \approx 37.01 \text{ cm}^2$), a larger area was coated than one surface of a microscope slide ($SA \approx 19.76 \text{ cm}^2$) and so a larger total coating mass was expected. The average total mass applied on the slides was 0.0335 g, but the average total mass applied to the samples was 0.1002 g, thus there was either overlapping of the coating on the sample when both sides were coated or the side of the glass slides coated were not fully covered. Warming the samples may also have played a role in the larger masses applied on the samples than on the slides compared to what might be expected in relation to SA.

The average total coating mass for Cosmoloid H80 on the samples was 0.0418 g, less than half the Paraloid B72 coating mass, but approximately double its average total coating mass applied on the glass slides (0.0217 g). The difference between the mass of coating on slides and samples is roughly what would be expected for the SA of each coated. The distribution of mass between the layers for the coating on the sample is fairly even, more so than the Paraloid B72 coating, as there is approximately a third applied in each layer ($33\% \pm 3$).

The average total coating mass for Siliglide 10 was 0.0069 g much less than for either Paraloid B72 (0.1002 g) that is roughly 14.5 times its mass or Cosmoloid H80 (0.0418 g), which is six times its mass. Of the Siliglide 10 layers the second layer (19%) of the coating had a much smaller mass than the first (43%) or third (38%) layers.

Whether the coating was applied to cleaned samples or to partially pre-corroded samples the Paraloid B72 coatings had the largest masses, Cosmoloid H80 had the second largest coating masses and Siliglide 10 had the smallest masses. The partially pre-corroded samples had larger ranges in the masses collected but there were also 10 samples with partially pre-corroded surfaces for each coating compared to 5 samples with just cleaned surfaces. Thus the surface treatment did not have much of an influence on the mass of coating applied.

Brush application was a suitable application method for all of the coatings, but for samples coated with Paraloid B72 warming the samples prior to coating application

may not have been suitable. Applying Paraloid B72 to cold samples may reduce the number of bubbles due solvent evaporation as more solvent may be able to escape before the coating dries. Both Paraloid B72 and Cosmoloid H80 are considered suitable for conservation, but Siliglide 10 is a new coating and has not been trialed in conservation before. The biggest concern about Siliglide 10 is its reversibility and this is an area which requires further work. The PROMET project found the combination of silanes they called silane A was reversible in 5M NaOH (Argyropoulos, 2008) and this is a treatment that could be tested on Siliglide 10.

7.2.6 Effects on oxygen measurements

7.2.6.1 Solvent choice

Prior to testing the coatings on samples they were tested on glass slides. In addition to their appearances and masses being analysed the effect of the coatings and carrier solvents on the O₂ sensor spots were also tested. Xylene had a larger impact on the sensor spots than acetone and so the use of xylene with Paraloid B72 was ruled out of the testing on sample material.

Paraloid B72 is known for retaining solvents for prolonged periods, so acetone which also influenced the sensor spots, but not as significantly was retested. Fresh slides coated with Paraloid B72 in acetone were de-gassed for 3 weeks before retesting their influence on the O₂ sensor spot. After 3 weeks de-gassing the data for these slides with the fluctuations of an empty jar removed from them only fluctuated within the error margins of the machine (± 2 hPa). Thus as long as the Paraloid B72 coating is allowed time to de-gas prior to measuring the O₂ levels, any future impact on the O₂ levels when used on samples should be as a result of O₂ being used up in the corrosion reaction.

Neither Cosmoloid H80 in white spirits or Siliglide 10 had a significant influence on the O₂ sensor spot. However, to keep the procedures standardised, all the coated samples were allowed 3 weeks for the coatings to de-gas in the climate chamber.

7.2.6.2 Oxygen consumption of coated cleaned steel

Paraloid B72

There is an increasing range in the data for the reduction in O₂ partial pressure for the cleaned Paraloid B72 coated samples over the 341 days of exposure at 80% RH, which with the control data subtracted fluctuate around 0 hPa (figure 140).

After 341 days the data is always within ± 3 hPa of 0 hPa. The final data points for these samples fell between -2.5 and 1.5 hPa giving a range of ± 2 hPa of the central point. From this data it is not possible to conclude that the samples are corroding and after almost a year of exposure to 80% RH may be corrosion free.

Cosmoloid H80

The data collected for the cleaned Cosmoloid H80 coated samples with the control data subtracted show a steady rate of O_2 consumption. Over the 341 days of exposure to 80% RH, the range in the data collected for the five samples increased, with the final values on figure 141 falling within ± 2.5 hPa of the midpoint. There is a slight curve to the trend in the data points on figure 141, indicating the rate of O_2 consumption and possibly the rate of corrosion are slowing a little. For these samples there is however, an increasing reduction over the 341 days, indicating that O_2 is being consumed and the samples are corroding. Corrosion is expected to slow as corrosion layers build up at failure points in the coating.

Siliglide 10

The clean Siliglide 10 coated samples were also found to consume O_2 . After 341 days of exposure the samples had consumed between 6 to 12 hPa (figure 142), thus all the values were within ± 3 hPa of the midpoint. The trend for these data points also shows a slight curve, but the curve for these data points indicate increasing trend rather than a slowing trend. This may indicate that the coating-metal chemical bonds are being broken, freeing up the metal surface for corrosion. Hydrolysis at high RH may be the cause of this coupled with potential lowering of pH from Fe^{2+} hydrolysis at anodes.

Comparison

Figure 143 shows the data collected for the fifteen clean and coated samples as well as a cleaned uncoated sample (CS = CS6) and an untreated sample (UT = UT6). It is clear from this graph that coating samples which are cleaned is beneficial. Even the highest reduction in O_2 partial pressure for a coated sample is less than a third of that for the cleaned uncoated samples. The untreated sample is consuming O_2 at a rate which is similar to the slowest consuming Cosmoloid H80 and Siliglide 10 clean coated samples.

After 200 days of exposure at 80% RH Paraloid B72 data does not overlap with any of the data shown for other samples on figure 143. However, all through the exposure period there are overlaps in the data collected for the Cosmoloid H80 and Siliglide 10 coated samples. Initially, Cosmoloid H80 coated samples consumed noticeably more O₂ than the Siliglide 10 coated samples, but after 300 days of exposure a Siliglide 10 coated sample became the fastest O₂ consuming coated sample. These two different coatings caused opposite behaviour of the samples as the O₂ consumption rate slowed for Cosmoloid H80 coated samples but for Siliglide 10 coated samples the O₂ consumption rate increased. This could be due to stable oxide and corrosion products forming on the Cosmoloid H80 coated samples and also due to coating-metal chemical bonds potentially being broken and allowing the surface to react with O₂ passing through the Siliglide 10 coating layers.

The boxplot in figure 144 shows the statistical summary of the final data points after 341 days of exposure to 80% RH analysed in terms of the reduction in O₂ partial pressure per day. Paraloid B72 clearly has the lowest median value, the lowest reduction in O₂ partial pressure and the smallest range (table 78). Although Siliglide 10 has a slightly higher range in the data on the last day of exposure than Cosmoloid H80, Siliglide 10 has a lower median value than Cosmoloid H80.

Figure 145 compares the data from figure 144 for the cleaned coated samples to the data for the cleaned uncoated sample data on figure 119. Again this highlights the need for a coating to be used and ferrous metal not to be left exposed to the impact of the environment.

7.2.6.3 Oxygen consumption of coated partially pre-corroded steel

Control data was not subtracted from the graphs in this section but instead was plotted alongside on the graphs, as the measurements were usually made 24 hours before or after.

Paraloid B72

There is a clear difference in the reduction of O₂ partial pressure for the partially pre-corroded Paraloid B72 coated samples and the control data (figure 146), indicating that O₂ was consumed by these samples and additional corrosion was likely to have taken place. The reduction in O₂ partial pressure was initially fairly steady, but after approximately 120 days the data for the samples levelled off and fluctuations were within the error margins of the meter (± 2.0 hPa). The implication here is that after

corroding for 120 days the samples stop corroding and are stable. Likely due to a build up of corrosion products at ingress points in the coating.

Cosmoloid H80

The initial reduction in O₂ partial pressure for the partially pre-corroded samples was quick (figure 147) but the rate gradually slowed, faster for some than for others indicating the unpredictability of the performance of Cosmoloid H80. Throughout the 342 days of exposure to 80% RH the range between the data points increased. The range within data after the final data points were collected (34.22 hPa) was fairly high.

Siliglide 10

The partially pre-corroded Siliglide 10 coated samples did not initially appear to reduce the O₂ partial pressure within the jars, as the data points were very close to the data for the jar with no sample (figure 148). Separation between the control data and the sample data began to show after roughly 120 days, but even for the final data points there was minimal difference between the control data and the Siliglide 10 coated sample reducing the O₂ partial pressure the least. The range between the samples data points was low up until roughly 180 days of exposure to 80% RH, when the range between the data points began to increase much more noticeably. Siloxane groups (Si-O-Si) can slowly hydrolyse to silanol groups that are much more hydrophilic, and so are not indefinitely stable (Ooij et al., 2005). Thus metals cannot be indefinitely protected by silane films as with continuous exposure even the most hydrophobic films hydrolyse allowing water to reach the interface. However, if partly hydrolysed films can dry out the siloxane groups can reform since siloxane hydrolysis is a reversible process. Further work in this area may reveal whether under cyclic conditions Siliglide 10 has better protective properties.

Comparison

When the final data points collected are compared in the boxplot (figure 149) and table 79 it is clear that Siliglide 10 coated samples have the smallest median value for the reduction in O₂ partial pressure, and Cosmoloid H80 has the largest median value. Cosmoloid H80 has the largest range in value and Paraloid B72 has the smallest range. For the final data points the range in the data shows overlaps between all of the coatings assessed.

Figures 150 and 151 show average data comparisons for the average partially pre-corroded coated and uncoated samples, as well as the untreated sample (UT6) and the cleaned uncoated sample (CS6). Figure 150 just shows the first 50 days and figure 151 shows the full 342 days for all the averaged and individual data points. Again it is clear that applying a coating is beneficial, as the average reduction of O₂ partial pressure for uncoated, partially pre-corroded samples was more than three times that of any of the coated, partially pre-corroded samples over the first 50 days of exposure to 80% RH (figure 150). Although it is clear the consumption of O₂ slows over the exposure period for the Cosmoloid H80 and Paraloid B72 coated samples, for Siliglide 10 coated samples which initially shows minimal O₂ consumption, there is an increase in O₂ consumption over the exposure period instead. Applying Siliglide 10 on partially pre-corroded samples slows O₂ consumption to below that of clean uncoated samples straight away. Likely due to its ability to bond with the oxides in the thin corrosion layer. With Paraloid B72 applied, after roughly 100 to 125 days the samples are consuming O₂ slower than the cleaned uncoated sample and before the end of the exposure period the samples coated with Cosmoloid H80 are also consuming O₂ slower than the cleaned uncoated samples. Thus towards the end of the exposure period (figure 151) the cleaned uncoated sample is consuming O₂ faster than all of the partially pre-corroded coated samples, again reinforcing the benefit of using a coating whether the samples are clean or partially corroded. Applying any of the three coatings used within this research slows the rate of O₂ consumption compared to no coating on a partially pre-corroded samples or clean uncoated sample after more than 300 days of exposure at 80% RH.

Graphs showing the average trends do not show the variation between samples treated in the same manner, thus in addition to figure 149, a further boxplot has been included (figures 152). Figure 152 compares the control data, the untreated sample, the clean uncoated sample, the clean coated samples and the partially pre-corroded coated samples interpreting their final data points as reduction in O₂ partial pressure per day. It compares all of the samples split into coating types and also into different treatments. This boxplots reveals the median value for the clean Siliglide 10 coated samples is higher than that of the partially pre-corroded Siliglide 10 coated samples. For both Paraloid B72 and Cosmoloid H80 the median values are significantly higher for the partially pre-corroded than the clean coated samples. Silanes are known to be more effective on inorganic oxides e.g. Fe₂O₃, than iron or steel (figure 82).

Thus figure 152 indicates that where possible ferrous metal should be cleaned if Paraloid B72 or Cosmoloid H80 are being used. Where there is corrosion that cannot be removed, the indication from these results is that Siliglide 10 is most likely the best option, but before a year is up further maintenance may be required. Thus, Siliglide 10 is the best choice for corroded surfaces over a short time period, as it initially stopped corrosion occurring.

7.2.6.4 Oxygen consumption of scribe coated cleaned steel

Although a scribe was introduced to each of the samples to potentially imitate damage to a coating by a scratch the results for this section are not as one might expect.

Paraloid B72

For the first 70 days of exposure at 80% RH, the O₂ consumption for the scribed Paraloid B72 coated samples displayed no visible trend (figure 153). There was an increase in O₂ in some of the jars, an explanation for this might be acetone still retained within the Paraloid B72 coating. The acetone as it was released from the coating may have affected the rubber seal of the lids used on the jars, allowing O₂ into the jars.

For the 148 days of exposure at 80% RH (figure 154), after photographing the samples and returning them to their jars and the chamber, the data showed only fluctuation around 0 hPa within ± 2 hPa reduction in O₂ partial pressure for all but one data point. Thus if corrosion is taking place, it is minimal as such low quantities of O₂ are being consumed.

When looking at the combined data in figure 155, after the first 50 days the changes in the O₂ partial pressure measurements are minimal. Scribed sample P1 appears to be reducing the O₂ partial pressure more than the other samples for both graphs, but overall for these 10 samples there is no clear trend for the time that they were monitored.

Cosmoloid H80 and Siliglide 10

The results achieved for the Cosmoloid H80 coated and Siliglide 10 coated samples scribed using a scalpel are not that dissimilar to those achieved for the Paraloid B72 coated scribed samples. Both fail to show a clear trend in the first 70 days and

when exposed for a further 148 days their data fluctuates within ± 2 hPa of 0 hPa. Thus, when combined for the total 218 days of exposure neither coating data shows a clear trend, but the ranges in the data are more than ± 2 hPa around the median values.

For these samples their appearances may provide more information than the reduction in O₂ partial pressure data.

7.2.7 Aesthetics of coatings on samples

Untreated samples

Prior to any treatment the samples are very dark in colour (figures 162 and 163) – dark red-brown with dark grey regions throughout and some have areas of historic dark green paint still attached. After exposure to 80% RH for 163 days there was minimal change in the appearance (figures 164 and 165). On closer inspection (figures 166 and 167) small areas of uniform corrosion were visible, yellow-orange brown in colour. These small areas of corrosion confirm the reduction in O₂ partial pressure data for the untreated samples, which indicated corrosion was taking place. If more corrosion is taking place under paint layers there are no obvious signs.

Cleaned samples

Prior to cleaning the samples they looked much like the untreated samples prior to exposure at 80% RH, although the amount of historic green paint varied depending on the sample (figures 168 and 169). On some samples there was more than one layer of green paint, which was visible due to the top layer being a lighter green than the dark green layer underneath. The cleaned samples surfaces (figures 170 and 171) showed varying numbers of pits and troughs in the white-silver surface. There were also some small darker grey areas.

The corrosion on these samples was darker in colour than the corrosion on the untreated sample as it was red-brown in colour. The corrosion pattern appears to be linked in part to the peaks and trough in the sample's air abraded surface (figures 172 and 173). Figure 172 shows the surface of the sample which faced away from the conditioned silica gel, whereas figure 173 shows the surface of the sample that faced down towards the silica gel. Leidheiser Jr. (1987) stated that filiform corrosion can in some cases develop on uncoated steel but connected this to small quantities

of salt contaminants being present on the surface. Although neither salt solution nor coatings were applied to these samples a large amount of filiform corrosion was visible (figure 174 and 175).

Partially Pre-Corroded samples

The first two stages for these samples (figures 176 – 179) are much the same as those described above for the untreated and the cleaned samples. After cleaning these samples were partially pre-corroded using salt-spray of a similar formulation to de-icing salt. Figure 180 was blanked off and was free from salt-solution and thus did not corrode prior to exposure at 80% RH, but slight darkening in a small area of the surface indicated it had oxidised slightly. Figure 181 was the side sprayed with salt-solution, which corroded quickly and in a fairly uniform manner, producing yellow-orange brown corrosion that was slightly darker at the edges. The corroded surface was placed face-up, away from the silica gel during the exposure to 80% RH.

After exposure at 80% RH both sides of the sample (figures 182 and 183) had dark red-brown corrosion present that was not present before. This darker corrosion did not appear uniform in nature and filaments were clear on the previously clean side (figure 184). The darker corrosion over the pre-corroded area (figure 185) also looked localised compared to the initial corrosion resulting from the salt spray, and may also be filiform corrosion.

Further research is needed into the accelerated corrosion method used, including identifying the corrosion products initially formed (figure 181) and what corrosion products were present after exposure to 80% RH (figure 183). Both the colour and nature of the corrosion products indicate they are likely to be different.

7.2.7.1 Cleaned and Coated Samples

These samples are also much the same as those described above for the untreated, the cleaned samples and the partially pre-corroded samples before and after cleaning. Thus the images start after the samples have been cleaned so the cleaned surfaces can be compared to the coated surfaces.

Cleaned and Coated with Paraloid B72

There were noticeable differences between the samples before and after coating with Paraloid B72 (figures 186 - 189). With coating applied the surface is darker and

glossy. Brush marks are not noticeable in the images but bubbles developed in some areas on the surface and around the edges. These areas with bubbles present were expected to be weak areas of the coating, and possible areas where corrosion would develop. After exposure at 80% RH for 341 days hardly any corrosion is visible (figures 190 and 191). A closer look (figures 192 and 193) reveals very small areas of filiform corrosion mostly located at the edges, but the amount of corrosion present is minimal considering the exposure time and this was evidenced by the reduction in O₂ partial pressure fluctuating around 0 hPa.

Cleaned and Coated with Cosmoloid H80

Again there were clear differences between the appearance of the samples before and after coating (figure 194 -197). With the coating applied the surface is a darker shade of grey, but matt. Where there were pits and grooves in the surface the coating collected and became white and opaque, however, these areas were very small.

The corrosion for these samples appeared more uniform (figures 198 and 199), although the peaks and trough in the surfaces appeared to have some influence, which side was facing down in the jar (figure 198) was also influential. Closer examination (figures 200 and 201) also showed a couple of small cracks had formed in the coating at the edge of the sample. The orange-brown corrosion that formed did so without any visible damage to the coating with the exception of these cracks at the edges.

Coated with Siliglide 10

As with Paraloid B72 and Cosmoloid H80 there were differences in the appearance of the samples before and after coating (figures 202 – 205). In the case of Siliglide 10 the differences were not quite as significant, with only a slight darkening of the surfaces and between a satin and a semi-gloss finish (figures 204 and 205).

After exposure to 80% RH for 341 days corrosion was present on both sides of the sample (figures 206 and 207), but it was more significant on the side facing down (figure 206) towards the silica gel. The yellow/orange-brown corrosion appeared more uniform than localised in nature, it also appeared influenced by the surface profile of the sample (figures 208 and 209). The sample shown is one which had slid off the SEM tripod clips used to raise the sample above the silica gel and allow circulation around the sample inside the jar. The corrosion which formed on this

sample was focused on the side and edge which was dislodged and lent into the silica gel. However, there were no visible signs of damage to the coating and corrosion was occurring quite freely.

7.2.7.2 Partially Pre-corroded and Coated Samples

For each of the samples shown in this section only one side of the samples are shown, the surface which was pre-corroded, as the clean sides will appear similar to the images above. Again for comparison purposes the cleaned surface images are also included.

Partially Pre-corroded Paraloid B72 Coated

The cleaned surface (figure 210) with white-silver metal and pre-corroded surface (figure 211) with scattered areas of yellow-brown corrosion within the darker brown corrosion were very different. With Paraloid B72 applied (figure 212) the corrosion appeared darker brown and a few bubbles were trapped within the gloss coating. After exposure at 80% RH for 342 days (figure 213), the corrosion had spread over the surface covering the edges, there was a slight change in colour and the surface profile no longer appeared as smooth. The colour of the corrosion had a slightly pinkish tinge and a close up (figure 214) revealed filaments of corrosion at the edge of the sample.

Further corrosion in addition to the pre-corroded area had clearly taken place on these samples and this was also evident from the reduction in O₂ partial pressure compared to the clean coated samples.

Partially Pre-corroded Cosmoloid H80 Coated

As with the Paraloid B72 coated sample above there was a clear difference between the clean (figure 215) and pre-corroded (figure 216) stages, with scattered areas of yellow/orange-brown corrosion within the darker brown corrosion covering the bulk of the surface. The darker brown corrosion dominated around the outer edge of the corroded area.

With the Cosmoloid H80 coating applied (figure 217) the colour of the corrosion was muted/greyed appearing a much lighter shade. However, after exposure at 80% RH for 342 days the corrosion had spread to the edges of the sample (figure 218) and changed to an orange-brown corrosion. Additionally, the corrosion over much of the

surface was powdery, which is visible in the higher magnification image (figure 219). Areas of coating may have detached as the volume of corrosion increased.

Partially Pre-corroded Siliglide 10 Coated

As with the samples above they were white-silver once cleaned (figure 220). After the samples were pre-corroded dark brown corrosion dominated around the outer edge of the corrosion and scattered areas of yellow-brown corrosion were present on the surface (figure 221). When the Siliglide 10 coating was applied (figure 222) it was barely visible to the naked eye and the corrosion layer looked thinner as if some had been wiped away while applying the coating. Around the edge of the samples bare metal was still clearly visible before exposure at 80% RH for 342 days. After the prolonged exposure to high RH (figure 223) new areas of corrosion had developed, which the higher magnification image (figure 224) revealed to be powdery in appearance and orange-brown in colour. There was minimal change in the appearance of this sample which is in agreement with the data as there was also only a small reduction in O₂ partial pressure.

Comparison

The additional corrosion which formed under the Paraloid B72 coating looked aggressive, probably due to the dark glossy colouring, however after the high corrosion rate during the initial period, the corrosion rate slowed significantly. This may be due to the corrosion reaching the edge of the surface where filaments can be seen progressing away from the bulk corrosion. The damage caused by filiform corrosion increases with higher environmental salinity, but as a rule only visual damage is caused by filiform corrosion (Bautista, 1996).

Both the Cosmoloid H80 and Siliglide 10 coatings allowed friable general corrosion to form highlighting that in these cases the corrosion formed is likely to be porous and have poor protective properties. Loss of historic material by the formation of friable corrosion products whilst coated is a cause for concern within the conservation sector. For Cosmoloid H80 coated samples in particular, with the O₂ consumption also in mind, the friable corrosion products indicate that Cosmoloid H80 is especially unsuitable for these conditions. Siliglide 10 had very good O₂ consumption results until the latter part of the year. It is therefore highly likely that if the samples had an additional coating layer applied in the latter part of the year it may have prevented the production of the friable corrosion. Siliglide 10 can be

applied by immersion and although this method has not been tested in this research, immersion may reduce the time required for application of an additional layer.

Both the visual and O₂ consumption results for these samples are in agreement with the electrochemical impedance spectroscopy (EIS) results of Cano et al. (2010), revealing that Paraloid B72 provided better protection than microcrystalline wax (Renaissance wax was used within their tests).

7.2.7.3 Scribed coated samples

The images for this section start after the clean coated samples have had a 2 cm scribe cut through the coating with a scalpel and salt solution had been brushed down the scribe. The scribes on the samples were allowed to begin corroding prior to exposure at 80% RH.

Scribed Paraloid B72 Coated Samples

In figure 225 prior to exposure at 80% RH, corrosion was hardly visible down the scribe, but as seen previously clusters of bubbles are visible in the Paraloid B72 coating. The data for the reduction in O₂ partial pressure indicated that corrosion may not have been taking place, so after 70 days the samples were removed and photographed (figure 226). As filiform corrosion was clearly taking place the samples were returned to their jars and assessed for a further 148 days (figure 227). Research discussed in section 2.3.2.5 described the conditions used for these samples as optimal conditions for filiform corrosion to develop. Thus on their continued exposure to 80% RH filiform corrosion continued and spread further but the data still did not provide a clear trend. The filaments were focused but not limited to the area around the scribe. The higher magnification image of the scribe (figure 228) reveals how aggressive the filiform corrosion appeared but the data collected for the reduction in O₂ partial pressure was not in agreement with the visual results. This highlights the superficial nature of filiform corrosion, thus what appeared aggressive is likely to be minimal and hardly affected the reduction in O₂ partial pressure measurements.

Further work on filiform corrosion and O₂ consumption is needed as it could provide more interesting information about its superficial nature. Questions regarding the best method for treating filiform once it is discovered are also raised. Is the best option to deactivate the filament by sealing the tail, dehydrate the filament by

reducing the RH to below 60% or should samples be cleaned and recoated as filiform corrosion causes loss of adhesion of the coating.

Scribed Cosmoloid H80 Coated Samples

The Cosmoloid H80 coating looked much the same as it did on the clean coated samples, but in this case included a scribe through the coating on the samples (figure 229). After exposure to 80% RH for 70 days (figure 230) yellow/orange brown corrosion was visible in the scribe and small amounts were visible over the surface and on the edges but not as filiform corrosion. A further 148 days exposure (figure 231) led to an increased amount of corrosion present. The top end of the scribe in the higher magnification image (figure 232) was the area experiencing the most aggressive corrosion, with the friable corrosion visible. Again the corrosion was not limited to the scribe location and the reduction in O₂ partial pressure data was inconclusive. The nature of the Cosmoloid H80 coating means it does not support filiform corrosion, in contrast to Paraloid B72.

Scribed Siliglide 10 Coated Samples

The Siliglide 10 coating looked much the same as it did on the clean coated samples, as the scribe through the coating was barely visible (figure 233). After exposure to 80% RH for 70 days (figure 234) orange brown corrosion was visible in the scribe. A further 148 days exposure (figure 235) led to an increased amount of corrosion present, but only in the scribe. Removing the Siliglide 10 coated samples from exposure to 80% RH temporarily, may have been beneficial for the coating allowing siloxane groups to reform if they had begun to partially hydrolyse. The top end of the scribe in the higher magnification image (figure 236) was the area experiencing the most aggressive corrosion, with friable corrosion visible. As the corrosion was focused at the top end of the scribe, more questions are raised such as, was the sample damaged when the coating was scribed? Did some of the de-icing salt solution collect in a pit? Is it localised pitting corrosion taking place? These questions and more which have not been asked reveal the need for further work in this area.

Comparison

There were obvious visual differences in the corrosion which formed in these tests with filiform corrosion occurring when Paraloid B72 was used but not when

Cosmoloid H80 or Siliglilide 10 were used. As all the samples were treated in the same manner apart from the coating used, the type of corrosion which forms must be due to the nature of the coating adherence to the substrate and the barrier properties of the coatings. Failure of these coatings create different outcomes, but which outcome is worst? As discussed above filiform corrosion is usually only visually damaging compared to the general corrosion Cosmoloid H80 coated samples experienced.

Paraloid B72 can be used as an adhesive so should create a strong physical bond with the steel surface. Cosmoloid H80 relies on keyed surfaces and the warmth of the metal when it was applied to create a protective layer over the surface, but as it is not an adhesive there is not a strong physical bond and the wax lays over the steel. Siliglilide 10 on the other hand forms chemical bonds with the steel surface, predominantly inhibiting corrosion by acting as a hydrophobic barrier coating preventing the transport of water/ions to the metal-coating interface unless the siloxane bonds begin to hydrolyse (Ooij et al., 2005). As mentioned above removing the samples temporarily from the chamber may have been beneficial for the Siliglilide 10 coating, although it probably had no real impact on the Paraloid B72 or Cosmoloid H80 coatings.

Due to the filiform corrosion which formed with the use of Paraloid B72 in the PROMET research they recommended that Paraloid B72 should not be considered as a possible protection system on its own in Mediterranean countries (Argyropoulos, 2008). With its performance in these tests it has been shown to be a feasible option, but in future work it may be worth considering Paraloid B72 in combination with the Siliglilide 10.

7.2.8 Compatibility of clear coatings with paints

Preliminary compatibility tests were carried out with paints used by the TM and the clear coatings. Using glass slides in these tests made some of the compatibility issues more visible. It is clear from the photographs that compatibility is an issue, although this could be due to the paint layers being recently coated. Sensitivity to solvents is reduced by aging of films and stoving produces a similar effect (Hess et al., 1979).

The formation of the wrinkled films in figures 237a and 240a is due to the action of acetone in the Paraloid B72 coating attacking the paint film. Acetone, is a strong

solvent, so attacks the paint film rapidly. The semi-gloss black paint in figure 239a was partially dissolved by the acetone in the Paraloid B72 coating and spread by the brush.

Cosmoloid H80 does not cause the same damage to the paint layers as Paraloid B72 perhaps partly due to using the weaker solvent white spirit, which is one of the least harmful solvents. Cosmoloid H80 does however leave a wax layer behind, with visible microcrystalline particles in most cases where it has been used. These microcrystalline particles cause a greying effect where they overlap the paint layers which is visible in figures 237b and 240b and less significantly in some of the others.

Although the Siliglide 10 coating itself is not visible to the naked eye once it has cured, it is still carried in the solvent isoamyl acetate, a strong solvent like acetone. Siliglide 10 has caused a little damage in figures 238c, 239c, 240c and 242c lifting a small amount of the paints in each case.

To have a better idea of the compatibility of these coatings with the paints, ideally the paints should aged for a longer time period before overlapping them with the clear coatings. This may reduce the impact of the strong solvents used with Paraloid B72 and Siliglide 10. If this is the case it would then also impact the visual appearance. An initial recommendation if these coatings are used with the paints, is to have minimal overlap so there is less area for these defects to occur.

Further tests may also be worth carrying out to test the compatibility of these paints with different solvents that can be used with these clear coatings. However, this is not possible for Siliglide 10 as it was used as sold.

8 Conclusion

This study assessed the occurrence of chloride induced corrosion by collecting corrosion product samples from historic sites in Scotland. At present atmospheric corrosion products cannot be predicted due to the complex nature of the terrain and atmosphere. The occurrence of akaganéite is not limited to marine atmospheres as de-icing salt is in common use and this aligns with data from the snow-belt in the northern states of the US. Using de-icing salts increases the risk of aggressive corrosion forming locally in Scotland and throughout the UK.

The core of this study however focuses on the anti-corrosive performance of clear coatings on historic armoured steel donated by the Tank Museum, which is based close to the South coast of England. Thus the museum environment has been assessed. Although the Tank Museum is continually working to improve the display and storage environments in which it houses its vehicles, it still face many challenges. The new Vehicle Conservation Centre (VCC) is beneficial as housing vehicles indoors dramatically reduces the time of wetness (TOW) they experience and makes it practically impossible for chloride ions from the external atmosphere to induce corrosion. However, the range in RH data both inside and outside of the vehicles shows wetting and drying induced corrosion will be occurring on the surfaces of the vehicles, with the exception of those subject to radiant heating. The workshop/shed environments pose the highest risk to their vehicles due to high RH, but RH data collected from the micro-environments inside the vehicles also indicate that these hidden environments are highly corrosive. These micro-environments within the vehicles would benefit from further research, testing the impact of silica gel.

All the coatings used within this research offer protection (at least twice as much O_2 is consumed per day when no coating is applied to a clean surface compared to when a coating is applied), but good surface preparation is needed. Corroded surfaces retaining some paint with continuous oxide layer and no pitting, offer protection and are more protective than stripping and not applying a coating, which is a high risk strategy.

The coatings offered protection irrespective of their relative barrier properties. In continuous high RH in the dark they provide good protection (reducing the O_2 consumption) on cleaned surfaces and significantly reduced corrosion even on surfaces with large amounts of accelerated corrosion on them. In the light the

coatings may suffer deterioration especially when exposed to ultra-violet (UV) light which disrupts and breaks covalent bonds of organic molecules. A bad scenario would be to strip the metal and not coat it when it is situated in a marine context or near a road regularly treated with de-icing salt.

Where coatings are damaged the corrosion type is influenced by the nature of the coating with filiform corrosion forming with acrylic but general corrosion forming with micro-crystalline wax and the silane.

Of the 3 coatings tested Siliglide 10 performed best with chloride in a high RH climate but may begin to fail towards the end of a year. It is therefore probably better suited for use indoors. Cosmoloid H80 performed worst overall in these tests and so cannot be recommended. Paraloid B72 can be recommended as it performed consistently well. It reduced corrosion on cleaned surfaces, with only superficial minimal filiform corrosion forming. It also performed reasonably well on contaminated surfaces. However, when using Paraloid B72 care needs to be taken with existing paint layers as acetone can cause solvent lifting, a possible solution could be to substitute acetone for xylene, but xylene is more toxic than acetone so there are additional health and safety implications. For the samples with salt solution applied to the scribed damage in the coatings there was not a great deal of difference between anti-corrosion performances of the coatings. Thus, the recommendation for protecting an area of local paint loss is to clean the surface and coat using 3 layers of Paraloid B72.

This research project has introduced Siliglide 10, a clear silane coating, as a potential coating of the future for conservation, although more research is needed. It has also provided both a methodology and a small amount of the research and data that is needed for creating a standard. There is a need for standards within the 'Heritage' conservation sector to provide quantified evidence based guidelines and advice for preserving specific materials in different states of repair to be stored in specific environmental conditions. Although it is only a small contribution, it is a significant contribution and by using this methodology, changing one variable at a time e.g. RH % or the metal substrate used, more and more data can be collated within a database and progress will be made towards creating standards for conservation practise, for the use of conservation practitioners

Another important area where further research is required included the solvent retention of Paraloid B72 with different solvents. Following this, comparison of O₂ consumption data using the coating Paraloid B72 with different solvents would

confirm whether using xylene instead of acetone is a feasible option for corrosion reduction. Potentially it may be that a Siliglide 10 and Paraloid B72 coating combination offers the best protection. However, as the performance of these coatings has not been tested in fluctuating RH, light and temperature conditions this is another area which requires further investigation in order to predict how they would perform in field-tests.

9 Bibliography

Abe, Y. and T. Gunji. 2004. Oligo- and polysiloxanes. *Progress in Polymer Science* 29(3), pp. 149-182.

Almeida, E., D. Santos and J. Uruchurtu. 1999. Corrosion performance of waterborne coatings for structural steel. *Progress in Organic Coatings* 37(3–4), pp. 131-140.

Amada, S. and T. Hirose. 1998. Influence of grit blasting pre-treatment on the adhesion strength of plasma sprayed coatings: fractal analysis of roughness. *Surface and Coatings Technology* 102(1-2), pp. 132-137.

Amada, S., T. Hirose and T. Senda. 1999. Quantitative evaluation of residual grits under angled blasting. *Surface and Coatings Technology* 111(1), pp. 1-9.

Antunes, R. A., R. U. Ichikawa, L. G. Martinez and I. Costa. 2014. Characterization of Corrosion Products on Carbon Steel Exposed to Natural Weathering and to Accelerated Corrosion Tests. *International Journal of Corrosion* 2014, p. 9.

Argyropoulos, V. 2008. *Final Activity Report - PROMET (Developing New Analytical Techniques and Materials for Monitoring and Protecting Metal Artefacts From the Mediterranean Region)*. Athens, Greece: Technological Educational Institution of Athens.

Argyropoulos, V., S. Boyatzis and M. Giannoulaki. 2013. The role of standards in conservation methods for metals in cultural heritage. In: Dillmann, P., D. Watkinson, E. Angelini and A. Adriaens eds. *Corrosion and conservation of cultural heritage metallic artefacts*. Vol. 65. Cambridge: Woodhead Publishing Limited, pp. 478-517.

Argyropoulos, V., D. Charalambous, A. Kaminari, A. Karabotsos, K. Polikreti, A. Siatou, E. Cano, D. M. Bastidas, I. Cayuela, J.-M. Bastidas, C. Degriigny, D. Vella, J. Crawford and S. Golfomitsou. 2007a. Testing of a new wax coating Poligen ES 91009 and corrosion inhibitor additives used for improving coatings for historic iron alloys. In: Degriigny, C., R. Van Lang, I. Joosten and B. Ankersmith eds. *Metal 07. Proceedings of the interim meeting of the ICOM-CC Metal WG*.

Argyropoulos, V., M. Giannoulaki, G. P. Michalakakos and A. Siatou eds. 2007b. *A survey of the types of corrosion inhibitors and protective coatings used for the conservation of metal objects from museum collections in the Mediterranean basin*. Strategies for saving our cultural heritage. Proceedings of the international conference on conservation strategies for saving indoor metallic collections, Cairo.

Arkles, B. 1977. Tailoring surfaces with silanes. *Chemtech* 7(12), pp. 766-778.

- Arkles, B. 2006. *Hydrophobicity, Hydrophilicity and Silanes*. Paint & Coatings Industry. pp. 114-132.
- Arnold, D. 2006. Preserving Your Antique Arms Collection. *GCA Journal*, pp. 19-23.
- Arroyave, C. and M. Morcillo. 1995. The effects of nitrogen oxides in atmospheric corrosion of metals. *Corrosion Science* 37(2), pp. 293-305.
- Asami, K. and M. Kikuchi. 2003. In-depth distribution of rusts on a plain carbon steel and weathering steels exposed to coastal–industrial atmosphere for 17 years. *Corrosion Science* 45(11), pp. 2671-2688.
- Ashley-Smith, J. 2013. *Risk assessment for object conservation*. Routledge, Taylor & Francis Group.
- ASTM. 2009. Section 1. Metallurgy - Introduction. In: Bringas, J. E. ed. *DS70 - Handbook of Steel Data: American and European*. pp. 1-20.
- Badea, G., P. Cret, M. Lolea, A. Setel and L. Marin. 2010. Principles of Atmospheric Corrosion Evaluation. *Nonconventional Technologies Review* 2/2010, pp. 10-15.
- Balasubramaniam, R. and A. V. Ramesh Kumar. 2000. Characterization of Delhi iron pillar rust by X-ray diffraction, Fourier transform infrared spectroscopy and Mössbauer spectroscopy. *Corrosion Science* 42(12), pp. 2085-2101.
- BASF. 2011. *Binders and Resins - Functionality & Performance - Solutions & Technologies - BASF Dispersions & Pigments*: [Online]. Available at: https://www.dispersions-pigments.basf.com/portal/basf/ien/dt.jsp?setCursor=1_570325 [Accessed: 19 November 2015].
- Bauccio, M. and American Society for Metals. 1993. *ASM Metals Reference Book, 3rd Edition*. ASM International.
- Baumann, K. and R. Bender. 2008. D1. Coatings and linings. In: Kreysa, G. and M. Schutze eds. *Corrosion Handbook: Atmosphere - D. Materials with special properties*. Wiley-VCH Verlag GmbH & Co. KGaA, pp. 300-330.
- Bautista, A. 1996. Filiform Corrosion in Polymer-Coated Metals. *Progress in Organic Coatings* 28, pp. 49-58.
- Bhaskaran, R., N. Palaniswamy, N. S. Rengaswamy and M. Jayachandran. 2005. A review of differing approaches used to estimate the cost of corrosion (and their relevance in the development of modern corrosion prevention and control strategies). *Anti-Corrosion Methods and Materials* 52(1), pp. 29-41.

Bierwagen, G. P. and A. M. Huovinen. 2010. 4.11 - Paint Formulation. In: Cottis, B., M. Graham, R. Lindsay, S. Lyon, T. Richardson, D. Scantlebury and H. Stott eds. *Shreir's Corrosion*. Vol. 4. Oxford: Elsevier, pp. 2643-2665.

Bird, S. and J. Langfeldt. 2013. Protection of Objects on Open Display at the Science Museum. *Amazing Technicolour Dreamcoats: Protective surface finishes for metals*. ICON Metals Group Conference and AGM at The Wallace Collection, London.

Blackshaw. 1982. An Appraisal of Cleaning Methods for the use on Corroded Iron Antiquities. In: Clarke, R. and S. Blackshaw eds. *Conservation of Iron, National Maritime Museum, Monograph No. 53*.

Bortak, T. N. 2002. *Guide to Protective Coatings Inspection and Maintenance*. U.S. Department of the Interior, Bureau of Reclamation.

Bos, W. M. 2008. *Prediction of coating durability: Early detection using electrochemical methods*. PhD, Technical University of Delft.

Brightman, M. 2012. Is the Conservation of the United Kingdom's Built Heritage Sustainable? *Reinvention: An International Journal of Undergraduate Research* (British Conference of Undergraduate Research (BCUR) - Special Issue).

Brimblecombe, P. and B. Ramer. 1983. Museum display cases and the exchange of water vapour. *Studies in Conservation* 28(4), pp. 179-188.

Brown, P. W. and L. W. Masters. 1982. Factors Affecting the Corrosion of Metals in the Atmosphere. In: Ailor, W. H. ed. *Atmospheric Corrosion*. New York: Wiley Interscience Publication, pp. 31-49.

Building Design Online. 2009. *Building Analysis: King Shaw Associates keep it simple at Tank Museum* [Online]. Building.co.uk, bdonline.co.uk. Available at: <http://www.building.co.uk/building-analysis-king-shaw-associates-keep-it-simple-at-tank-museum/3146744.article>, <http://www.bdonline.co.uk/building-analysis-king-shaw-associates-keep-it-simple-at-tank-museum/3146744.article> [Accessed: 20th March 2015].

Cáceres, L., T. Vargas and L. Herrera. 2009. Influence of pitting and iron oxide formation during corrosion of carbon steel in unbuffered NaCl solutions. *Corrosion Science* 51(5), pp. 971-978.

Cameron, C. 2004. Inorganic and Hybrid Coatings. In: Marrion, A. R. ed. *The chemistry and physics of coatings*. 2nd ed. Cambridge: The Royal Society of Chemistry, pp. 237-266.

Cano, E., D. M. Bastidas, V. Argyropoulos, S. Fajardo, A. Siatou, J. M. Bastidas and C. Degriñy. 2010. Electrochemical characterization of organic coatings for protection of historic steel artefacts. *Journal of Solid State Electrochemistry* 14(3), pp. 453-463.

Cano, E., D. M. Bastidas, V. Argyropoulos and A. Siatou. 2007. Electrochemical techniques as a tool for testing the efficiency of protection systems for historical steel objects. In: Argyropoulos, V., A. Hein and M. Abdel Harith eds. *Strategies for Saving our Cultural Heritage. Proceedings of the International Conference on Conservation Strategies for Saving Indoor Metallic Collections*. Cairo, Egypt 25 February - 1 March.

Castaño, J. G., C. A. Botero, A. H. Restrepo, E. A. Agudelo, E. Correa and F. Echeverría. 2010. Atmospheric corrosion of carbon steel in Colombia. *Corrosion Science* 52(1), pp. 216-223.

Chan, C.-M. and S. Venkatraman. 2006. Coating Rheology. In: Tracton, A. A. ed. *Coatings Technology: Fundamentals, Testing, and Processing Techniques*. Boca Raton, FL, USA: CRC Press, pp. 2.1-2.14.

Chapman, S. and D. Mason. 2003. Literature Review: The Use of Paraloid B-72 as a Surface Consolidant for Stained Glass. *Journal of the American Institute for Conservation* 42(2), pp. 381-392.

Chatterjee, U. K., S. K. Bose and S. K. Roy. 2001. *Environmental Degradation of Metals*. New York: Marcel Dekker, Inc.

Chen, Y. Y., H. J. Tzeng, L. I. Wei and H. C. Shih. 2005a. Mechanical properties and corrosion resistance of low-alloy steels in atmospheric conditions containing chloride. *Materials Science and Engineering: A* 398(1-2), pp. 47-59.

Chen, Y. Y., H. J. Tzeng, L. I. Wei, L. H. Wang, J. C. Oung and H. C. Shih. 2005b. Corrosion resistance and mechanical properties of low-alloy steels under atmospheric conditions. *Corrosion Science* 47(4), pp. 1001-1021.

Cole, I. and P. Corrigan. 2011. Predicting the service life of buildings and components. *Proceedings of the Institute of Civil Engineers (ICE) - Construction Materials* [Online] 164. Available at: <http://www.icevirtuallibrary.com/content/article/10.1680/coma.2011.164.6.305>.

Cole, I. S. 2010. 2.16 - Atmospheric Corrosion. In: Cottis, B., M. Graham, R. Lindsay, S. Lyon, T. Richardson, D. Scantlebury and H. Stott eds. *Shreir's Corrosion*. Vol. 2. Oxford: Elsevier, pp. 1051-1093.

Cole, I. S., W. Y. Chan, G. S. Trinidad and D. A. Paterson. 2004a. Holistic model for atmospheric corrosion Part 4 – Geographic information system for predicting airborne salinity. *Corrosion Engineering, Science and Technology* 39(1), pp. 89-96.

Cole, I. S., W. D. Ganther, A. M. Helal, W. Chan, D. Paterson, G. Trinidad, P. Corrigan, R. Mohamed, N. Sabah and A. Al-Mazrouei. 2013. A corrosion map of Abu Dhabi. *Materials and Corrosion* 64(3), pp. 247-255.

Cole, I. S., W. D. Ganther, D. A. Paterson, G. A. King, S. A. Furman and D. Lau. 2003a. Holistic model for atmospheric corrosion: Part 2 - Experimental measurement of deposition of marine salts in a number of long range studies. *Corrosion Engineering, Science and Technology* 38(4), pp. 259-266.

Cole, I. S., D. Lau and D. A. Paterson. 2004b. Holistic model for atmospheric corrosion Part 6 – From wet aerosol to salt deposit. *Corrosion Engineering, Science and Technology* 39(3), pp. 209-218.

Cole, I. S., T. H. Muster, N. S. Azmat, M. S. Venkatraman and A. Cook. 2011. Multiscale modelling of the corrosion of metals under atmospheric corrosion. *Electrochimica Acta* 56, pp. 1856-1865.

Cole, I. S., T. H. Muster, D. Lau and W. D. Ganther. 2004c. Some recent trends in corrosion science and their application to conservation. In: *Metal 04*. The National Museum of Australia,

Canberra ACT, 4–8 October 2004.

Cole, I. S. and D. A. Paterson. 2004. Holistic model for atmospheric corrosion Part 5 – Factors controlling deposition of salt aerosol on candles, plates and buildings. *Corrosion Engineering, Science and Technology* 39(2), pp. 125-130.

Cole, I. S., D. A. Paterson and W. D. Ganther. 2003b. Holistic model for atmospheric corrosion Part 1 - Theoretical framework for production, transportation and deposition of marine salts. *Corrosion Engineering, Science and Technology* 38(2), pp. 129-134.

Cole, I. S., D. A. Paterson, W. D. Ganther, A. Neufeld, B. Hinton, G. McAdam, M. McGeachie, R. Jeffery, L. Chotimongkol, C. Bhamornsut, N. V. Hue and S. Purwadaria. 2003c. Holistic model for atmospheric corrosion: Part 3 - Effect of natural and man made landforms on deposition of marine salts in Australia and south-east Asia. *Corrosion Engineering, Science and Technology* 38(4), pp. 267-274.

Cook, D. C. 2005. Spectroscopic identification of protective and non-protective corrosion coatings on steel structures in marine environments. *Corrosion Science* 47(10), pp. 2550-2570.

Cornell, R. M. and U. Schwertmann. 2006. *The Iron Oxides: Structure, Properties, Reactions, Occurrences and Uses*. Wiley-VCH.

Corvo, F., J. Minotas, J. Delgado and C. Arroyave. 2005. Changes in atmospheric corrosion rate caused by chloride ions depending on rain regime. *Corrosion Science* 47(4), pp. 883-892.

Corvo, F., T. Perez, L. R. Dzib, Y. Martin, A. Castañeda, E. Gonzalez and J. Perez. 2008. Outdoor–indoor corrosion of metals in tropical coastal atmospheres. *Corrosion Science* 50(1), pp. 220-230.

Cremer, N. D. 1989. Prohesion Compared to Salt Spray and Outdoors: Cyclic Methods of Accelerated Corrosion Testing. In: *Federation of Societies for Coatings Technology, 1989 Paint Show*.

Dalewicz-Kitto, S., F. McLaughlan, E. Schmuecker and J. Hood. 2013. Japanese armour and the conservation of a Sakakibara family armour at the Royal Armouries. *Journal of the Institute of Conservation* 36(1), pp. 35-52.

Davey, A. 2007. *The Maintenance of Iron Gates and Rainlings*. Historic Scotland, Longmore House, Salisbury Place, Edinburgh, EH9 1SH: Historic Scotland

Davidson, A. and G. W. Brown. 2012. Paraloid B-72: Practical Tips for the Vertebrate Fossil Preparation. *Collection Forum* 26((1-2)), pp. 99-119.

De Graeve, I., J. Vereecken, A. Franquet, T. Van Schaftinghen and H. Terryn. 2007. Silane coating of metal substrates: Complementary use of electrochemical, optical and thermal analysis for the evaluation of film properties. *Progress in Organic Coatings* 59(3), pp. 224-229.

de la Fuente, D., I. Díaz, J. Simancas, B. Chico and M. Morcillo. 2011. Long-term atmospheric corrosion of mild steel. *Corrosion Science* 53(2), pp. 604-617.

Deflorian, F. and L. Fedrizzi. 1999. Adhesion characterization of protective organic coatings by electrochemical impedance spectroscopy. *Journal of Adhesion Science and Technology* 13(5), pp. 629-645.

Degrigny, C. 2010. Use of artificial metal coupons to test new protection systems on cultural heritage objects: manufacturing and validation. *Corrosion Engineering, Science and Technology* 45(5), pp. 367-374.

Delaney, J. 2015. 'Tank in a Bag' Project - Building 104 to: Lawson, A. Received 23 April 2015.

Delplancke, J. L., S. Berger, X. Lefèbvre, D. Maetens, A. Pourbaix and N. Heymans. 2001. Filiform corrosion: interactions between electrochemistry and mechanical properties of the paints. *Progress in Organic Coatings* 43(1–3), pp. 64-74.

Dillmann, P., F. Mazaudier and S. Hœrlé. 2004. Advances in understanding atmospheric corrosion of iron. I. Rust characterisation of ancient ferrous artefacts exposed to indoor atmospheric corrosion. *Corrosion Science* 46(6), pp. 1401-1429.

Dumfries and Galloway Council. 2016. *About the Midsteeple* [Online]. Communications Unit, Council Offices, English Street, Dumfries, DG1 2DD, United Kingdom. Available at: <http://www.dgboxoffice.co.uk/index.aspx?articleid=13714> [Accessed: 25/04/2016].

Emmerson, N. and D. Wakinson. 2013. Preparing Historic Wrought Iron for Protective Coatings: Quantitative Assessment to Produce Evidence-Based Protocols. In: Hyslop, E., V. Gonzalez, L. Troalen and L. Wilson eds. *Metal 2013*. Edinburgh, Scotland, 16th – 20th September 2013.

Emmerson, N. J. and D. E. Watkinson. 2016. Surface preparation of historic wrought iron: Evidencing the requirement for standardisation. *Materials and Corrosion* 67(2), pp. 176-189.

Evans, U. R. 1972. *The Rusting of Iron: Causes and Control*. Edward Arnold Limited.

Finnie, I. 1995. Some reflections on the past and future of erosion. *Wear* 186–187,(Part 1), pp. 1-10.

Fitzsimons, B. and T. Parry. 2010. 4.17 - Paint and Coating Failures and Defects. In: Cottis, B., M. Graham, R. Lindsay, S. Lyon, T. Richardson, D. Scantlebury and H. Stott eds. *Shreir's Corrosion*. Vol. 4. Oxford: Elsevier, pp. 2728-2745.

Ganther, W. D., I. S. Cole, A. M. Helal, W. Chan, D. A. Paterson, G. Trinidad, P. Corrigan, R. Mohamed, N. Sabah and A. Al-Mazrouei. 2011. Towards the development of a corrosion map for Abu Dhabi. *Materials and Corrosion* 62(11), pp. 1066-1073.

Gelest Inc. 2007. *Gelest: Optical Materials* Gelest Inc.

Gelest Inc. 2013. *Reactive Silicones: Forging new polymer links*. Gelest Inc. Morrisville PA 19067 USA

Godfraind, S., R. Pender and B. Martin eds. 2012. *Metals, English Heritage: Practical Building Conservation Series*. Farnham, Surrey, UK: Ashgate Publishing Limited.

Graedel, T. E. and R. P. Frankenthal. 1990. Corrosion Mechanisms for Iron and Low Alloy Steels Exposed to the Atmosphere. *Journal of Electrochemical Society* 137(8), pp. 2385-2394.

Griffiths, B. J., D. T. Gawne and G. Dong. 1996. The erosion of steel surfaces by grit-blasting as a preparation for plasma spraying. *Wear* 194(1–2), pp. 95-102.

Grossman, D. M. 1996. *More realistic tests for atmospheric corrosion*. ASTM Standardisation news. April 1996, pp. 34-39.

Groysman, A. 2010. *Corrosion for Everybody*. Springer.

Gustafsson, M. E. R. and L. G. Franzén. 1996. Dry deposition and concentration of marine aerosols in a coastal area, SW Sweden. *Atmospheric Environment* 30(6), pp. 977-989.

Gustafsson, M. E. R. and L. G. Franzén. 2000. Inland transport of marine aerosols in southern Sweden. *Atmospheric Environment* 34(2), pp. 313-325.

Guy, A. 2004. Coatings Components Beyond Binders. In: Marrion, A. R. ed. *The Chemistry and Physics of Coatings*. Cambridge: The Royal Society of Chemistry, pp. 267-316.

Harris, A. F. and A. Beevers. 1999. The effects of grit-blasting on surface properties for adhesion. *International Journal of Adhesion and Adhesives* 19(6), pp. 445-452.

Hashimoto, K., K. Asami, A. Kawashima, H. Habazaki and E. Akiyama. 2007. The role of corrosion-resistant alloying elements in passivity. *Corrosion Science* 49(1), pp. 42-52.

Hastuty, S., A. Nishikata and T. Tsuru. 2010. Pitting corrosion of Type 430 stainless steel under chloride solution droplet. *Corrosion Science* 52(6), pp. 2035-2043.

Herting, G., I. O. Wallinder and C. Leygraf. 2008. Corrosion-induced release of the main alloying constituents of manganese-chromium stainless steels in different media. *Journal of Environmental Monitoring* 10(9), pp. 1084-1091.

Hess, M., T. A. Banfield, S. T. Harris and H. Brunner. 1979. *Hess's Paint Film Defects: Their Causes and Cures*. 3rd ed. London, UK: Chapman and Hall Ltd.

Historic Scotland. 2005. *Boundary Ironwork - A guide to re-instatement*. Historic Scotland, Longmore House, Salisbury Place, Edinburgh, EH9 1SH: Historic Scotland

HITEK-nology Solutions. 2013. *Case Study #22 Imperial War Museum WW2 Tanks* [Online]. Online: Available at: <http://www.hitektechnologysolutions.co.uk/assets%5Ccase%20studies%5CLong%20Ter>

[m%20Preservation%5CImperial%20War%20Museum%20Tanks.pdf](#) [Accessed: 24 April 2015].

Hoar, T. P. 1976. Review Lecture - Corrosion of Metals: its cost and control. *Proceedings of the Royal Society of London. A. Mathematical and Physical Sciences* 348, pp. 1-18.

Hœrlé, S., F. Mazaudier, P. Dillmann and G. Santarini. 2004. Advances in understanding atmospheric corrosion of iron. II. Mechanistic modelling of wet-dry cycles. *Corrosion Science* 46(6), pp. 1431-1465.

Horie, V. 2010. *Materials for Conservation - Organic consolidants, adhesives and coatings*. 2nd ed. Oxford, UK: Elsevier Ltd.

Hougardy, H., W. Dahl and H. J. Grabke. 2003. Steel, 6. Uses: Microstructures, Properties, and Heat Treatment. *Ullmann's Encyclopedia of Industrial Chemistry*. Completely Revised 6th ed., Vol. 34. Wiley-VCH Verlag GmbH & Co. KGaA, pp. 125-181.

Houska, C. 2009. Deicing Salt – Recognizing the Corrosion Threat. *International Molybdenum Association, Pittsburgh, TMR Consulting*, pp. 1-11.

Jenkins, G. J., M. C. Perry and M. J. Prior. 2008. *The Climate of the United Kingdom and Recent Trends*. Met Office Hadley Centre, Exeter, UK.

Jones, D. A. 2013. *Principles and prevention of corrosion*. 2nd ed. Essex, United Kingdom: Pearson Education Limited.

Kennell, G. F. and R. W. Evitts. 2009. Crevice corrosion cathodic reactions and crevice scaling laws. *Electrochimica Acta* 54(20), pp. 4696-4703.

King, D. 2006. Bovington's defence strategy. *Building Services Journal* [Online]. Available at: <http://www.douging.co.uk/PDFs/BSJ%20Jul06%20Bovington%20Defence%20Strategy.pdf>, <http://www.building.co.uk/conserving-architectural-treasures-bovington/3070075.article> [Accessed: 14th October 2013].

Knasiak, G. J., A. Lukacs, R. W. Mouk and A. E. Abel. 2003. Polysilazane/polysiloxane block copolymers. In: United States Patent and Trademark Office ed. United States: Kion Corporation, Huntingdon Valley, PA (US).

Koch, G. H., M. P. H. Brongers, N. G. Thompson, Y. P. Virmani and J. H. Payer. 2001. *Executive Report: Corrosion Cost and Preventive Strategies in the United States*. CC Technologies Laboratories, Inc. and NACE International.

- Kucera, V. and E. Mattsson. 1987. Atmospheric Corrosion. In: Mansfeld, F. ed. *Corrosion mechanisms*. New York: Marcel Dekker, Inc., pp. 211-284.
- Lau, N. T., C. K. Chan, L. I. Chan and M. Fang. 2008. A microscopic study of the effects of particle size and composition of atmospheric aerosols on the corrosion of mild steel. *Corrosion Science* 50(10), pp. 2927–2933.
- Lawson, L., C. Flack and S. Taylor. 2013. Come Rain or Shine: Maintaining the Barbara Hepworth Sculpture Garden. *Amazing Technicolour Dreamcoats: Protective surface finishes for metals*. ICON Metals Group Conference and AGM at The Wallace Collection, London.
- Laycock, N. J., J. Stewart and R. C. Newman. 1997. The initiation of crevice corrosion in stainless steels. *Corrosion Science* 39(10–11), pp. 1791-1809.
- Le Pera, M. E. 2004. Prepositioning Military Vehicles and Equipment. *Tribology & Lubrication Technology* 60(5), pp. 28-34.
- LeBozec, N., N. Blandin and D. Thierry. 2008. Accelerated corrosion tests in the automotive industry: A comparison of the performance towards cosmetic corrosion. *Materials and Corrosion* 59(11), pp. 889-894.
- Lee, E. W. 2010. *A Study of the Effectiveness of Paraloid B72 as a Coating System Depending on Differing Number of Application*. MSc Dissertation, Cardiff University.
- Leidheiser Jr., H. 1987. Coatings. In: Mansfeld, F. ed. *Corrosion mechanisms*. New York: Marcel Dekker, Inc., pp. 165-209.
- Li, C. 2006. Biodeterioration of acrylic polymers Paraloid B-72 and B-44: Report on field trials. *Anatolian Archaeological Studies* 15, pp. 283-290.
- Lukacs, A. and G. J. Knasiak. 2003. Thermally stable, moisture curable polysilazanes and polysiloxazanes. In: United States Patent and Trademark Office ed. Kion Corporation, Huntingdon Valley, PA (US).
- Lyon, S. B. 2010. 3.01 - Corrosion of Carbon and Low Alloy Steels. In: Cottis, B., M. Graham, R. Lindsay, S. Lyon, T. Richardson, D. Scantlebury and H. Stott eds. *Shreir's Corrosion*. Oxford: Elsevier, pp. 1693-1736.
- Ma, Y., Y. Li and F. Wang. 2009. Corrosion of low carbon steel in atmospheric environments of different chloride content. *Corrosion Science* 51(5), pp. 997-1006.
- Maréchal, L., S. Perrin, P. Dillmann and G. Santarini. 2007. Study of the Atmospheric Corrosion of Iron by Aging Historical Artefacts and Contemporary Low-Alloy Steel in a Climatic Chamber: Comparison with Mechanistic Modelling. In:

Dillmann, P., G. Beranger, P. Piccardo and H. Matthiesen eds. *Corrosion of Metallic Heritage Artefacts: Investigation, Conservation and Prediction of Long Term Behaviour: Investigation, Conservation and Prediction of Long Term Behaviour*. Cambridge: Woodhead Publishing, pp. 131-151.

Marrion, A. R. e. ed. 2004. *The chemistry and physics of coatings*. 2nd ed. Cambridge: The Royal Society of Chemistry.

Marrow, T. J., L. Babout, A. P. Jivkov, P. Wood, D. Engelberg, N. Stevens, P. J. Withers and R. C. Newman. 2006. Three dimensional observations and modelling of intergranular stress corrosion cracking in austenitic stainless steel. *Journal of Nuclear Materials* 352(1–3), pp. 62-74.

Martin, J. W., S. C. Saunders, F. L. Floyd and J. P. Wineburg. 1996. Methodologies for Predicting the Service Lives of Coating Systems. In: Brezinski, D. and T. J. Miranda eds. *Federation Series*. Blue Bell, Pennsylvania, USA: The Federation of Societies for Coating Technology.

Matthiesen, H. 2007. A Novel Method to Determine Oxidation Rates of Heritage Materials in Vitro and in Situ. *Studies in Conservation* 52(4), pp. 271-280.

McCafferty, E. and A. C. Zettlemyer. 1971. Adsorption of water vapour on α -Fe₂O₃. *Discussions of the Faraday Society* 52, pp. 239-254.

Mendoza, A. R. and F. Corvo. 1999. Outdoor and indoor atmospheric corrosion of carbon steel. *Corrosion Science* 41, pp. 75-86.

Military Factory. 2015. *Alvis FV603 Saracen Armored Personnel Vehicle / Armored Car (1952)* [Online]. Available at: http://www.militaryfactory.com/armor/detail.asp?armor_id=576 [Accessed: 14-09-2016].

Momber, A. 2008. *Blast Cleaning Technology*. Berlin, Heidelberg: Springer-Verlag Berlin Heidelberg.

Momber, A. W., Y. C. Wong, R. Ij and E. Budidharma. 2002. Hydrodynamic profiling and grit blasting of low-carbon steel surfaces. *Tribology International* 35(4), pp. 271-281.

Monnier, J., S. Réguer, E. Foy, D. Testemale, F. Mirambet, M. Saheb, P. Dillmann and I. Guillot. 2014. XAS and XRD in situ characterisation of reduction and reoxidation processes of iron corrosion products involved in atmospheric corrosion. *Corrosion Science* 78, pp. 293-303.

Morcillo, M., D. de la Fuente, I. Diaz and H. Cano. 2011. Atmospheric Corrosion of Mild Steel. *Revista De Metalurgia* 47(5), pp. 426-444.

Mottner, P., H. Roemich, M. Pilz, S. Brueggerhoff and J. Kiesenberg. 2001. Investigations of transparent coatings for the conservation of iron and steel outdoor industrial monuments. In: MacLeod, I. D., J. M. Theile and C. Degriigny eds. *METAL 2001, Proceedings of the International ICOM Committee for Conservation Metals Working Group*,. Santiago de Chile,, 2 - 6 April 2001. Western Australian Museum.

Murphy, B. S. 1904. *English and Scottish Wrought Ironwork*. George Waterston & Sons, Edinburgh.

Museums Galleries Scotland. 2014. *Advice Sheet: Caring for metal collections in museums*.

Nasu, S., T. Kamimura and T. Tazaki. 2002. Investigation of Rust Formed on Steel Surfaces and Related Oxyhydroxides. *Hyperfine Interactions* 139(1), pp. 175-182.

NHIG. 2012. Conservation of Architectural Ironwork In: *Conservation Studies CPD Course*. Edinburgh, 22-23 October 2012. (First published: Topp, C. 2008. *Journal of Architectural Conservation*. 14(2)) National Heritage Ironwork Group,.

Nilsson, J.-O. 1992. Super duplex stainless steels. *Materials Science and Technology* 8(8), pp. 685-700.

Nishimura, T., H. Katayama, K. Noda and T. Kodama. 2000. Effect of Co and Ni on the corrosion behavior of low alloy steels in wet/dry environments. *Corrosion Science* 42(9), pp. 1611-1621.

Nishimura, T. and T. Kodama. 2003. Clarification of chemical state for alloying elements in iron rust using a binary-phase potential–pH diagram and physical analyses. *Corrosion Science* 45(5), pp. 1073-1084.

Oliveira, C. G. and M. G. S. Ferreira. 2003. Ranking high-quality paint systems using EIS. Part II: defective coatings. *Corrosion Science* 45(1), pp. 139-147.

Ooij, W. J. v., D. Zhu, M. Stacy, A. Seth, T. Mugada, J. Gandhi and P. Puomi. 2005. Corrosion Protection Properties of Organofunctional Silanes — An Overview. *Tsinghua science and technology* 10(6), pp. 639-664.

Otaduy, P. J. and A. Karagiozis. 2010. Corrosion Prediction in Buildings Based on Simulation of Temporal Distribution of Humidity and Temperatures and the International Standard ISO-9223. In: ASHRAE ed. *Buildings XI*. December 2010. American Society of Heating, Refrigerating and Air-Conditioning Engineers, Inc.

Overdiep, W. S. 1986. The levelling of paints. *Progress in Organic Coatings* 14(2), pp. 159-175.

Palanivel, V., D. Zhu and W. J. van Ooij. 2003. Nanoparticle-filled silane films as chromate replacements for aluminum alloys. *Progress in Organic Coatings* 47(3–4), pp. 384-392.

Pardo, A., M. C. Merino, M. Carboneras, F. Viejo, R. Arrabal and J. Muñoz. 2006. Influence of Cu and Sn content in the corrosion of AISI 304 and 316 stainless steels in H₂SO₄. *Corrosion Science* 48(5), pp. 1075-1092.

Pardo, A., M. C. Merino, A. E. Coy, F. Viejo, R. Arrabal and E. Matykina. 2008a. Effect of Mo and Mn additions on the corrosion behaviour of AISI 304 and 316 stainless steels in H₂SO₄. *Corrosion Science* 50(3), pp. 780-794.

Pardo, A., M. C. Merino, A. E. Coy, F. Viejo, R. Arrabal and E. Matykina. 2008b. Pitting corrosion behaviour of austenitic stainless steels – combining effects of Mn and Mo additions. *Corrosion Science* 50(6), pp. 1796-1806.

Parslow, G. I., D. J. Stephenson, J. E. Strutt and S. Tetlow. 1997. Paint layer erosion resistance behaviour for use in a multilayer paint erosion indication technique. *Wear* 212(1), pp. 103-109.

Peguet, L., B. Malki and B. Baroux. 2007. Influence of cold working on the pitting corrosion resistance of stainless steels. *Corrosion Science* 49(4), pp. 1933-1948.

Perkins, B. N. 2003. The de-electrification and re-electrification of historic lighting fixtures at Winterthur Museum. *Journal of the American Institute for Conservation* 42 (3), p. 457 to 462.

Pickering, H. W. 1995. The role of electrode potential distribution in corrosion processes. *Materials Science and Engineering: A* 198(1–2), pp. 213-223.

Pilz, M. and H. Römich. 1997. Sol-Gel Derived Coatings for Outdoor Bronze Conservation. *Journal of Sol-Gel Science and Technology* 8(1), pp. 1071-1075.

Podany, J., K. M. Garland, W. R. Freeman and J. Rogers. 2001. Paraloid B-72 as a Structural Adhesive and as a Barrier within Structural Adhesive Bonds: Evaluations of Strength and Reversibility. *Journal of the American Institute for Conservation* 40(1), pp. 15-33.

Poorna Chander, K., M. Vashista, K. Sabiruddin, S. Paul and P. P. Bandyopadhyay. 2009. Effects of grit blasting on surface properties of steel substrates. *Materials & Design* 30(8), pp. 2895-2902.

Prosek, T., M. Kouril, M. Dubus, M. Taube, V. Hubert, B. Scheffel, Y. Degres, M. Jouannic and D. Thierry. 2013. Real-time monitoring of indoor air corrosivity in

cultural heritage institutions with metallic electrical resistance sensors. *Studies in Conservation* 58(2), pp. 117-128.

Punckt, C., M. Bölscher, H. H. Rotermund, A. S. Mikhailov, L. Organ, N. Budiansky, J. R. Scully and J. L. Hudson. 2004. Sudden Onset of Pitting Corrosion on Stainless Steel as a Critical Phenomenon. *Science* 305(5687), pp. 1133-1136.

Rashidi, N., S. Alavi-Soltani and R. Ashmatulu. 2007. Crevice Corrosion Theory, Mechanisms and Prevention Methods. In: *Graduate Researchers and Scholarly Projects Symposium*. Wichita State University.

Redman, K. and B. Hall. 2013. Establishing suitable tests for determining the appropriate coating for your external metalwork; explaining the pros and cons of paints, waxes, lacquers, gilding and nothing. *Amazing Technicolour Dreamcoats: Protective surface finishes for metals*. ICON Metals Group Conference and AGM at The Wallace Collection, London.

Reedy, C. L., R. A. Corbett, D. L. Long, R. E. Tatnall and B. D. Krantz. 1999. *Article: Evaluation of three protective coatings for indoor silver objects*. Objects Specialty Group Postprints. pp. 41-69.

Reynolds, P. A. 1994. The Rheology of Coatings. In: Marrion, A. R. ed. *The Chemistry and Physics of Coatings*. Herts, UK: Royal Society of Chemistry, pp. 28-46.

Reynolds, P. A. 2004. The Rheology of Coatings. In: Marrion, A. R. ed. *The Chemistry and Physics of Coatings*. 2nd ed. Cambridge, UK: The Royal Society of Chemistry, pp. 26-45.

Rimmer, M., D. Thickett, D. Watkinson and H. Ganiaris. 2013. *Guidelines for the storage and display of archaeological metalwork*. London: English Heritage.

Roberge, P. R., R. D. Klassen and P. W. Haberecht. 2002. Atmospheric corrosivity modeling - a review. *Materials and Design* 23, pp. 321-330.

Rohm and Haas. 2007. *Paraloid B-72 100% - Technical Data Sheet*. Online at: <http://www.conservation-support-systems.com/system/assets/images/products/B72tech.pdf>; Rohm and Haas Company

Rosknecht, G. F., W. P. Elliott and F. L. Ramsey. 1973. The Size Distribution and Inland Penetration of Sea-Salt Particles. *Journal of Applied Meteorology* 12(5), pp. 825-830.

Royal Airforce Museum. 2013. *Saracen: Construction* [Online]. Available at: <http://www.nationalcoldwarfarexhibition.org/research/collections/saracen/construction/> [Accessed: 14-09-2016].

Saeed, A. 2013. *Sustainable Methodology of Conserving Historic Military Vehicles*. Bournemouth University.

Santana Rodríguez, J. J., F. J. Santana Hernández and J. E. González González. 2002. XRD and SEM studies of the layer of corrosion products for carbon steel in various different environments in the province of Las Palmas (The Canary Islands, Spain). *Corrosion Science* 44(11), pp. 2425-2438.

Santarini, G. 2007. Corrosion Behaviour of Low-Alloy Steels: From Ancient Past to Far Future. In: Dillmann, P., G. Beranger, P. Piccardo and H. Matthiesen eds. *Corrosion of Metallic Heritage Artefacts: Investigation, Conservation and Prediction of Long Term Behaviour: Investigation, Conservation and Prediction of Long Term Behaviour*. Cambridge: Woodhead Publishing, pp. 18-30.

Schauwinhold, D., U. Kalla and G. Kalwa. 2003. Steel, 6. Uses: Classification of Steels and Steel Products and Types of Steel. *Ullmann's Encyclopedia of Industrial Chemistry*. Completely Revised 6th ed., Vol. 34. Wiley-VCH Verlag GmbH & Co. KGaA.

Schindelholz, E. and R. G. Kelly. 2012. Wetting phenomena and time of wetness in atmospheric corrosion: a review. *Corrosion Reviews* 30(5-6), pp. 135-170.

Schmuecker, E., R. Lees and T. Richardson. 2010. The Examination and Conservation of a 17th Century Indian Horse Armour. In: Mardikian, P., C. Chemello, C. Watters and P. Hull eds. *Metal 2010*. Charleston, South Carolina, USA.

Schweitzer, P. A. 2003. *Metallic Materials: Physical, Mechanical, and Corrosion Properties*. New York: Marcel Dekker, Inc.

Schweitzer, P. A. 2010. *Fundamentals of Corrosion: Mechanisms, Causes, and Preventative Methods*. Boca Raton, Florida: CRC Press, Taylor & Francis Group.

Schwertmann, U. and H. Fechter. 1994. The Formation of Green Rust and its Transformation to Lepidocrocite. *Clay Minerals* 29, pp. 87-92.

Selwyn, L. 2004. *Metals and Corrosion: A Handbook for the Conservation Professional*. Ottawa, Canada: Canadian Conservation Institute

Shashoua, Y. and H. Matthiesen. 2010. Protection of iron and steel in large outdoor industrial heritage objects. *Corrosion Engineering, Science and Technology* 45(5), pp. 357-361.

- Shreir, L. L. 1976. Localised Corrosion. In: Shreir, L. L. ed. *Corrosion: Metal/Environment Reactions*. 2nd ed., Vol. 1. London, UK: Newnes- Butterworths pp. 1:130-175.
- Siatou, A., V. Argyropoulos, D. Charalambous, K. Polikreti and A. Kaminari. 2007. Testing New Coating Systems for the Long-Term Protection of Copper and Iron Alloy Collections Exposed in Uncontrolled Museum Environment. In: Argyropoulos, V., A. Hein and M. Abdel Harith eds. *Strategies for Saving our Cultural Heritage. Proceedings of the International Conference on Conservation Strategies for Saving Indoor Metallic Collections*. Cairo, Egypt, 25 February - 1 March.
- Slabaugh, W. H. and M. Grotheer. 1954. Mechanism of Filiform Corrosion. *Industrial & Engineering Chemistry* 46(5), pp. 1014-1016.
- Sorensen, P. A., S. Kiil, K. Dam-Johansen and C. E. Weinell. 2009. Anticorrosive coatings: a review. *Journal of Coatings Technology and Research* 6(2), pp. 135-176.
- Soum, A. 2001. Polysilazanes. In: Jones, R. G., W. Ando and J. Chojnowski eds. *Silicon-containing polymers: the science and technology of their synthesis and applications*. Dordrecht/Boston/London: Kluwer Academic Publishers, pp. 353-373.
- Ståhl, K., K. Nielsen, J. Jiang, B. Lebech, J. C. Hanson, P. Norby and J. van Lanschot. 2003. On the akaganéite crystal structure, phase transformations and possible role in post-excavational corrosion of iron artifacts. *Corrosion Science* 45(11), pp. 2563-2575.
- Stoye, D. and W. Freitag. 2007a. Paint Additives. *Paints, Coatings and Solvents*. 2nd (Completely Revised) ed. Weinheim, Germany: Wiley-VCH Verlag GmbH, pp. 159-171.
- Stoye, D. and W. Freitag. 2007b. Paint Application. *Paints, Coatings and Solvents*. 2nd (Completely Revised) ed. Weinheim, Germany: Wiley-VCH Verlag GmbH, pp. 195-218.
- Stoye, D. and W. Freitag. 2007c. Paint Systems. *Paints, Coatings and Solvents*. 2nd (Completely Revised) ed. Weinheim, Germany: Wiley-VCH Verlag GmbH, pp. 101-141.
- Stoye, D. and W. Freitag. 2007d. Types of Paints and Coatings (Binders). *Paints, Coatings and Solvents*. 2nd (Completely Revised) ed. Weinheim, Germany: Wiley-VCH Verlag GmbH, pp. 11-100.
- Stratmann, M., K. Bohnenkamp and H.-J. Engell. 1983. An Electrochemical Study of Phase-Transitions in Rust Layers. *Corrosion Science* 23(9), pp. 969-985.

- Stratmann, M. and M. Rohwerder. 2001. Materials science: A pore view of corrosion. *Nature* 410(6827), pp. 420-423.
- Syed, S. 2006. Atmospheric corrosion of materials. *Emirates Journal for Engineering Research* 11(1), pp. 1-24.
- Tada, E., K. Sugawara and H. Kaneko. 2004. Distribution of pH during galvanic corrosion of a Zn/steel couple. *Electrochimica Acta* 49(7), pp. 1019-1026.
- Tata Steel, SCI and BCSA. 2015. *Standard corrosion protection systems for buildings* [Online]. Available at: http://www.steelconstruction.info/Standard_corrosion_protection_systems_for_buildings#Introduction [Accessed: 23rd October 2015].
- Tavakkolizadeh, M. and H. Saadatmanesh. 2001. Galvanic Corrosion of Carbon and Steel in Aggressive Environments. *Journal of Composites for Construction* 5(3), pp. 200–210.
- Thackray, A. and D. Stevens. 2013. Lacquering a the V&A, Past, Present and Furniture Mounts. *Amazing Technicolour Dreamcoats: Protective surface finishes for metals*. ICON Metals Group Conference and AGM at The Wallace Collection, London.
- The Tank Museum. 2016. *The Tank Musuem - About Us* [Online]. Available at: <http://www.tankmuseum.org/about-us> [Accessed: 05/04/2016].
- The World Bank Group. 1999. Sulfur Oxides: Pollution Prevention and Control. In: The World Bank Group in Collaboration with the United Nations Environment Programme and the United Nations Industrial Development Organization ed. *Pollution Prevention and Abatement Handbook 1998: Towards Cleaner Production*. Washington, D.C., USA.
- Tidblad, J. 2013. Atmospheric Corrosion of Heritage Metallic Artefacts: Processes and Prevention. In: Dillmann, P., D. Watkinson , E. Angelini, A. Adriaens and on behalf of the Working Party 21 on Corrosion of Archaeological and Historical Artefacts eds. *Corrosion and Conservation of Cultural Heritage Metallic Artefacts*. Cambridge, UK: Woodhead Publishing Limited, pp. 37-52.
- Topp, C. 2009. Heritage Ironwork Training: A call for specialist training and accreditation. [Online]. Available at: <http://www.buildingconservation.com/articles/ironworktraining/ironworktraining.htm> [Accessed: 16 August 2016].
- Townsend, H. E. 2001. Effects of Alloying Elements on the Corrosion of Steel in Industrial Atmospheres. *Corrosion* 57(6), pp. 497-501.

Trethewey, K. R. and J. Chamberlain. 1995. *Corrosion for science and engineering*. 2nd ed. Longman Group Limited.

Tsutsumi, Y., A. Nishikata and T. Tsuru. 2007. Pitting corrosion mechanism of Type 304 stainless steel under a droplet of chloride solutions. *Corrosion Science* 49(3), pp. 1394-1407.

Tullmin, M. and P. R. Roberge. 2000. Atmospheric Corrosion. In: Winston Revie, R. ed. *Uhlig's Corrosion Handbook*. Second ed. John Wiley & Sons, Inc.

Turgoose, S. 1982. The Nature of Surviving Iron Objects. In: Clarke, R. and S. Blackshaw eds. *Conservation of Iron, National Maritime Museum, Monograph No. 53*.

Turner, G. P. A. 1988. *Introduction to Paint Chemistry and Principles of Paint Technology*. 3rd ed. London, UK: Chapman & Hall.

Uhlig, H. H. 1963. Section II. Corrosion in Liquid Media, the Atmosphere, and Gases: Pitting in Stainless Steels and Other Passive Metals. In: Uhlig, H. H. ed. *The Corrosion Handbook*. New York, USA: John Wiley & Sons, Inc., pp. 165-173.

van der Wel, G. K. and O. C. G. Adan. 1999. Moisture in organic coatings — a review. *Progress in Organic Coatings* 37(1–2), pp. 1-14.

Vera Cruz, R. P., A. Nishikata and T. Tsuru. 1996. AC Impedance monitoring of pitting corrosion of stainless steel under a wet-dry cyclic condition in chloride-containing environment. *Corrosion Science* 38(8), pp. 1397-1406.

Walker, P. 1982a. Organosilanes as adhesion promoters for organic coatings. Part 1: silanes on the metal surface. *Journal of the Oil and Colour Chemists Association* 65(11), pp. 415-423.

Walker, R. 1982b. The corrosion and preservation of iron antiques. *Journal of Chemical Education* 59(11), p. 943.

Walker, R. 1982c. The Role of Corrosion Inhibitors in the Conservation of Iron. In: Clarke, R. and S. Blackshaw eds. *Conservation of Iron, National Maritime Museum, Monograph No. 53*.

Walton, J. C., G. Cragolino and S. K. Kalandros. 1996. A numerical model of crevice corrosion for passive and active metals. *Corrosion Science* 38(1), pp. 1-18.

Watkinson, D. 2010. 4.43 - Preservation of Metallic Cultural Heritage. In: Cottis, B., M. Graham, R. Lindsay, S. Lyon, T. Richardson, D. Scantlebury and H. Stott eds. *Shreir's Corrosion*. Oxford: Elsevier, pp. 3307-3340.

Watkinson, D. and M. Rimmer. 2013. Quantifying Effectiveness of Chloride Desalination Treatments for Archaeological Iron Using Oxygen Measurement. In: Hyslop, E., V. Gonzalez, L. Troalen and L. Wilson eds. *Metal 2013 Interim Meeting of the ICOM-CC Metal Working Group*. Edinburgh, 17th September 2013. Historic Scotland.

Weissenrieder, J. and C. Leygraf. 2004. In Situ Studies of Filiform Corrosion of Iron. *Journal of The Electrochemical Society* 151(3), pp. B165-B171.

Wensink, H. 2002. *Fabrication of microstructures by powder blasting*. PhD, University of Twente.

Whitehouse, N. R. 2010. 4.10 - Paint Application. In: Cottis, B., M. Graham, R. Lindsay, S. Lyon, T. Richardson, D. Scantlebury and H. Stott eds. *Shreir's Corrosion*. Vol. 4 - Management and Control of Corrosion. Oxford: Elsevier, pp. 2637-2642.

Wicks, Z. W. and F. N. Jones. 2013. Coatings. *Kirk-Othmer Encyclopedia of Chemical Technology*. John Wiley & Sons, Inc.

Wicks, Z. W., F. N. Jones, S. P. Pappas and D. A. Wicks. 2006a. Adhesion. *Organic Coatings: Science and Technology*. 3rd ed. Hoboken, NJ, USA: John Wiley & Sons, Inc., pp. 121-136.

Wicks, Z. W., F. N. Jones, S. P. Pappas and D. A. Wicks. 2006b. Application Methods. *Organic Coatings: Science and Technology*. 3rd ed. Hoboken, NJ, USA: John Wiley & Sons, Inc., pp. 473-489.

Wicks, Z. W., F. N. Jones, S. P. Pappas and D. A. Wicks. 2006c. Corrosion Protection by Coatings. *Organic Coatings: Science and Technology*. 3rd ed. Hoboken, NJ, USA: John Wiley & Sons, Inc., pp. 137-158.

Wicks, Z. W., F. N. Jones, S. P. Pappas and D. A. Wicks. 2006d. Film Defects. *Organic Coatings: Science and Technology*. 3rd ed. Hoboken, NJ, USA: John Wiley & Sons, Inc., pp. 490-510.

Wicks, Z. W., F. N. Jones, S. P. Pappas and D. A. Wicks. 2006e. Flow. *Organic Coatings: Science and Technology*. 3rd ed. Hoboken, NJ, USA: John Wiley & Sons, Inc., pp. 41-67.

Wicks, Z. W., F. N. Jones, S. P. Pappas and D. A. Wicks. 2006f. Solvents. *Organic Coatings: Science and Technology*. 3rd ed. Hoboken, NJ, USA: John Wiley & Sons, Inc., pp. 349-381.

Williams, J. 2009a. *The role of science in the management of the UK's heritage*. Historic England.

Williams, J. 2009b. *The use of science to enhance our understanding of the past*. English Heritage.

Wolfram, J., S. Bruggerhoff and G. Eggert. 2010. Better than Paraloid B72? Testing Poligen Waxes as Coatings for Metal Objects. In: Mardikian, P., C. Chemello, C. Watters and P. Hull eds. *METAL 2010*. Charleston, South Carolina, USA, 11-15 October 2010.

Wranglen, G. 1974. Pitting and sulphide inclusions in steel. *Corrosion Science* 14(5), pp. 331-349.

Zhao, X. and G. S. Frankel. 2007. Quantitative study of exfoliation corrosion: Exfoliation of slices in humidity technique. *Corrosion science* 49(2), pp. 920-938.

Zorll, U. 2006. Adhesion Testing. In: Tracton, A. A. ed. *Coating Technology: Fundamentals, Testing, and Processing Techniques*. Boca Raton, FL, USA: CRC Press, pp. 6.1-6.13.

10 Appendix

10.1 Summarised TM environment data

The individual tables provide summarised data for different areas of the museum.

Table 81 Summary of environment in the British Steel Hall on the Tortoise Tank.

Monitoring period	Start date	End Date	Temperature (°C)			Relative Humidity (%)		
			Min	Ave	Max	Min	Ave	Max
Oct - Nov '11	24/10/2011	16/11/2011	18.8	19.1	23.0	47.4	61.6	72.7
Nov '11 – Jan '12	16/11/2011	19/01/2012	15.9	18.8	22.9	25.0	46.7	65.5
Jan – Mar '12	19/01/2012	05/03/2012	14.8	18.5	23.2	17.4	39.1	62.1
Mar – May '12	05/03/2012	01/05/2012	17.7	18.7	24.6	25.3	41.8	58.7
May – Jun '12	01/05/2012	22/06/2012	18.0	20.3	24.8	32.4	51.8	73.8
Jun – Aug '12	22/06/2012	29/08/2012	18.9	21.3	25.2	39.2	62.5	80.9

Table 82 Data summary collected in the Discovery Centre on the Mark 10

Monitoring period	Start date	End Date	Temperature (°C)			Relative Humidity (%)		
			Min	Ave	Max	Min	Ave	Max
Oct - Nov '11	24/10/2011	16/11/2011	16.79	17.81	25.71	47.16	66.57	79.91
Nov '11 – Jan '12	16/11/2011	19/01/2012	14.19	17.44	22.79	28.52	50.63	69.77
Jan – Mar '12	19/01/2012	05/03/2012	12.86	17.42	22.93	18.63	41.37	61.81
Mar – May '12	05/03/2012	01/05/2012	17.06	18.11	22.95	25.73	43.19	60.21
May – Jun '12	01/05/2012	22/06/2012	17.10	19.66	25.03	32.95	53.91	78.81
Jun – Aug '12	22/06/2012	29/08/2012	17.98	20.81	25.81	41.23	65.03	82.40

Table 83 Summarised data collected in the New Display Hall on the Firefly

Monitoring period	Start date	End Date	Temperature (°C)			Relative Humidity (%)		
			Min	Ave	Max	Min	Ave	Max
Oct - Nov '11	24/10/2011	16/11/2011	17.96	19.49	22.94	45.54	59.98	71.54
Nov '11 – Jan '12	16/11/2011	19/01/2012	15.81	18.75	22.94	26.21	46.13	64.45
Jan – Mar '12	19/01/2012	05/03/2012	17.27	18.77	23.50	19.11	38.05	73.16
Mar – May '12	05/03/2012	02/05/2012	15.99	18.60	29.09	24.58	42.48	95.05
May – Jun '12	02/05/2012	22/06/2012	16.16	20.00	24.34	34.14	54.01	92.50
Jun – Aug '12	22/06/2012	29/08/2012	19.32	21.75	25.44	41.17	61.91	77.25

Table 84 Summary of data by the TM in the New Display Hall inside the Firefly

Monitoring period	Start date	End Date	Temperature (°C)			Relative Humidity (%)		
			Min	Ave	Max	Min	Ave	Max
Nov '11 – Jan '12	17/11/2011	19/01/2012	16.87	18.78	23.14	28.46	45.66	61.50
Jan – Mar '12	19/01/2012	05/03/2012	16.36	18.91	23.04	17.38	37.34	57.11
Mar – May '12	05/03/2012	01/05/2012	16.55	18.67	25.38	28.00	41.53	86.65
May – Jun '12	01/05/2012	22/06/2012	16.94	19.98	23.48	39.55	53.41	68.29

Table 85 Summary of data collected by the TM in Nev's Shed

Monitoring period	Start date	End Date	Temperature (°C)			Relative Humidity (%)		
			Min	Ave	Max	Min	Ave	Max
Nov '11 – Jan '12	17/11/2011	19/01/2012	-0.82	8.14	24.55	47.90	91.77	100.00
Jan – Mar '12	19/01/2012	05/03/2012	-6.12	5.54	22.76	41.65	91.19	100.00
Mar – May '12	05/03/2012	01/05/2012	1.47	9.32	22.88	30.86	81.21	100.00
May – Jun '12	01/05/2012	22/06/2012	4.42	14.28	27.76	30.41	80.79	100.00
Jun – Aug '12	22/06/2012	29/08/2012	10.86	17.45	29.33	38.57	83.72	100.00

Table 86 Summary of the data collected by the TM in the New Shed

Monitoring period	Start date	End Date	Temperature (°C)			Relative Humidity (%)		
			Min	Ave	Max	Min	Ave	Max
Nov '11 – Jan '12	17/11/2011	19/01/2012	5.28	10.05	23.52	47.94	82.86	100.00
Jan – Mar '12	19/01/2012	05/03/2012	1.82	7.65	22.91	40.65	80.23	100.00
Mar – May '12	05/03/2012	01/05/2012	7.12	11.69	23.30	31.13	69.98	96.63
May – Jun '12	01/05/2012	22/06/2012	10.32	16.27	32.35	29.52	71.29	100.00
Jun – Aug '12	22/06/2012	29/08/2012	15.03	19.39	29.55	40.17	74.84	97.47

Table 87 Summary of data collected by the TM in Shed 1

Monitoring period	Start date	End Date	Temperature (°C)			Relative Humidity (%)		
			Min	Ave	Max	Min	Ave	Max
Nov '11 – Jan '12	17/11/2011	19/01/2012	-1.74	7.65	23.11	48.43	96.86	100.00
Jan – Mar '12	19/01/2012	05/03/2012	-6.94	5.39	22.83	40.67	93.74	100.00
Mar – May '12	05/03/2012	01/05/2012	0.64	9.78	23.70	28.58	80.76	100.00
May – Jun '12	01/05/2012	22/06/2012	3.54	15.28	32.01	29.05	78.83	100.00
Jun – Aug '12	22/06/2012	29/08/2012	10.03	18.55	32.53	36.09	81.82	100.00

Table 88 Summary of data collected by the TM in the Shed 1 Extension

Monitoring period	Start date	End Date	Temperature (°C)			Relative Humidity (%)		
			Min	Ave	Max	Min	Ave	Max
Nov '11 – Jan '12	17/11/2011	19/01/2012	-2.61	7.83	23.47	37.79	93.90	100.00
Jan – Mar '12	19/01/2012	05/03/2012	-7.37	5.64	23.24	41.42	90.95	100.00
Mar – May '12	05/03/2012	01/05/2012	0.19	10.09	28.83	22.50	79.31	100.00
May – Jun '12	01/05/2012	22/06/2012	2.75	15.80	37.35	19.56	75.65	100.00
Jun – Aug '12	22/06/2012	29/08/2012	9.39	19.04	41.85	21.80	78.52	100.00

Table 89 Summarised data collected in the Tamiya Hall, at the Sentry Post

Monitoring period	Start date	End Date	Temperature (°C)			Relative Humidity (%)		
			Min	Ave	Max	Min	Ave	Max
Oct - Nov '11	24/10/2011	16/11/2011	15.28	16.63	22.60	50.53	72.45	80.81
Nov '11 – Jan '12	16/11/2011	19/01/2012	15.62	21.05	30.80	20.55	44.31	78.11
Jan – Mar '12	19/01/2012	05/03/2012	12.32	20.53	23.78	15.38	33.62	55.07
Mar – May '12	05/03/2012	01/05/2012	17.98	20.79	25.16	22.84	36.95	57.09
May – Jun '12	01/05/2012	22/06/2012	17.89	20.62	27.04	30.10	51.95	74.32
Jun – Aug '12	22/06/2012	29/08/2012	17.77	20.92	28.28	45.51	65.96	79.19

Table 90 Summary of data collected by the TM in the WW1 Hall, display case

Monitoring period	Start date	End Date	Temperature (°C)			Relative Humidity (%)		
			Min	Ave	Max	Min	Ave	Max
Apr '12	19/04/2012	25/04/2012	15.66	16.75	23.13	32.75	42.03	71.44
Apr – May '12	25/04/2012	01/05/2012	14.89	16.50	21.56	40.64	47.63	60.51
Jun – Aug '12	22/06/2012	29/08/2012	18.02	21.40	27.84	39.95	63.03	79.74

Table 91 Summary of data collected by the TM in the WW1 Hall, CW

Monitoring period	Start date	End Date	Temperature (°C)			Relative Humidity (%)		
			Min	Ave	Max	Min	Ave	Max
Oct - Nov '11	24/10/2011	16/11/2011	17.61	19.15	26.73	37.29	59.63	77.33
Nov '11 – Jan '12	16/11/2011	19/01/2012	16.50	18.81	22.68	23.40	45.91	68.35
Jan – Mar '12	19/01/2012	05/03/2012	13.14	18.73	23.27	15.48	37.26	57.01
Mar – May '12	05/03/2012	01/05/2012	14.14	18.08	23.06	24.80	67.57	42.72
May – Jun '12	01/05/2012	22/06/2012	14.78	19.11	26.06	32.03	55.53	76.52
Jun – Aug '12	22/06/2012	29/08/2012	18.02	21.40	27.84	39.95	63.03	79.74